IAEA TECDOC SERIES

IAEA-TECDOC-1929

IAEA-TECDOC-1929

Geochemical and Mineralogical Characterization of Uranium and Thorium Deposits

Final Report of a Coordinated Research Project

IAEA
International Atomic Energy Agency

GEOCHEMICAL AND MINERALOGICAL CHARACTERIZATION OF URANIUM AND THORIUM DEPOSITS

The following States are Members of the International Atomic Energy Agency:

AFGHANISTAN
ALBANIA
ALGERIA
ANGOLA
ANTIGUA AND BARBUDA
ARGENTINA
ARMENIA
AUSTRALIA
AUSTRIA
AZERBAIJAN
BAHAMAS
BAHRAIN
BANGLADESH
BARBADOS
BELARUS
BELGIUM
BELIZE
BENIN
BOLIVIA, PLURINATIONAL STATE OF
BOSNIA AND HERZEGOVINA
BOTSWANA
BRAZIL
BRUNEI DARUSSALAM
BULGARIA
BURKINA FASO
BURUNDI
CAMBODIA
CAMEROON
CANADA
CENTRAL AFRICAN REPUBLIC
CHAD
CHILE
CHINA
COLOMBIA
COMOROS
CONGO
COSTA RICA
CÔTE D'IVOIRE
CROATIA
CUBA
CYPRUS
CZECH REPUBLIC
DEMOCRATIC REPUBLIC OF THE CONGO
DENMARK
DJIBOUTI
DOMINICA
DOMINICAN REPUBLIC
ECUADOR
EGYPT
EL SALVADOR
ERITREA
ESTONIA
ESWATINI
ETHIOPIA
FIJI
FINLAND
FRANCE
GABON
GEORGIA
GERMANY
GHANA
GREECE
GRENADA
GUATEMALA
GUYANA
HAITI
HOLY SEE
HONDURAS
HUNGARY
ICELAND
INDIA
INDONESIA
IRAN, ISLAMIC REPUBLIC OF
IRAQ
IRELAND
ISRAEL
ITALY
JAMAICA
JAPAN
JORDAN
KAZAKHSTAN
KENYA
KOREA, REPUBLIC OF
KUWAIT
KYRGYZSTAN
LAO PEOPLE'S DEMOCRATIC REPUBLIC
LATVIA
LEBANON
LESOTHO
LIBERIA
LIBYA
LIECHTENSTEIN
LITHUANIA
LUXEMBOURG
MADAGASCAR
MALAWI
MALAYSIA
MALI
MALTA
MARSHALL ISLANDS
MAURITANIA
MAURITIUS
MEXICO
MONACO
MONGOLIA
MONTENEGRO
MOROCCO
MOZAMBIQUE
MYANMAR
NAMIBIA
NEPAL
NETHERLANDS
NEW ZEALAND
NICARAGUA
NIGER
NIGERIA
NORTH MACEDONIA
NORWAY
OMAN
PAKISTAN
PALAU
PANAMA
PAPUA NEW GUINEA
PARAGUAY
PERU
PHILIPPINES
POLAND
PORTUGAL
QATAR
REPUBLIC OF MOLDOVA
ROMANIA
RUSSIAN FEDERATION
RWANDA
SAINT LUCIA
SAINT VINCENT AND THE GRENADINES
SAN MARINO
SAUDI ARABIA
SENEGAL
SERBIA
SEYCHELLES
SIERRA LEONE
SINGAPORE
SLOVAKIA
SLOVENIA
SOUTH AFRICA
SPAIN
SRI LANKA
SUDAN
SWEDEN
SWITZERLAND
SYRIAN ARAB REPUBLIC
TAJIKISTAN
THAILAND
TOGO
TRINIDAD AND TOBAGO
TUNISIA
TURKEY
TURKMENISTAN
UGANDA
UKRAINE
UNITED ARAB EMIRATES
UNITED KINGDOM OF GREAT BRITAIN AND NORTHERN IRELAND
UNITED REPUBLIC OF TANZANIA
UNITED STATES OF AMERICA
URUGUAY
UZBEKISTAN
VANUATU
VENEZUELA, BOLIVARIAN REPUBLIC OF
VIET NAM
YEMEN
ZAMBIA
ZIMBABWE

The Agency's Statute was approved on 23 October 1956 by the Conference on the Statute of the IAEA held at United Nations Headquarters, New York; it entered into force on 29 July 1957. The Headquarters of the Agency are situated in Vienna. Its principal objective is "to accelerate and enlarge the contribution of atomic energy to peace, health and prosperity throughout the world''.

IAEA-TECDOC-1929

GEOCHEMICAL AND MINERALOGICAL CHARACTERIZATION OF URANIUM AND THORIUM DEPOSITS

FINAL REPORT OF A COORDINATED RESEARCH PROJECT

INTERNATIONAL ATOMIC ENERGY AGENCY
VIENNA, 2020

COPYRIGHT NOTICE

For further information on this publication, please contact:

Nuclear Fuel Cycle and Materials Section
International Atomic Energy Agency
Vienna International Centre
PO Box 100
1400 Vienna, Austria
Email: Official.Mail@iaea.org

Printed by the IAEA in Austria
November 2020

IAEA Library Cataloguing in Publication Data

Names: International Atomic Energy Agency.
Title: Geochemical and mineralogical characterization of uranium and thorium deposits / International Atomic Energy Agency.
Description: Vienna : International Atomic Energy Agency, 2020. | Series: IAEA TECDOC series, ISSN 1011–4289 ; no. 1929 | Includes bibliographical references.
Identifiers: IAEAL 20-01355 | ISBN 978–92–0–118920–2 (paperback : alk. paper) |
ISBN 978–92–0–119020–8 (pdf)
Subjects: LCSH: Uranium ores — Geology. | Thorium ores. | Mineralogical chemistry. | Analytical geochemistry.

FOREWORD

A long term, sustainable supply of uranium (and potentially thorium in the future) is an essential part of the nuclear fuel cycle. It is also important to ensure that the mining, extraction and processing of uranium (and thorium) are efficient and environmentally friendly. Over the past few decades there have been significant advancements in geochemical techniques and geological assessment methodologies. These advancements can be used to elucidate the genesis of uranium and thorium deposits in various geographical and geological environments for enhanced resource evaluation and to characterize deposits for improvements in mining, extraction and processing.

In 2015, the IAEA launched a coordinated research project entitled Geochemical and Mineralogical Characterization of Uranium and Thorium Deposits. The goal of the project was to improve the understanding of the genesis of uranium and thorium deposits using new methodologies and geochemical techniques. The project, which involved 12 research contract holders (from Argentina, China (2), Egypt, Ghana, Islamic Republic of Iran, Kenya, Madagascar, Mongolia, the Philippines, Ukraine and the Bolivarian Republic of Venezuela), one technical contract holder (Canada) and one agreement holder (France), was concluded in October 2018.

This publication presents a summary of the research and selected papers from the project's partners. The results are expected to enhance exploration programmes, resource evaluation and sustainable supply of uranium and thorium for peaceful purposes.

The IAEA would like to acknowledge the support provided by the following partners: School of Nuclear and Allied Sciences, University of Ghana; Department of Earth Science, University of Ghana; National Nuclear Research Institute, Ghana Atomic Energy Commission; University of Lorraine-GeoRessources Laboratory-CREGU; National University of Córdoba, Argentina; United States Geological Survey, Colorado office; and National Institute of Nuclear Sciences and Techniques, Madagascar. The IAEA would also like to thank all the participants for their contributions, in particular the late K. Kyser for facilitating and hosting the second research coordination meeting. The IAEA officer responsible for this publication was A. Hanly of the Division of Nuclear Fuel Cycle and Waste Technology.

EDITORIAL NOTE

This publication has been prepared from the original material as submitted by the contributors and has not been edited by the editorial staff of the IAEA. The views expressed remain the responsibility of the contributors and do not necessarily represent the views of the IAEA or its Member States.

Neither the IAEA nor its Member States assume any responsibility for consequences which may arise from the use of this publication. This publication does not address questions of responsibility, legal or otherwise, for acts or omissions on the part of any person.

The use of particular designations of countries or territories does not imply any judgement by the publisher, the IAEA, as to the legal status of such countries or territories, of their authorities and institutions or of the delimitation of their boundaries.

The mention of names of specific companies or products (whether or not indicated as registered) does not imply any intention to infringe proprietary rights, nor should it be construed as an endorsement or recommendation on the part of the IAEA.

The authors are responsible for having obtained the necessary permission for the IAEA to reproduce, translate or use material from sources already protected by copyrights.

The IAEA has no responsibility for the persistence or accuracy of URLs for external or third party Internet web sites referred to in this publication and does not guarantee that any content on such web sites is, or will remain, accurate or appropriate.

CONTENTS

SUMMARY

1. BACKGROUND

With increased need for uninterrupted, long-term and sustainable supply of uranium (and potentially thorium in the future), it has become important to consider further evaluation of regions for increasing the resource base, and at the same time, making the mining and extraction more efficient and environmentally friendly. A deeper understanding of the genesis of uranium and thorium deposits under various geological environments with complex mineralization processes is required. This can be obtained through technological advancements which includes the analysis of the geochemical and mineralogical characteristics of each deposit. Such information will be helpful in guiding further exploration and optimization of extraction and production, and in effective environmental management.

The objectives of the Coordinated Research Project (CRP) were accomplished through a variety of methods, some of which were project specific. The main methods comprised obtaining geochemical and mineralogical data including major, minor and trace elements; stable and radioactive isotopes; identification of major uranium, thorium and other ore minerals; scanning electron microscopy and fluid inclusion studies. The outputs are expected to assist in understanding the global distribution of uranium and thorium resources in a consistent manner and thus provide valuable inputs for exploration strategies, resource evaluation and their sustainable development.

2. OBJECTIVE

This publication is a summary of the results and an overview of activities that were carried out under the CRP, Geochemical and mineralogical characterization of uranium and thorium deposits that was launched in 2015 and terminated in 2018.

3. STRUCTURE

This publication comprises an introduction of the background and objectives of the CRP and a brief summary of the fourteen studies. An individual brief summary of all studies that were part of the CRP has been provided as not all contract holders provided a research summary paper, and papers for this publication were voluntary due to the different levels of research undertaken. The remainder of the publication consists of eight papers that are more detailed reports of research undertaken in association with the CRP.

4. SCOPE

Twelve research contracts, one agreement and one technical contract were implemented for this CRP. The Member States involved, institutions, chief investigators and title of the individual projects are outlined in Table 1. Researchers were encouraged to publish their results and some of the preliminary results were presented at the IAEA International Symposium on Uranium Raw Material for the Nuclear Fuel Cycle: Exploration, Mining, Production, Supply and Demand, Economics and Environmental Issues (URAM-2018) held in Vienna, Austria, 25–29 June 2018 (see Appendix 1).

Argentina, China, and Ukraine focused on comprehensive studies of specific deposit types; broad studies of an international scope were undertaken by the researchers from Canada and France; Ghana, Madagascar, Mongolia and the Philippines focused on aspects of characterizing and evaluating national uranium resources; Kenya focused on development of analytical techniques; Egypt, the Islamic Republic of Iran, and the Bolivarian Republic of Venezuela undertook characterization and assessment of the uranium potential of phosphate type deposits.

5. CRP ACHIEVEMENTS

New geochemical and mineralogical data from the research conducted under this CRP has resulted in a better understanding of the genesis of uranium and thorium, improved the evaluation of uranium and thorium resources, and in some cases will have implications for processing and production.

Several collaborations were developed among CRP partners from a number of countries that were involved in the CRP including: Argentina, Canada, China, France, Madagascar, Ukraine, and the Bolivarian Republic of Venezuela, and one country not directly involved in the CRP (the United States of America). Collaborations were also developed amongst institutions within the countries.

A field trip, which shared some of the research conducted by the Ukraine was held in the Ukraine from 2–6 July 2018 with 25 international participants.

Twenty-eight publications (Appendix 1), and eight graduate degrees (PhD and MSc, Appendix 2) were reported in association with the CRP activities.

TABLE 1. IAEA MEMBER STATES, INSTITUTIONS, TITLE OF RESEARCH PROJECTS AND CHIEF SCIENTIFIC INVESTIGATORS FOR CRP

IAEA Member State	Institute City	Title	Chief Scientific Investigator(s)
Argentina	Comisión Nacional de Energía Atómica Buenos Aires	Metallogenesis of granite-related uranium deposits in Argentina	Mr Juan Oscar Álvarez Mr Luis López
Canada	Queens University Kingston	Geochemical and mineralogical characterization of various uranium deposits	Mr Kurt Kyser
China	Beijing Research Institute of Chemical Engineering and Metallurgy Beijing	Mineralogical characterization of sandstone uranium deposits in China	Mr Liao Weng-Sheng
China	East China University of Technology/Jiujiang University Nanchang	The relations of A-type igneous rocks to uranium mineralization in south China	Mr Liu Xiaodong
Egypt	Nuclear Materials Authority Cairo	Geochemical and mineralogical characterization of uranium and thorium in Egyptian phosphate deposits	Mr Hado Gady
France	Centre de Recherches sur la Géologie de l'Uranium (CREGU) Nancy	Geochemistry of uranium oxides; tracing the uranium deposit types	Mr Michel Cuney
Ghana	Ghana Atomic Energy Commission Accra	Geochemical and mineralogical studies of potential co-products; uranium resources in Ghana	Mr Samuel B. Dampare
Islamic Republic of Iran	Nuclear Science and Technology Research Institute Tehran	Investigation of the uranium potential of Islamic Republic of Iran's sedimentary phosphatic rocks	Mr Khoshnoodi Khalegh

TABLE 1 (Cont.). IAEA MEMBER STATES, INSTITUTIONS, TITLE OF RESEARCH PROJECTS AND CHIEF SCIENTIFIC INVESTIGATORS FOR CRP

IAEA Member State	Institute City	Title	Chief Scientific Investigator(s)
Kenya	University of Nairobi Nairobi	Multimodal spectrometric characterization of uranium and thorium bearing mineral ores from Kenya's high background radiation areas	Mr Hudson Angeyo Kalambuka
Madagascar	Office des Mines Nationales et des Industries Stratégiques Antananarivo	Morondova uranium project	Ms Dinamalala Ranaivosoana
Mongolia	Nuclear Research Center National University of Mongolia Ulaanbaatar	Elemental Characterization of Uranium Ore Deposits from Mongolia	Ms Tserenpil Shurkhuu
Philippines	Philippine Nuclear Research Institute Quezon City	Geochemical and radiometric characterization of the Cu-Mo-U occurrences in the Larap-Paracale mineralized district, Camarines Norte, Phillipines	Mr Vargas Edmondo Mr Rolando Reyes
Ukraine	M.P. Semenenko Institute of Geochemistry, Mineralogy and Ore Formation Kyiv	Geochemical and mineralogical characterization of Palaeoproterozoic albitite-type uranium deposits of the Ukrainian Shield	Mr Leonid Shumlyanskyy
Bolivarian Republic of Venezuela	Universidad Simon Bolivar Caracas	Geochemical and mineralogical study of the U-bearing phosphatic rocks of Navay Formation, Tachira State, Bolivarian Republic of Venezuela	Mr John Luis Manrique Mr Haydn Barros

BRIEF SYNOPSIS OF THE STUDIES CARRIED OUT UNDER THIS CRP

This section provides individual partner summaries of research objectives and key results of studies carried out under this CRP.

1. ARGENTINA

1.1. Objective

To characterize mineralogical and geochemical aspects of uranium deposits related to granites and define the felsic igneous (granitic) rocks that have played the most relevant role as uranium sources, including understanding key processes such as successive fractionation in the different magmatic complexes, magmatic uranium enrichment and hydrothermal processes, alteration and uranium mobility.

1.2. Key results

The studies allowed refinement of the metallogenetic model of uranium deposits related to granitic rocks which will also aid in formulation of guidelines to better plan exploration activities. Granites play an important role as a uranium source and hosting diverse types of uranium mineralization and the knowledge gained from this research will assist in development of new uranium prospects and resources related to granites in Argentina.

2. CANADA

2.1. Objective

To increase the understanding of the genesis of various types of uranium deposits in diverse geographical and geological environments via analyses of their geochemical and mineralogical characteristics.

2.2. Key Results

Geochemical data obtained during the first two years of the CRP were shared with the IAEA and participants in the CRP. The second research coordination meeting was held at Queen's University, Canada. The chief scientific investigator, Mr Kyser provided mentoring and advice to many of the CRP participants and organized a tour of the excellent laboratory facilities at the university.

3. CHINA

China had two projects, focusing on sandstone-type and granite-type environments, respectively.

Mineralogical characterization of sandstone uranium deposits in China

3.1. Objective

To identify additional uranium resources, develop guidelines on uranium mining and production and to enrich databases on sandstone-type uranium deposits.

3.2. Key results

Ten major sandstone-type uranium deposits in China have been studied and estimated resources were increased by 100–500 tU. The outcomes of this study will aid in the comparison of various deposits and in particular in the establishment of the relationships between permeability, uranium mineralization and uranium recovery by leaching. This will also be used to predict the leaching properties for newly discovered deposits. There is an expression of interest from organizations in China to use the outcomes of this study in order to develop a software establishing a database which relates the mineralogy of deposits with leaching methods to predict the leaching technology.

The relations of A-type igneous rocks to uranium mineralization in south China

3.3 Objective

To determine the genesis of A-type syenite and granite assemblages and sodium-metasomatic uranium deposits in the Jiling area.

3.4. Key results

Paleozoic A-type syenite and granites in the Jiling area were formed by mixing between crustal- and mantle- derived magmas. Ore forming fluid was derived from mixing between magmatic fluid and meteoric water, and the uranium was derived from the host A-type granitic rocks. The results of this programme will be used to formulate guidelines for future exploration in the area and other areas with similar lithologies.

4. EGYPT

4.1 Objective

Evaluation of P_2O_5 and uranium in El-Sebaiya and Abu-Tartur areas to determine the added value (recovery of uranium and rare earth elements (REE)) from phosphate deposits in Egypt.

4.2. Key results

The inferred phosphate resources in El-Sebaiya area are about 80 million tons with an average of 90 ppm uranium and is depleted in REE and low in thorium. The Abu-Tartur phosphate is enriched in REE with about 0.2% but poor in uranium and thorium (25 and 4 ppm respectively).

The El-Sebaiya area has the best potential for added value through recovery of uranium and Abu-Tartur through recovery of REE.

5. FRANCE

5.1 Objective

To improve the understanding of the genesis of uranium deposits by measuring and comparing the REE from a wide range of deposits from variable geological settings (from deep magmatic to surficial conditions).

5.2. Key results

It was determined that the REE patterns are specific to each deposit type and that they directly reflect the conditions of their genesis. REE patterns and associated trace elements may represent an efficient tool for: (i) constraining geological models of uranium deposits; (ii) genetically discriminating new uranium discoveries; and (iii) forensic studies (isotopic tracing of deposits). However, additional experimental work is needed to improve the interpretations.

6. GHANA

6.1. Objective

To investigate the potential of the late Devonian to early Carboniferous Takoradi Shale Formation (TSF) in Ghana to host uranium, thorium and other trace elements.

6.2. Key results

The rocks have a uranium content of 6.9 to 9.0 ppm with an average concentration of 8.3 ppm, thorium contents range from 18.1 to 22.1 ppm and total REE range between 271 ppm and 368 ppm. Thorium, zirconium, niobium, tantalum, vanadium, total REE and titanium, which are typically enriched in uraniferous black shales, are also enriched in the Takoradi Shale Formation (TSF). However, the black shales of the TSF have lower concentrations of uranium compared to typical uraniferous black shales and therefore are of limited interest as a potential source of uranium.

7. ISLAMIC REPUBLIC OF IRAN

7.1. Objective

Investigation of uranium mineralization potential of Islamic Republic of Iran's sedimentary phosphates using geochemistry and mineralogy.

7.2. Key results

The major factors controlling uranium enrichment in sedimentary phosphates include environment of formation; phosphate mineralogy; amount of organic matter; P_2O_5 grade; redox conditions, (Eh and pH) at the time of phosphate deposition; paleo-climatic conditions; and weathering. According

to the above factors, the phosphorite horizons of Pabdeh Formation have the potential for uranium enrichment. Uranium in phosphorite horizons of Sheikh Habil, Kuh-e Kumeh, Choram, Khormoj and Kuh-e Rish deposits are in a range of 88 to 108 ppm, 17 to 69 ppm, 19 to 57 ppm, 12 to 40 ppm and 10 to 41 ppm uranium, respectively. In the phosphate deposits of Pabdeh Formation, the main host of uranium is apatite.

8. KENYA

8.1. Objective

To develop and utilize machine learning to enable multimodal spectrometric methodologies for direct geochemical characterization of Kenya's high background area comprising thorium and uranium bearing rocks.

8.2. Key Results

Machine learning was developed and applied/tested to a number of techniques including: laser induced breakdown spectroscopy (LIBS) and its new extension, laser ablation molecular isotopic spectrometry (LAMIS); energy dispersive X-ray fluorescence and scattering (EDXRFS) spectrometry; laser Raman microspectrometry (LRM); laser induced fluorescence (LIF) spectroscopy; and laser scanning microscopy (LSM), to develop a multimodal protocol for direct geochemical analysis and characterization of thorium and uranium bearing mineral rocks from Kenya's alkaline-carbonatite complexes. This work will be used towards development of a multimodal protocol relevant to mineralogical and geochemical characterization of uranium and thorium, as well as to their extraction and sustainable exploitation.

9. MADAGASCAR

9.1. Objective

To find a new deposit of uranium in the Morondava sedimentary basin (Makay Formation) in Madagascar.

9.2. Key results

Due to issues with procurement of equipment required for the geochemical analyses, this work was not fully completed. However, the field work and sample collection were completed, and the analytical work will be undertaken once the equipment is received through the related IAEA Technical Cooperation project.

10. MONGOLIA

10.1. Objective

To determine elemental fingerprints including rare earth element (REE) distribution patterns of Mongolian uranium deposits.

10.2. Key results

As a result of complications to obtain UO_2 concentrates, bulk samples from the Mongolian uranium deposits were studied instead. A REE pattern with light rare earth element (LREE) enrichment was noted for Zoovh Ovoo, a sandstone-type deposit which represents a significant part of the total uranium resources of Mongolia. This geochemical signature can be used as a comparison tool for other potential deposits in Mongolia.

11. PHILIPPINES

11.1. Objective

To conduct a re-evaluation of known uranium-bearing base metal and iron deposits in Larap-Paracale mineralized district in Camarines Norte, Philippines and to verify previously identified areas with anomalous radioactivity, to assess the REE contents, and to determine if more detailed evaluations should be recommended for future studies.

11.2. Key results

The historical uranium anomalies previously delineated in the San Isidro and Capacuan area did not show anomalous uranium concentrations but showed relatively high thorium concentrations (equivalent thorium (eTh) of 1.7 to 23.2 ppm with an average of 9.9 ppm). The uranium content in the Paracale National-Sta Rosa Sur anomaly is approximately 13 ppm equivalent uranium (eU) based on radiometric data. The high uranium concentrations detected by gamma spectrometry at Nakalaya were confirmed. Data also indicated high uranium concentrations that were associated with the base metals such as copper, molybdenum, zinc, lead and iron.

12. UKRAINE

12.1. Objective

To investigate sources of the fluids and uranium for the sodium-metasomatites of the Central Ukrainian Uranium Province (CUUP) and to establish links with major crust-forming events.

12.2. Key results

The project provided a detailed mineralogical, geochemical and isotope-geochemical (Sr-Nd-Pb isotopes) characterization of the albitite-type uranium deposits. The results indicate a prevailing crustal source of the metasomatizing fluids. However, a plume-related mantle source is also important, as plume provided not only heat required for generation of hot fluids, but also contributed to elevated concentrations of a characteristic set of elements such as heavy rare earth

elements (HREE) and transitional metals (nickel, cobalt, copper, and zinc). These new results are important for the understanding of the nature and causes of sodium-metasomatism and related uranium mineralization, and for further exploration of albitite-type uranium deposits in other areas.

In association with the research conducted for this CRP, an international field trip, Uranium and Thorium Deposits of the Central Ukrainian Uranium Province was held 2–6 July 2018 with 26 researchers from nine countries (Australia; China; Ecuador; Estonia; France; India; Islamic Republic of Iran; Ukraine; and Bolivarian Republic of Venezuela attending).

13. BOLIVARIAN REPUBLIC OF VENEZUELA

13.1. Objectives

Geochemical and mineralogical characterization of the uranium-bearing phosphate rocks of the Navay deposit.

13.2. Key results

The phosphate rocks of the Navay Formation are an important source for manufacturing phosphorus fertilizer. Phosphate rocks of the Navay Formation have relatively high concentrations of uranium and yttrium and the range of total rare earth elements are higher than the average of other phosphate deposits that have been reported in the literature. As a follow up to the studies carried out under the CRP it was recommended that a more detailed study be undertaken to identify the total REE contents of individual sedimentary beds of the Navay Formation, in order to establish if the phosphate deposits could be economically mined for rare earth elements.

GRANITE-RELATED URANIUM DEPOSITS IN ARGENTINA. GEOLOGICAL CONTEXT AND NEW METALLOGENETIC STUDIES*

L. LÓPEZ, J. ÁLVAREZ, F. PARRA, P. ANZIL,
C. BELLO, E. CEBALLOS, M. SALVATORE, L. SCARLATTA,
S. MIYNO, E. FELKAI, P. FERREYRA, A. ZELAYA
National Atomic Energy Commission (CNEA)
Buenos Aires, Argentina

M. CUNEY, J. MERCADIER
Université de Lorraine
Nancy, France

A. HANLY
International Atomic Energy Agency
Vienna, Austria

R. LIRA
CONICET- FCEF y N- Universidad Nacional de Córdoba
Córdoba, Argentina

*Preliminary results and some parts of this paper were presented at the IAEA International Symposium on Uranium Raw Material for the Nuclear Fuel Cycle: Exploration, Mining, Production, Supply and Demand, Economics and Environmental Issues (URAM-2018). Vienna, Austria, 25-29 June 2018.

Abstract

In Argentina, Devonian-Carboniferous magmatism has played a very relevant role in uranium metallogenesis, driving magmatic and late-magmatic preconcentration processes, both within and in the periphery of the granitic massifs. This research has characterized different types and subtypes of uranium deposits linked to that fertile magmatism. These new studies on uranium minerals from uranium sites of interest have improved the metallogenetic knowledge of the granite-related uranium deposits, which in turn could aid the exploration for similar uranium deposits. It was determined that granites play an important role both as a uranium source and hosts of diverse types of uranium mineralization. Additionally, it is thought that, at the existing level of knowledge, there are prospects for the discovery and development of new uranium resources related to granites in Argentina.

1. INTRODUCTION

The National Atomic Energy Commission of Argentina (CNEA), in cooperation with the National University of Córdoba, has carried out the project entitled 'Metallogenesis of Granite-Related Uranium Deposits in Argentina' within the framework of an IAEA coordinated research project (CRP), entitled, 'Geochemical and Mineralogical Characterization of Uranium and Thorium Deposits'. The project, whose main results are summarized in this paper, pursues the aim of improving the general knowledge of the granite-related uranium deposits to a better understanding of their potential to delineate new uranium resources [1].

Late Paleozoic magmatic activity is well developed in the central-western part of Argentina including San Luis, Cordoba, La Rioja, San Juan, Catamarca, Santiago del Estero and Tucuman provinces (Figure 1). This Devonian-Carboniferous magmatism has played a very relevant role in uranium metallogenesis, driving magmatic and late-magmatic preconcentration processes, both within and in the periphery of the granitic massifs. In addition, these granitic rocks are considered good sources of uranium for the formation of more recent sedimentary deposits.

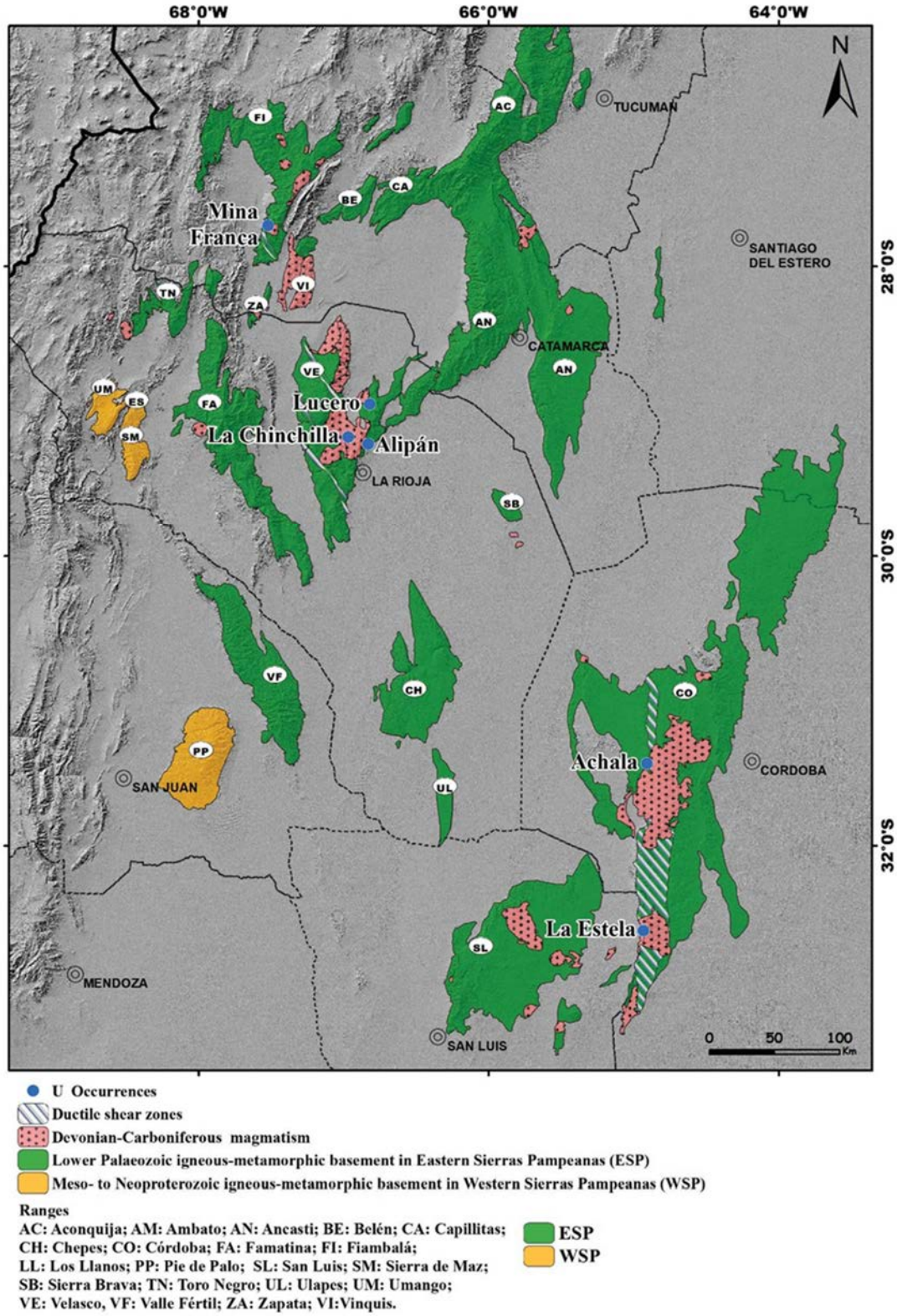

FIGURE 1. Regional geologic map of Devonian–Carboniferous magmatism in Sierras Pampeanas Range, Argentina. Modified from [2].

The voluminous magmatic activity that occurred between ca. ca. 359–322 Ma (Carboniferous magmatism) [3] and 390–365 Ma (Achalian Orogeny) [4] and consists of both batholiths and plutons that were emplaced in metamorphic or granitic complexes, some with differentiated S-type signature, whereas other have A-type characteristics.

This research allowed the characterization of different types and subtypes of uranium deposits linked to fertile magmatism. Several metallogenetic studies have been carried out in order to improve the geological, structural, geochemical and mineralogical knowledge of uranium deposits related to granites. Additionally, efforts have been made to define those felsic igneous rocks that have played the most relevant role as uranium sources and to characterize the relationship between magmatic uranium enrichment and hydrothermal deposits, alteration and uranium mobility.

Intragranitic episyenite-subtype deposits with disseminated uranium mineralisation (pitchblende, pyrite, and hexavalent uranium minerals) hosted in the peraluminous leucogranites of the Achala batholith (368 Ma) are comparable to those from the Middle European Variscian chain. The La Estela deposit corresponds to an endogranitic vein-type model and is located in the Cerro Áspero – Alpa Corral batholith (358 Ma); the mineralisation occurs as fluorite-pitchblende veins (uranophane, autunite, and gummite) hosted in high K calc-alkaline granites. There are also exposures of the perigranitic vein/stockworks subtype located in the metamorphic basement enclosing high potassium calc-alkaline granites. An example of this type of deposit is the Franca deposit, located in the periphery of the Los Ratones granite (335–340 Ma) in the Sierra de Fiambalá (north-western Pampean Ranges). The mineralisation is mainly controlled by N to NE fracture zones to the west and northwest border of the pluton, and dominantly consists of pitchblende and hexavalent uranium minerals. This perigranitic subtype is also represented by the Alipan and Lucero deposits (sooty pitchblende, pyrite, and hexavalent uranium minerals), located in the Velasco Ranges and related to the Huaco (358–330 Ma) and Pinchas granitoids. La Chinchilla leucogranitic pluton corresponds to the intrusive type, plutonic (quartz monzonite) subtype uranium deposits with magmatic oxyuranopyrochlore-columbite-(Fe) accessory assemblage and a supergene carlosbarbosaite and uranophane low-grade disseminated mineralisation.

2. METHODOLOGY

General tasks carried out during the project include both geological field work and specific metallogenetic determinations at specialized laboratory facilities of different institutions.

Eight field trips were carried out at different sites of uranium interest in order to perform geological characterization, sampling and ground gamma-ray radiometric surveys. Geologic-structural mapping, alteration studies, systematic radiometry and complementary gamma-ray spectrometric measurements were carried out in anomalous uranium sectors.

Specific petrographic, mineralogical and chemical determinations can be summed up as follows:

- Petrographic and mineralogical studies of thin polished sections by using polarized light microscopy (transmitted and reflected light) at the CNEA laboratories

- Chalcographic studies and alpha-autoradiographies of uranium perigranitic mineralization hosted in metamorphic rocks, including different types of alteration and uranium minerals at the CNEA laboratories;

- Thin polished sections of selected unaltered minerals were analysed using a CAMECA SX100 electron microprobe (EPMA) at the GeoRessources Laboratory, Lorraine University (Nancy, France). The major elements were measured (U, Pb, Th, Ca, Si, Al, Ti, Fe, Mn, V, Na, Nb, La and Y);
- U-oxide geochemistry of selected mineralisation was determined using Laser Ablation-Inductively Coupled Plasma Mass Spectrometry (LA-ICPMS) at the GeoRessources Laboratory. For each experiment, 14 REE (La, Ce, Pr, Nd, Sm, Eu, Gd, Tb, Dy, Ho, Er, Tm, Yb and Lu), U-238, Pb total and a series of trace elements were analysed;
- Thin sections of gneisses and granites were analysed by Scanning Electron Microscopy (SEM) and electron probe microanalyser (EPMA). SEM was performed using a QUANTA FEG 450 instrument while EPMA was implemented using a JEOL JXA8900R instrument. Both instruments belong to the Denver Microbeam Laboratory, USGS, Denver;
- Mineralogical determination of perigranitic uranium mineralisation by X-Ray Diffraction (XRD) with a Philips PW 1800 instrument of the LAMARX Laboratory, National University of Córdoba was done. These samples were also analysed with a portable XRF Thermo Niton equipment at the CNEA;
- Major and minor geochemical analyses of granite, aplite and pegmatite dykes, phyllite, schist and granitic mylonite samples and determination of beta and gamma radiometric U, total chemical U, major and trace elements of U minerals were carried out at CNEA laboratories;
- Chemical analyses of granites, pegmatites and schist samples by Neutron Activation Analysis (NAA) were accomplished at the Argentine Research Reactor RA-3 (CNEA);
- Petrographic, X-Ray Diffraction, short wave infrared spectrometry (SWIR) reflectance spectrometry, portable infrared mineral analyzer (PIMA) and scanning electron microscopy studies were performed in trench samples to characterize hydrothermal/supergenic alteration belts in the metamorphic host. These studies were carried out in cooperation with the Argentine Geological Mining Survey (SEGEMAR).

Previously completed and new results have been interpreted within a general magmatic-metallogenic context and taking into consideration IAEA World Distribution of Uranium Deposits (UDEPO) criteria [5].

3. GEOLOGICAL SETTING

The Sierras Pampeanas of Argentina are elongated blocks of crystalline basement that were exposed by tilting during Cenozoic Andean tectonics. Caminos [6] was the first to recognize different groups based on lithological differences; an eastern group of sierras dominated by abundant Paleozoic granites and metasedimentary rocks (Eastern Sierras Pampeanas), and a western group characterized by ultrabasic and carbonatic rocks (Western Sierras Pampeanas) (Figure 2).

The Eastern Sierras Pampeanas are mainly made of low-to-high grade metasedimentary rocks of Paleoproterozoic to Early Ordovician age and extensive granites of Paleozoic age, including Cambrian (Pampean), Early Ordovician (Famatinian) and Devonian–Carboniferous (Achalian and Gondwanan) magmatisms. The present study is focused on the last group of igneous rocks.

Devonian to Carboniferous granitoids can be divided into two groups according to their absolute ages and geological characteristics, as follows: Middle to Upper Devonian granitoids (e.g. Achala and Cerro Áspero batholiths) and Lower Carboniferous granitoids (e.g. Huaco, Los Ratones, Pinchas and Chinchilla). These two groups of granitoids belong to different tectono-magmatic events that developed in the Eastern Sierras Pampeanas. The first group correspond to the Achalian event and the second group to an Early Gondwanan event [7, 8]. Intrusive bodies appear aligned along prominent shear zones involving ductile and brittle-ductile deformation developed during the Famatinian orogeny and was reactivated during Devonian and Carboniferous times.

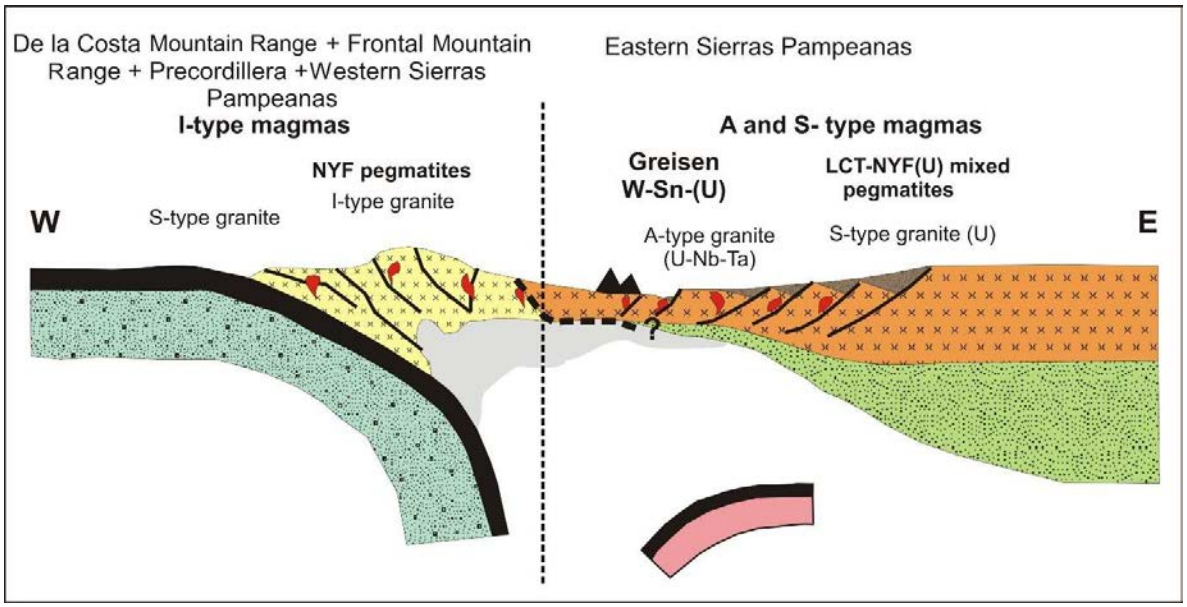

FIGURE 2. Tectonic environment of Carboniferous uranium-rich magmatism and related mineralisation events. Modified from [9].

4. STUDY AREAS

4.1. Achala batholith U District

The 'Hercynian' peraluminous Achala batholith (approx. 2 500 km^2) located in the Sierras de Córdoba is composed of several magmatic suites and numerous facies (Figure 3) [10]. Two-mica monzogranites are the most exposed lithology. Muscovite (± almandine-rich garnet) monzogranite is the most evolved rock that occurs as marginal plutons or facies. The magmatic cycle ends with intragranitic niobium-yttrium-fluorine (NYF) or mixed family pegmatites of the beryl-columbite-phosphate subtype, enriched in Be and U and aplitic-pegmatitic dikes of simple mineralogy [11]. U-Pb dating of zircon for the most important granite type (i.e. coarse grained to porphyritic two-mica monzogranite) yielded an Upper Devonian age. Rb/Sr and K/Ar dating obtained from whole granite rock and pegmatitic muscovites, respectively, have yielded a Carboniferous age [12].

The uranium occurrences of the Achala batholith are located in the western part of the massif (Figure 3). On the one side, the batholith exhibits on its surface numerous hexavalent uranium mineralisations hosted in feldspar episyenites, which are generated by the intensive

dequartzification and sodium metasomatism of the granite. These episyenites are distributed along magmatic shear zones and host both hexavalent uranium minerals and Fe-oxyhydroxide, produced as the result of the oxidation of the pitchblende–pyrite paragenesis [13].

On the other side, in Don Alberto and Sala Grande sites, mineralisation lies in metamorphic rocks [14], where the mineral assemblage has been described as 'cordierite-apatite-uraninite-muscovite-biotite-chlorite-feldspar-quartz' in nodules within pegmatites penetrating gneissic roof pendants [15]. Additionally, at the Los Riojanos site, the fracture that hosts uranium mineralisation lies in muscovite granite.

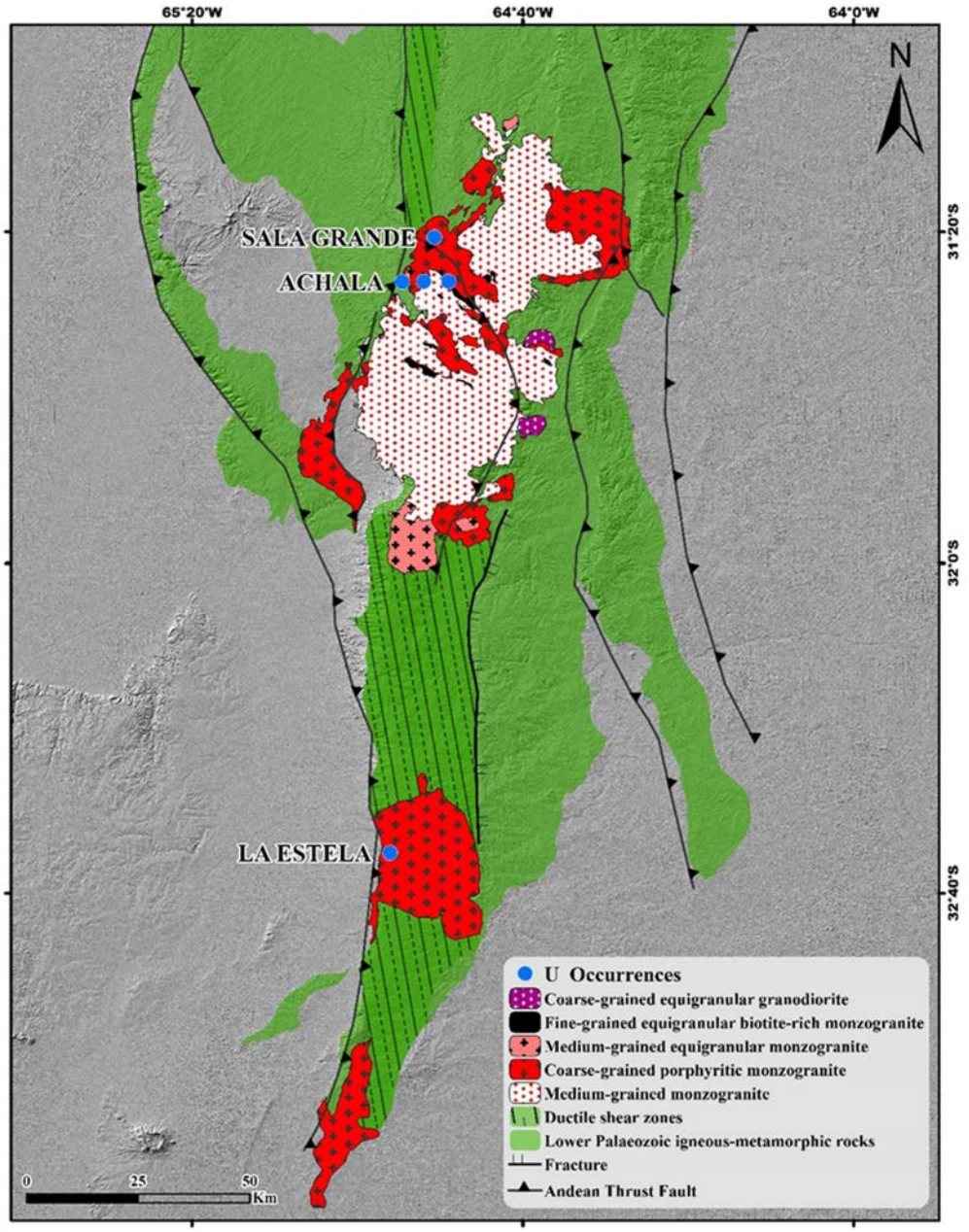

FIGURE 3. Hillshade Aster GDem image with geological map of Achala and Cerro Áspero batholiths and pre-Devonian basement, modified from [16].

4.1.1. Don Alberto U mineralisation

Uranium mineralisation is hosted in biotite gneiss intruded by porphyritic two mica granite and later, in the contact surface, by a cordierite-bearing pegmatite body that corresponds to late-magmatic activity. Cordierite shows two textural varieties: idioblastic and xenoblastic. The latter is poikilitic with biotite, zircon, apatite and euhedral uraninite inclusions (Figures 4a, b). Also, uraninite is included in biotite and muscovite showing concentric radioactive halos and marked radial fractures (Figures 4c, d).

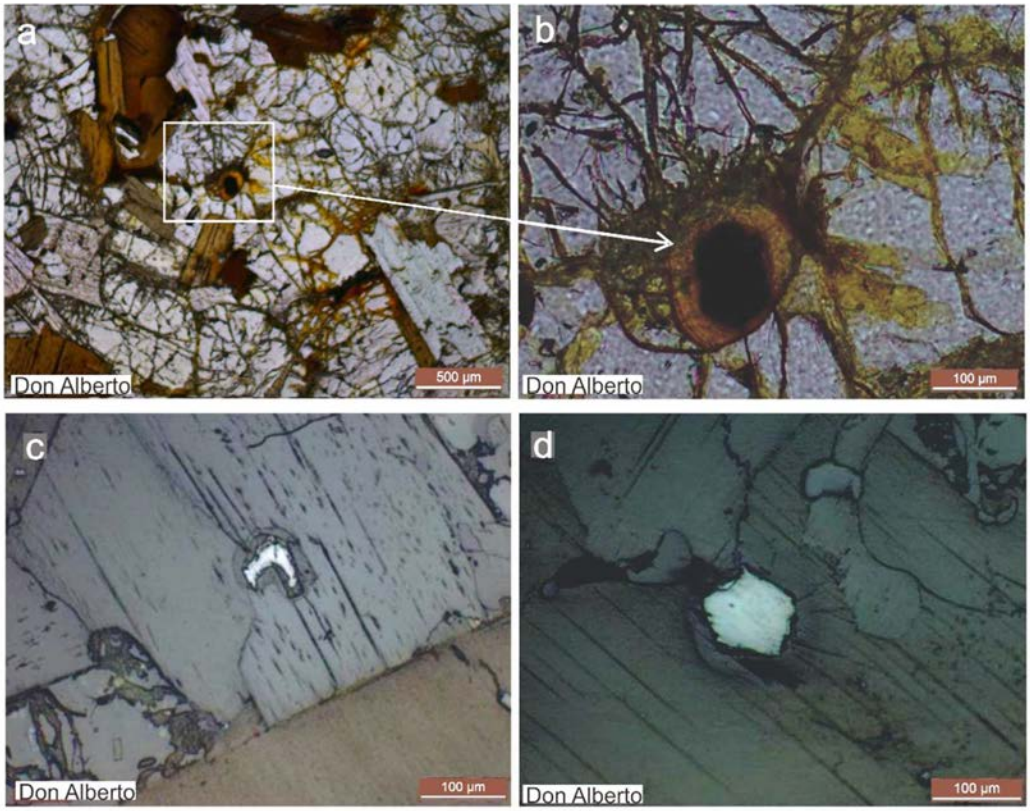

FIGURE 4. Microphotographs of euhedral uraninite: a- Gneiss texture and mineral assemblage (quartz, cordierite, biotite and plagioclase); b- Detail of uraninite with metamict halo, oxidized border and radial fractures in cordierite (transmitted light); c- Euhedral uraninite with metamictic halo and radial fractures in muscovite (reflected light); d- Radial fractures in biotite and muscovite (reflected light).

Uranium oxides from Don Alberto are euhedral uraninite grains and analyses show significant Th content (about 1 wt% ThO_2) which indicates a high temperature origin (Figure 5). They have between 2.7 and 3.8 wt% PbO corresponding to chemical ages between 255 and 325 Ma. Their yttrium content is not significantly enriched (0.07 to 1 wt% Y_2O_3), but the highest value corresponds to an altered U-oxide (characterized by the lowest UO_2: 86.2 wt% and PbO: 0.1 wt% and the highest SiO_2: 7.58 wt% and CaO: 3.18 wt%, compared to the other analyses).

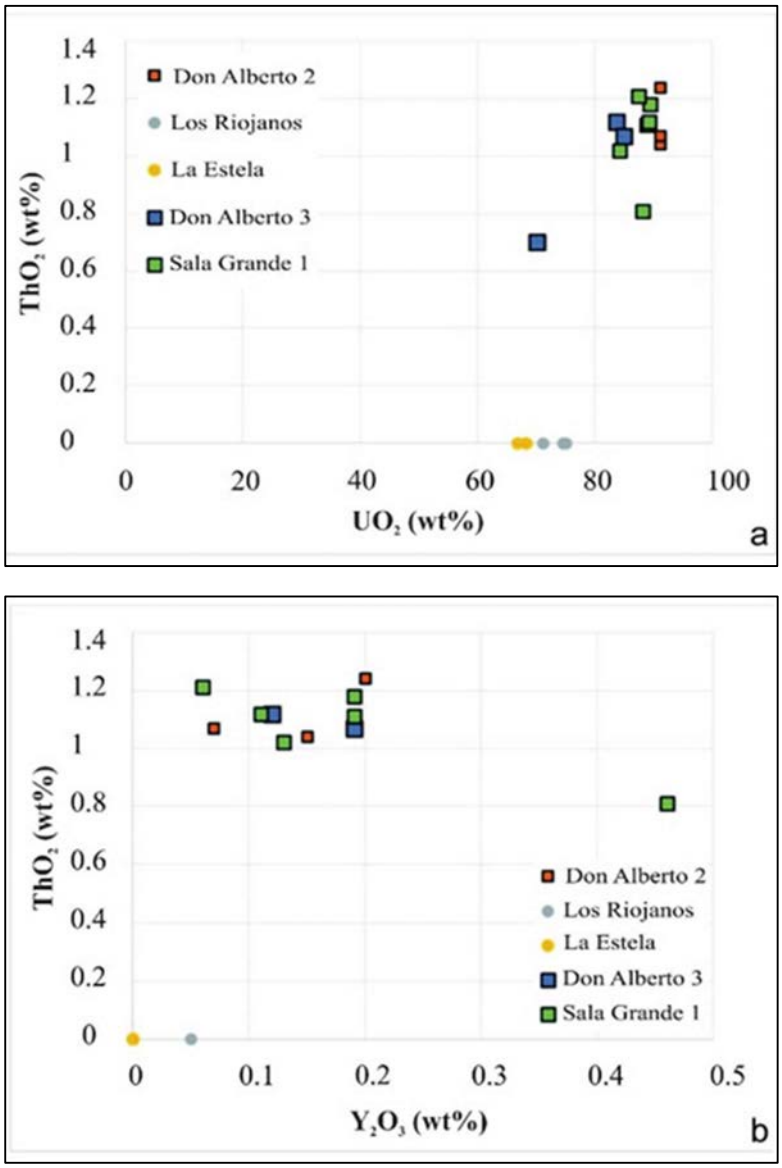

FIGURE 5. a) UO_2 vs ThO_2 and b) Y_2O_3 vs ThO_2 for the U-oxides from different sites.

The global fractionation of the REE patterns and the high REE contents of the U-oxides have been studied in two samples (Don Alberto 2 and 3). Figure 6 shows the results of sample Don Alberto 3, where points DON 3.2 and DON 3.3 are identical and only analysis of point DON 3.1 has slightly lower REE contents. These patterns are similar to those found for magmatic uraninite of the Rössing deposit in Namibia [17], but with lower total REE.

The other trace element patterns of these U-oxides are also similar, with significant enrichment in W, Zr and Mn and more limited enrichments in B, As, W, except two points sampled (DON 2.1 and DON 2.2) which are not enriched in Mo, W and Ti. They are all very poor in Nb.

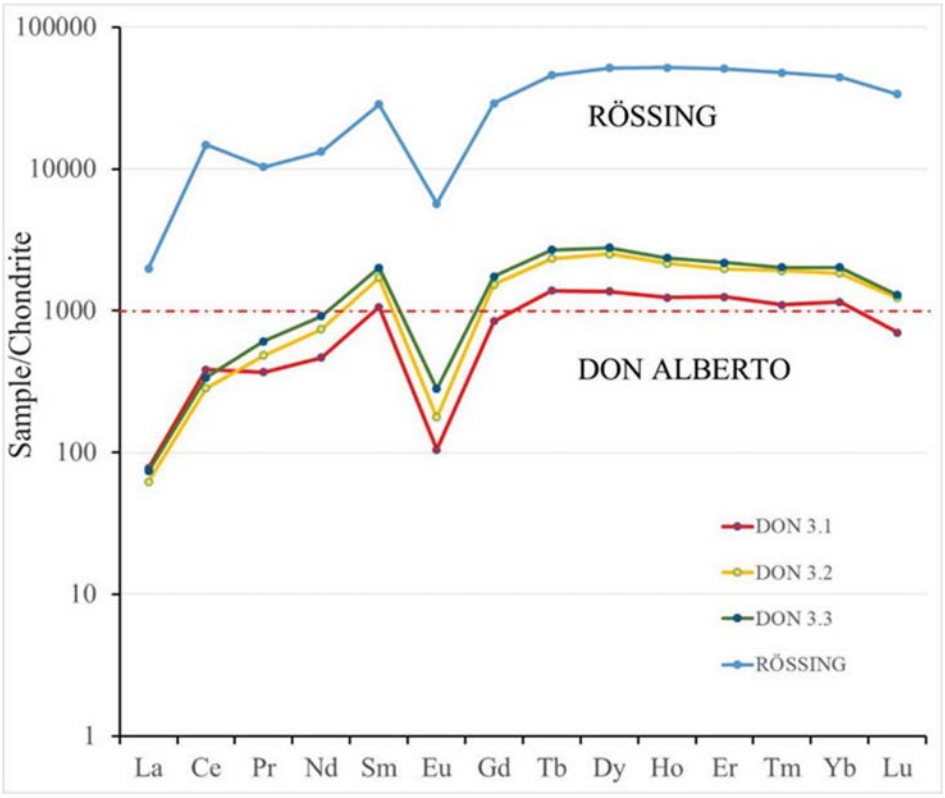

FIGURE 6. Chondrite normalized REE patterns of U-oxides from Don Alberto 3 (DON 3.1, 3.2, 3.3) and Rössing U deposit.

4.1.2. Sala Grande U mineralisation

Uranium mineralisation occurs in the subhorizontal contact between biotite (± sillimanite) gneiss and the granitic surface of the Achala batholith. In this site, the metamorphic host is a roof relict that has been transformed by contact metamorphism to a hornfels at hornblende facies. The granitic facies in Sala Grande is a two-mica porphyry, similar to Don Alberto. The hornfels contains hexagonal-shaped uraninite and zircon inclusions, both with pleochroic halos. Uraninite is partially altered to yellow oxidized uranium mineral (possibly uranophane) (Figures 7 a, b).

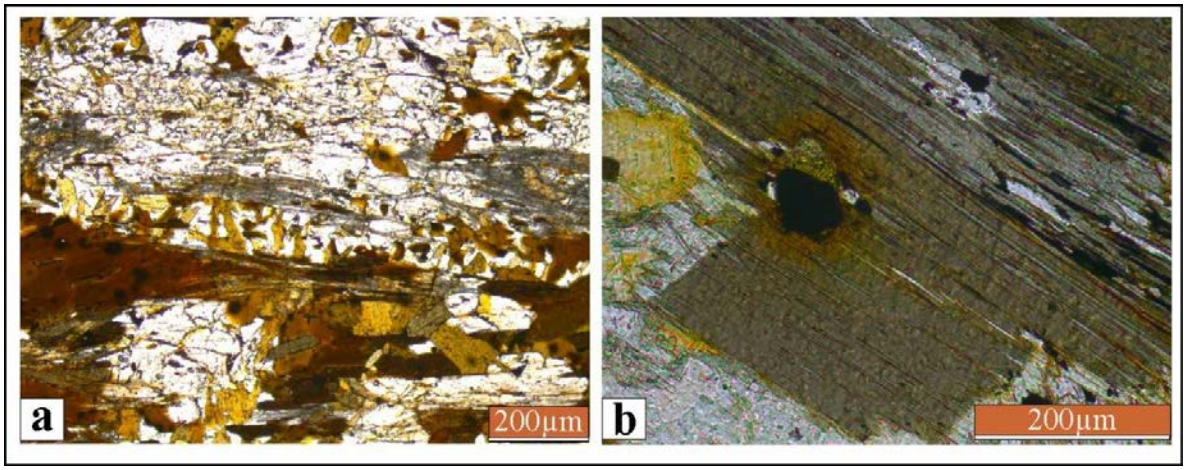

FIGURE 7. Transmitted light photomicrographs: a) spaced foliation microtexture of biotite-cordierite gneiss; b) Partially altered euhedral uraninite included in biotite.

Uranium oxides from Sala Grande 1 has a ThO_2 content of about 1% indicating high temperature uraninite (see Figure 5). REE contents are equivalent to those of Don Alberto occurrences, which indicates a similar environment and formation processes. REE patterns of the sample studied (2 analytical points) from Sala Grande are shown in Figure 8.

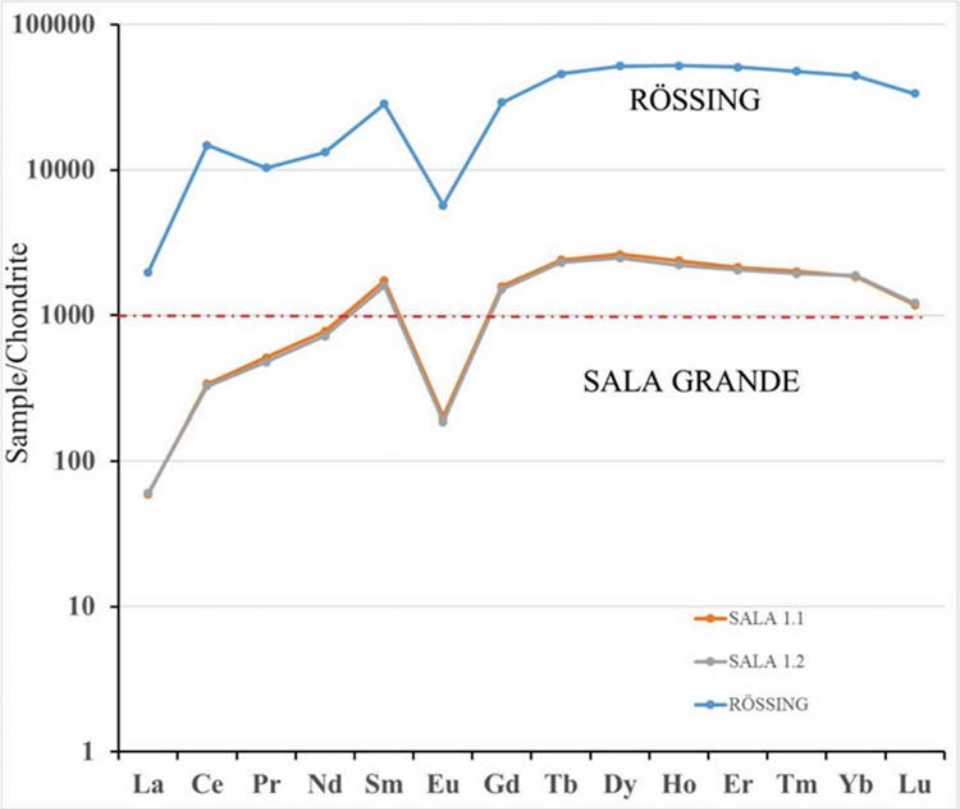

FIGURE 8. Chondrite normalized REE patterns of U-oxides from Sala Grande occurrence in comparison with Rössing U deposit.

4.1.3. Los Riojanos uranium mineralisation

The main uranium mineralisation is hosted in a cataclastic belt affecting the equigranular muscovite granite. These cataclastics are made of recrystallized fine-grained granitic matrix and low temperature hydrothermal quartz. The sample studied is from drill core (44 m depth). The uranium mineralisation occurs within a 0.5 mm thick vein, associated with pyrite and quartz (Figures 9 a, b). This vein shows a mortar texture formed by crushed and recrystallized quartz grains. Both the vein and small cavities are filled with pyrite and sooty pitchblende [18].

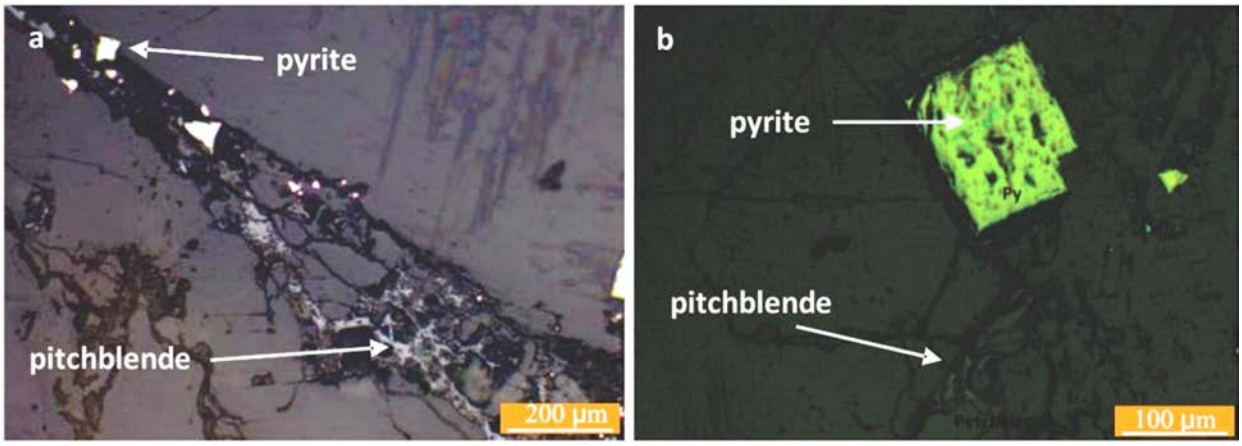

FIGURE 9. Reflected light microphotographs of mineralized fractures: a- Fissure filled with cubic pyrite and sooty pitchblende; b- Detail of cubic pyrite crystal with grey pitchblende filling micro-fractures.

Uranium oxides from Los Riojanos have no detectable thorium content but have significant yttrium (0.47–1.01 wt% Y_2O_3) and calcium (3.49–4.46 wt% CaO) concentrations with low to moderate silica contents (1.7–3.21 wt% SiO_2), indicating a low temperature hydrothermal origin.

4.2. Cerro Áspero U District

The Middle to Late Devonian Cerro Áspero batholith (440 km^2) was formed by the emplacement of Alpa Corral, El Talita, and Los Cerros plutons which are aligned in a NNW direction, intruding the Guacha Corral mylonite shear zone (Lower Paleozoic). This batholith shows a geochemical evolution characterized by a progressive increase in alkalinity and aluminosity [19]. For the Alpa Corral pluton a Rb/Sr isochron established a crystallization age of 369 ± 9 Ma (Early Devonian) [20]. Granites belong to the high K series with initial $^{87}Sr/^{86}Sr$ higher than 0.704, which would suggest a cortical anatexis origin [20].

There are some 15 post-batholitic vein-type fluorite-chalcedony deposits that can also host uranium minerals. These deposits occur as veins uniformly distributed throughout the border zone of the Cerro Áspero batholith, and they are closely related to pervasive silicification and argillitic alteration of the host granite [17]. In La Estela mine, fluorite is spatially associated with pitchblende and other uranium minerals such as uranophane and meta-autunite.

4.2.1. La Estela U deposit

La Estela deposit belongs to the endogranitic model and was emplaced in the Cerro Áspero batholith in the western slope of the Sierra de Comechingones. This deposit was mined from 1953 to 1990 and produced 36 tU at an average grade of 0.07% U. Resources are estimated at 1500 tU.

The U mineralisation is linked to black fetid fluorite veins (antozonite) filling a poly-phase brecciated granite (Figures 10 a, b, c). Primary minerals include pitchblende, fluorite, pyrite and probably chalcopyrite in a silica gangue. These minerals appear in surface and in drill cores at up to 120 meters deep. Secondary uranium minerals are uranophane and to a lesser amount autunite and meta-autunite. Yellow to reddish-brown mixtures of hydrous oxides of uranium ('gummite') are associated with botryoidal pitchblende nodules (Figure 10 d). These minerals are disseminated and covered fractured areas close to the mineral body.

According to SEM studies 10 μm coffinite and pitchblende inclusions in pyrite with antozonite and second stage fluorite assemblage precipitated at 136–122°C (microthermometry of fluid inclusions) [18]. Neutron activation data also show 123 ppm U content in antozonite crystals whereas fluorite from other stages has only 0.5 ppm U. Pitchblende age according to [19] U/Pb method is 23 ± 1 Ma (early Miocene), with other pulses that give ages of 10 and 12 Ma.

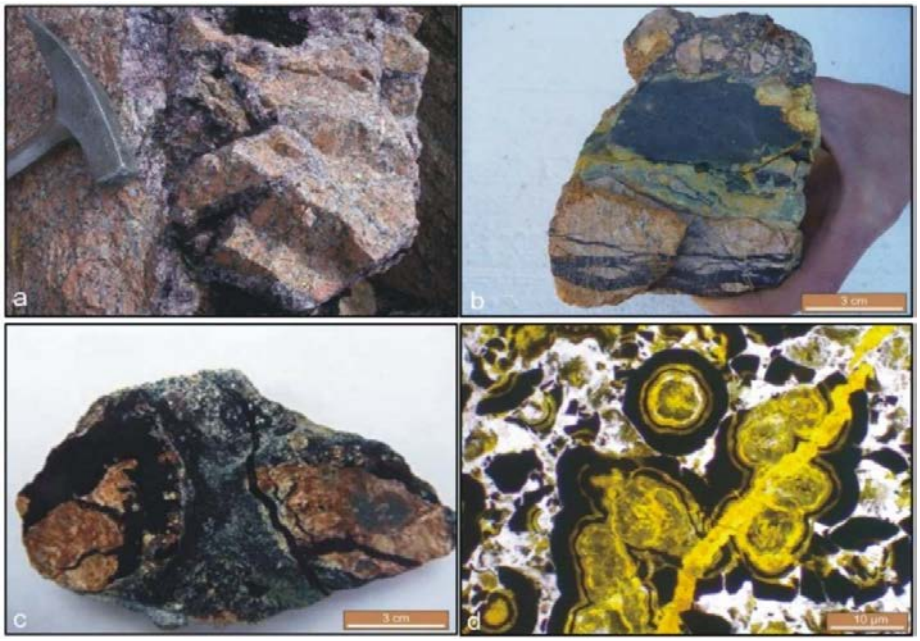

FIGURE 10. a) Outcrop showing granite with mineralized fluorite stockwork; b) Lenticular pitchblende partially altered to yellow oxidized uranium minerals and fractures with antozonite; c) Fluorite-pitchblende-pyrite breccia granite; d) Microphotograph of botryoidal pitchblende surrounded and cut by yellow hexavalent uranium minerals.

Uranium minerals from the La Estela deposit do not have detectable thorium and yttrium contents (see Figure 4) and shows relatively high Si (14.82 and 15.47 wt% SiO_2) and Ca concentrations (6.91 and 6.67 wt% CaO), corresponding to a coffinite type composition [20].

REE patterns of U-oxides are similar to deposits associated with granites, but with an important negative Ce anomaly indicating the involvement of highly oxidized conditions being able to oxidize Ce^{3+} to the weakly mobile Ce^{4+} and a very high abundance in total REE (Figure 11).

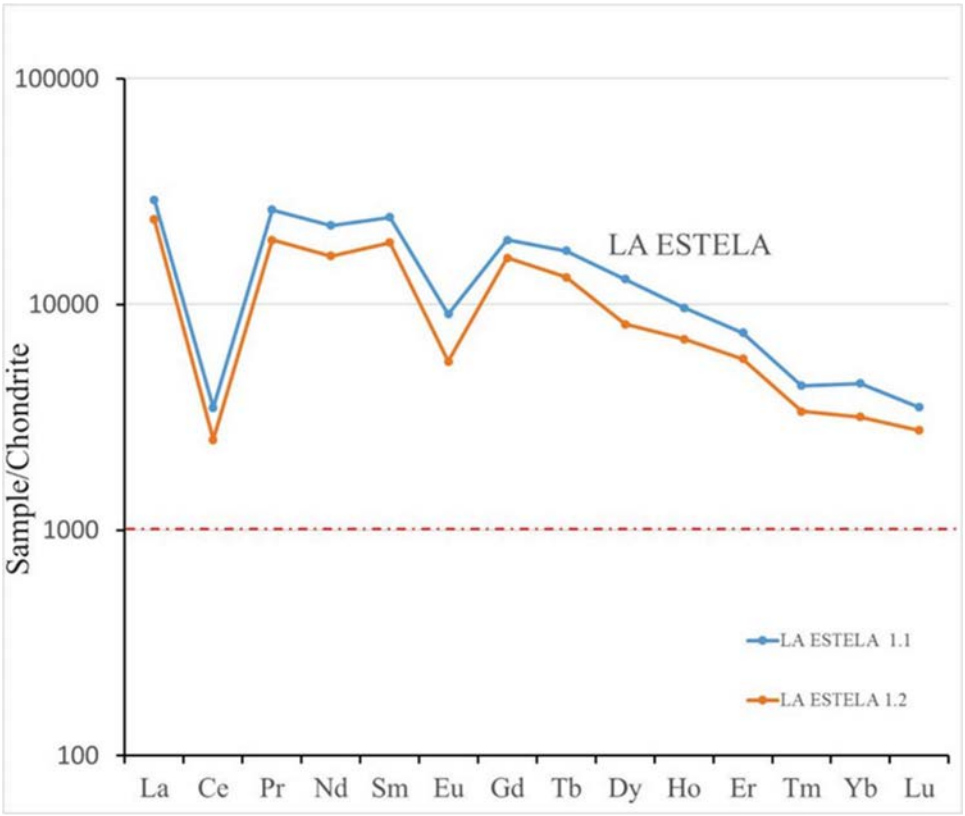

FIGURE 11. Chondrite normalized REE patterns of U-oxides from La Estela deposit.

Their trace element patterns (Figure 12) are characterized by a very high abundance of elements associated with hydrothermal granite related deposits (B, As, Mo, W, Mn) but also less mobile elements such as Ti, Nb and Zr.

Figure 13 shows primary REE and a series of other trace element contents determined by LA-ICPMS of Achala and Cerro Áspero U deposits. The procedure described in [17] has been followed, where after electron microprobe analysis only the unaltered areas of uranium oxides and with a crystal size exceeding the diameter of the ablation spot were analysed.

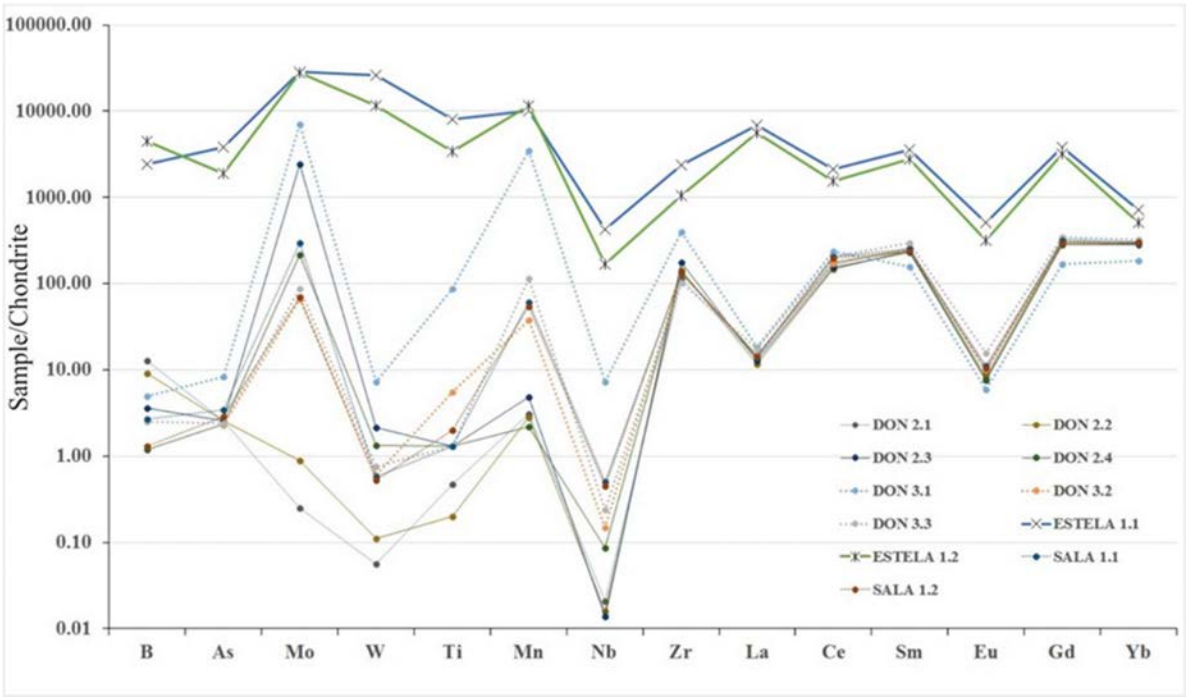

FIGURE 12. Trace element spider plots of the U-oxides from different uranium deposits from Argentina. LA-ICP-MS analyses. DON = Don Alberto 2 and 3, ESTELA = La Estella, SALA = Sala Grande.

4.3. Sierra de Velasco U District

Sierra de Velasco range extends in La Rioja province and constitutes the greatest plutonic outcrop of the Pampean Ranges [21]. Most of the plutons are made of peraluminous granites of Ordovician age generated during the Famatinian orogeny [22]. These Famatinian granites have been locally intruded by several Upper Devonian to Lower Carboniferous plutons, three of which were studied in this research: Huaco granitic complex related to the Alipan deposit; La Chinchilla pluton and Pinchas granite related to the Lucero deposit (Figure 13). Several ages have been reported for the Huaco granite: zircon U-Pb, LA-ICP-MS age of 354 ± 4 Ma [23] and monazite U-Pb, ID-TIMS ages between 350 ± 5 and 358 ± 5 Ma [24].

4.3.1. Alipan U deposit

Alipan uranium deposit is located in the eastern flank of Sierra de Velasco (Figure 14). The host rock belongs to the Ordovician basement of La Cebila metamorphic complex. This basement is in intrusive and tectonic contact with the Carboniferous Huaco granite to the west, and in tectonic or erosive contact with Tertiary piedmont deposits to the east.

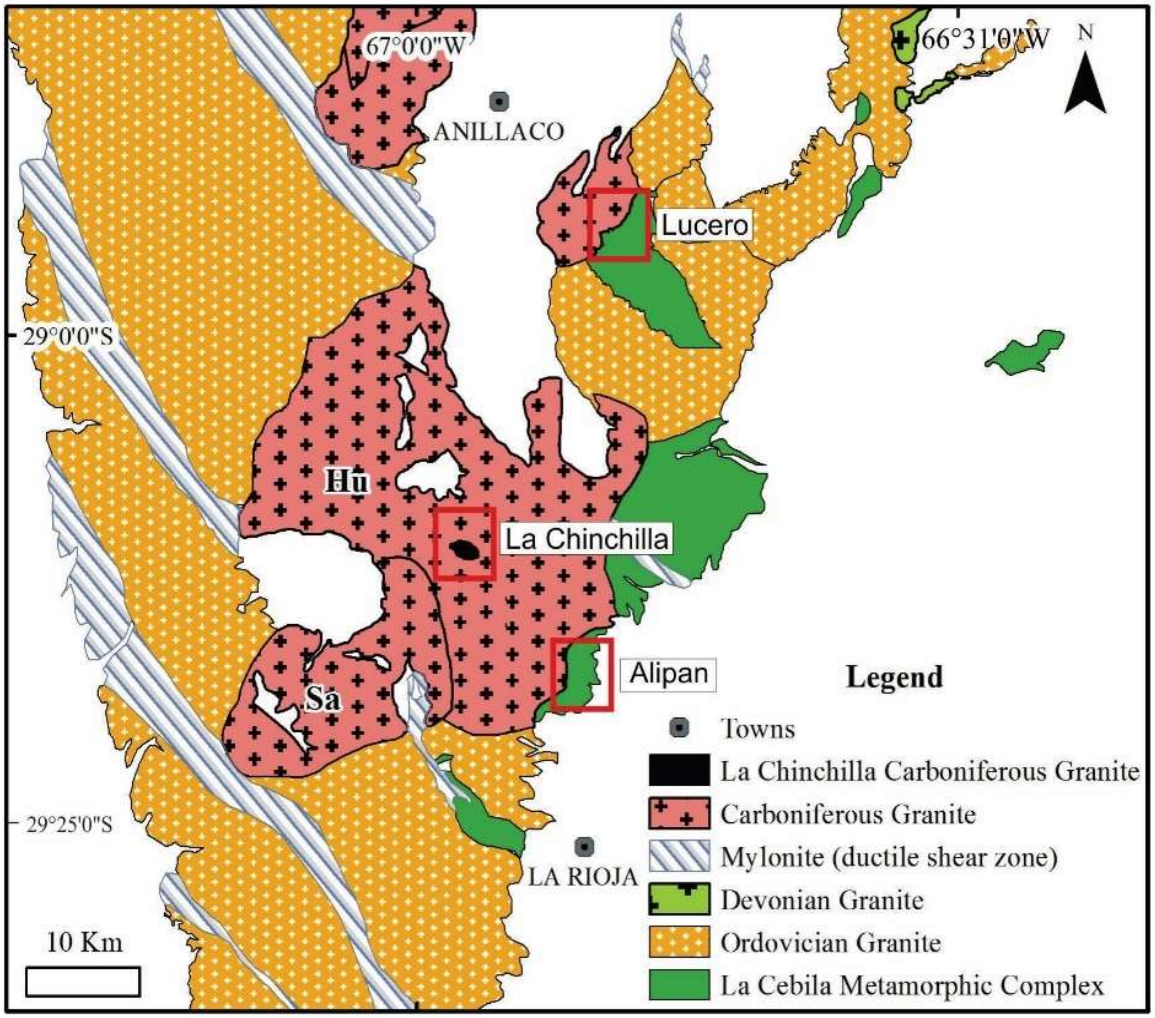

FIGURE 13. Regional geologic map of northern Velasco range with three main uranium sites: Alipan, La Chinchilla and Lucero occurrences.

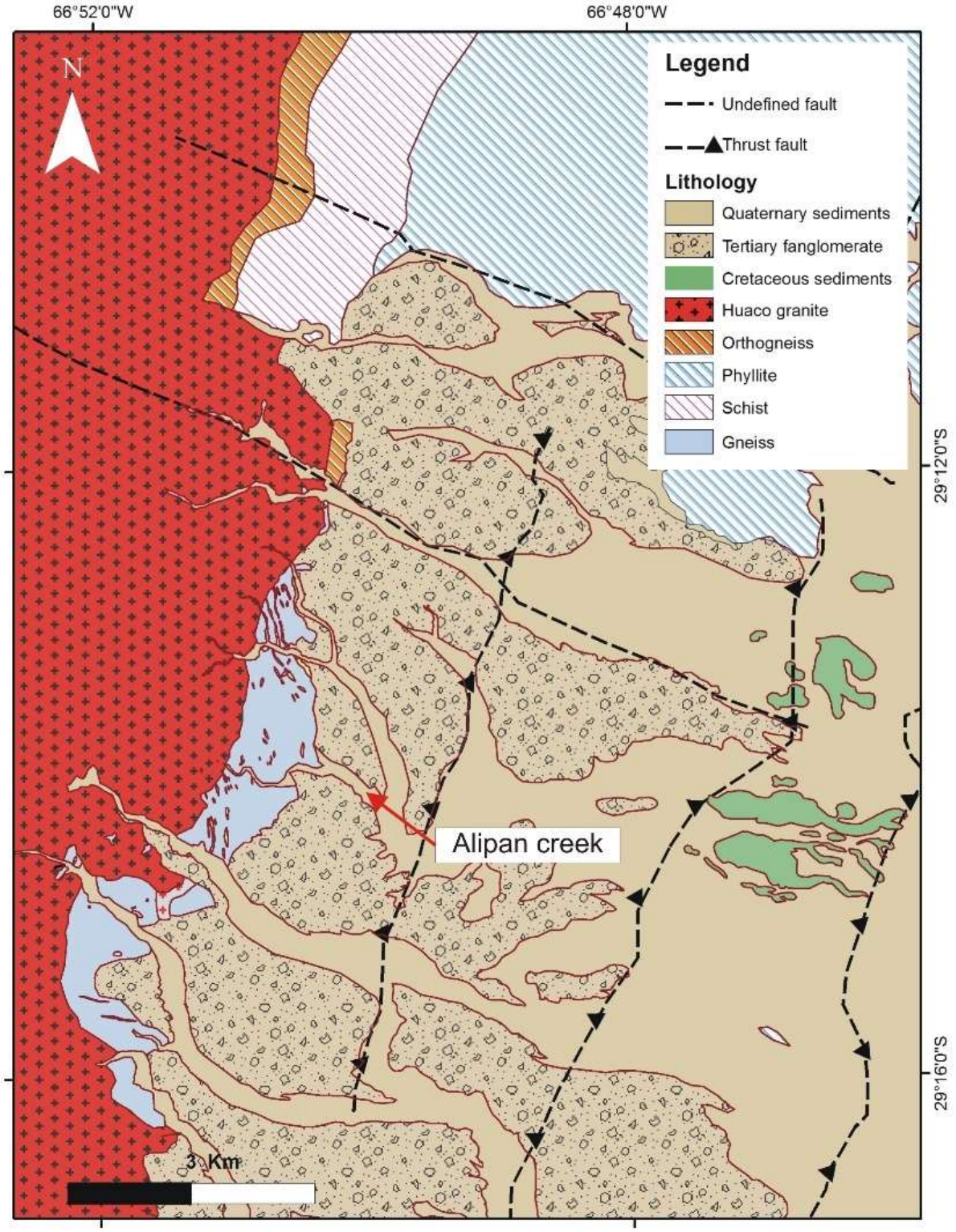

FIGURE 14. Detailed geologic map of Alipan uranium deposit.

A radioactive gamma-ray anomaly at surface is 2.5 km long and 300 m wide within a north-south discontinuous medium to high-grade metamorphic belt. Borehole information clearly defines a vertical, irregular and fault-controlled redox zone. An oxidized halo developed 30 m from surface hosts the main uranium mineralisation. Above approx. 30 m, the reduced zone contains quartz-pyrite and calcite, vertical veins that are crosscut by sooty pyrite and pitchblende in vertical fragile fissures and fractures.

Uranium minerals of the oxidized zone, such as uranophane and meta-autunite, can be observed at a macroscopic scale. They appear coating pores and fractures from 1 mm to 1 cm thick (Figure 15 a). Under the optical microscope, uranophane is present as greenish yellow crystals with micaceous or acicular habit (Figure 15 c). Meta-autunite is green, with platy habit. Samples of drill core from the reduced zone contain tetravalent uranium minerals such as pitchblende and coffinite (Figures 15 b, d) [25, 26]. Both are black minerals under transmitted light, and light grey with low reflectance under reflected light. They have a crustiform texture, filling fractures as monominerals or are associated with calcite and pyrite (Figure 15 e). Textural analysis in fractures has identified different mineralisation events, of which the most frequently observed is successive pulses of pyrite cut by veins with different amounts of silica and uranium.

There are different types of fractures. Breccia texture with euhedral grains of pyrite, plagioclase, calcite, muscovite and quartz inside a matrix are composed of different amount of silica and uranium (Figure 15 f). Furthermore, there is a zonal variation in composition with the edges being richer in pyrite and calcite and the core richer in uranium minerals. In other fractures the uranium minerals fill interstitial space between calcite crystals. These minerals are also disseminated in the rock, isolated or associated to different minerals: mica cleavage, partial or total substitution of cordierite and/or adsorbed in rutile. Pitchblende also occurs with botryoidal texture in corroded pyrite.

Chemical composition of pitchblende (average of n=11) is UO_2 80%, SiO_2 4.6% and CaO 3.9%, with minor amounts of Al_2O_3 (1%) and FeO (0.96%). The average chemical composition of coffinite (n=14) is UO_2 66.3%, SiO_2 13.3%, CaO 3.8%, Al_2O_3 2.54% and FeO 2%. There is evidence of an increase in the concentration of SiO_2 and a decrease in UO_2, which is likely due to the process of coffinitization of pitchblende. Analysis of uranophane (average of n=12) UO_2 64%, SiO_2 13.8%, CaO 4.5% and minor constituents Al_2O_3 (0.4%), K_2O (1.77%) and FeO (0.4%). No appreciable radiogenic lead concentrations were found in any of the minerals.

XRD was performed on the samples with uranium minerals and uranophane was most abundant with other uranium minerals identified including, β-uranophane, meta-autunite, phurcalite and pitchblende [27]. The analysis was also performed on a fracture filled with uranium minerals obtained from a drill core sample with 2 600 cps (measured by a SPP2 type scintillometer) in which it was determined by XRD that the sample contained uraninite and quartz [28].

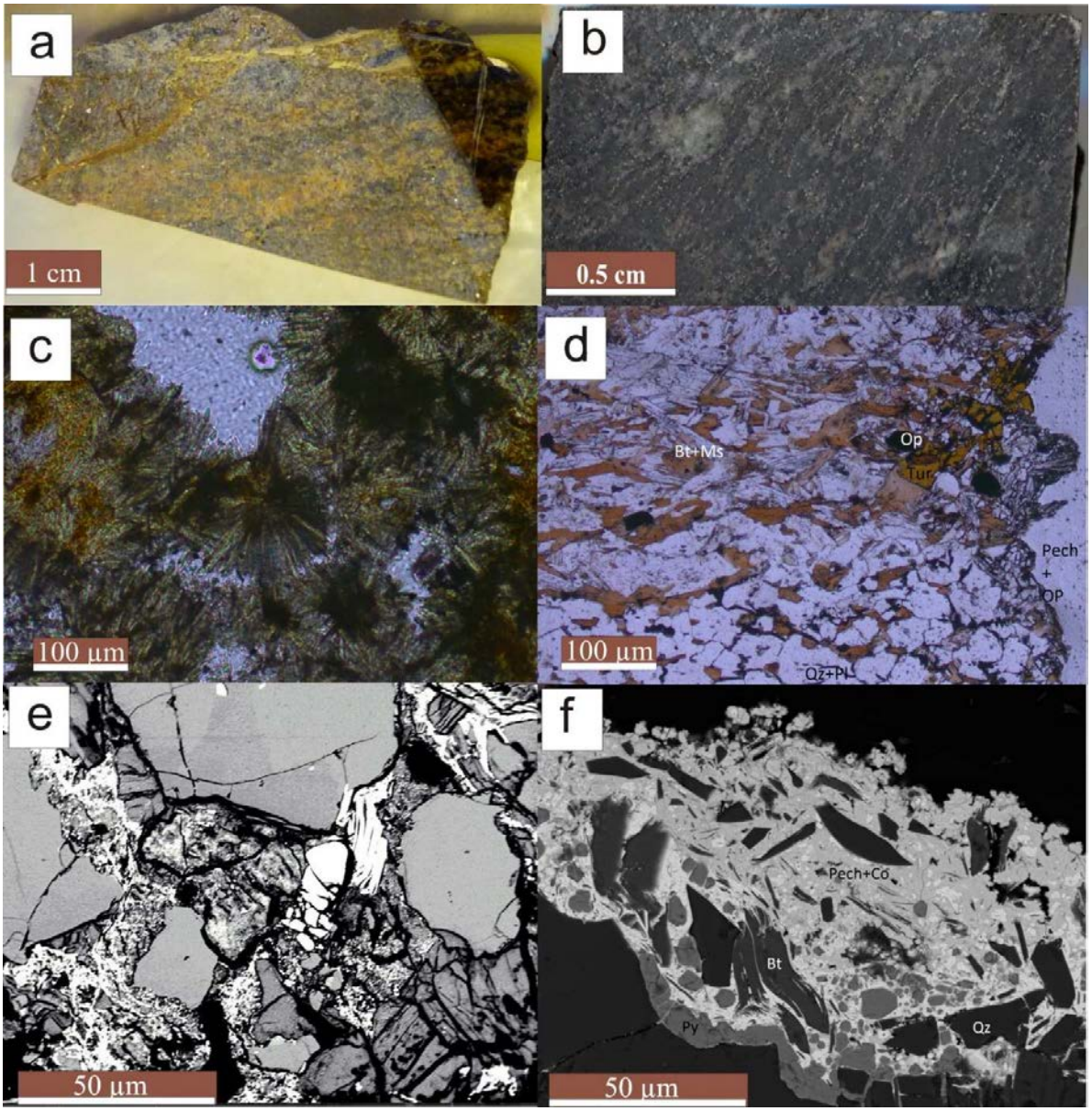

FIGURE 15. a) Photograph of mineralized gneiss with fractures filled with uranophane; b) Photograph of mineralized gneiss with pitchblende and coffinite in a reduced environment (2 cm bar); c) Radial uranophane micrograph; d) Microphotography of gneiss with pitchblende and coffinite as opaque mineral; e) Backscattered electron (BSE) image of uranophane (white) filling spaces between grains); f) Backscattered electron (BSE) image of fracture filled with a matrix of pitchblende (white) and coffinite (grey) and clasts of pyrite, biotite and quartz. Abbreviations: Pech: pitchblende; Co: coffinite; Py: pyrite; Bt: biotite; Ms: muscovite; Qz: quartz.

4.3.2. La Chinchilla U deposit

The Chinchilla pluton, located in the Sierra de Velasco Range, has been the subject of numerous investigations due to its complex and distinctive geochemistry, its varied and valuable accessory mineralogy and its high uranium content (Figure 16).

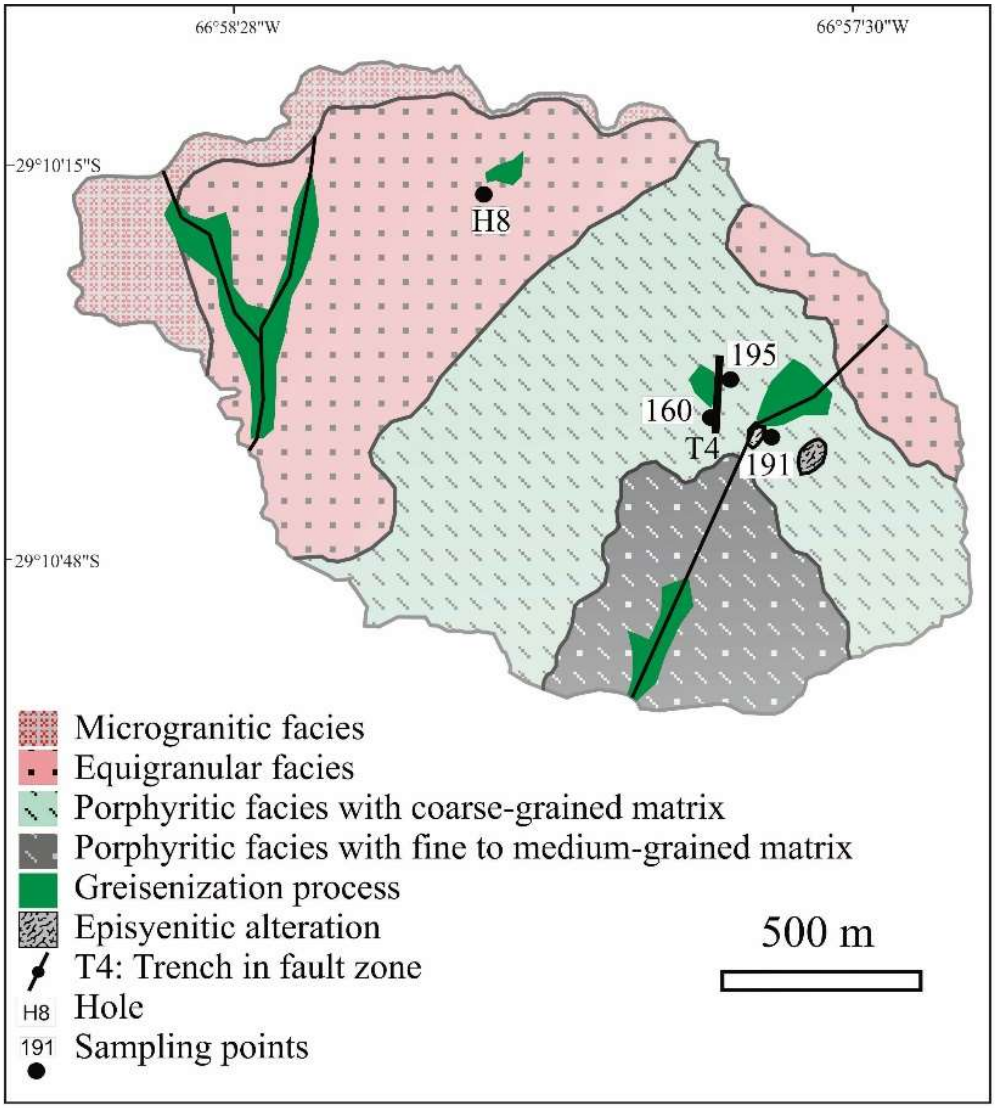

FIGURE 16. Detailed geologic-alteration map of La Chinchilla pluton [30].

La Chinchilla granite is an epizonal, sub-ellipsoidal shape intrusive body of about 3.75 km^2, with its major axis-oriented ESE. A 344.5 ± 1.4 Ma crystallization age was established according to U-Pb dating of monazite [24].

According to its textural and radiometric characteristics, three main granite facies have been distinguished: porphyritic (differentiated into fine and coarse matrix subfacies), equigranular and microgranite [29] (see Figure 16). The dominant equigranular and porphyritic facies corresponds to miarolitic-pegmatite and micromiarolitic granites, respectively [30].

The geochemical characteristics of the La Chinchilla granite are very distinctive. It is weakly peraluminous, rich in SiO_2, alkalis (8.4%) and F (accessory fluorite), with ferrous affinity (high Fe/Mg ratios), relatively poor in Fe_2O_3, MgO, CaO, Sr and Ba and very impoverished in P; shows enrichment in HFSE, mainly Y, Nb, Ta, Th, U, HREE and Li, Rb and Be [24]. With respect to

trace element values, although U and Th are found in high proportions in the three facies, the equigranular facies has the highest uranium and thorium contents (average: 119 ppm U and 32 ppm Th). Average Th/U ratio for equigranular facies is 0.38, 1.6 for porphyritic facies and 0.29 for microgranitic facies.

Accessory minerals of the porphyritic facies have been previously studied in detail [30]. For the current study identification of accessory minerals was carried out using BSE images and analysed by EDS and WDS. Oxyuranopyrochlore which occurs as inclusions in late smoky quartz and muscovite were investigated. EDS identified columbite-(Fe) which is commonly associated with oxyuranopyrochlore. Ilmenite has appreciable amounts of Nb that indicates a differentiated character of the intrusive. In addition to the previously mentioned minerals, xenotime and uranophane (rich in Nb, Ti and Th) inclusions in zircon have been described in drill cores.

Regarding the mineralogy of miarolitic pegmatites of equigranular facies, amazonite, beryl, oxy-calcio pyrochlore and cassiterite are identified, which reflects the NYF nature of the melt [31].

In addition, the supergene mineral carlosbarbosaite [$(UO_2)_2Nb_2O_6$ $(OH)_2$*$2H_2O$] has been identified in altered areas of granite [32] and also as secondary accessory phases disseminated in the unaltered micromiarolitic porphyritic granite. It occurs in intergranular contacts, fractures and/or cavities in aggregates of fine fibres. Microscopically it appears pale yellow to cream in colour, is slightly pleochroic from yellow to yellow greenish and EDS analysis exhibits compositions similar to those reported by Atencio et al. [33].

It is interpreted that fluids of meteoric origin affected the granite transforming the primary association oxyuranopyrochlore and columbite-(Fe) into carlosbarbosaite; no further evidence is available to establish a precise and balanced alteration reaction.

According to the level of current geological knowledge, the preliminary estimation of resources made in the equigranular facies indicates speculative resources of 990 tU @ 0.0159% U [34].

4.3.3. Lucero U deposit

Lucero uranium deposit is located in the northeast sector of the Sierra de Velasco range (Figure 17). The present metamorphic sequences of low to medium grade belongs to La Cébila metamorphic complex. These constitute an elongated NNE-SSW belt limited to both the ESE and WNW by syntectonic to post-tectonic granitoids. The main syntectonic unit is the Huaco granite where crystallization ages range from 481 ± 2.8 Ma dates for zircon by the SHRIMP U-Pb method [22] and 476.4 ± 1.5 to 461 ± 2.2 Ma dates from monazites by conventional U-Pb method [35]. Towards the NW of Lucero site, these units are intruded by the post-tectonic Pinchas granite, through a net and semi-circular contact. This granite is a pink to yellowish grey porphyritic to equigranular granite. Pinchas does not exhibit evidence of deformation and is assigned to the Lower Carboniferous magmatic event as well as the Huaco and the Chinchilla granites.

The Pinchas granite crops out in La Punta range and has two main facies: a pink porphyritic granite, with K-feldspar mega crystals and a light grey leucocratic equigranular granite. In addition, there is a set of aplitic and late banded pegmatitic dikes with synmagmatic contacts with the granite facies. Pegmatites emplaced in metamorphic rocks have banded texture and a varied mineralogy.

The sub circular-shaped pegmatites found in Pinchas are generally zoned, with a quartz core and quartz-albite-muscovite dominated wall zone. Well crystallized tourmaline and beryl are common in the wall zone with phengitic muscovite and Nb-Ta oxides with important U content. Geochemically, it is a peraluminous granite with an aluminium saturation index between 1.22 and 1.31 [36] and the sum of Na_2O and K_2O reaches normal to high values (7.2 to 8.0%).

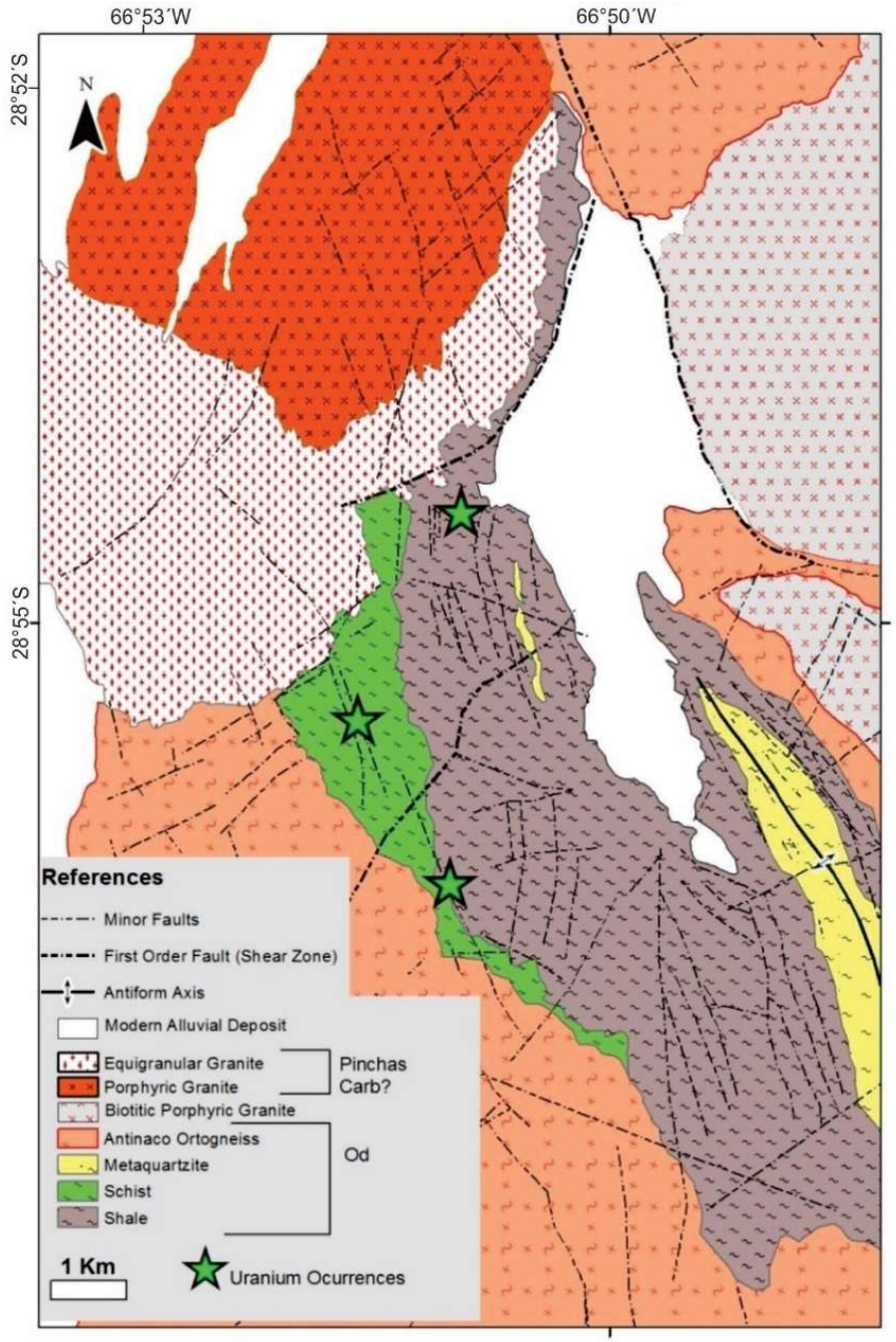

FIGURE 17. Geologic map of Pinchas granitic facies and La Cébila metamorphic complex.

There are uranium occurrences both in aplitic/pegmatitic facies of Pinchas granite and in the metamorphic rocks intruded by this granite. Pinchas granite shows albitization, which affected both the magmatic microcline and plagioclase, and the formation of secondary muscovite replacing biotite and feldspars. Phyllite and mylonitic schists of the La Cébila metamorphic complex host the most important uranium mineralisation within fractures or foliation planes. This schist displays an intense fracturing, hematite alteration and has been intruded by granite and pegmatitic dikes assigned to the Pinchas granite.

Mineralisation is composed of Na-uranospinite which has greenish-yellow, pale green and lemon-yellow colours, micaceous habit and strong green fluorescence (Figure 18 a). Phurcalite and uranophane are also present in fissures as powdery yellow-orange crusts or forming small fibrous aggregates of vitreous lustre on iron oxides (Figure 18 b).

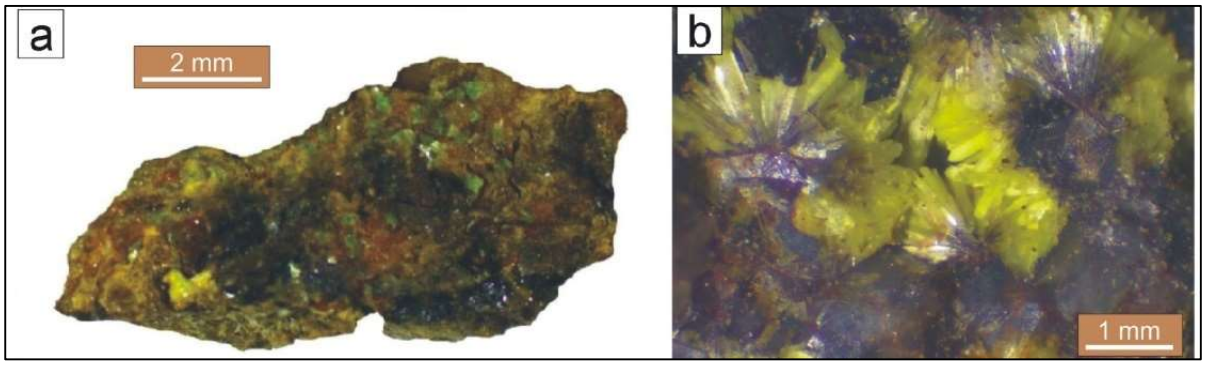

FIGURE 18. a) Sodium-uranospinite in phyllite; b) Phurcalite in quartz vein in phyllite.

Uraninite was observed as inclusion of zircon crystal in an isolated way. Both in aplites/pegmatites and porphyritic granite facies a Nb-Ta-U oxide (Figures 19 a, b) was identified which could preliminarily be classified as carlosbarbosaite [36] and/or other undefined species.

In metamorphic rocks the uranium mineralisation impregnates veins or is infilling cavities. When it is associated with tourmaline the uranium mineral is vyacheslavite $U^{4+}(PO_4)$ $(OH)•2.5H_2O$ and is the first time that it has been identified in Argentina (Figures 19 c, d) [37].

Autunite, meta-autunite, uranophane, natrouranospinite and phurcalite appear near the contact with Pinchas Granite [36]. They are associated with quartz, fluorite veins and iron oxy-hydroxides in fragile and fragile-ductile structures.

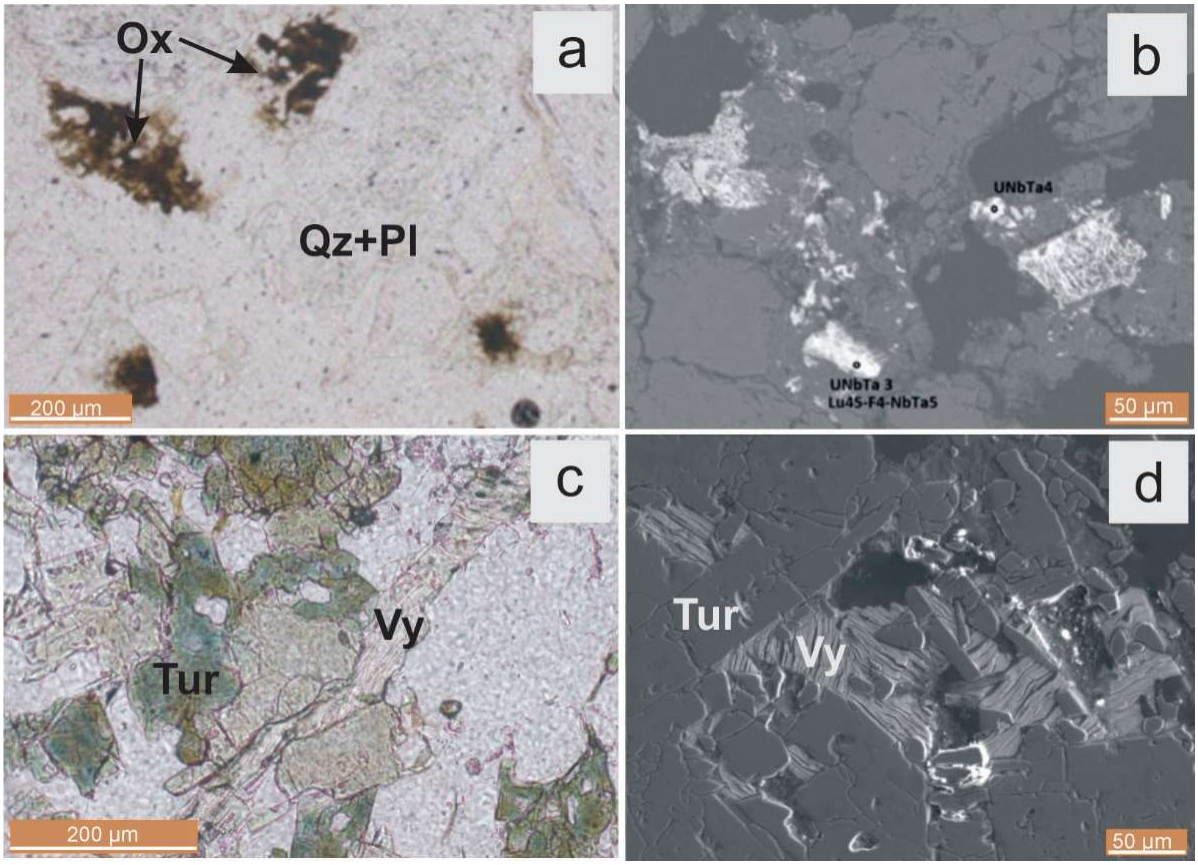

FIGURE 19. Microphotographs of: a- Nb-Ta-U ± Si oxide; b- BSE image from these oxides; c- Vyacheslavite vein in tourmalinite lenses; d- SEM relief image of Vyacheslavite. References: Ox: oxide; Qz: quartz; Pl: plagioclase; Tur: tourmaline; Vy: Vyacheslavite.

4.4. Fiambala U District

The Sierra de Fiambala is composed of a variable composition and grade of metamorphic rocks (phyllite, schist, gneiss, marble, amphibolite, meta-gabbro and migmatite). There are two large groups of intrusive rocks according to their field setting and age. One group of plutons of Neoproterozoic to Lower Palaeozoic age (545–480 Ma) [38] are deformed bodies that are generally concordant with the foliation of the metamorphites. The second group of intrusives are of Neopalaeozoic age (close to 330 Ma) [38, 39, 40]. They are discordant with the internal structure of the host rock and are located in more superficial levels than the previous group. These intrusives have been linked to different mineralisations of Sn-W-U.

4.4.1. Franca U deposit

The Franca mine area is composed of pelitic and quartz-feldsphathic metasediments of Upper Precambrian to Lower Palaeozoic age. These have been intruded by the Los Ratones pluton of Carboniferous age (325 Ma in monazite) [41]. Los Ratones is a peraluminous/metaluminous granite and outcrops in the central sector of the Sierra de Fiambalá [42]. It contains two dominant facies with sharp contacts; one is porphyritic and the other is equigranular facies. Petrological characteristics of granites evolved from the high-K granite series are rich in fluorine.

There are five altered-mineralized belts in N-S direction. The largest of them is 1500 meters long and 300 meters wide. Studies of alteration carried out using a portable infrared mineral analyser (PIMA) confirm the presence of sericite, illite-smectite, montmorillonite, kaolinite, quartz, calcite and associated chlorite [43]. The altered belt has topaz, muscovite, fluorite and cassiterite indicating the presence of a greisen system that is well recognized in the sector [42, 44] (Figures 20 a–f). This greisen system affects both the metamorphic rocks and Los Ratones granite which exhibits albitization and microclinization [42].

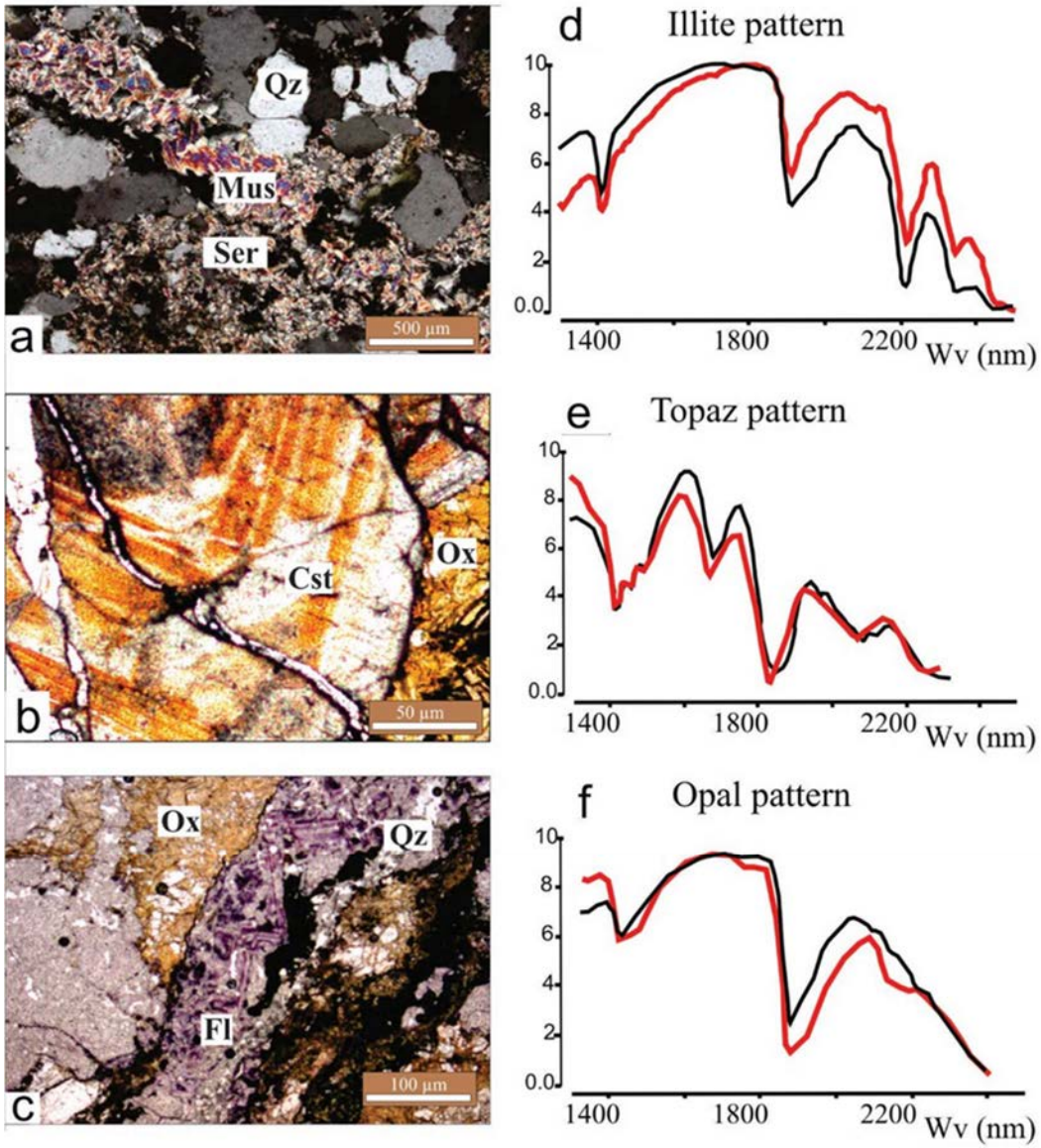

FIGURE 20. Photomicrographs : a) Argillic-sericitic alteration (Qz=quartz; Mus=muscovite; Ser=sericite); b) cassiterite (Cst) crystal, oxides (Ox); c-Fluorite (Fl) vein and associated silica (Qz) and oxides (Ox); d, e and f) infrared spectra obtained by PIMA corresponding to samples shown in adjacent photomicrographs [43].

The primary mineralisation is composed of pyrite and pitchblende associated with chalcopyrite, pyrrhotite, galena, sphalerite, electrum and subordinated cassiterite and wolframite. Based on textural and field relationships the following paragenetic sequence was established: cassiterite–wolframite; pitchblende–pyrite; chalcopyrite–pyrrhotite–melnikovite–galena–sphalerite–electrum. Sn-W mineralisation was intimately associated with the greisenization process, and mineralisation of uranium and pyrite is spatially linked to fluorite [44, 45]. The pitchblende appears in reniform masses, as spherulites of 1–4 mm in diameter, surrounded by euhedral crystals of blackish to bluish-violet fluorite. This association was replaced by a supergene paragenesis with torbernite, autunite, meta-autunite, meta-torbernite, saleeite, kasolite, coffinite, uranophane, phurcalite and parsonsite [46].

EDS and EPMA analyses were performed on oxidized samples with abundant presence of secondary uranium minerals [47]. The predominant uranium mineral is uranophane and the second most dominant one is kasolite, where the aluminium content seems to be higher (Figure 21).

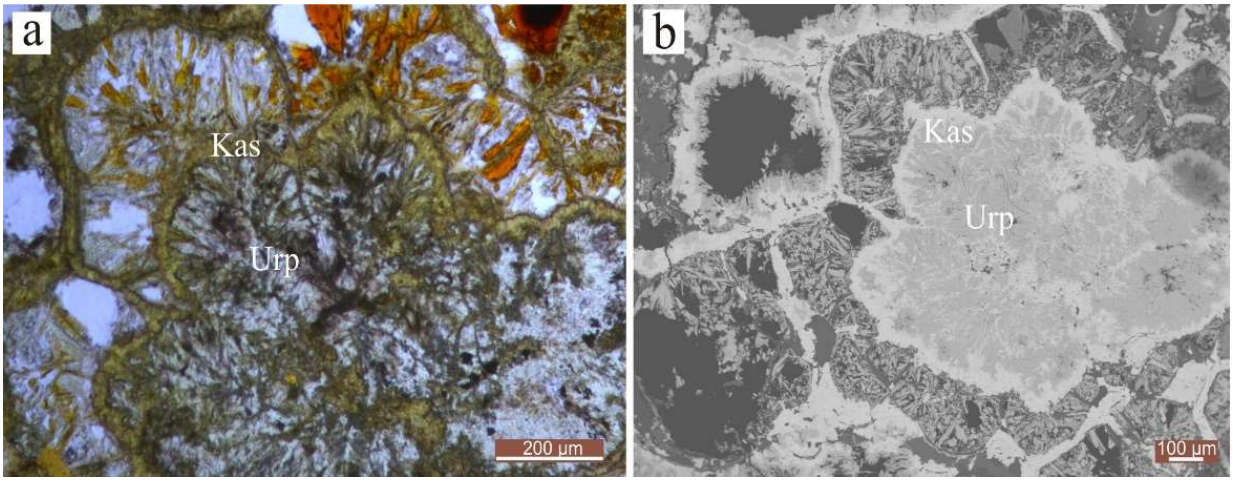

FIGURE 21. a) Photomicrography of kasolite (Kas) and uranophane (Urp); b) Backscattered electron image from the same association.

The only mineralisation age of 114–113 Ma was obtained by Morello [48]. This age was achieved by two different methods. One was by the measuring the A0 parameter of the pitchblende cell by XRD. The other age was acquired by the Pb^{207}/U^{235} isotopic method which provided two ages, one of 113.6 Ma and another of 51.4 Ma.

5. MAGMATISM CHARACTERIZATION AND ASSOCIATED MINERALISATION

Data and interpretations obtained during this study in conjunction with information published by other authors, have allowed the characterization of the different magmatic uranium sources.

In an A-B chemical mineralogical diagram [49] (Figure 22), it was observed that in general all samples correspond to highly differentiated magmatism. Most of the samples (except for a set of samples corresponding to La Chinchilla) plot in the peraluminous domain. Within this domain a

high percentage of samples plot in the leucogranitic field, more specifically in field I, with predominance of muscovite over biotite. Other samples corresponding to the Cerro Áspero, Achala, Huaco and to a lesser extent Los Ratones plot in the field II with biotite > muscovite and III with biotite.

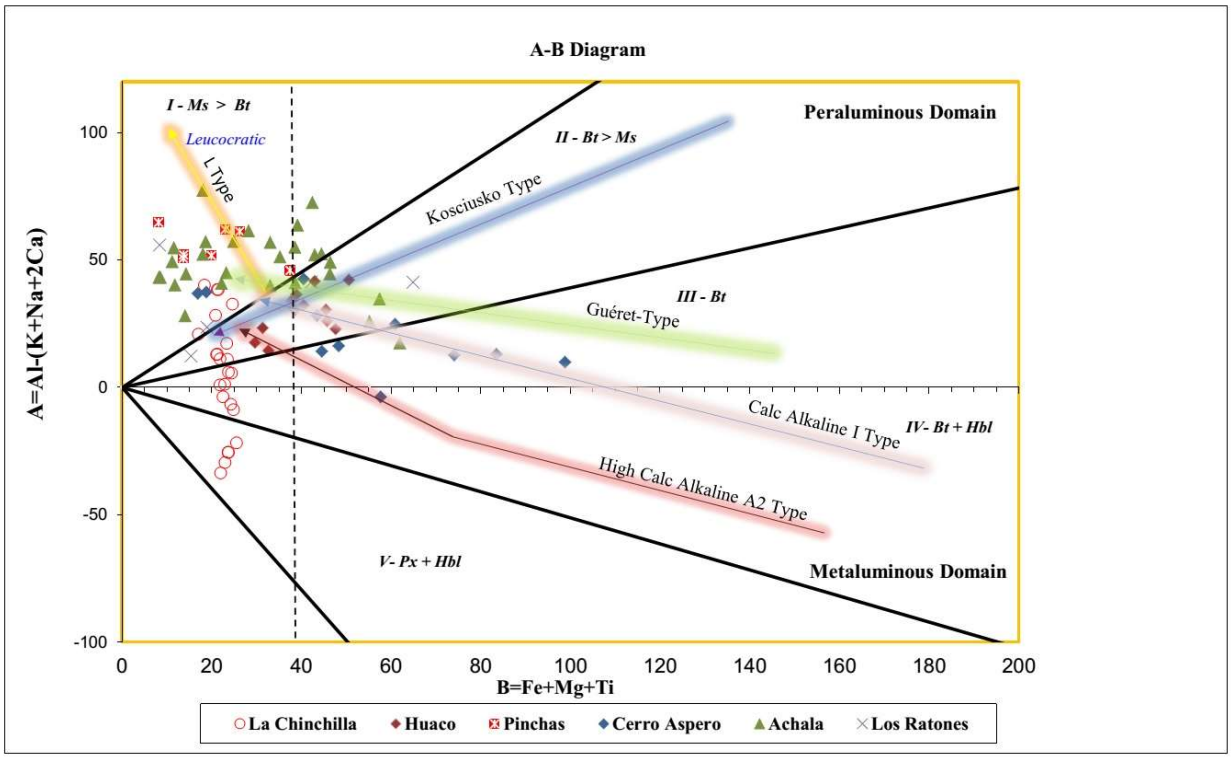

FIGURE 22. Peraluminous index (A = Al – [Na+K+2Ca]) versus differentiation index (B = Fe+Mg+Ti) diagram of [49]. Modified from [50].

Devonian magmatism is clearly differentiated in the diagram discriminating igneous rocks (Figure 22), where the samples corresponding to Achala, plot mainly in the peraluminous field (ASI> 1), while those of Cerro Áspero plot in the metaluminous field (ASI <1) with a slight tendency to peraluminosity. This indicates that for the middle to upper Devonian period there are two distinctive uranium fertile magmatic events; high-K calc-alkaline metaluminous to peraluminous represented by Cerro Áspero batholith and another peraluminous one represented by two-mica A- and S-type Achala batholith.

Lower Carboniferous magmatism varies from the metaluminous to slightly peraluminous fields for La Chinchilla and Huaco granites; whereas Los Ratones granite is located in the slightly peraluminous field. The Pinchas granite is clearly peraluminous and represents together with the Achala batholith, highly polymerized magmas (ASI > 1.1) (see Figure 23).

During this period the dominant magmatism was metaluminous to slightly peraluminous, of high-K calc-alkaline series, represented mainly by A-type plutons such as La Chinchilla, Huaco and Los Ratones. Only Pinchas represents clearly peraluminous two-mica granitoids.

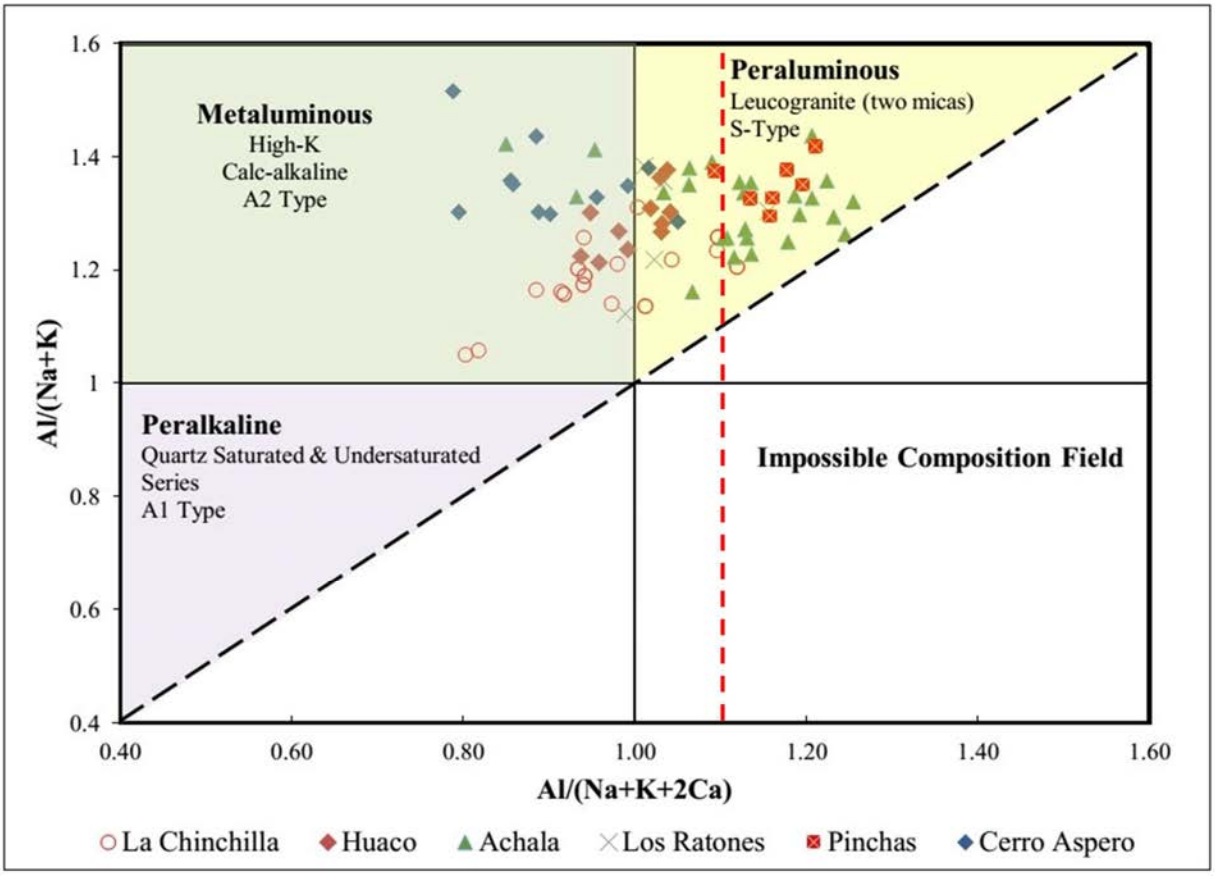

FIGURE 23. Diagram discriminating peraluminous, metaluminous and peralkaline igneous rocks. Only the uranium-rich igneous rocks have been indicated with their corresponding designation in the alphabetic classification. Red dashed line represents ASI=1.1. Modified from [51].

Figure 24 shows Th/U ratios for all the granitoids studied. Those with lower Th/U ratios are Pinchas and La Chinchilla, but uraninite is not observed as a common accessory mineral. Only in Pinchas granite has uraninite been found as scarce small inclusions in zircon [36].

In both granites, accessory minerals such as columbite-(Fe), tantite and oxyuranopyrochlore are common. Alteration under low temperature oxidizing conditions formed disseminated carlosbarbosaite [30], common in both granites.

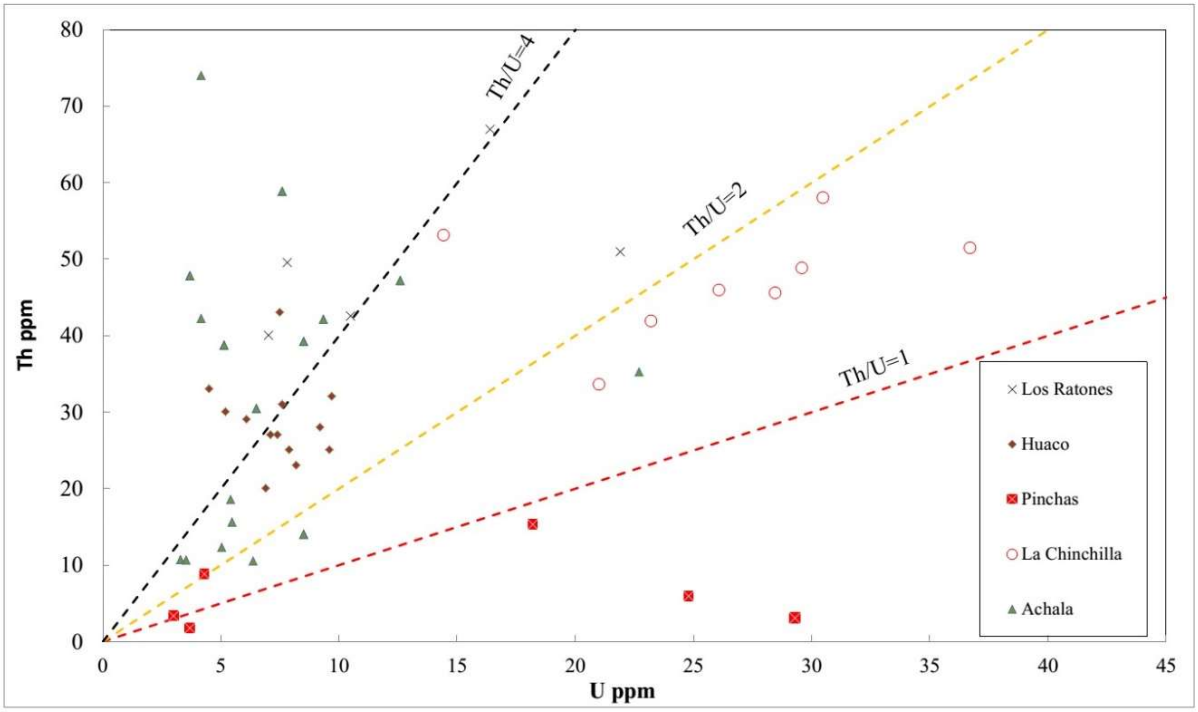

FIGURE 24. Th/U ratios from different Devonian – Carboniferous granites.

The Pinchas granite and some samples from La Chinchilla and Achala have Nb/Ta ≤ 5 and Zr/Hf >18 ratios indicating fertility and good mineralizing potential with evidence of magmatic-hydrothermal interaction processes such as secondary muscovitization and greisenization [52] (Figure 25).

Most of the samples belonging to the Pinchas granite fall in the domain of granites related to Sn-W (U) mineralisation as well as some samples of La Chinchilla and Achala granite. This is corroborated with what was observed with EDS and WDS in La Chinchilla and Pinchas, with the presence of cassiterite as an accessory phase in pegmatitic miaroles [31] and wolframite-quartz veins and accessory cassiterite included in quartz and muscovite of the equigranular facies and aplites of the Pinchas granite [53]. Some samples of Pinchas also plot in the rare metals related granite mineralisation field.

There is a set of samples from La Chinchilla and Los Ratones that plot outside established fields. Although they have values of Zr/Hf less than 25, which indicates granite fertility and association to Sn-W(U)-Be and Ta mineralisation [54], they have values of Nb/Ta between 5 and 7. However, at the level of current metallogenetic knowledge of both granites [30, 42, 55] they can be considered granites of high fertility and related to mineralisation.

The majority of the Achala and Huaco samples and two samples from Los Ratones plot in the barren granite field because of their low Ta content. There are no data available concerning the Nb/Ta and Zr/Hf ratios for the Cerro Áspero granite.

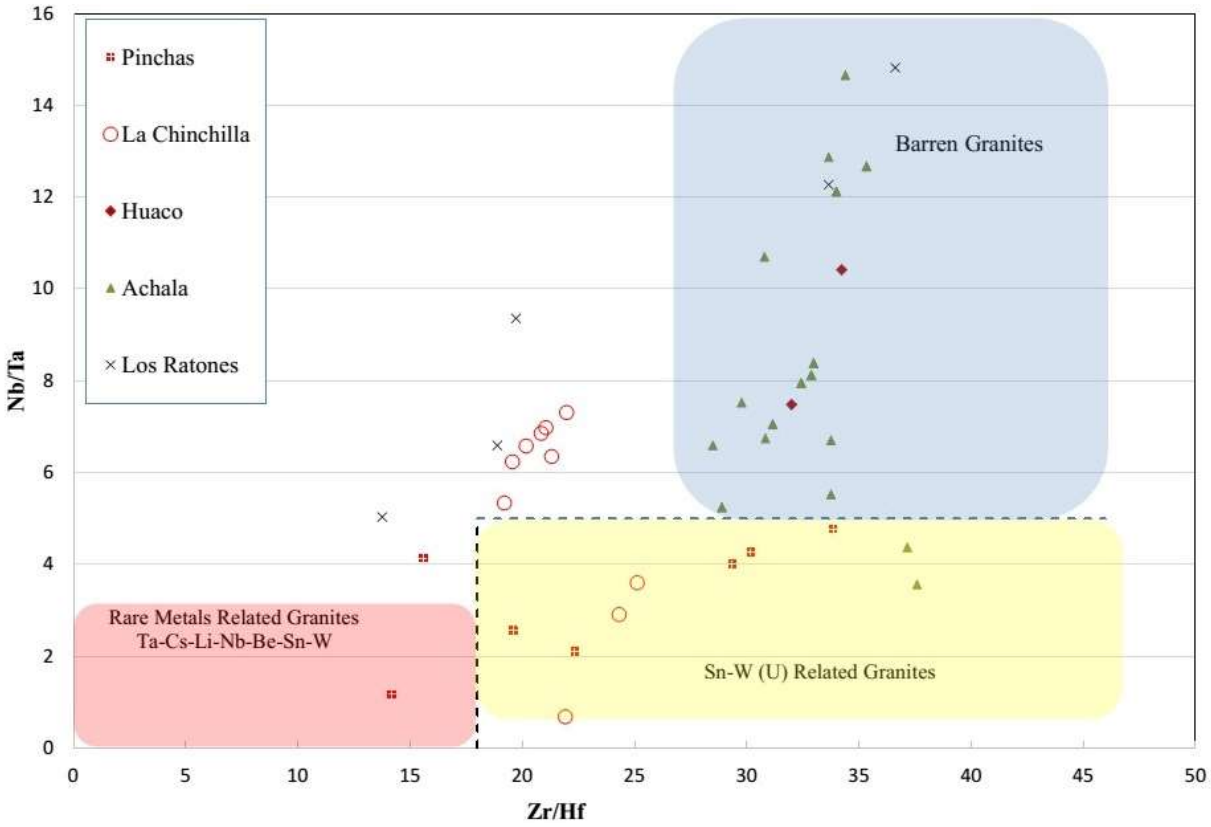

FIGURE 25. Nb/Ta versus Zr/Hf diagram differentiating barren and ore-bearing peraluminous granites. Modified from [52].

The set of granitoids studied indicates that the Devonian to Carboniferous magmatism of the Sierras Pampeanas geological province generated granites enriched in U, Sn, W, Nb, Ta, Li, Be and F. Two major types of uranium-rich igneous rock are described: metaluminous to slightly peraluminous high-K calc-alkaline granites and peraluminous (two-mica) leucogranites. The first group corresponds to La Chinchilla, Huaco, Cerro Áspero and Los Ratones granites with Al/(Na+K)≈1. This group represents fertile U magmas especially in highly fractionated facies with a high U/Th ratio and where metamictization/alteration processes have acted on the silicates containing uranium (i.e. U-thorite, allanite, zircon). In particular, La Chinchilla has very low P_2O_5 contents with Fe-Li rich mica (phengite, zinnwaldite), Al/(Na+K)<1.15 and intermediate REE, Y, Zr, Hf, Th contents that were derived from a highly fractionated melt of A-type magmas with Nb-Ta (columbite), U-Nb-Ta (oxyuranopyrochlore) and Sn (cassiterite) mineralisation.

The second group includes the peraluminous Achala and Pinchas granitoids. These represent fertile magmas and very good uranium sources with uraninite as a common accessory mineral present mainly as high P_2O_5 leucogranitic peraluminous (Al/(Na+K)>1.15) facies. Evidence from new outcrops at the Achala sites (Don Alberto and Sala Grande) suggests that the uraninite from the western slope of the Sierra Grande was derived from pegmatitic melts fractionated from the Achala monzogranite. These are peraluminous pegmatite bodies (cordierite-andalusite) emplaced between the porphyritic granite and the country rock biotite-gneisses.

6. CONCLUSIONS

The interpretation of new studies on uranium minerals from several uranium sites of interest improved the metallogenetic knowledge of the granite-related uranium deposits, which could in turn improve exploration guidelines.

Granites played an important role both as a uranium source and as host of diverse types of uranium mineralization. Additionally, it is thought that at the existing level of knowledge there is good potential to develop new uranium resources related to granites in Argentina.

ACKNOWLEDGEMENTS

The CRP paper was part of a larger study on granite-related uranium deposits that has been carried out under the National Uranium Favourability Program and investment projects of "Program 24 – Fuel Cycle", which pursued the objective to increase the resources for nuclear fuel in Argentina. The CNEA would like to acknowledge the invaluable scientific and financial support of this research through the IAEA CRP. Besides, it must be noted that several metallogenic studies described in this contribution were accomplished in cooperation with the University of Lorraine-Geo Ressources Laboratory-CREGU Nancy (France), the National University of Córdoba (Argentina) and the US Geological Survey at Colorado (United States of America). An earlier discussion on metallogenic aspects of granite-related uranium deposits of Argentina was given in [56].

REFERENCES

[1] ÁLVAREZ, J., LOPEZ, L., Annual Progress Reports for Contracts under the Coordinated Research Activities, Metallogenesis of Granite-Related Uranium Deposits in Argentina. IAEA Internal Rep., IAEA, Vienna, 2016–2018 (Unpublished internal report).

[2] DAHLQUIST, J. A., ALASINO, P. H., BASEI, M. A., CÁMERA, M. M. M., GRANDE, M. M., NETO, M. D. C. C., Petrological, geochemical, isotopic, and geochronological constraints for the Late Devonian–Early Carboniferous magmatism in SW Gondwana (27–32° LS): an example of geodynamic switching. International Journal of Earth Sciences **107** 7 (2018) 2575–2603.

[3] ALASINO, P. H., DAHLQUIST J.A., PANKHURST, R.J., GALINDO, C., CASQUET, C., RAPELA, C.W., LARROVERE, M.A., FANNING, C.M., Early Carboniferous sub-to mid-alkaline magmatism in the Eastern Sierras Pampeanas, NW Argentina: A record of crustal growth by the incorporation of mantle-derived material in an extensional setting. Gondwana Research **22** 3–4 (2012) 992–1008.

[4] PANKHURST, R. J., RAPELA, C.W., The proto-Andean margin of Gondwana: an introduction. Geological Society, London, Special Publications 142 1 (1998): 1–9.

[5] INTERNATIONAL ATOMIC ENERGY AGENCY (IAEA), UDEPO – World Uranium Deposits and Resources (2017) https://infcis.iaea.org/UDEPO/Deposits.

[6] CAMINOS, R. Sierras Pampeanas de Tucumán, Catamarca, La Rioja y San Juan. In: TURNER, J.C. (Ed.): Segundo Simposio de Geología Regional Argentina, Academia Nacional de Ciencias, Córdoba, Argentina (1979) 41–79.

[7] DAHLQUIST, J.A., ALASINO, P.H., EBY, G.N., GALINDO, C., CASQUET, C., Fault controlled Carboniferous A-type magmatism in the proto-Andean foreland (Sierras Pampeanas, Argentina): geochemical constraints and petrogenesis. Lithos **115** (2010) 65–81.
[8] GORUSTOVICH, S., GUIDI, F., ZELAYA, A., PARRA, F., MORELLO, O., ALVAREZ, J., LÓPEZ, L., SALVATORE, M., BIANCHI, R., Depósitos de minerales nucleares del noroeste argentino. In: MURUAGA, C.M. y GROSSE, P. (Eds.), Ciencias de la Tierra y Recursos Naturales del NOA. Relatorio del XX Congreso Geológico Argentino, San Miguel de Tucumán (2017) 1003–1024.
[9] ZAPPETTINI, E.O., Metalogénesis del noroeste argentino. Relatorio del XI Congreso Argentino de Geología Económica, Salta (2016) 41 pp.
[10] DEMANGE, M., ÁLVAREZ, J.O., LOPEZ, L., ZARCO, J.L., The Achala Batholith (Córdoba, Argentina): A composite intrusion made of five independent magmatic suites: Magmatic evolution and deuteric alteration. International Journal of Earth Sciences **91** 2(1996) 11–25.
[11] GALLISKI, M. A., SFRAGULLA, J., Las pegmatitas graníticas de las sierras de Córdoba. 19° Congreso Geológico Argentino, Relatorio Asociación Geológica Argentina, Córdoba (2014): 365–388.
[12] LIRA, R., SFRAGULLA J., El magmatismo devónico-carbonífero: el batolito de Achala y plutones menores al norte del cerro Champaquí. Geología y Recursos Naturales de la Provincia de Córdoba. 19º Congreso Geológico Argentino Relatorio Asociación Geológica Argentina, Córdoba (2014) 293–347.
[13] LIRA, R., Episienitas feldespáticas y su relación con depósitos uraníferos en el Batolito de Achala, Provincia de Córdoba. Revista Asociación Geológica Argentina 42.3–4 (1987): 388–406.
[14] LIRA, R., Un nuevo modelo metalogenético uranífero en el basamento cristalino de las sierras Pampeanas: uranio en metamorfitas de contacto (batolito de Achala, Provincia de Córdoba), Boletín de la Asociación Geológica de Córdoba **7** (1985) 438–451.
[15] GORDILLO, C. E., SCHREYER, W., WERDING, G., ABRAHAM, K., Lithium in NaBe-cordierites from El Peñón, Sierra de Córdoba, Argentina. Contributions to Mineralogy and Petrology **90** 1 (1985) 93–100.
[16] ZARCO, J. J., Geología estructural y petrología estructural del complejo granítico peraluminoso de Achala en relación con la génesis y la localización de la mineralización de Uranio (Sierras Pampeanas, Argentina). PhD. Thesis, Universidad Nacional de Salta 2006 (Unpublished internal report) 94 pp.
[17] MERCADIER, J., CUNEY, M., LACH, P., BOIRON, M.C., BONHOURE, J., RICHARD, A., LEISEN, M., KISTER, P., Origin of uranium deposits revealed by their rare earth element signature. Terra Nova **23** (2011) 264–269.
[18] LIRA, R., Manifestación Nuclear "Los Riojanos": Estudio mineralógico de testigos de perforación, sondeo L.R. ex-15. Comisión Nacional de Energía Atómica Internal Report, CNEA, Córdoba 1983 (Unpublished internal report).
[19] CONIGLIO, J. E., Evolución petrológica y metalogenética del batolito Cerro Áspero en relación con el ciclo geoquímico endógeno del flúor, Sierra de Comechingones, Córdoba, Argentina. PhD Thesis, Universidad Nacional de Río Cuarto 2006 (Unpublished internal report).

[20] PINOTTI, L., TUBÍA, J.M., D'ERAMO, F., VEGAS, N., SATO, A.M., CONIGLIO, J., ARANGUREN, A., Structural interplay between plutons during the construction of a batholith (Cerro Áspero batholith, Sierras de Córdoba, Argentina). Journal of Structural Geology **28** 5 (2006) 834–849.
[21] TOSELLI, A. J., DURAND, F.R., ROSSI DE TOSELLI, J.N., SAAVEDRA, J., SIAL, A.N., Granitos peraluminosos de la Zona Batolítica Central de Sierras Pampeanas (NW Argentino): Relaciones y significado geotectónico. Memorias del XII Congreso Geológico de Bolivia **2** (1996): 755–768.
[22] PANKHURST, R., RAPELA, C. Y., FANNING, C., Age and origin of coeval TTG, I - and S- type granites in the Famatinian Belt of NW Argentina. Transactions of the Royal Society of Edinburgh: Earth Sciences **91**(2000): 151–168.
[23] SÖLLNER, F., VERDES, A., GROSSE, P., TOSELLI, A., U-Pb age determinations by LA-ICPMS on zircons of the Huaco granite, Sierra de Velasco (NW-Argentina): a long-term history of melt activity within an igneous body. Proceeding 20° Colloquial, Latin American Earth Science **1** (2007): 57–58.
[24] GROSSE, P., SÖLLNER, F., BÁEZ, M., TOSELLI, A., ROSSI, J., DE LA ROSA, J.D., Lower Carboniferous post-orogenic granites in central eastern Sierra de Velasco, Sierras Pampeanas, Argentina: U-Pb monazite geochronology, geochemistry and Sr-Nd isotopes. International Journal of Earth Sciences **98** (2008) 1001–1025.
[25] MORELLO, O., APARICIO, P., Informe preliminar: Mineralización en la Sierra de Velasco- La Rioja. Resultados DRX y SEM. Comisión Nacional de Energía Atómica Internal Report, Buenos Aires, 2010 (Unpublished internal report) 4pp.
[26] ANZIL, P.A., SALVATORE, M.A., PARRA, F.J., SCARLATTA, L.R., MIYNO, S.S. y BELLO, F.C., Análisis textural y química mineral de la mineralización de uranio Alipán, Sierra de Velasco, La Rioja. Implicancias sobre la edad de la mineralización. 20° Congreso Geológico Argentino, Actas. San Miguel de Tucumán (2017) 2pp.
[27] MORELLO, O., APARICIO, P., Mineralización de uranio en la Sierra de Velasco, La Rioja. Revista de la Asociación Geológica Argentina **70** 3 (2013): 335–340.
[28] ANZIL, P.A., SALVATORE, M.A., Análisis por DRX de muestras mineralizadas de las áreas: Alipán, Lucero y Maggi. Comisión Nacional de Energía Atómica Internal Report, Córdoba 2018 (Unpublished internal report) 18pp.
[29] SALVATORE, M., PARRA, F.J., SÁNCHEZ, D.L., ÁLVAREZ, J.O., BELLO, C., ZARCO AMBROSIO, J.J., Caracterización litogeoquímica del granito La Chinchilla y su relación con el uranio, Sierra de Velasco, Provincia de La Rioja. Revista de la Asociación Geológica Argentina **70** (2013): 341 –350.
[30] BARDELLI, F.M., PARRA, F.J., LIRA, R., Minerales accesorios y procesos de alteración del granito La Chinchilla, sierra de Velasco, La Rioja: aspectos mineralógicos y geoquímicos en su relación con mineralización uranífera. Revista de la Asociación Geológica Argentina **75** 1(2018): 134–151.
[31] LIRA, R., PARRA, F., BARDELLI, F.M., GALLISKI, M.Á. y SCARLATTA, L.R., Amazonite from miarolitic NYF-pegmatites and primary accessory minerals of the A-type La Chinchilla granite, Sierra de Velasco, La Rioja province, Argentina. 7th International Symposium on Granitic Pegmatites, PEG, Książ (2015) 40–41.
[32] MORELLO, O., Nuevo hallazgo del óxido de uranio-niobio-tantalio en Argentina. I Reunión Latinoamericana de Cristalografía. IX Reunión Anual de la Asociación Argentina de Cristalografía **1**(2013) 2 pp.

[33] ATENCIO, D., ROBERTS, A.C., COOPER, M.A., MENEZES FILHO, L.A.D., COUTINHO, J.M.V., STIRLING, J.A.R., VENANCE, K.E., BALL, N.A., MOFFATT, E., CHAVES, M.L.S.C., BRANDÃO, P.R.G., ROMANO, A.W., Carlosbarbosaite, ideally $(UO_2)_2Nb_2O_6(OH)_2 \bullet 2H_2O$, a new hydrated uranyl niobate mineral with tunnels from Jaguaraçu, Minas Gerais, Brazil: description and crystal structure. Mineralogical Magazine **76** (2012) 75–90.
[34] URQUIZA, L.A., Estimación de recursos. Cateo El Gallo. La Rioja. Comisión Nacional de Energía Atómica. Comisión Nacional de Energía Atómica Internal Report, Mendoza 2011 (Unpublished internal report) 20 pp.
[35] DE LOS HOYOS, C., LAZO, M., ROSSI, J., Caracterización petrológica y geoquímica del Granito Señor de La Peña, sierra de Velasco, La Rioja, Argentina. 16º Congreso Geológico Argentino, La Plata. Actas publicadas en CD (2005) 8 pp.
[36] CIMA, A., COLOMBO, F., SALVATORE, M., Caracterización petrológica y geoquímica del plutón La Punta y sus manifestaciones uraníferas asociadas (Sierra de Velasco, La Rioja). Universidad Nacional de Córdoba, Bachelor final project 2016 (Unpublished internal report) 161 pp.
[37] ANZIL, P., MIYNO, S., SALVATORE, M., PARRA, F., SCARLATTA, L, FELKAI, E., BELLO, C., ÁLVAREZ, J., Cateo Lucero: Análisis con EDS y WDS en minerales de uranio y asociados. Comisión Nacional de Energía Atómica Internal Report, Córdoba 2018 (Unpublished internal report) 30 pp.
[38] GRISSOM, G., DE BARI, S., SNEE, L., Geology of the Sierra de Fiambalá, northwest Argentina: implications for Early Palaeozoic Andean tectonics. In: PANKHURST, R. J., RAPELA, C. W. (Eds.), The proto-Andean margin of Gondwana. Geological Society, London, Special Publications **142** (1998) 291–323.
[39] ARROSPIDE, A., Las manifestaciones de greisen de la Sierra de Fiambalá, Catamarca. Revista de la Asociación Geológica Argentina **40** 1–2(1985) 97–113.
[40] ÁVILA, J.C., RUBINSTEIN, N., MORELLO, O., FOGLIATA, A.S., Edad y caracterización de una mica de litio asociada a un sistema de greisen en Mina La Rosario, Sierra de Fiambalá, Catamarca. Revista de la Asociación Geológica Argentina **63** 1(2008) 43–48.
[41] GRISSOM, G.; DE BARI, S.; PAGE, S.; PAGE R.; VILLAR, L; COLLEMAN, R; VIRUEL DE RAMÍREZ, M., The deep crust of an Early Paleozoic Arc; The Sierra Fiambalá, Northwestern Argentina. In: HARMON R. S., RAPELA C.W. (Eds.): Andean Magmatism and its Tectonic Setting. Geological Society of America, Special Paper 265 (1991) 189–200.
[42] FOGLIATA, A., Depósitos de greisen asociados agranitos carboníferos post-orogénicos con potencial mineralizador, Sierra de Fiambalá, Catamarca, Argentina Boletín Geológico y Minero **118** 4 (2008) 385–400.
[43] CEBALLOS E., ZELAYA A., GORUSTOVICH, S., Estudios Complementarios de alteración hidrotermal en el depósito de uranio Mina Franca, Catamarca, Argentina. Actas del XX Congreso Geológico Argentino S9 (2017) 16–19.
[44] RUBINSTEIN, N., MORELLO, O., BURGOS, J., El yacimiento de uranio Las Termas, Catamarca, Argentina. Revista Asociación Geológica Argentina **56** 1(2001) 91–98.
[45] MORELLO, O., RUBINSTEIN, N., BURGOS, J., Nuevos avances sobre la metalogénesis de la Manifestación Las Termas-Fiambalá, Argentina. 3° Reunión de Mineralogía y Metalogenia, La Plata (1996) 153–156.
[46] DE LA HOZ, M., Mineralización supergénica del depósito de uranio Las Termas, sierra de Fiambalá, Catamarca. Actas del XI Congreso de Geología Ecónomica (2016) 4pp.

[47] CEBALLOS E., ANZIL P.A., Mina Franca: muestras analizadas por microscopio electrónico y microsonda. Comisión Nacional de Energía Atómica Internal Report 2017 (Unpublished) 6 pp.
[48] MORELLO, O., Edad de la mineralización de uranio. Depósito Las Termas, Fiambalá, Catamarca. Actas del 17° Congreso Geológico Argentino **2** (2008): 641–642.
[49] DEBON, F., LE FORT, P.A., Chemical – mineralogical classification of common plutonic rocks and associations. Transactions of the Royal Society of Edinburgh: Earth Sciences **73** (1982) 135–149.
[50] CUNEY, M., KYSER, K., Deposits related to Na-metasomatism and high-grade metamorphism. In Recent and Not-so-Recent Developments in Uranium Deposits and Implications for Exploration. Short Course Series 39. Quebec: Mineralogical Association of Canada (2008) 257 pp.
[51] CUNEY, M., Felsic magmatism and uranium deposits. Bulletin de la Société Géologique de France **185** 2(2014) 75–92.
[52] BALLOUARD, C., POUJOL, M., BOULVAIS, P., BRANQUET, Y., TARTÈSE, R., VIGNERESSE, J. L., Nb-Ta fractionation in peraluminous granites: A marker of the magmatic-hydrothermal transition. Geology **44** 3(2016) 231–234.
[53] ANZIL, P.A., SALVATORE, M.A., LOPEZ PINTO, M.R., SCARLATTA, L.R., MIYNO, S.S., FELKAI, E.F., BELLO, F.C., PARRA, F.J., ÁLVAREZ, J.O., Cateo Lucero: Análisis de las rocas ígneas mineralizadas. Potenciales fuentes de uranio. Comisión Nacional de Energía Atómica Internal Report, Córdoba 2019 (Unpublished) 60 pp.
[54] ZARAISKY, G.P., AKSYUK, A.M., DEVYATOVA, V.N., UDORATINA, O.V., CHEVYCHELOV, V.Y., The Zr/Hf ratio as a fractionation indicator of rare-metal granites: Petrology **17** (2009) 25–45.
[55] MORELLO, O., RUBINSTEIN, N., HONGN, F., FERREIRA, L., ANESA, J., ARIAS A., Modelo metalogenético del yacimiento de uranio Las Termas, Fiambalá, Catamarca, Argentina. Boletín Geológico y Minero **122** 3 (2011) 325–332.
[56] ÁLVAREZ, J., LÓPEZ, L., CUNEY, M., MERCADIER, J., HANLY, A., PARRA, F., BELLO, C., LIRA, R., ANZIL, P., MIYNO, S., SALVATORE, M., SCARLATTA, L., FELKAI, E., FERREYRA, P., New Studies of the Uranium Deposits Related to Granites in Argentina. In: International Atomic Energy Agency (IAEA). International Symposium on Uranium Raw Material for the Nuclear Fuel Cycle: Exploration, Mining, Production, Supply and Demand, Economics and Environmental Issues (URAM2018). Vienna, Austria 25–29 June 2018. Book of abstracts and extended abstracts (2018) 33–36.

MINERALOGICAL CHARACTERIZATION OF SANDSTONE URANIUM DEPOSITS IN CHINA

WENSHENG LIAO, PO LI, ZHENGBANG LIU,
LIMIN WANG, GUOPING JIANG, KE HE,
Beijing Research Institute of Chemical Engineering and Metallurgy
Beijing, China

Abstract

In uranium mineralizing processes in sedimentary environments, uranium deposition is related to complex geological and hydrogeological processes, mainly with relation to reductive minerals and permeability of the formation. In this project, five typical sandstone uranium deposits were studied: the north belt of the Shihongtan in Tuhar Basin; Mengqigur in Yili Basin located in Xinjiang; Shashagetai in Erdos Basin; Bayanwula in Erlian Basin; and Qianjiadian in Tongliao Basin located in Inner Mongolia. Through chemical analysis and determination of the mineral composition, the behaviour of reductive minerals and clay minerals in the deposits were investigated, revealing the relations between the behaviour of reductive minerals, clay minerals and permeability of mineralized horizons and the microscopic genesis of sandstone uranium deposits. The results show that reductive materials such as organic matter and pyrite determine the degree of enrichment and extent of uranium. The richest mineralized body usually occurs in sandstone with high contents of organic matter and/or sulphur. For those deposits with high contents of clay minerals, such as the Shashagetai and the north belt of Shihongtan deposits, the adsorption of uranium by clay minerals also plays a relatively important role in uranium mineralization. In addition, the permeability of sand bodies promotes the enrichment, transport and distribution of uranium. Reductive media are also critical and as a result uranium mineralization tends to occur in sand bodies with good permeability and high content of organic matter.

1. INTRODUCTION

China has been changing its uranium prospecting direction from ‘hard rock’ types to in-situ leach amenable sandstone uranium deposits since the 1990s. As a result of this effort, many sandstone uranium deposits were found in Xinjiang and Inner Mongolia. In comparison with similar deposits in other countries the deposits that have been discovered in China, so far, have smaller resources which feature lower grades and GT (Grade-Thickness) and have poorer geologic and hydrogeological conditions such as low permeability and thick aquifers. These characteristics lead to smaller productivities of an individual mining unit and higher costs.

For historical reasons, the institutions/organizations for geologic exploration in China are separate from the departments of mining uranium. The exploration organizations are responsible for finding the uranium resource, analysing the origin of uranium deposits and formation, and characterizing the mineralogy of the uranium deposit. Commonly similar results were reported when an exploration institution/company investigated the genesis of uranium deposits, geochemistry of formation, and the characteristics of minerals among those deposits which were in different strata or zones within an area. However, because of the heterogeneity of the formation, the varieties of the mineral species, and the distribution and amounts of reductive materials in partially oxidized zones, there may be a striking difference in the quantity, species and/or occurrence of uranium. Additionally, the minerals in the formation, especially the species, amount and distribution of clays may also have led to heterogeneity of the fluids flowing in porous media and the mineralization. Exploration organizations are frequently lacking high precision data and this lack of detailed information for each uranium deposit makes it difficult to guide in-situ leaching and further exploration.

In uranium mineralizing processes in sedimentary environments the uranium deposition is related to complex geological environments and particularly the presence of reductive minerals and permeability of the formation. Strongly reducing environments and moderate permeabilities of the formation may lead to good uranium mineralization. During recovery of uranium from well development fields, the relatively good mineralization often occurs just before or after the redox front, with one or more drill holes containing higher concentrations of uranium.

It is necessary to perform detailed mineralogical characterization and analyse the related permeability conditions. Not only is this precise information important to mining uranium, but it can also guide further exploration for increasing the reserve.

In the past, we have performed some work on mineralogical characterization and its relationship with permeability [1]. There were three deposits analysed in the same way which are located in Erdos, Tongliao in Inner Mongolia autonomous area, and Tengchong in Yunnan province.

In this project, five typical sandstone uranium deposits in different regions were selected to conduct the research. The deposits are located in Ordos, Erlian, Tongliao of Inner Mongolia, and Yili and Tuhar in Xinjiang Urgur autonomous region. Field tests or industrial production were performed in the deposits studied. Drill holes were planned in the studied areas in a way that would ensure adequate sampling for mineralogical characterization.

2. TECHNIQUES AND METHODOLOGIES

2.1. Sampling and preparation of samples

The mineralized and host rock samples were collected in plastic bags at each drill hole. The mineralized samples were then wrapped in a protective wax that has a melting point of 56–58°C. The underground water in the uranium-bearing aquifer was bottled.

After unpacking at the laboratory, samples were classified according to their lithology, sizes and uranium-bearing properties. Samples for chemical analysis were milled to -200 mesh with a final quantity of 100–200 g. The large-diameter cores for tests of porosity and permeability were re-drilled into a rod shape with a diameter of 2.5 cm using core boring equipment. Then, the ends of the rod-shaped core were flattened with a cutting and burnishing machine. The samples for analysis by XRD, SEM and polarizing microscope were prepared in accordance with the requirements of relevant standards of preparation.

2.2. Chemical analysis of the solid and water samples

Fluorescent spectrometry, ICP-MS, and ICP-AES for chemical analysis were utilized to analyse the concentrations of cationic and anionic ions of solid and water samples.

2.3. Mineralogical characterization

A RINT 2000 automated powder X-ray diffractometer (Rigaku, Japan) was utilized to determine the mineralogy of rocks and to identify clay minerals. A polarizing microscope and SEM scanning

electron microscope were used for visualization of the featured minerals and extent and type of cementation.

2.4. Determination of porosity and permeability

A porosimeter permeameter and AutoPoreTM III 9500 mercury porosimeter were used to determine the porosity, permeability, and the pore size distribution of core samples.

3. NORTH BELT OF SHIHONGTAN URANIUM DEPOSIT

3.1. Geological setting

The Shihongtan uranium deposit is located in the southwest of the Turpan-Hami Basin in Xinjiang Uygur autonomous region. The Turpan-Hami Basin is surrounded by mountains, with Bogeda mountain in the north, Kalawucheng Mountain in the west, Harlike Mountain in the east, and Jueluotage Mountain in the south.

The topography of the studied area is low in the north and east, and high in the south and west, and its altitudes are 118.0–315.0 m. The Jueluotage Mountain, with altitudes of 500–2500 m, is the provenance area of the Shihongtan deposit. The Aiding Lake, located to the northeast of Shihongtan deposit and with an altitude -154 m, is the discharge area of the deposit.

The outcrop strata in the Shihongtan deposit are mainly Shuixigou Group, Lower and Middle Jurassic (J_{1-2}). Shuixigou Group consists of three formations: Badaowan Formation (J_1b), Lower Jurassic; Sangonghe Formation (J_1s), Middle Jurassic; and Xishanyao Formation (J_2x), Middle Jurassic [2]. The mineralization occurs in the Xishanyao Formation, which can be divided into 4 lithological members (J_2x^1, J_2x^2, J_2x^3 and J_2x^4). The formation is composed of conglomerate, gravel-bearing coarse grained sandstone, and medium-grained sandstone and is attributed to braided stream, fluvial-swamp and fluvial delta depositional systems [3].

3.2. Uranium deposit and mineralization characteristics

The Shihongtan uranium deposit is located in the west of Aiding Lake clinoform belt. According to the spatial and stratigraphic distribution of uranium mineralization, the Shihongtan uranium deposit can be divided into three belts: south, middle and north belts. Because there are many works that have already been conducted at the south belt [2–5], in this study, the north belt was investigated.

The north belt is located in the north of the Yingzuiya Fault. Uranium mineralization occurs in the third lithological member of the Middle Jurassic Xishanyao Formation (J_2x^3), which belongs to a braided-swamp depositional system. The J_2x^3 is composed of two layers of sand bodies, namely J_2x^{3-1} and J_2x^{3-2}, which are loose-subloose, grey coloured and permeable mineralized layers with the amount of clasts generally higher than 90%. The cements account for less than 10% and are mainly clay minerals and minor carbonate [4]. The total length of the north belt is about 6000 m, and widths range from 200–600 m. The depths of upper and lower ore bodies are 230–330 m and 270–400 m, respectively. Uranium orebodies show complex roll and tabular forms in section, and irregular snake-like forms in plan view. The behaviour is almost the same as that of the redox front

of the interlayer oxidation zones. There is a heterogeneous distribution of organic matter such as carbonized plant debris and disseminated pyrite in the ores, with the richest mineralization located in the roll front.

The thickness of the upper ore body ranges from 1–8 m, with an average of 4.4 m, whereas that of the lower ore body ranges from 1–12 m, with an average of 5.3 m. The grade of the upper ore body ranges from 0.0128% to 0.0840% U, with an average of 0.0375% U, and the grades of the lower ore body are between 0.0105% to 0.1432% U, with an average of 0.0408% U. In general, the thickness and grade of the ore bodies vary considerably. The uranium contents in upper and lower orebodies are 1.04–6.31 kgU/m^2 and 1.04–11.76 kgU/m^2, with an average value of 2.62 kgU/m^2 and 3.76 kgU/m^2, respectively, showing that uranium mineralization is very heterogeneous.

Uranium occurs as uranium minerals and adsorbed uranium. Enrichments of associated elements such as Mo, V, Se, Ge, Re, Ga and Sc are variable and have been found in lithological members of the Xishanyao Formation within the North Belt, especially at the redox transitional zone, with minor enrichment phenomena occurring within the oxidation or reducing zone [6].

U-Pb isotopic dating of mineralization yields three representative ages of 81 Ma, 24 Ma and 8.8 Ma, which correspond to the Late Lower Cretaceous, the Late Oligocene and the Late Miocene, respectively. These results are similar to those of the south belt [2, 4].

3.3. Results and discussion

3.3.1. Chemical compositions

Chemical analyses for 106 samples (Table 1) show that the average contents of SiO_2, Al_2O_3, K_2O, and Na_2O in mineralized samples from the North Belt are 72.38%, 11.72%, 2.75% and 1.16%, respectively, indicating that samples have low contents of quartz but have high contents of feldspar and/or clay minerals. The average value for total Fe (calculated on basis of Fe_2O_3) is 2.05%, with FeO accounting for over two thirds of total Fe. The average value of loss on incineration for samples reaches 5.62%.

TABLE 1. AVERAGE CONTENTS OF MAJOR ELEMENTS IN MINERALIZED SAMPLES FROM THE NORTH BELT OF THE SHIHONGTAN DEPOSIT (%)

Sample No.	U	SiO_2	Al_2O_3	CaO	MgO	K_2O	Na_2O	Fe_2O_3	FeO	TiO_2	MnO	P_2O_5	Loss on incineration
106	0.109	72.38	11.72	1.93	0.90	2.75	1.16	2.05	1.60	0.44	0.03	0.09	5.62

The characteristic elements, such as U, TOC (total organic carbon), CO_2, ΣS (total sulphur), ΣFe (total iron) in the ore were analysed. The results listed in Table 2 indicate a relatively high content of reductive materials in the ore, which is consistent with a positive correlation among uranium, carbonized fragments and pyrite.

TABLE 2. CONTENT OF CHARACTERISTIC ELEMENTS IN THE MINERALIZED SAMPLES OF THE NORTH BELT

Sample No.	U%	TOC%	$CO_{2\%}$	∑S%	Fe^{2+}%	Fe^{3+}%	Fe^{2+}/Fe^{3+}	∑Fe（%）
121	0.056	0.62	0.84	0.43	0.89	0.71	1.34	1.60

The organic carbon in the mineralized samples is relatively high, with an average of 0.62% but its distribution is not uniform. The average content of sulphur (∑S) in the ore is 0.43% and is generally uniform. The content of total iron (∑Fe) is relatively stable, with an average value of 1.60%. Iron mainly occurs as in-situ precipitates from rocks with no obvious transportation during oxidation process but there is a variation in valence state. The ratio of Fe^{2+}/Fe^{3+} is about 1.4:1, indicating that iron in the ore rocks mainly occurs as Fe^{2+}.

3.3.2. Mineralogical compositions

The mineralization of the North Belt is composed of grey, grey-white, grey-black and yellowish coloured clastic sandstone, minor feldspathic lithic sandstone and debris quartz sandstone. The main minerals in ores consist of the major rock-forming minerals (i.e. quartz, feldspar, biotite and muscovite) (Figure 1), heavy minerals, pyrite, carbonaceous plant fragments, clay minerals, calcite and clast, etc. Generally, clay minerals contents are high in the uranium mineralization.

The heavy minerals are mainly epidote, tourmaline, apatite, garnet, titanite, zircon, ilmenite, brookite, monazite, spinel, rutile, and rarely brannerite. Pyrite and carbonaceous plant fragments are about 0.1–1.5%. Carbonized fragments occur as strip and sharp-edged forms distributed heterogeneously in rocks. Occasionally, a wood cell texture filled with pyrite was observed in carbonaceous fragments. Pyrite usually occurs as anhedral crystals disseminated in rocks, and less commonly as cubes or pentagonal dodecahedron fine grains. Some pyrite is a product of alteration from biotite or detritus.

The content of clay minerals in the mineralized samples is 15–25%. About 50% of the clays are microscopic kaolinite, scale-like illite and chlorite which coexist with micro-lithic fragments distributed between detrital grains, and the others are alteration products of rock fragments, feldspar and biotite. X-ray diffraction of the clay minerals showed that they are mainly composed of kaolinite, illite, chlorite and montmorillonite (Table 3, Figure 2), with average contents of 37.71%, 23.00%, 18.50%, and 20.79% respectively. The relatively high contents of kaolinite and illite and low contents of chlorite and montmorillonite suggest that the environment of uranium deposition was relatively acidic, a condition which favours uranium mineralization.

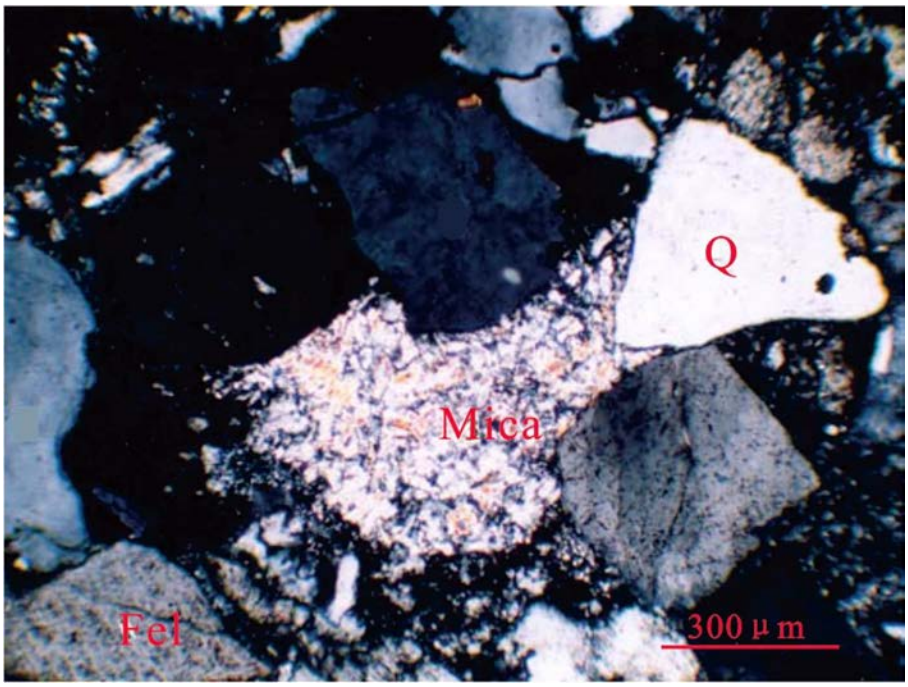

FIGURE 1. Lithic sandstone containing biotite and muscovite (mica), Q=quartz, Fel=Feldspar.

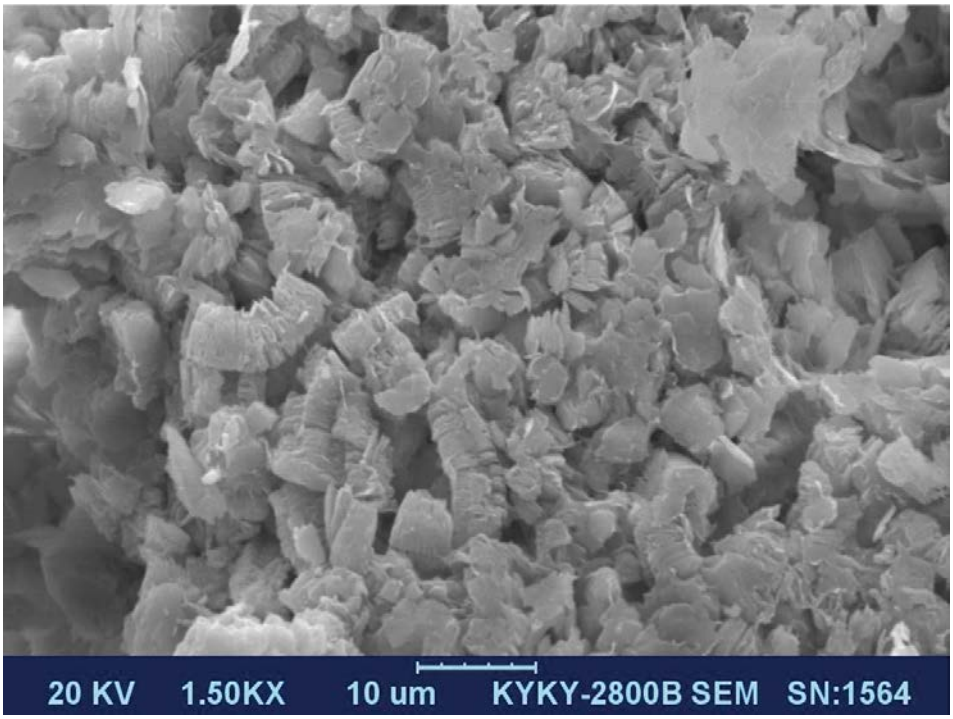

FIGURE 2. SEM image of intergranular authigenic foliaceous kaolinite aggregates

TABLE 3. RELATIVE CONTENTS OF CLAY SPECIES IN MINERALIZED SAMPLES

Rock type	Sample No.	Lithology	U (%)	Kaolinite (%)	Illite (%)	Chlorite (%)	Montmorillonite (%)
Uranium ores	T06Kr—45	Grey medium sandstone	0.0394	36	14	23	27
	T06Kr—47	Grey medium sandstone	0.1680	43	18	25	14
	T08Kr—15	Grey coarse sandstone	0.2140	38	24	21	17
	T08Kr—26	Grey gravel-containing coarse sandstone	0.0744	36	24	19	21
	T08Kr—54	Grey coarse sandstone	0.0296	43	19	16	22
	T08Kr—103	Grey gravel-containing coarse sandstone	0.0174	41	26	21	12
	T08Kr—113	Grey coarse sandstone	0.0845	32	27	16	25
	T08Kr—185	Grey medium sandstone	0.0137	39	23	17	21
	T08Kr—204	Grey-white medium sandstone	0.0276	33	28	20	19
	T08Kr—261	Grey medium sandstone	0.0340	37	21	18	24
	T08Kr—281	Grey medium sandstone	0.0417	21	21	14	44
	T08Kr—332	Grey fine sandstone	0.0259	41	24	18	17
	T09Kr—164	Grey gravel-containing coarse sandstone	0.0321	42	28	16	14
	T09Kr—167	Grey gravel-containing coarse sandstone	0.0439	46	25	15	14
Average			0.0604	37.71	23.00	18.50	20.79

3.3.3. Relations between reductive minerals and uranium mineralization

Chemical analyses (Table 2) showed that there is abundant organic carbon in the ore-bearing horizon with heterogeneous distribution. High contents of organic carbon are usually accompanied by high uranium grades, indicating that the uranium enrichment is related to adsorption by carbonaceous matter. Sulphur mainly occurs as nodular pyrite in host rocks but also occurs as disseminated, microcrystalline pyrite and marcasite in ore with colloidal texture. Sulphur-bearing minerals play a significant role in uranium precipitation and coexist or are associated with uranium minerals in colloidal form.

The content of total iron (∑Fe) is relatively uniform with an average of 1.60%. The ratio of Fe^{2+}/Fe^{3+} suggests that iron mainly occurs in two-valence form in the mineralization and that the rocks are in a weakly reductive condition. There is a relationship between uranium mineralization and valence status of iron. Based on mineral compositions, iron in two-valence (2+) state may occur within chlorite, mica, pyrite, marcasite, or montmorillonite, while iron with a higher valence (3+) may occur as hematite and limonite.

From a metallogenetic point of view, the mineralized bodies in the North Belt occur in the redox transitional zone and the weakly oxidized subzone of the third member of the Middle Jurassic Xishanyao Formation (J_2x^3). The mineralized rocks are mainly grey and dark grey coloured, with powdery fine-grained pyrite and minor powdery carbonized debris. The organic carbon in mineralization significantly increases (0.62%), the ratio of Fe^{3+}/Fe^{2+} (0.75) is lower than 1, and total sulphur (0.43%) rises to some extent.

The zoning characteristics of interlayer oxidation zones are obvious. The geochemical parameters, such as the colour of rocks, the mineralogical composition and geochemical characteristics, show regular changes. From the entirely oxidized subzone to reductive zone, iron-bearing minerals in the rock change gradually from limonite to hydrogeothite, hydrohematite, then to powdery microcrystalline pyrite, and finally to coarse grained pyrite. Carbonaceous matter almost disappears in the entirely oxidized subzone and significantly increases from the weakly oxidized subzone, to the transitional zone, and then to the reducing zone.

Chemical compositions were determined for host rocks of various subzones in the interlayer oxidation zone. The results are listed in Table 4, showing the regular changes of contents of characteristic elements.

TABLE 4. CHARACTERISTIC ELEMENTS IN ROCKS OF VARIOUS SUBZONES ALONG EXPLORATION LINE 39 IN NORTH BELT

Interlayer oxidation zone	Drill hole No.	U% (10^{-4})	Th% (10^{-4})	TOC (%)	Fe^{3+}/Fe^{2+}	∑Fe (%)	∑S (%)	CO_2 (%)
Oxidation subzone	ZK39-3	6.35	8.70	0.035	1.10	1.40	0.02	0.13
	ZK39-5	5.70	6.03	0.08	2.22	1.94	0.013	0.12
Redox transitional subzone	ZK39-W5G	177.50	7.04	0.20	0.80	1.17	0.29	4.09
	ZK39-4	67.0	6.30	0.17	1.54	2.13	0.16	0.10
Original rock subzone	ZK39-6	3.50	6.90	0.05	0.24	1.14	0.17	0.37

The elements sensitive to the redox environment, such as iron, total sulphur (∑S) and total organic carbon (TOC), show obvious regular variations in different subzones. In the oxidation subzone, iron occurs in two- and three-valence state with the ratio of Fe^{3+}/Fe^{2+} between 1.10–2.22, and the ∑S and TOC contents are lower. In the redox transition subzone, the ratio of Fe^{3+}/Fe^{2+} is slightly lower with values of 0.80–1.54 and have the highest contents of TOC and ∑S with up to 0.20% and 0.29%, respectively. In the original rock subzone, the ratio of Fe^{3+}/Fe^{2+} is lowest with a value of 0.24, and the contents of TOC and ∑S are also low with values of 0.05% and 0.17%, respectively. The total iron content in different subzones fluctuates between 1.14%–2.13% but with no obvious regularity.

Corresponding to the content changes of reductive minerals, the content of uranium is lower in the oxidation subzone and original rock zone and is higher in the redox transitional subzone. The uranium ore bodies are located near the redox front, within 10–100 m of the interlayer oxidation zones. The largest and most abundant uranium ore bodies usually occur in the thick and large sand bodies of the oxidation-reduction transitional zone.

3.3.4. Relations between the permeability of the deposit and uranium metallogenesis

The mineralogical study shows that sediments of the North Belt are detrital sandstone with low contents of quartz and feldspar and a high content of clay minerals of up to 20%. The rocks are not well sorted, leading to low permeability aquifers with hydraulic conductivities of 0.21–0.68 darcies.

Various lithologies from the ore-bearing aquifer were chosen to conduct tests of porosity and permeability. The results (Table 5) show a broad range of changes in permeability (K) indicating a strong heterogeneity. The permeability of mineralized samples is generally better than that of host rocks. The average ratio of permeability of mineralized samples from the lower aquifer to that of host rocks (K_{ore}/K_{host}) is 1.2 whereas the average ratio for the upper aquifer is 1.37.

The results suggest that uranium mineralization is related to permeability of sand bodies. Good uranium mineralization occurs in loose-subloose, coarse-grained sandstones within redox transitional zones which have better permeability. Uranium mineralization is also related to higher contents of pyrite and organic matter. For fine-grained sandstone with low permeability, uranium mineralization is poor.

TABLE 5. PERMEABILITY OF ROCKS FROM ORE-BEARING AQUIFER OF NORTH BELT

Aquifer	Rock type	Sample no.	Range (m/d)	Average (m/d)	Coefficient of variation (%)
Lower	Conglomerate	23	0.03–1.25	0.50	66.5
	Coarse sandstone	104	0.04–2.34	0.42	88.5
	Medium sandstone	82	0.01–2.54	0.39	125.4
	Fine sandstone	34	<0.01–0.41	0.17	108.3
K_{ore}/ K_{host}*		12**	0.4–2.7	1.20	51.3
Upper	Conglomerate	29	0.05–4.51	0.68	133.6
	Coarse sandstone	86	0.02–3.03	0.40	110.7
	Medium sandstone	26	0.01–0.58	0.39	75.1
	Fine sandstone	34	＜0.01–0.74	0.12	163.7
K_{ore}/ K_{host}*		22**	0.6–3.0	1.37	61.0

* The ratio of permeabilities between mineralized and host rocks
** Number of wells
m/d=millidarcies

4. MENGQIGUER URANIUM DEPOSIT

4.1. Geological setting

The Mengqiguer uranium deposit is located in the transition zone between the eastern tectonic active region and western tectonic stable region in the southern margin of Yili Basin, at the southeast limb of a drawer-like syncline of Zhajistan [7]. The basal lithologies of Mengqiguer area are Carboniferous-Permian marine volcanic rocks, tuffs and terrigenous clastic rocks. The cover strata in this area consist mainly of Quaternary, Paleogene, Cretaceous, Jurassic and Triassic rocks. Uranium mineralization of the Mengqiguer deposit mainly occurs in sand bodies of the Middle-Lower Jurassic Sangonghe Formation and Xishanyao Formation.

Three faults (F1, F2 and F3) are observed in the deposit. The F1 fault, located in the southeast of the deposit, is part of basin-controlling thrust faults in the southern provenance zone of the Yili Basin. The transection of F1 into the ore-bearing strata connects the hydrodynamic system of the

provenance zone. Uranium-bearing and oxygen-bearing water in the provenance zone flows straight to the ore-bearing strata, forming and improving the recharge, runoff and discharge system of groundwater [8].

4.2. Uranium deposit and mineralization characteristics

The Mengqiguer uranium deposit, occurring in four strata, is a typical multilayer uranium deposit. Uranium ore bodies are hosted in the sand bodies of the lower member (J_1S_1) and upper member of the Sangonghe Formation (J_1S_2), and lower member (J_2X_1) and upper member of the Xishanyao Formation (J_2X_3), Middle-Lower Jurassic [7]. Not only is each stratum of the ore bodies controlled by the corresponding interlayer oxidized zone, but each stratum also exhibits specific metallogenic characteristics and metallogenic regularity.

Except for the sand body of the upper member of the Xishanyao Formation (J_2X_2) which disappears or merges into J_2X_1 in some places, the remaining ore bodies of the three members develop continuously in section. The clay aquicludes are stable and sand bodies have developed relatively independently in the formations. The ore bodies trend in a SE direction with strike angles of 142°–158°, with an average of 149°, and dip in a NE direction with dip angles of 31°–48°, with an average of 45°, within the scope of the deposit. The depth of the sand body is such that the southwest is shallower than the northeast.

The mineralized bodies occur in the redox transition zone. The formation of the mineralized bodies is mainly dominated by the redox front of the interlayer oxidation zones, lithology and uniformity of sand bodies. The forms of the ore bodies are tabular, lenticular and roll. Tabular mineralized bodies generally occur in the limbs, extending about 200–600 m, with smaller thicknesses of 0.2–1.5 m. Lenticular mineralized bodies also occur in the limbs, often near the roll, with a smaller width of about 100–300 m and thickness of 1.5–3.2 m. The roll mineralized bodies are generally located in the redox front of the interlayer oxidation zones, with greater thicknesses than the other types (3.2–8.6 m) and widths of about 100–300 m.

In general, the thickness of the mineralized body ranges from 0.55–0.80 m but the thickness in the roll part is often greater than 2.50 m. Variation of ore grades are moderate with values between 0.0192% U to 0.4430% U and an average of 0.1643% U [9]. Uranium mainly occurs as uraninite, coffinite and brannerite. Some uranium occurs in monazite and zircon in isomorphic form and some uranium is adsorbed onto clay minerals.

The behaviour of elements which may be geochemically associated with uranium such as Se, Mo, Re, Ge, Ga and V are similar to that of uranium in the interlayer oxidation zone. The migration and enrichment of Se, Mo, Re is significant.

U-Pb isotopic dating indicates that the metallogenic epoch is relatively recent. Dating by $^{206}Pb/^{238}U$ yielded ages of 4.1–11.5 Ma which represent Middle and Late Miocene to Early Miocene [9].

4.3. Results and discussion

4.3.1. Chemical compositions

Chemical analysis of 246 samples of mineralized and host rock selected from the redox transition zone of the Mengqiguer deposit was conducted and the results are shown in Table 6. The average contents of SiO_2, Al_2O_3, K_2O and CaO in mineralized samples indicate higher quartz and lower feldspar and/or clays. The concentrations of elements in the host rock are similar to those in mineralized samples, but SiO_2 is slightly higher, corresponding to lower Ca, Mg and Fe. The ratio of FeO/Fe_2O_3 is not high, which is 0.54 for mineralized samples, and 0.61 for the host rock. The results indicate that the redox transition zone is in a partial oxidation state.

TABLE 6. CHEMICAL COMPOSITIONS OF MENGQIGUER URANIUM DEPOSIT (%)

Rock type	Number of Samples	SiO_2	Al_2O_3	K_2O	Na_2O	CaO	MgO	Fe_2O_3	FeO	TiO_2	MnO	P_2O_5	Loss on incineration
Ore	121	82.92	7.47	2.13	0.40	1.17	0.47	0.94	0.51	0.18	0.16	0.19	2.64
Host rock	125	84.13	7.60	1.92	0.35	1.02	0.46	0.70	0.43	0.19	0.13	0.09	2.59

4.3.2. Mineralogy

Mineralogical analysis of mineralized samples and host rock from the Mengqiguer uranium deposit was conducted and the results are shown in Table 7 and Table 8. The results indicate that there are no significant differences between ore and host rock mineral composition. They are all silicate mineral aggregates consisting of clastics and interstitial materials. The sand bodies are mainly composed of quartz, debris and feldspar. Interstitial materials include argillaceous matrix and clay minerals or partial calcite cement with weak to very weak cementation.

TABLE 7. MINERALOGY OF HOST ROCKS OF THE MENGQIGUER DEPOSIT BASED ON PETROGRAPHIC STUDIES (88 SAMPLES)

	Clastic content (%)				Cement (%)
	Quartz	Feldspar	Debris	Total clastics	
Average	45.8	10.1	44.1	88	10.9

TABLE 8. MINERALOGICAL COMPOSITIONS OF MINERALIZED ROCKS IN THE MENGQIGUER DEPOSIT BASED ON PETROGRAPHIC STUDIES (15 SAMPLES)

	Clastic content (%)							Total clays (%)
	Quartz	Feldspar	Debris	Mica	Pyrite	Carbon debris	Heavy minerals	
Average	49.3	12.9	34.0	0.7	2.6	1.4	0.7	3.9

In the samples, there is local calcite cementation. The amount of matrix is low and is comprised of fibrous-like sericite or tan-black coloured aphanitic clay minerals. Porosity is relatively well developed.

The argillaceous and fine-grained clasts are the main interstitial materials. For most of the mineralized and host rocks, the interstitial materials consist of over 90% matrix and less than 10% cements which are mainly clay minerals.

The amount of clay minerals in the Mengqiguer deposit is only about 3.1–5.3% and consist mainly of kaolinite, illite, illite/montmorillonite (I/M) mixed layer, chlorite and minor montmorillonite (Table 9). There was no significant difference in the types of clay minerals between mineralized and rock samples.

TABLE 9. RELATIVE CONTENT OF CLAY MINERALS IN THE MENGQIGUER DEPOSIT (%)

Sample No.	Layer	Kaolinite	Montmorillonite	I/M mixed layer	Illite	Chlorite
13	J_1s_1	75.5	12.3	14.5	9.3	0.6
8	J_1s_2	75.7	-	13.6	8.2	0
22	J_2x_1	74.2	-	13.1	11.5	1.2
13	J_2x_3	62.3	24.1	9.7	13.2	3.2
Average values		71.9	9.1	12.7	10.6	1.3

The contents of mica (0.6–1.9%), pyrite (1.0–5.4%) and carbon plant debris (0.6–2.6%) are significantly higher in the mineralized samples. Autogenic pyrite usually occurs as strawberry and nodule shapes. Pyrite formed in the mineralizing phase usually shows idiomorphic, hypidiomorphic or xenomorphic forms. Mineralization rich in uranium often contain higher contents of disseminated pyrite associated with leaf-like, slightly veined marcasite. Carbon debris are carbonized fragments of ancient wood. Microscopically, the cell structure is visible for debris that have undergone a low degree of metamorphism. The cell cavities are often filled with clays, matrix, pyrite, sphalerite and sometimes pitchblende.

The biggest difference between the mineralized and host rock is the increase of a small amount of minerals formed during the mineralizing phase. The quantity of crystalline idiomorphic,

hypidiomorphic, and xenomorphic pyrite increases in mineralization, as well as the clay minerals such as kaolinite, illite and montmorillonite formed in the water-rock interaction within interlayer oxidation zone.

4.3.3. Relations between reductive minerals and uranium mineralization

Interlayer oxidation was responsible for formation of the Mengqiguer uranium deposit. The migration and enrichment of uranium were a result of oxidation reactions as a result of interactions with oxygen-containing water in the aquifer and the physicochemical reactions in the redox transition zone. The total iron in the ore body is not high, occurring mainly as Fe^{3+}, which indicates that the mineralized bodies are in the partial oxidation state in the redox environment (Table 6). There are low amounts of clay minerals of which kaolinite is the main clay mineral (Tables 8 and 9). Therefore, there is only weak adsorption of uranium on clay minerals. In addition, Table 8 also shows that carbon debris and sulphide (pyrite, marcasite) are the two most common types of reducing substances in the deposit. Chemical analysis of organic carbon and total sulphur on samples of mineralized and host rock was carried out (Table 10). The results show that the amount of organic matter and sulphur compounds are, as expected, lowest in the oxidation zone, higher in the reduction zone, and the highest contents are in the transition zone. This indicates there is a direct correlation between organic matter and sulphur compounds and uranium minerals.

TABLE 10. CHARACTERISTIC ELEMENTS OF VARIOUS ZONES IN MENGQIGUER DEPOSIT

Interlayer oxidation zone	U% (10^{-6})	Th% (10^{-6})	∑S (%)	Fe^{2+} (%)	Fe^{3+} (%)	Fe^{3+}/Fe^{2+}	Sample No.
Oxidation zone	5.87	5.66	0.02	0.13	0.36	2.80	76
Redox transition zone	>100	6.53	0.10	0.20	0.35	1.75	63
Original reduction zone	10.19	6.36	0.10	0.27	0.29	1.07	160

The correlation between the amounts of organic carbon and uranium in the various geochemical zones are nearly the same indicating that organic matter plays an important role in the precipitation and enrichment of uranium which is adsorbed and/or reduced by organic matter [9].

The total sulphur in the oxidation zone is the lowest, and in the transition zone and the reduction zone it is 5 times higher than that of the oxidation zone and the total iron in this area is relatively constant (Table 10). Fe^{2+} in the formation shows an increasing trend from the oxidation zone to the transition zone and reduction zone, but Fe^{3+} tends to decrease, which results in Fe^{3+}/Fe^{2+} ratios that are gradually reduced from 2.8 in the oxidation zone to 1.07 in the original reduction zone. Additionally, as shown in Table 6, the FeO/Fe_2O_3 ratio in the host rocks are higher than that of mineralized zones, indicating that uranium mineralization is not related to iron.

Uranium is the highest in the transition zone, followed by the reduction zone, and the oxidized zone has the lowest level of uranium, which is consistent with the spatial position of the uranium ore body in the interlayer oxidation zone and corresponding with reductive materials. Additionally, this observation supports the metallogenic mechanism of uranium migration and enrichment occurs in the transition zone.

4.3.4. Relationship between permeability of the deposit and uranium metallogenesis

Core samples with various lithologies in the ore-bearing horizon and host rock were chosen to conduct testing of porosity and permeability. The results show that pores develop in aquifers with good connectivity between the pores. The values of porosity and permeability coefficients are 25.3–32.7% and 0.15–1.33 darcies, respectively. However, most of the mineralization is very loose and unconsolidated and cannot be prepared as core samples for porosity and permeability testing. The degree of cementation of the test sample is relatively high and therefore the values are likely to be lower than the actual average values of porosity and permeability of the deposit as these samples are not representative of the majority of the ore materials.

Results of permeability testing are listed in Table 11 and indicates that the permeability of mineralized samples is generally better than that of host rock samples. Groundwater containing uranium can preferentially flow into the ore body and the relationship between permeability and mineralization is positive.

TABLE 11. RESULTS OF PERMEABILITY TESTING

Drill No.	Sampling depth (m)	Permeability (darcies)	Lithology	Mineralization	K_{ore}/K_{host}
SKP3500-1	527.30-527.40	0.52	Grey Coarse	Host rock	1.75
	527.65-527.75	0.40	Grey Coarse	Host rock	
	527.85-527.95	0.27	Grey Coarse	Host rock	
	527.95-528.05	0.60	Grey Coarse	Host rock	
	529.04-529.20	1.05	Grey Coarse	Ores	
	529.74-529.84	0.52	Grey gravel containing coarse	Ores	
SKP3528	439.90-440.10	0.38	Grey medium	Ores	1.52
	459.40-459.60	0.43	Grey fine	Ores	
	459.60-459.70	0.29	Grey fine	Ores	

TABLE 11 (Cont.). RESULTS OF PERMEABILITY TESTING

Drill No.	Sampling depth (m)	Permeability (darcies)	Lithology	Mineralization	Kore/Khost
SKP 3538 (cont.)	462.20-462.35	0.30	Light red sandy conglomerate	Host rock	
	467.00-467.20	0.72	Light red sandy conglomerate	Ores	
SKP3528-1	455.70-455.80	0.49	Grey coarse	Ores	2.21
	457.20-457.30	1.06	Grey coarse	Ores	
	468.80-469.00	0.35	Red coarse	Host rock	
SK320-1	452.42-452.52	1.33	Grey Coarse	Ores	2.26
	453.62-453.73	0.59	Grey Coarse	Host rock	
P1120	444.98-445.08	0.49	Grey Coarse	Ores	
P1120-1	445.38-445.48	0.32	Grey Coarse	Host rock	
SK726	417.27-417.37	0.42	Grey Coarse	Ores	1.91
	418.07-418.17	0.22	Grey Coarse	Host rock	
510II-YZH-SC-1	648.38-648.41	0.19	Grey Coarse	Host rock	
510II-YZH-SC-2	650.48-651.01	0.60	Grey Coarse	Ores	
510II-YZH-SC-5	651.13-651.16	0.44	Grey medium	Ores	
510II-YZH-SC-6	652.20-652.23	0.47	Grey medium	Ores	
510II-YZH-SC-7	652.25-652.28	0.15	Grey fine	Ores	
510II-YZH-SC-12	656.75-656.78	0.25	Grey fine	Ores	
510II-YZH-SZ-4	651.70-657.75	0.41	Grey medium	Ores	

Statistical analyses were conducted on the distribution of uranium in various sandstone lithologies. Uranium mineralization in the lower member of the Sangonghe Formation (J_1S_1) is distributed mainly in the glutenite, accounting for 53.5% of total reserves and in coarse-grained sandstone accounts for 22.6%. Uranium in the upper member of Sangonghe Formation (J_1S_2) mainly occurs in the coarse-grained sandstone, accounting for 53.4% of total reserves, with glutenite accounting for 23.3%. Uranium in the lower member of the Xishanyao Formation (J_2X_1) is mainly distributed in the coarse-grained sandstone, accounting for 54.7% of total reserves, with glutenite accounting for 17.5%. In the upper member of the Xishanyao Formation (J_2X_3), uranium is mainly distributed in coarse sandstone, accounting for 61.7% of the total uranium reserves, and 20.0% is in the fine sandstone. The proportion of uranium in calcareous sandstone is very low. Deposition and enrichment of uranium, therefore, is most favourable in coarse sandstone.

5. SHASHAGETAI URANIUM DEPOSIT

5.1. Geological setting

The Shashagetai uranium deposit is located in the northern part of the Ordos Basin at altitudes of 1100–1500 m. The Ordos Basin belongs to a Mesozoic inland mega sag depositional basin located in the western part of the North China plate. The basin is about 250 000 km^2 and is an important basin which is rich in coal, petroleum, natural gas and uranium [10–11].

The ore-bearing horizon lies in the lower member of the Middle Jurassic Zhiluo Formation. The formation consists of sand bodies of a multi-period, incised valley braided river depositional system formed under humid climatic conditions, covering conformably or by false conformity the coal seam of the Middle Jurassic Yan'an Formation [12]. The area is weakly folded and fractured and the outcropping formations are mainly Jurassic and Cretaceous, and less commonly Tertiary and Quaternary rocks [13].

5.2. Uranium deposit and mineralization characteristics

The uranium deposit of Shashagetai occurs mainly in the braided river sand body of the lower member of the Zhiluo Formation which developed along the front of a paleo-interlayer oxidation zone which is within a faulted tectonic structure. The length of the deposit is 6.8 km in a west-east direction and ranges from 0.2 to 1.3 km in a north-south direction. The burial depths of the upper part of the sand bodies range from 111.75–209.75 m, while the burial depths of the lower limits are between 115.35–219.20 m. The mineralized body has an average thickness of 3.68 m, an average grade of 0.0521% uranium, and an average uranium content by square meter of 3.59 kgU/m^2. The morphologies of the mineralized bodies in plan view show roll, tabular and lenticular types [14].

The ore-bearing horizon mainly consists of fine and medium-grained sandstone, with a small amount of silty mudstone and coarse-grained sandstone. Uranium occurs as two types, the uranium minerals and the absorbed uranium which comprises more than 70% of the reserves. The reductive state of U is the main existing form and 60% of the uranium belongs to U^{4+} compounds.

U-Pb isotopic dating of mineralized samples yields three representative mineralization ages of 76±4 Ma, 84±4 Ma and124±6 Ma, which represent Early Cretaceous and Late Cretaceous [15].

5.3. Results and discussion

5.3.1. Chemical compositions

Chemical analysis of 500 samples was conducted and the results are listed in Table 12. The average contents of SiO_2 and Al_2O_3 are 69.54% and 11.30%, respectively, which indicates a relatively low content of quartz and high feldspar and/or clay compared to that of the Shihongtan deposit and Mengqiguer deposit (i.e. compared with Table 2 and Table 6).

TABLE 12. CHEMICAL ANALYSIS OF MINERALIZED SAMPLES FROM SHASHAGETAI DEPOSIT (AVERAGE VALUES)

No. of samples	Uranium %	SiO_2 %	Al_2O_3 %	FeO %	Fe_2O_3 %	CaO %	MgO %	K_2O %	Na_2O %	MnO %	P_2O_5 %	TiO_2 %	Loss on incineration/%
500	0.10	69.54	11.30	1.69	1.35	5.04	1.80	2.75	2.02	0.08	0.18	0.62	7.81

In addition, analysis of U, CO_2, total sulphur (ΣS), total iron (ΣFe) and ferrous iron was conducted with the results shown in Table 13.

The average content of ∑Fe is 1.52% with the majority of values between 1–1.5% ∑Fe and some values as high as between 2–3% ∑Fe, among which Fe^{+2} is 60% of the total. The average content of sulphur which is mainly attributed to pyrite is 0.29%, with the largest value of about 0.5% in some samples. The mineralized samples are rich in Fe^{+2}, and pyrite cementation is frequently seen in the samples, showing that the ore-bearing horizon is in a reductive condition. The average values of Ca, Mg and inorganic carbon are 1.97%, 0.92% and 0.61%, respectively, indicating a high content of carbonate.

TABLE 13. AVERAGE VALUES FOR CHARACTERISTIC ELEMENTS FROM SAMPLES OF THE SHASHAGETAI DEPOSIT

∑U%	*U^{6+}%*	*∑S%*	*∑Fe%*	*Fe^{2+}%*	*Ca%*	*Mg%*	*CO_2%*
0.10	0.04	0.29	1.52	1.05	1.97	0.92	2.24

5.3.2. Mineralogy

The lithology of the Shashagetai deposit is dark-light grey sandstones, formed in a low-grade diagenetic environment. Clasts make up >85% and carbonate cement is relatively high, which makes the mineralization alkaline.

The proportion of quartz, feldspar, debris and mica in clasts are 40.0–45.0%, 30.5–35.0%, 20.0–25.0% and 2.0–5.0%, respectively. Feldspar is comprised of mainly potassium feldspar with minor

amounts of plagioclase. Feldspar tends to argillization, with kaolinization for potash feldspar and hydromicatization, epidotization and chloritization for plagioclase. Approximately 1/3 of the feldspar has been affected by argillization. Mica is composed of green and brown coloured biotite and chlorite and occurs as penninite (after chloritization). Moreover, carbonized plant debris, organic matter and heavy minerals are also present.

Mineral analysis using X-ray diffraction was conducted on 28 samples. The content of whole rocks and the relative content of clay minerals were quantitatively determined (Table 14).

TABLE 14. AVERAGE MINERAL COMPOSITIONS BY XRD FROM THE SHASHAGETAI DEPOSIT (%)

Quartz	Plagioclase	Potash feldspar	Calcite	Ankerite	Pyrite	Clay minerals				
						Kaolinite	Montmorillonite	Chlorite	Illite	Total
36.8	14.8	17.8	13.10	0.1	0.3	3.2	10.8	2.1	0.9	17.1

According to Table 14, the main minerals of the deposit are quartz, feldspars, clay and calcite. In addition, pyrite (Figure 3), goethite and a small amount of ankerite are also present. Calcite frequently occurs as coarse grains on the surface of, or among particles, and blocks the pores (Figure 4).

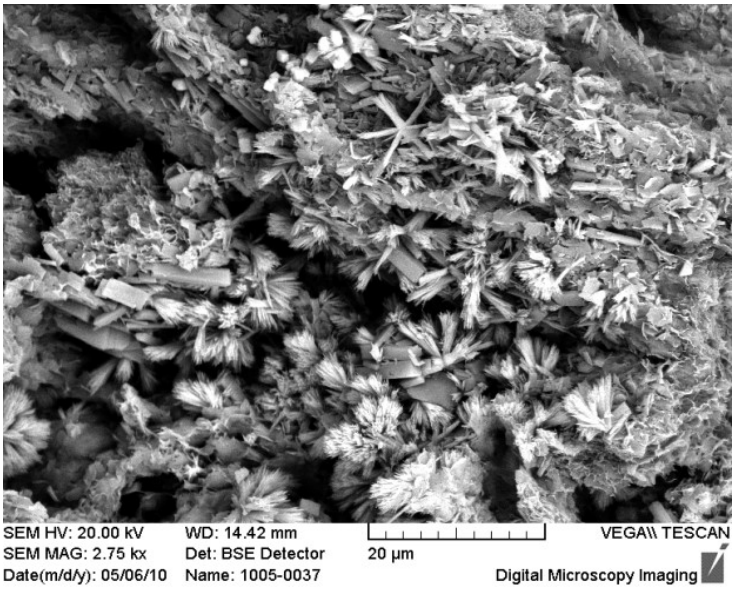

FIGURE 3. Needle-like goethite and cubic pyrite between granules (sample S43-32).

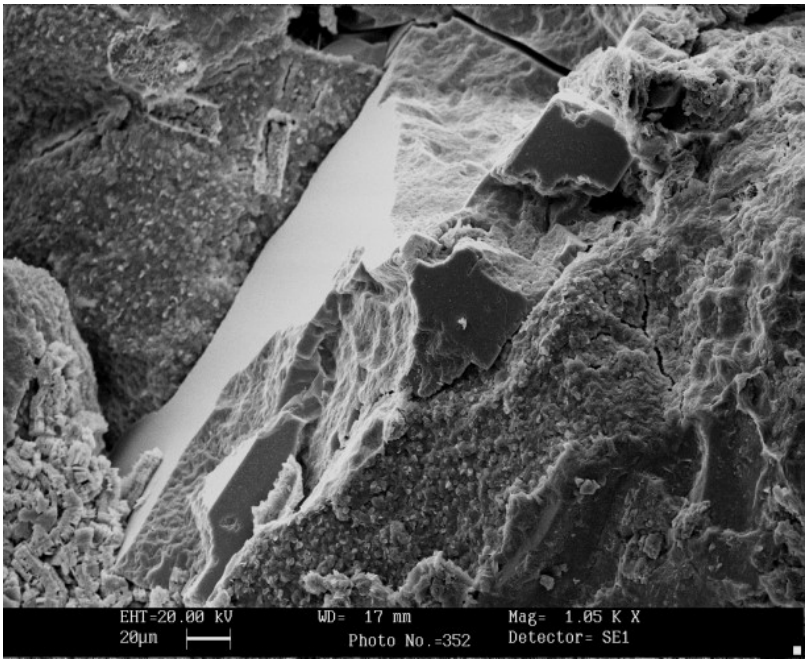

FIGURE 4. Intergranular calcite blocking pores (sample SZ01-7).

The amount of clay minerals is high which includes from highest to lowest concentrations, montmorillonite, seen as inter-granules and on the surface of particles (Figure 5); chlorite (Figure 6); kaolinite and illite.

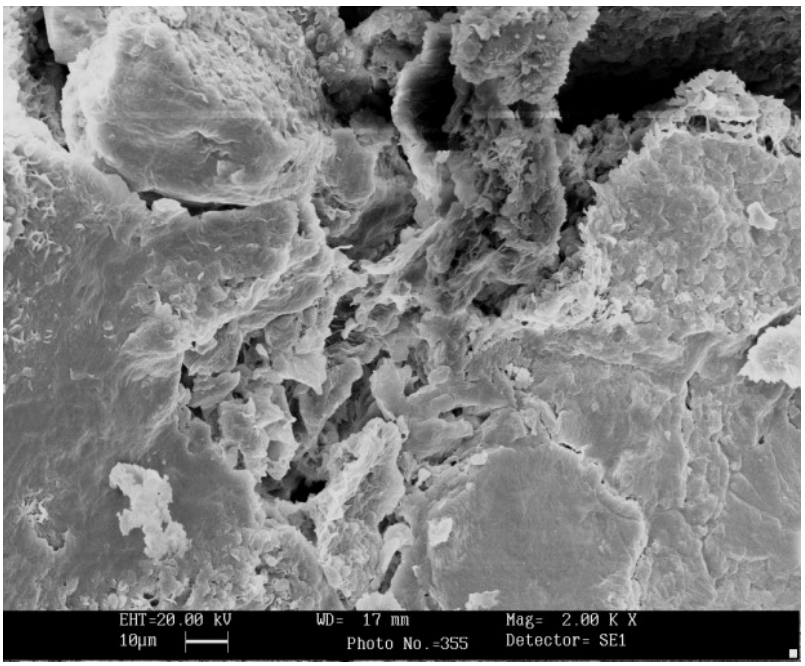

FIGURE 5. Intergranular secondary porosity and chlorite (sample SZ01-7).

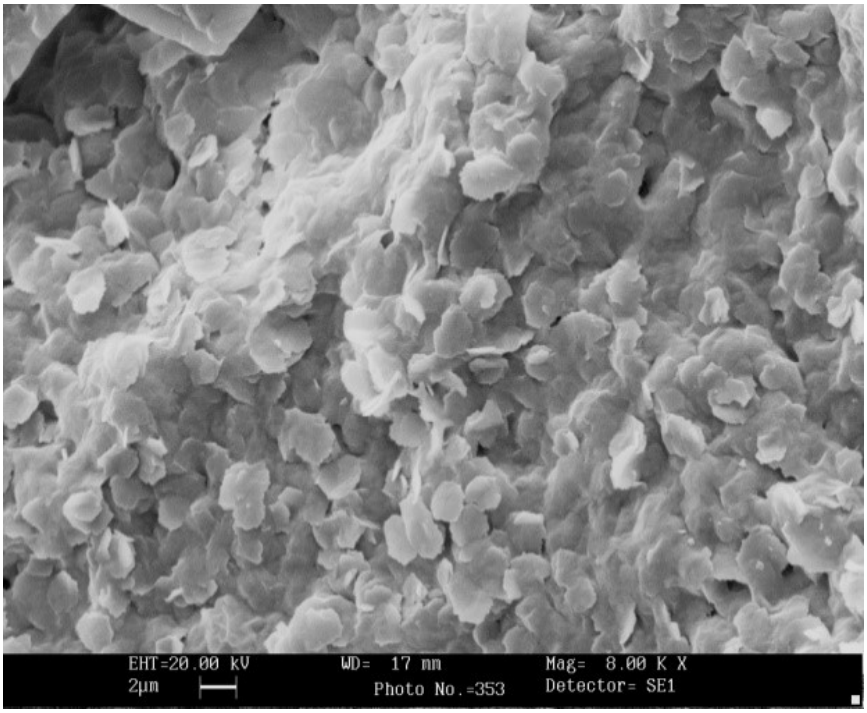

FIGURE 6. Leaf-shaped montmorillonite on the surface of grain (sample SZ01-7).

5.3.3. Relationship between reductive minerals and mineralization

The alteration of host rocks include carbonation, pyritization and argillization. Carbonation has an irregular mass-like distribution. Pyritization has occurred in grey sandstone with a dispersed and disseminated distribution. The main patterns of argillization are widely dispersed chloritization, kaolinitization, and hydromicazation. The alteration has also occurred in the mineralized bodies; therefore, the host rock and mineralization have similar compositions in terms of mineral and chemical compositions.

The relationship and distribution of the characteristic elements and uranium mineralization is shown in Figure 7. In the ore-bearing horizon as uranium increases the content of sulphur rises while the amount of carbonate decreases.

In addition, the changes of characteristic elements in different zones were investigated. Low-valence sulphur is low in the completely oxidized zone and in the ancient oxidation zone with values of 0.14% and 0.12% (Table 15). The values of the original reductive zone and redox transition zone are 0.31% and 0.39% respectively, over two times larger than those of the former, and are highest in the mineralization. The result reveals a close relationship between the uranium mineralization and the S^{2-} contents.

The changing trend of total organic carbon (TOC) is similar to that of sulphur with the highest in the redox transition zone, the next highest is in the originally reduced zone, and the lowest in the completely oxidized zone. This indicates that in the completely oxidized zone the organic debris

has been consumed by oxidative combustion. The TOC in grey sandstone and mineralization are between 0.24–0.33 % which is higher than the values in other rocks.

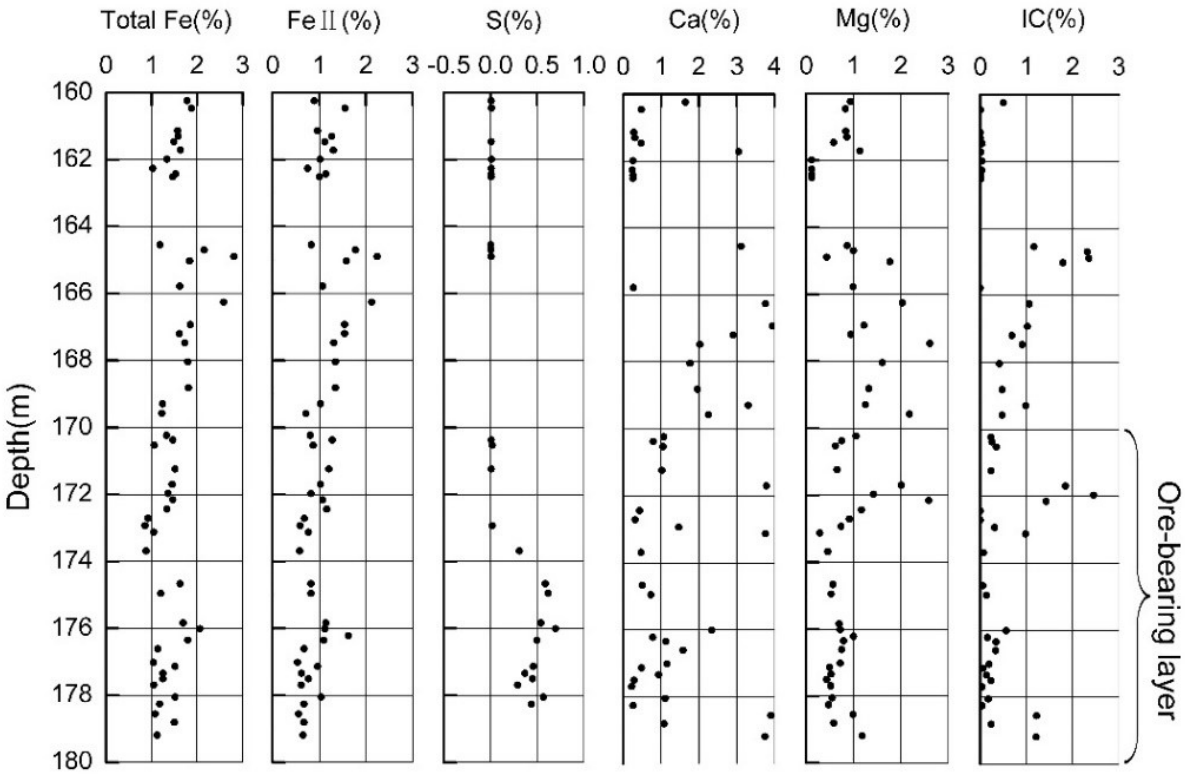

FIGURE 7. Longitudinal distribution of characteristic elements in well S43. IC=inorganic carbon.

TABLE 15. CHARACTERISTIC ELEMENTS OF DIFFERENT ZONES IN SHASHAGETAI DEPOSIT

Lithology	TOC (%)	∑S(%)	S^{2-}(%)	Fe^{2+}(%)	Fe^{3+}(%)	Fe^{2+}/Fe^{3+}
Completely oxidized zone (green sandstone)	0.16	0.30	0.14	1.44	0.77	1.86
Redox transition zone (ores)	0.33	0.63	0.39	1.31	0.94	1.39
Ancient oxidized zone residue (red calcareous sandstone in main)	0.19	0.36	0.12	1.00	0.97	1.03
Original reduced zone (grey sandstone)	0.24	0.67	0.31	1.28	0.95	1.35

Uranium in absorbed forms is associated with carbon plant debris, partially oxidized ilmenite and clay minerals in the redox transition zone. They mainly reside in the matrix or on the edge of ilmenite. The content of uranium in carbon plant debris can reach a high of 10.13–12.42%. The contents in smectite and chlorite are 1.67–4.57% and 1.73–2.61%, respectively. Uranium is also found on the edges of pyrite. The uranium minerals are intimately associated with pyrite and disseminated asphalt-bearing carbon debris.

In general, the uranium mineralization mainly occurs in association with high amounts of organic matter, pyrite and clay minerals. The enrichment of uranium has a close relationship with absorption onto organic matter, clay minerals, and pyrite and for pyrite there is additionally a close association with uranium minerals.

5.3.4. Relationship between formation permeability and uranium mineralization

The upper and lower aquicludes of the Shashagetai deposit are both continuous and stable. The mineralized zones and host rock are sub-loose, and the average porosity is 24.69%. The permeability coefficient of the ore-bearing aquifer is 0.026–0.160 darcies. The upper part of the ore-bearing aquifer consists of medium- and fine-grained sandstone with poor permeability, while the middle and lower parts within which ores occur, are made up of coarse and medium to coarse-grained sandstone with moderate permeability.

Carbonate content is a key factor relating to the amount of permeability of the formation (Figure 8). Uranium mineralization has mainly developed in locations which have relatively high permeability, low carbonate content and are rich in sulphur (Figures 7 and 8). The uranium mineralization also has a close relationship with sulphur.

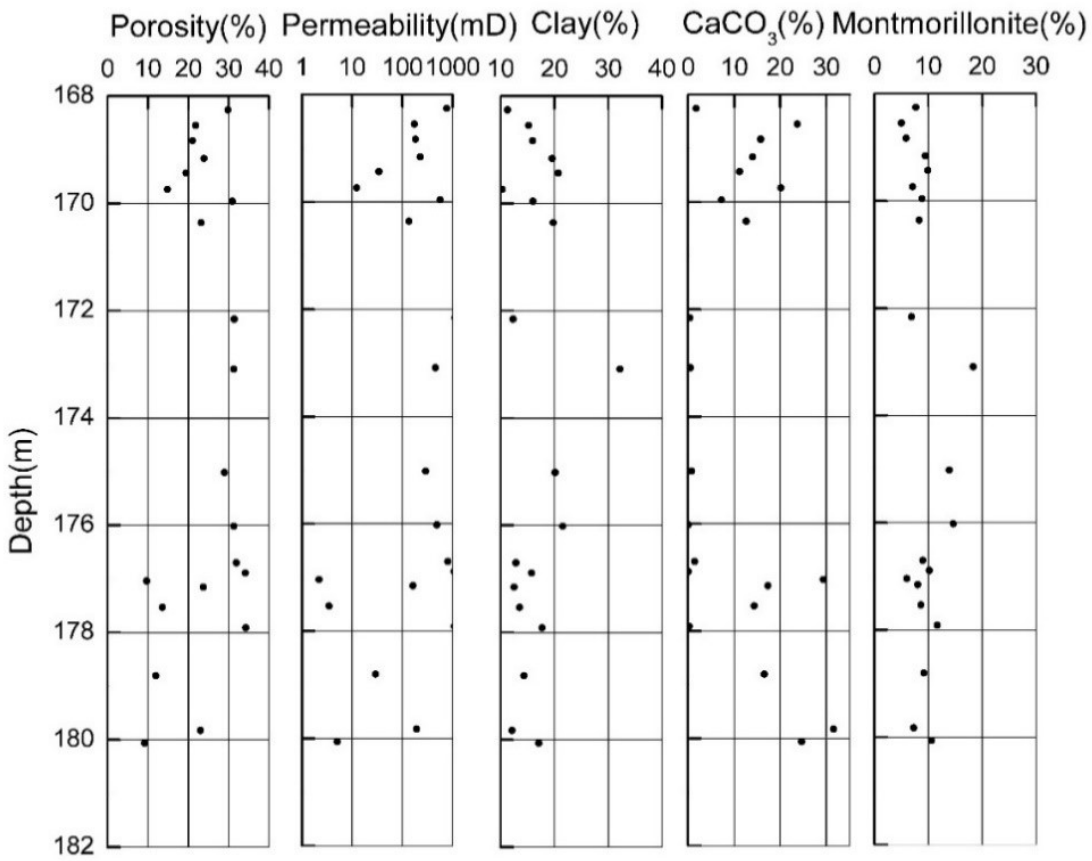

FIGURE 8. Longitudinal distribution of porosity, permeability and cements in well S43.

6. BAYANWULA URANIUM DEPOSIT

6.1. Geological setting

The Bayanwula deposit is located in the western Manite depression of the Erlian Basin. The Erlian Basin is in the suture of the Asian plate and Siberian plate, located in the north-central Inner Mongolia Autonomous Region. The elevation of the deposit is about 900–1100m. The eastern terrain, which was affected by the lava plateau of Abaga county, is relatively higher than the western part [16]. Groundwater flows from east to west and the topography of the deposit is flat.

The deposit is associated with Jurassic, Cretaceous, Paleogene, Neogene, and Quaternary sedimentary strata [17]. The Lower Jurassic is composed of a set of volcanic clastic rock layers. The Upper Cretaceous is absent and the Lower Cretaceous is the main sedimentary host of the deposit. Paleogene and Neogene rocks are not common in the region.

Based on lithologies and sedimentary environment, the Lower Cretaceous strata can be divided into Aershan Formation (Fm), Tengger Fm and the Saihan Fm. The Saihan Fm is the main ore-host and can be divided into two parts, the upper member and lower member, with conformable contact [18]. The lower member of Saihan Fm (K_1s^1) was formed in a fault-depression depositional system during the conversion period, with alluvial fan, braided river and delta sedimentary environments.

The upper member of Saihan Fm (K_1s^2) is the main fluvial system within the sedimentary basin. The general direction of the ancient river valley was from the southwest to the northeast, and the formation received materials continuously from the side uplift. The main sedimentary environment is a braided river or braided river delta. The Bayanwula deposit lies in the middle of an ancient river valley in a braided river system.

6.2. Uranium deposit and mineralization characteristics

The upper member of the Saihan Formation, ore-bearing stratum, is a set of braided river sand bodies which were formed by constant accretion of multi-material sources. The strip-like sand bodies spread northeast and accumulated thicknesses of between 30–100 m. Sandstone is coarse-to-fine grained and comprises a fining-upward sequence. Generally, the sandstone also contains fine gravel. The structural features include crossbedding, argillaceous cementation and massive structure and unconsolidated sandstones with good permeability.

The main mineralized body of the Bayanwula deposit is large in scale, with a NE trend of 8100 m in length and 100–800 m in width. It is relatively continuous in plan, but it shows the roll and tabular shapes in cross-section. The thickness of the body is generally 0.50–22.05 m, with an average value of about 6.80 m. Grade is between 0.0108–0.2477% U, with an average of 0.0201% U. Uranium content in kilogram per square meter is 1.01–7.36 kgU/m^2, with an average of 2.27 kgU/m^2.

Uranium occurs mainly as forms of adsorbed uranium with lesser amounts of uranium minerals and uranium-bearing minerals.

The main associated elements are Re (rhenium), Se (selenium), Mo (molybdenum), Sc (scandium) and V (vanadium). Their contents are greater than the values of the average crustal values, indicating enrichment of these five elements.

Results of whole-rock U-Pb isotopic dating indicate that the age of uranium mineralization is 7 ± 0 Ma and 44 ± 5 Ma. This corresponds to the Neogene (N1), and Eocene (E2) metallogenic epochs, respectively [19].

6.3. Result and discussion

6.3.1. Chemical composition

According to the results of chemical analysis (Table 16), the main component in the ores of the Bayanwula deposit is SiO_2.

TABLE 16. CHEMICAL COMPOSITION OF MINERALIZED SAMPLES (%)

Lithology	SiO_2	FeO	Fe_2O_3	Al_2O_3	TiO_2	MnO	CaO	MgO	P_2O_5	K_2O	Na_2O	Loss on incineration	No. of samples
Sandstone	76.50	0.86	2.41	9.94	0.42	0.02	0.88	0.61	0.08	3.65	2.31	2.82	215

The characteristic components FeS_2, CO_2, and total organic carbon (TOC), were analysed and the results are shown in Table 17 and Table 18. Mineralized samples are rich in reducing minerals/matter. The CO_2 values and carbon, which occurs mainly as organic carbon is low. The total carbon in mudstones are higher than that of sandstones indicating that muddy siltstone and mudstone are more reducing than sandstone.

TABLE 17. CHARACTERISTIC COMPONENTS IN WELL BTZ-01

Sample	Depth(m)	Lithology	FeS_2 (%)	CO_2 (%)	TOC (%)	Loss on incineration (%)	U (%)
BTZ-01-31	111.60-111.80	Yellow medium-coarse grained sandstone	0.028	<0.01	0.029	0.43	0
BTZ-01-1	117.30-117.50	Grey gravelly Fine-grained sandstone	0.197	<0.01	0.063	0.20	0.0173
BTZ-01-4	117.80-117.95	Grey fine-grained sandston	0.125	<0.01	0.044	1.01	0.0103
BTZ-01-12	120.75-120.90	Grey gravelly Fine-grained sandstone	0.192	<0.01	0.232	1.64	0.0143
BTZ-01-18	124.15-124.30	Grey muddy siltstone	0.466	<0.01	0.057	1.36	0.0086
BTZ-01-29	127.70-127.90	Grey mudstone	0.708	<0.01	0.423	2.14	0.0072

6.3.2. Mineralogy

The Bayanwula deposit is composed mainly of clastic rocks with small amounts of clay minerals, organic carbon and pyrite [20].

TABLE 18. CHARACTERISTIC COMPONENTS IN WELL BTC-01

Sample	Depth (m)	Lithology	Total C (%)	Inorganic C (%)	FeS_2 (%)	U (%)
BTC-01-48	110.2–110.4	Light yellow gravelly sandstone	0.53	0.08	<0.02	0.003
BTC-01-6	116.9–117.1	Grey medium-grained gravelly sandstone	0.48	0.07	0.398	0.009
BTC-01-10	117.8–118.0	Grey muddy sandstone	0.28	0.05	<0.02	0.009
BTC-01-18	119.4–119.6	Grey muddy fine-grained sandstone	0.25	0.04	<0.02	0.009
BTC-01-22	120.2–120.4	Grey fine-grained sandstone	-	-	<0.02	0.007
BTC-01-28	121.2–121.4	Grey muddy fine-grained sandstone	0.19	0.04	0.286	0.011
BTC-01-33	122.1–122.3	Grey muddy sandstone	-	-	0.158	0.007
BTC-01-39	122.8–123.0	Grey muddy fine-grained sandstone	0.20	0.04	0.069	0.010
BTC-01-44	123.5–123.7	Grey muddy fine-grained sandstone	0.21	0.02	0.497	0.007
BTC-01-47	126.3–126.5	Mudstone with some carbon	0.71	0.03	<0.02	0.017

Clastic rocks in the mineralized zone consists of quartz, feldspar, debris, organic carbon, matrix and cements (Table 19).

TABLE 19. COMPOSITION OF CLASTIC ROCKS OF THE BAYANWULA DEPOSIT

Ore type	Composition of clastic rock (%)								Matrix (%)		Cements (%)		No. of samples
	Quartz		Feldspar		Debris		Organic carbon						
	Range	Ave.	Range	Ave.	Range	Ave.	Range	Ave.	Range	Ave.	Range	Ave.	
Sandstone	32.4–65.9	56.2	15.4–36.4	22.9	0–19.4	4.9	0–1.6	0.4	0–20.0	10.3	0–28.0	5.2	20
Conglomerate	6.8–30.8	14.4	8.5–13.8	13.7	31.2–77.4	58.1	0–2.7	0.4	0–12.0	7.8	1–15.0	5.5	10

Quartz in clasts is mainly derived from granite, occurring as quartz crystals and polycrystalline quartz. Feldspar occurs mainly as lath-like crystals with minor plagioclase and microcline. Debris mainly comes from granites with lesser amounts contributed from tuff, rhyolite, slate, and occasionally mudstone debris.

Clay minerals mainly occur as matrix. Clay minerals consist of smectite, illite, llite/smectite (I/S) and minor kaolinite, which occur as curved sheets or fragment-like aggregates in clastic particles (Figures 9 and 10). According to the results of Liu [17] and the analyses made in this study (Table 20), clay mineral abundance is relatively high in the mineralization zone and grey sandstone zone with smectite and/or I/S comprising the majority. Clay minerals tend to adsorb uranium and uranium absorbed onto clay was commonly identified with the electron microscope.

6.3.3. Relationship between reductive substances and mineralization

The reductive substances in ores are mainly organic carbon and FeS_2. TOC in mineralized samples is higher than that of the host rock, as shown in Tables 17 and 18. Carbonized plant debris occurs as veinlets and as root-shaped fragments, most of which have a clear cell structure (Figures 11 and 12). Veinlets of carbon debris consists of opaque and black coloured carbonized matter occurring along the stratification. The root-shaped carbon debris is randomly distributed. It is opaque-translucent and black-dark brown coloured and consists of carbonized matter and brown matter.

TABLE 20. CLAY MINERALS IN THE BAYANWULA DEPOSIT

No.	Total clays (%)	Relative content (%)			Ratio of I/S (%S)
		K	I	I/S	
1	17.0	12	17	71	70
2	18.2	12	14	74	60
3	16.3	8	15	77	65
4	10.4	8	14	78	70
5	16.0	6	11	83	70
6	16.9	10	10	80	60
7	16.3	10	15	75	55
8	15.5	5	8	87	65
9	16.5	15	17	68	55
Average	15.9	10	13	77	63

* K-Kaolinite, I-Illite, S-Smectite, I/S Mixed layer of illite and smectite

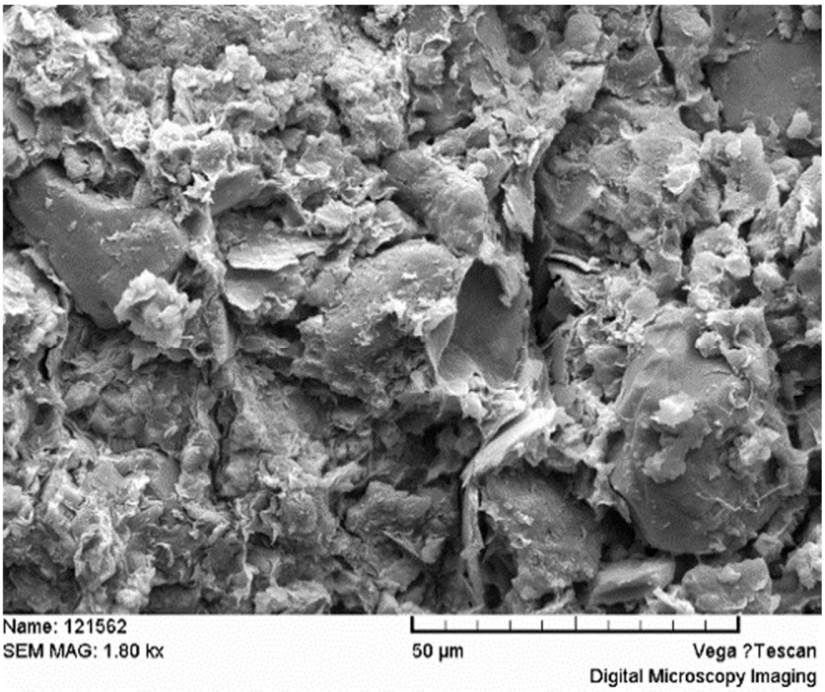

FIGURE 9. Curved sheet of smectite and illite in medium to coarse-grained sandstone.

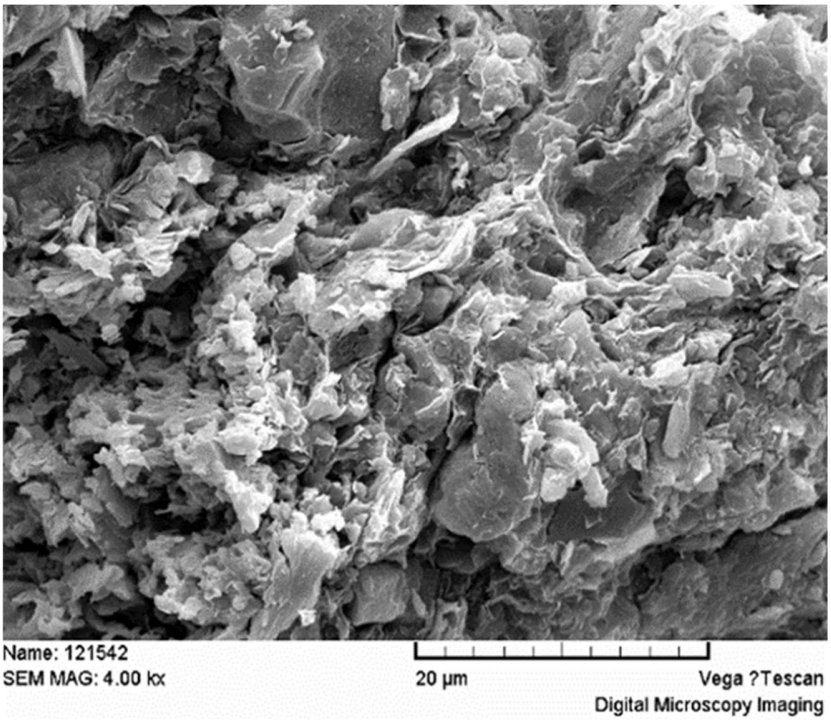

FIGURE 10. Curved fragments of smectite and illite in fine-grained sandstone

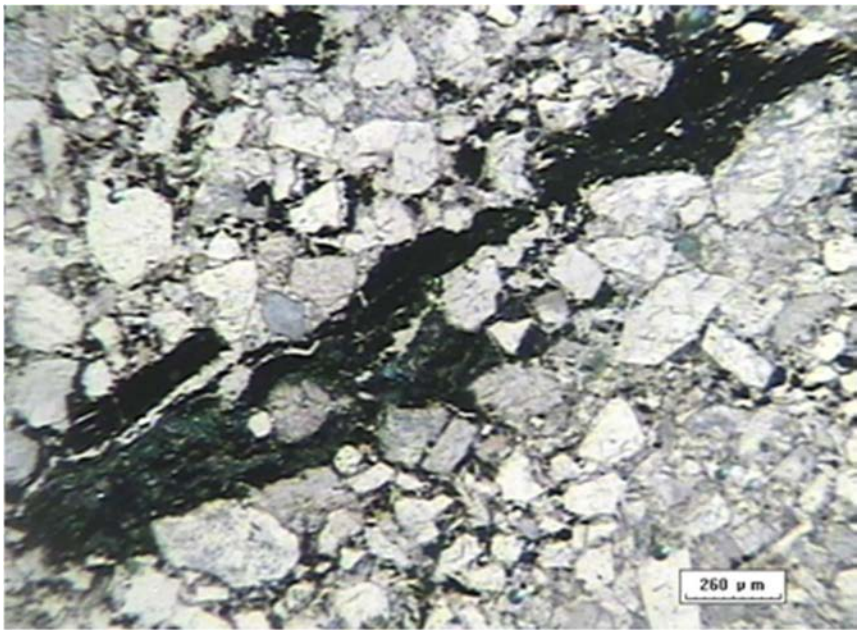

FIGURE 11. Veined carbon debris.

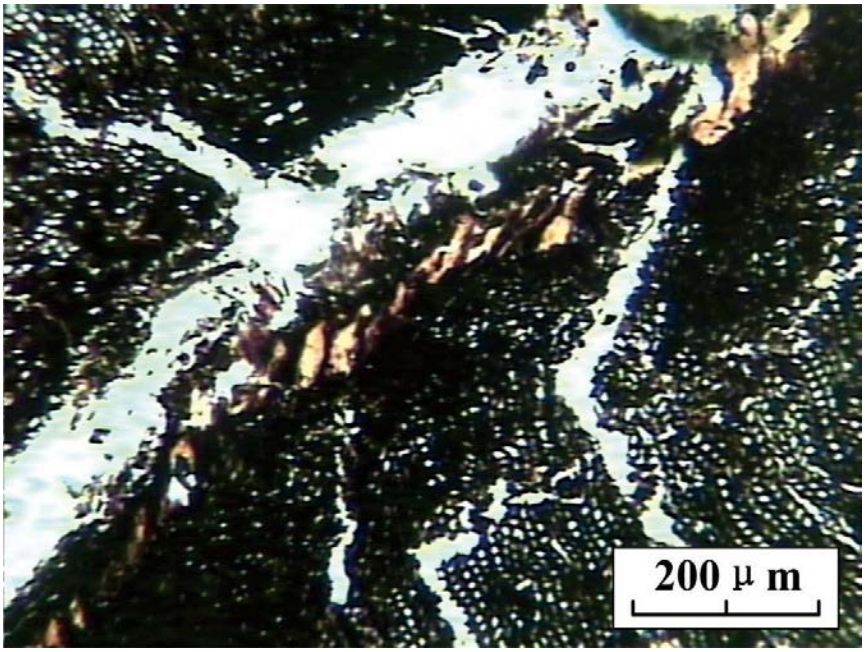

FIGURE 12. Carbon debris with cell structure.

Research shows that iron hydroxides in grey sandstone of the redox transition zone basically disappear, and the carbonized plant debris is preserved. The colour of the rock is mainly grey and light grey, partially blue-grey and green-grey. Carbon is mainly organic carbon with an uneven

distribution as shown in Tables 17 and 18. There is a trend that the higher the contents of organic carbon, the richer the uranium is. Scanning electron microscopy images show that uranium occurs in carbon debris of clastic rocks, which indicates that the enrichment of uranium was related to the adsorption and reduction by organic matter.

Fine-grained pyrite was observed in the grey coloured sand body. There is a higher content of pyrite in the mineralized samples with a value of about 1%, which can reach much higher values, with a range of 10–28%. The majority of pyrite occurs as cement. The single pyrite crystals occur as dusty, micro-spherical, granular, and cube shapes. The aggregates show a variety of shapes including strawberry, nodular, veinlets, dendrite, and massive. As shown in Table 17, the FeS_2 and uranium contents in sandstone are positively correlated to each other, and the contents of uranium in samples of BTZ-01-4, BTZ-01-12 and BTZ-01-1 increase with increasing FeS_2. The results of electron probe analysis show that the uranium minerals are usually closely associated with pyrite (Figure 13), and pyrite cement is also an important substrate for the adsorption of uranium.

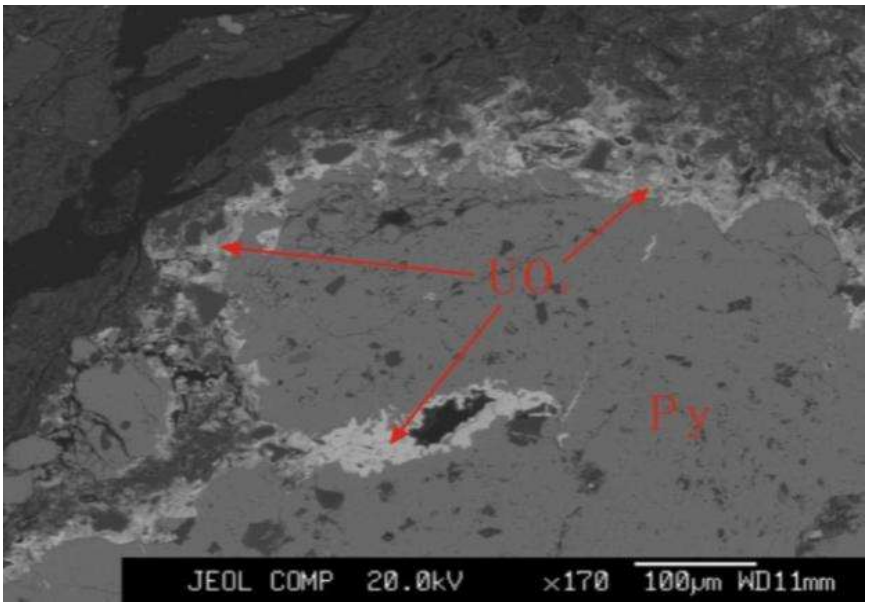

FIGURE 13. Co-occurrences of pitchblende (UO_2) and pyrite (Py).

6.3.4. Relationship between heterogeneous permeability and mineralization

Mineralogical studies show that sandstone-type mineralization is dominated by quartz, and conglomerate-type is dominated by clastics. Clay minerals account for about 10%, and clastics are well sorted. The ore-bearing aquifer has very good permeability and a good hydraulic conductivity of 2.90–13.20 darcies (Table 21).

TABLE 21. HYDROGEOLOGICAL PARAMETERS OF THE BAYANWULA DEPOSIT

Well No.		Thickness of aquifer (m)	Static water table (m)	Water-head (m)	Drop-down (m)	Water yield		Specific yield (l/s·m)	Hydraulic conductivity (darcies)	Conductivity coefficient (m^2/d)
						l/s	m^3/d			
ZK399-105	CDII-1	46.5	19.72	48.38	10.78	4.78	412.80	0.44	2.90	130.70
SWZK383-97		63.6	18.99	40.01	3.83	5.41	467.32	1.41	5.97	379.69
BZK367-85	CDIII-1	38.8	21.17	64.24	2.17	4.73	408.00	2.18	13.20	483.10
	CDI-2	59.7	20.92	61.48	3.18	5.41	467.28	1.70	9.50	569.48
SWZK335-83		75.5	26.02	71.48	0.40	1.57	135.60	3.92	7.16	514.10
CDI-2		58.1	/	/	/	/	/	/	11.27	654.49

Hydraulic conductivity was determined for core samples taken from mineralization, host rocks, and the lower and upper confining layers of well SWZK335-83 (Table 22). The results show that the hydraulic conductivity of host rocks of the aquifer is 0.1–5.15 darcies, and the grain size of the rocks are positively related to the hydraulic conductivity. The hydraulic conductivity varies greatly, showing strong heterogeneity in the formation. According to observations in the field, the structure and tectonic setting and mineral composition of the mineralized zones are basically the same as the host rock. Notably some parameters could not be obtained because the column cores for permeability testing could not be made for the unconsolidated samples. Nevertheless, it can be concluded that the mineralized and host rocks have the same characteristics of a positive correlation between the grain size of the sandstone and hydraulic conductivity.

The grain size distribution of different grades was determined (Table 23). The results indicate that the grade is closely related to the particle size distribution. Samples with higher grade are mainly hosted by mixed sandy conglomerates and fine-grained sandstones, while samples with lower grade are sandy conglomerates.

TABLE 22. RESULTS OF PERMEABILITY TESTING OF SAMPLES FROM WELL SWZK335-83

No.	Sample	Sampling depth (m)	Lithology	Hydraulic conductivity (darcies)	Remarks
1	BS2004-10	96.60	Grey-green mudstone with sand and gravel	/	Upper confining layer
2	BS2004-5	110.80	Grey medium-grained sandstone	0.15	Host rock
3	BS2004-8	124.50	Grey sandy conglomerate	Broken	Ores
4	BS2004-9	127.00	Grey gravelly medium-grained sandstone	0.2	Host rock
5	BS2004-1	131.80	Grey-black muddy fine-grained sandstone	0.015	Ores
6	BS2004-2	142.50	Grey sandy conglomerate	0.83	Host rock
7	BS2004-3	143.10	Grey fine-grained sandstone with carbon debris	0.10	Host rock
8	BS2004-4	146.30	Grey gravelly coarse-grained sandstone	5.15	Host rock
9	BS2004-6	159.10	Grey fine-grained sandstone	Broken	Ores
10	BS2004-7	152.20	Grey sandy conglomerate	1.16	Host rock
11	BS2004-11	177.85	Grey-black mudstone	0.002	Lower confining layer

TABLE 23. GRAIN SIZE DISTRIBUTION WITH URANIUM GRADE

Grade (%)	Lithology				No. of samples
	Gravel with sandstone (%)	Medium-coarse grained sandstone (%)	Medium-fine grained sandstone (%)	Fine grained sandstone (%)	
＞0.03	33.33	22.22	19.44	25.00	36
0.02 – 0.03	33.33	20.83	16.67	29.17	72
0.01–0.02	29.25	24.09	23.87	22.80	465
0.005–0.01	51.50	17.50	18.50	12.50	200

Table 23 shows that grades of uranium mineralization are closely related to the heterogeneity of the sandstone. Uranium mineralization mainly occurs in the sandy conglomerate and medium-coarse grained sandstones that are weakly consolidated and have good permeability. These coarse-grained ore-bearing rocks are mixed with some fine-grained sandstone with greater heterogeneity. In the fine-grained sandstones with relatively low permeability, the uranium grade is relatively low.

7. QIANJIADIAN URANIUM DEPOSIT

7.1. Geological setting

The Qianjiadian uranium deposit is located in the north of the Kailu depression of the Songliao Basin, which is a NNE trending long and narrow depression about 100 km long, 9–20 km wide and with an area of 1280 km^2 [21].

Kailu depression is in the southwest part of the Songliao Basin, and the central part of the depression is covered by Tertiary and Quaternary strata with altitudes of 200–300 m and elevation differences of 10–20 m. A set of Palaeozoic metamorphic rocks form the basement of the basin. The provenance area consists of Mesozoic volcanic rocks, Hercynian and Yanshanian granites and Palaeozoic metamorphic rocks. The cap rocks of the basin are composed of a set of Lower Cretaceous rift lacustrine sedimentary rocks, Upper Cretaceous fluvial and lacustrine sedimentary rocks, the Neogene Dagan Formation (N_1d) and loose sediments of the Quaternary period [19].

The main provenance area of the Qianjiadian deposit is the west slope of Zhangguangcai range which lies to the southeast of Qianjiadian. The paleo uplift comprised of acidic volcanic rocks, ancient crystalline rocks and metamorphic rocks, nearby, or further mountainous regions provided abundant uranium sources for the deposit. The widely developed braided river sand body provided a good aquifer for oxygen- and uranium-containing water, and also provided favourable conditions for the formation of smooth paleochannels from the recharge zone and a runoff zone to the discharge zone [22].

7.2. Uranium deposit and mineralization characteristics

The ore-bearing strata in the Qianjiadian deposit is the Cretaceous Yaojia Formation which has a typical mudstone-sandstone-mudstone sequence. The Yaojia Formation can be divided into two rhythmically graded sedimentary sequences, namely the lower member and the upper member, with similar thicknesses of 60–80 m. Mineralization develops mainly at the base, with a small part in the top and middle of the lower member of the Yaojia Formation. The overall strike of the mineralized sand is 37° NNE, and the trend is northwest with a dip angle of less than 10°.

The ore-bearing rocks are mainly fine-grained sandstone and medium-grained sandstone and uranium mineralization is lower in the siltstone and mudstone. The main clastic components in the ore-bearing sandstone are quartz, feldspar and minor debris, while the matrices are mainly comprised of clay minerals and the cements are carbonates. The mineralized body is 1100–1300 m in length and 380–1000 m in width and has a mainly tabular morphology but can also be lenticular and a combination of tabular and lenticular. The burial depth of the mineralized body is 251.8–298.31 m with a thickness of 6.46–15.75 m, an average grade of 0.03% uranium, and an average uranium content by square meter of 4.95 kgU/m^2.

The occurrences of uranium in the Qianjiadian deposit are absorbed uranium, uranium minerals and minor uranium-bearing minerals. The uranium minerals are pitchblende and the absorbed uranium mainly occurs in organic matter and clays, and the uranium-bearing minerals are mainly detrital zircons in sandstone. The ratio of U^{4+}/U^{6+} in the lower member of the Yaojia Formation is 0.266–1.116 and the average value is 0.761.

The associated elements of uranium in ore-bearing sandstone, such as Y, V, Sc, Se and Re, are relatively high, which indicates these elements were enriched during uranium mineralization [23]. The content of Se increased not only in the transition zone but in the oxidized sandstone, indicating that a certain amount of Se was precipitated in the oxidation zone and transient zone. Re is mainly enriched in the transition zone and the original reduced zone, and its content is much higher than in the oxidation zone.

U-Pb isotopic dating of mineralized samples of the grey muddy fine-grained sandstone and grey siltstone from the lower member of the Yaojia Formation yields an age of 96±14 Ma and the age for mineralized samples from the light grey fine-grained sandstone is 67±5 Ma. These two ages correspond to the middle and late stages of the Late Cretaceous. The middle of the Late Cretaceous is the syngenetic sedimentary and mineralization period, and the age of mineralization is the same as that of the sediments of the Yaojia Formation which is about 85 Ma.

7.3. Results and discussion

7.3.1. Chemical composition

The results of chemical analyses of samples from the Qianjiadian deposit are listed in Table 24.

TABLE 24. CHEMICAL COMPOSITIONS OF MINERALIZED SAMPLES (UPPER AND LOWER YAOJIA) AND HOST ROCK

Stratum	No. of samples	U% ($\times10^{-4}$)	SiO_2 (%)	Al_2O_3 (%)	CaO (%)	MgO (%)	K_2O (%)	Na_2O (%)	Fe_2O_3 (%)	FeO (%)	TiO_2 (%)	MnO (%)	P_2O_5 (%)	Loss on incineration (%)
Upper Yaojia	131	185.94	72.30	11.47	2.67	1.00	3.50	1.09	1.24	1.16	0.45	0.10	0.12	4.34
Lower Yaojia	195	230.08	71.88	16.82	2.93	1.21	3.24	0.99	1.29	1.12	0.41	0.07	0.12	5.00
Average	-	212.34	72.04	14.67	2.82	1.12	3.34	1.03	1.27	1.14	0.43	0.08	0.12	4.73
Host rock	206	< 100.00	72.54	11.23	2.56	1.09	3.47	1.05	1.07	1.10	0.41	0.08	0.11	-

As shown in Table 24, the average contents of SiO_2 and Al_2O_3 in the mineralized samples are 72.04% and 14.67%, respectively, indicating that the rock type may be arkose. The average contents of K_2O and Na_2O are 3.34% and 1.03%, respectively, which also means feldspar and/or clays are relatively high. The average contents of Fe_2O_3, FeO and CaO+MgO (CaO>MgO) are 1.27%, 1.14% and 3.95%, respectively, showing that there are a certain amount of iron minerals and carbonate (as calcite) in ores in accordance with a larger loss on incineration.

The composition of the upper member of Yaojia Formation is similar to that of the lower member. The average content of SiO_2 in the lower member of Yaojia Formation is slightly lower than that of upper member. However, Al_2O_3 content in the lower member of Yaojia Formation is significantly higher, which indicates higher amounts of detrital feldspar and lower quartz in comparison to the lower member.

Table 24 shows that the general chemical compositions of mineralization and the host rock are similar and the composition of the host rock is almost identical to that of upper member ores. The Al_2O_3 contents of the host rock is relatively low, indicating that quartz is higher. The contents of FeO in mineralized and host rocks are very similar, while the content of Fe_2O_3 in the mineralization is higher than in the host rock.

7.3.2. Mineralogy

The detrital minerals of the ore-bearing sandstone are mainly quartz, feldspar and minor debris. The matrix consists of clay minerals and cementing materials comprises of carbonate, iron and manganese minerals.

The main components of mineralization are quartz, potash feldspar, plagioclase, and relatively high amounts of clay minerals. Accessory minerals include ankerite and calcite. Heavy minerals include garnet, zircon, ilmenite, titanomagnetite, tourmaline, staurolite, epidote, kyanite, biotite, titanite and rutile. Authigenic minerals include pyrite, limonite, barite and anatase.

Mineralogical analysis shows that the main minerals in mineralized samples are quartz, potassium feldspar, plagioclase and clay minerals (Table 25). Carbonates are mainly dolomite and calcite with minor pyrite (Figures 14 and 15).

TABLE 25. MINERALOGY OF THE QIANJIADIAN URANIUM DEPOSIT (%; I/S= ILLITE/SMECTITE; NUMBER OF SAMPLES = 46)

Quartz	Potash feldspar	Plagioclase	Calcite	Dolomite	Pyrite	Clay minerals and relative contents				
						12.5				
61.6	11.7	9.8	1.2	3.0	0.14	Smectite	I/S mixed layer	Kaolinite	Chlorite	Illite
						1.9	12.7	73.9	2.4	8.7

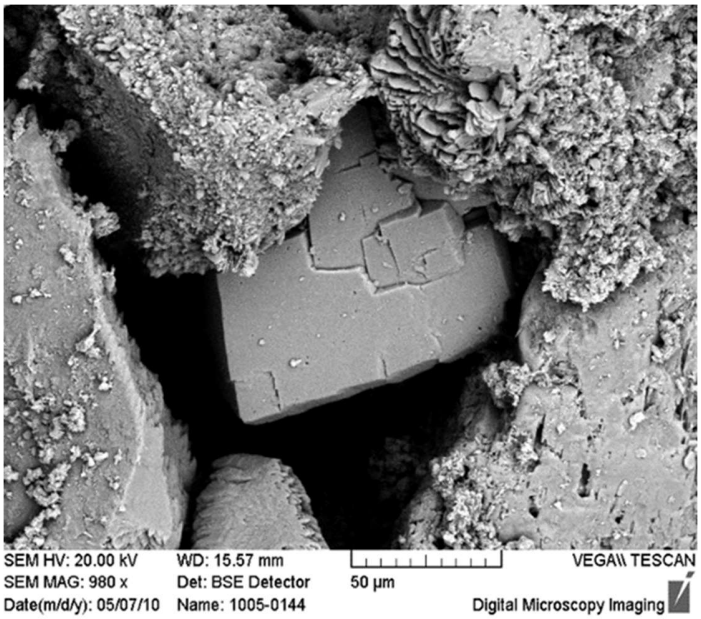

FIGURE 14. Intergranular authigenic calcite crystal and flaky kaolinite (sample TL-13).

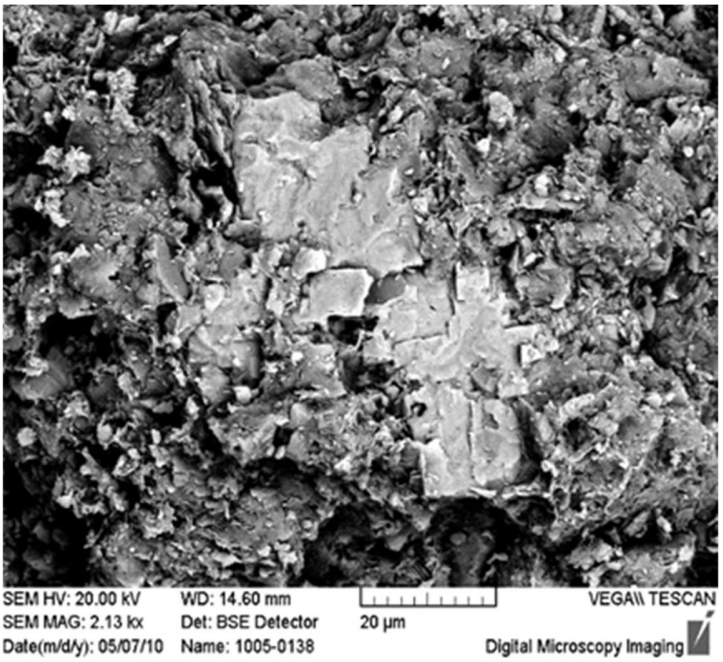

FIGURE 15. Clumpy pyrite found in clay minerals (sample TL-10).

Clay minerals are relatively abundant, and the majority is kaolinite which occurs as flakes and as vermicular grains (Figures 16 and 17). Illite is also present and occurs in flake form.

Pyrite can be divided into two types of forms: an aggregation of idiomorphic granular and powder crystals; and pyrite with a colloidal texture. Microscopically the aggregate pyrite of idiomorphic granular and powder crystals occurs in both the matrix and cementing material. Colloidal pyrite occurs with pitchblende as small veins. In some mineralized samples, authigenic minerals which

are mainly pyrite account for 44.9–87.3% of all the heavy minerals, indicating that the ore-bearing rocks have undergone strong epigenetic reduction.

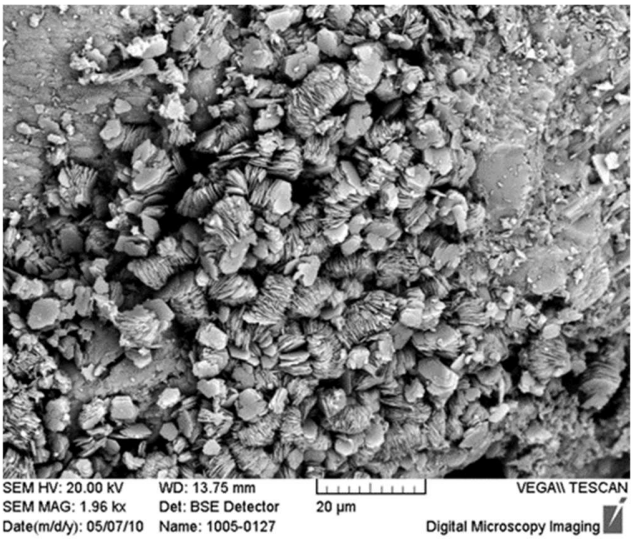

FIGURE 16. Intergranular flake and wormlike kaolinite (sample TL-1).

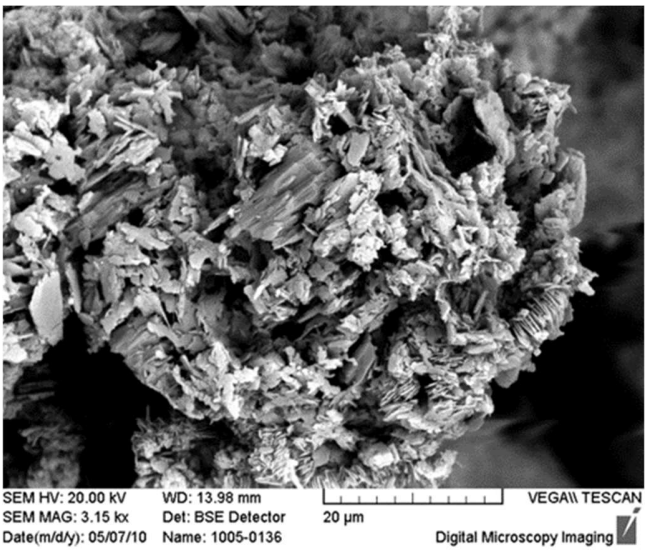

FIGURE 17. Leaching, dissolved pore of potash feldspar and kaolinite on the edge (sample TL-5).

7.3.3. Relations between reductive minerals and mineralization

Table 24 shows that host rocks and mineralization in the upper and the lower member of the Yaojia Formation are similar to each other in overall chemical composition but the average contents of Al_2O_3 and Fe_2O_3 are lower in the host rocks. In addition, similar values of FeO in host rock and mineralization are observed. The lower Fe_2O_3 and similar FeO values in the host rocks reflect a

stronger reductive atmosphere than that of the mineralization, which seems to be inconsistent with the general metallogenic principle. The ratios of Fe_2O_3/FeO (0.97–1.38) in sand bodies show the state of redox environment. The average ratio of Fe_2O_3/FeO of the ore-bearing stratum is 1.11, which means the state of the stratum is tending to partial oxidation in the redox transition zone.

In order to understand the redox environment of the deposit clearly, Chen et al. [23] conducted an analysis of samples from the oxidation zone, redox zone and the protogenic reductive zone and the study reported that ratios of Fe_2O_3/FeO in mineralization are higher than those in grey-white sandstone (host rocks) and original grey sandstone (reduction zone). This is consistent with the results of this study (refer to Table 24) and indicate that the contents of total sulphur and organic carbon are highest in the grey ore-bearing sandstone. This indicates that total sulphur and organic carbon play important roles in mineralization. All the described phenomena may also have a close relationship with reduction by hydrocarbons, oil and gas [24–25].

The average contents of total organic carbon (TOC) and sulphur (S) in the mineralized samples which are about 0.23% and 0.22%, respectively, and are not notably high. However, a notable trend is that the greater the TOC and S, the higher the grade of the uranium (Table 26).

TABLE 26. CHARACTERISTIC PARAMETERS OF THE QIANJIANDIAN DEPOSIT

Sample No.	U (%)	CO_2 (%)	TOC (%)	S (%)	FeO (%)	Fe_2O_3 (%)	FeO/Fe_2O_3
q-1	0.030	1.29	0.02	0.14	1.17	2.07	0.56
q-2	0.092	4.35	0.35	1.25	1.89	4.20	0.45
q-3	0.042	1.49	0.07	0.34	1.20	2.25	0.53
q-4	0.021	1.29	0.02	0.14	1.17	2.07	0.56

Therefore, TOC and sulphide minerals played important roles in mineralization in the Qianjiadian deposit, while iron did not have much significance.

7.3.4. Relationship between formation permeability and mineralization of uranium

The Yaojia Formation was formed in a braided fluvial sedimentary environment. The sandstone is a feldspathic quartz type sandstone with the majority comprised of light grey and grey-white coloured fine-grained sandstones and minor medium to fine-grained sandstones, siltstones and mudstones. The formation is rich in clay minerals and generally, the permeability of this type of lithological sequence is poor. That the sand bodies are thick and that grains in the debris are rounded and relatively well sorted, however, results in a relatively uniform permeability. A mercury porosimeter test (Table 27) shows that the distribution of pores is homogeneous, and the number of large pore channels are both high and centred. The pore throats which contribute to 99% of the permeability have diameters of 2.5–16 μm and have a high ratio to total pore number of 45.75% which means that the pores are large and well sorted, leading to good connectivity and relatively uniform permeability of the ore-bearing stratum.

TABLE 27. PARAMETERS OF PORE THROAT CHARACTERISTICS

Sample No.	Pore throat radius range/μm*	Ratio to total pore number /%	Contribution to permeability /%	Mean pore throat radius /μm	Porosity /%	Permeability /10^{-3}μm^2
TL04	4.0-10.0	38.58	98.84	0.59	32.0	186
TL07-1	2.5-10.0	45.83	99.19	1.35	34.2	210
TL15-1	6.3-16.0	42.56	98.53	2.16	30.8	833
TL19	6.3-16.0	45.81	98.61	3.66	36.3	1326
TL22	6.3-16.0	51.88	99.21	7.88	39.2	3813
TL25	4.0-16.0	49.71	99.50	3.85	32.2	893
Average	2.5-16.0	45.73	98.98	3.25	34.1	1210

* Pore throat radii that affect permeability > 1% were selected. Columns 3 and 4 were derived from the number of pores in column 2 relative to the total number of pores.

A series of tests of gas porosity and permeability on the Yaojia Formation was conducted. The results show that the porosity is between 12.4% to 36.7% with an average value of 30.7%. For the lower member of Yaojia Formation, the range of permeability is 1 to 4119×10^{-3}μm^2 with an average value of 503.7×10^{-3} μm^2 while the values for the upper member are between 1 to 1508×10^{-3} μm^2 with an average value of 246.2×10^{-3} μm^2. Overall, the permeability of the lower member is significantly higher than that of upper member of the Yaojia Formation.

In addition, a comparison of permeability between the ore-bearing horizon and host rock has been carried out and the results from 6 wells are shown in Table 28. The average value of permeability of the ore-bearing horizon is 0.177 darcies and for the host rock is 0.186 darcies. The ratio of the ore-bearing horizon to host rock is 0.95 which indicates that there is good uniformity of the sand body in the Yaojia Formation and the permeabilities of mineralization and host rocks are similar.

TABLE 28. COMPARISON OF PERMEATION BETWEEN MINERALIZATION AND HOST ROCK OF QIANJIADIAN DEPOSIT (WHERE K=PERMEABILITY)

Rock type	Thickness		Thickness of aquifer		Ave. content (silt+clay) (%)	Ave. K (darcies)	K_{ore}/K_{host}
	Range(m)	Ave. (m)	Range(m)	Ave. (m)			
Ore	8.40 – 10.35	9.13	21.50 – 29.43	25.39	19.72	0.177	0.95
Host rock	12.65– 20.78	16.26			20.61	0.186	

The results above show that the sorting is good, and permeability of the sand body is homogeneous in the Qianjiadian deposit. The braided river sedimentary environment generally has good aquifer characteristics which are favourable for ore-forming processes, promoting and sustaining the movement of uranium- and oxygen-containing water. In such a way, uranium in the fluids can be reduced, adsorbed and precipitated in the target zone through continuous recharge of the aquifer. Because TOC and sulphide is uniformly distributed in the deposit, which also has good sorting and permeability properties, the uranium occurrence is usually tabular, large in size and thick. These conditions formed the Qianjiadian uranium deposit with a thickness of 9 m, which is the thickest sandstone deposit in China.

8. CONCLUSIONS

Five typical sandstone type uranium deposits in China were studied, which include the north belt of the Shihongtan in Tuhar Basin, Mengqigur in Yili Basin located in Xinjiang, and the Shashagetai in Ordos Basin, Bayanwula in Erlian Basin, and Qianjiadian in Tongliao Basin located in Inner Mongolia. The behaviour of reductive substances and clay minerals in the deposits and the relationships between the reductive minerals and permeabilities of the sand bodies were investigated and the microscopic genesis of sandstone uranium deposits was revealed.

8.1. Redox characteristics of the interlayer oxidation zone determine the enrichment and extent of uranium mineralization

Uranium mineralization is mainly located in the redox transition zone, and most of the uranium occurs in the sandstone before and after the redox front of the interlayer oxidation zone. In the North belt of Shihongtan, 70% of the uranium resource occurs in the light yellow-grey coloured sandstone before and after the redox front of the interlayer oxidation zone.

Uranium mineralization is closely related to reductive materials such as organic matter and pyrite. Organic matter and pyrite are important for adsorption and/or reduction of uranium. Sand bodies with a high content of organic matter or clay interbeds favour the occurrence of uranium. The best mineralization usually occurs in sandstone with a high content of organic matter and/or sulphide. For those deposits with a high content of clay minerals, such as the Shashagetai deposits, the adsorption of uranium by clay minerals also play an important role in uranium mineralization.

8.2. Permeative property of sand bodies promotes the enrichment and distribution of uranium

Under the crucial condition of the presence of reductive media, uranium tends to occur in sand bodies that have good permeability and a high content of organic matter.

This investigation showed that uranium mineralization in the Shihongtan deposit tends to occur in the sand bodies that are mainly coarse-grained sandstone. The sand bodies which coexist with reductive media such as carbonized debris and powdery pyrite are very thick and are mainly unconsolidated sediments with good permeability. In the Mengqigur deposit, uranium occurs mainly in coarse-grained sandstone or sandy conglomerate and the permeability of mineralization containing sand bodies is greater than the host rock. Uranium mineralization in the Shashagetai deposit occurs in the sand bodies with low carbonate content and strongly reducing materials.

The sand bodies are unconsolidated to weakly consolidated with relatively good permeability with an abundance of pyrite and organic matter. Uranium in the Bayanwula deposit occurs mainly at the transition between coarse to fine-grained sandstone in the lower-middle part of a braided stream system which is represented by sandy conglomerates and medium to fine-grained sandstones that are weakly consolidated and have good permeability.

For the Qianjiadian uranium deposit, the grain size is relatively uniform, and cementation is relatively weak which gives the formation a homogeneous permeability allowing the groundwater to move along the sand body. The permeability of the ore-bearing horizon and host rock are similar, and the aquifer is quite thick. The uniformity of the sand body and the extensive distribution of reductive materials slowed the flow rate of the uranium-bearing and oxygen-bearing waters in the sand body, promoting the reduction and deposition of uranium. The hydrogeological conditions led to the formation of a large, thick, low grade, tabular uranium mineralization.

In the sandstone type uranium deposits studied, uranium mineralization is directly related to the reductive materials and permeability of the sand bodies. The best mineralized bodies occur in sandstones with high content of organic matter, and in most cases, with high permeability.

ACKNOWLEDGEMENTS

This work summarizes the results of studies carried out between 2004 and 2018 by Beijing Research Institute of Chemical Engineering and Metallurgy (BRICEM) and BRICEM would like to thank the support and publication of this research through the IAEA CRP. We also acknowledge Dr. Adrienne Hanly whose efforts helped to enhance the quality and value of this paper.

REFERENCES

[1] LIAO W.S., WANG L.M., JIANG G.P. JIANG Y., Factors affecting the permeability of low-permeability sandstone uranium deposits: A case study, CIM J. **5** (2014) 119–126.
[2] QUAN Z.G., LI Z.S., Geological characteristics and genesis of the Shihongtan sandstone-type uranium deposit, Xinjiang, Geological Review **48** (2002) 430–436 (In Chinese).
[3] CHEN H., LI J., CAO L. SHANG G., ZHOU W., TAN L., LIU J., WU Z., The geological survey report on the south belt of Shihongtan uranium deposit, Turpan, Xinjiang (Lines 31–32) (**2013)** (Unpublished internal report).
[4] WANG J., ZHANSHUANG L., ZHANYOU L., Geological and geochemical characteristics of Shihongtan uranium deposits, SW Turpan-hami Basin, Xinjiang autonomous region, IAEA Technical Reports Series No.1396 Vienna, Austria (2004) 59–68.
[5] ZHOU W, TAIYANG G., ZUYI C., JIANGHONG L., LITING F., WUWEI L., ISL-amenable sandstone-type uranium deposit: Global aspects and recent developments in China, IAEA Technical Reports Series No.1396 Vienna Austria (2004) 25–46.
[6] SHANG G.F., QIAO H.M., LIU Z. G., SONG Z., Geochemical characteristic of sandstone type uranium deposition interlayer oxidation zone, Baxiankou area, Advances in earth science. 27 Suppl. (2012) 245–250 (In Chinese)

[7] LIU T., ZHANG Z., P0-P55 line geological survey report of Mengqiguer uranium deposit in Chabuchaer, Xinjiang (2007) (Unpublished internal report).
[8] ZHANG Z., JIANG H., WANG M., Driving Factors of Metallogenesis of Mengquer Uranium and its Significances to Discover Uranium in Yili Basin, Mineral Deposits **29** (Supplement) (2010)165–166 (In Chinese).
[9] ZHANG X., Study on the causes of the uranium deposit from the southern margin of Yili Basin, Master Thesis, Beijing Research Institute of Geology (2012) (In Chinese).
[10] FAN A., Mineralization constraint of Jurassic diagenesis in Dongsheng uranium deposit, Ordos Basin, PhD Thesis, Northwest University (2007) (In Chinese).
[11] LIU Y., FENG Q., YANG R., FAN A., XING X., Discussion on genesis of sandstone-type uranium deposits in Dongsheng area, Ordos Basin, Acta Geologica Sinica **80** (2006)761–767 (In Chinese).
[12] WANG S., Coal accumulation and evaluation of coal resource in Ordos Basin. Peking: China Coal Industry Publishing House (1996) (In Chinese).
[13] XIAO X., The mineralization geochemistry of the low temperature fluid on the Dongsheng sandstone type uranium deposit, PhD Thesis, Beijing Research Institute of Geology (2004) (In Chinese).
[14] ZHU X., WANG Y., WANG Z., ZHANG C., LIU J., Trace element geochemistry of sandstone-type uranium deposits in Dongsheng area, Geology-Geochemistry **31** (2003) 39–44 (In Chinese).
[15] XIA Y., LIU H., Pre-enrichment and metallogeny of uranium in Zhiluo Formation sand bodies of Dongsheng area, Ordos Basin. World Nuclear Geoscience. **22** (2005) 187–191 (In Chinese).
[16] FAN X., NIE F., Discussion on age and paleo geographical environment of ore sandstone-type uranium deposits in Bayanwula area, Erlian Basin, Uranium Geology **24** (2008)150–154 (In Chinese).
[17] LIU W., KANG S., Characteristics of paleo-valley sandstone-type uranium mineralization in the middle of Erlian Basin, Uranium Geology **29** (2013)328-335 (In Chinese).
[18] LU C., PENG Y., Sedimentary backgrounds of sandstone-type uranium deposit in western Manite depression of Erlian Basin, Uranium Geology **29** (2013) 336–343 (In Chinese).
[19] XIA Y., LIN J., Research on geochronology of sandstone-hosted uranium ore-formation in major uranium-productive basins, northern China, Uranium Geology **19** (2003) 129–136 (In Chinese).
[20] ZHANG C., NIE F., Sources of sandstone-type uranium ore of intermountain basin, Journal of east china institute of technology **35** (2012) 230–237 (In Chinese).
[21] CAI YUQI, LI SHENGXIANG, Sedimentary environment analysis of Yaojia Formation - the ore-hosting stratum of Qianjiadian uranium deposit, Uranium Geology **24** (2008) 66–72 (In Chinese).
[22] YU W., DONG Q., ZOU J., FENG B., Analysis of metallogenic conditions of in-situ leachable sandstone type uranium deposit in the southeastern margin of Songliao Basin, Journal of Jilin University (Earth Science Edition) **36** (2006) 543–549 (In Chinese).
[23] CHEN X., FANG X., GUO Q., XIA Y., PANG Y., SUN Y., Redisscussion on uranium metallogenesis in Qianjiadian sag, Songliao Basin, ACTA GEOLO GICA SINICA **82** (2008) 553–561 (In Chinese).
[24] TIAN S., Analysis of uranium deposit diagenesis in Qianjiadian sag of Songliao Basin. Special Oil and Gas Reservoirs **12** (2005) 26–34 (In Chinese).

[25] GAO Y., YU B., YU W., LI Z., ZHANG Q., MIAO A., Analysis on uranium metallogenic conditions and ore-controlling factors of Qianjiadian-Jiamatu area, southwest of Songliao Basin, World Nuclear Geoscience **25** (2008) 150–156 (In Chinese).

GEOCHEMICAL AND MINERALOGICAL CHARACTERIZATION OF URANIUM, THORIUM AND RARE EARTH ELEMENTS IN EGYPTIAN PHOSPHATE DEPOSITS

H. MIRA, H. GADO, N. FARAG, I. ZIDAN
Nuclear Materials Authority
Cairo, Egypt

Abstract

Phosphate deposits in Egypt occur in three main locations: (1) Nile valley phosphate in El Sebaiya mine; (2) New valley phosphate in Abu Tarture plateau; and (3) Red sea phosphate in Safaga and Quseir area. Mineralogically, francolite and carbonate hydroxyl apatite are the most abundant varieties of apatite in phosphate rocks in Egypt. Geochemically, phosphate rocks range from 24 to 29% P_2O_5 for the high-grade phosphate ore in El Sebaiya. In addition, uranium content ranges from 50 to 132 ppm with an average of 91 ppm U. The inferred phosphate resource in El Sebaiya area is about 80 Mt P_2O_5. The phosphate rocks in Abu Tarture plateau are enriched in rare earth elements (REEs) and average about 0.2% and are depleted in uranium (average about 25 ppm) and thorium (average 4 ppm).

1. INTRODUCTION

Phosphate is the raw material for many important industries such as phosphatic fertilizers, phosphoric acid, soap, detergents, and food [1].

Phosphate rocks in Egypt belong to the North Africa to Middle East phosphogenic belt of Late Cretaceous to Paleogene age [2].

Geologically, in Egypt, the phosphorite-bearing sequence called the Duwi Formation occurs as thin widespread shallow marine deposits of an east-west trending belt. The phosphorite beds are intercalated with different lithofacies such as shales, marls, limestone, cherts, and oyster limestone. The phosphorite beds range from some tens of centimetres to meters.

In Abu Tarture, the phosphate beds are composed of coarse to fine phosphorite grains intercalated with dolomitic phosphorite, glauconitic shale and black shale.

2. MINERALOGICAL INVESTIGATION

The studied phosphorite rocks were investigated by X-Ray diffraction (XRD) and Scanning Electron Microscope (SEM). The obtained data show the presence of phosphatic and non-phosphatic minerals [3].

The phosphatic minerals include carbonate-fluorapatite (francolite, $Ca_5[(PO_4\text{-}CO_3)\ F, O]$) and carbonate-hydroxy apatite (dahllite, $Ca_5[(PO_4\text{-}CO_3)_3\ OH, O]$). These are the most abundant variations of apatite minerals in the phosphatic rocks.

The non-phosphatic minerals include quartz and calcite with minor gypsum and are embedded in the groundmass or as a cement materials.

3. RADIOACTIVITY, URANIUM, THORIUM AND REE CONTENTS

Marine phosphorites are considered as a good source of uranium, where they contain about 50-132 ppm uranium [3]. Uranium in phosphorites occurs in two oxidation states, the insoluble tetravalent state (U^{4+}) and the soluble hexavalent state (U^{6+}) as uranyl ions. Some authors have mentioned that the geochemical relation of uranium with some major and trace elements in phosphatic rocks were derived from sea water during deposition of phosphates (i.e. syngenetic origin) [4].

Uranium content in El Sebaiya area ranges from 50 to 132 ppm with an average of 91 ppm, thorium average 3 ppm and REEs average 200 ppm. In comparison, the phosphate rocks in Abu Tarture plateau are enriched in REEs elements with an average of about 0.2% and are depleted in uranium (average about 25 ppm) and thorium (average 4 ppm) [5].

During 2016, about 6 million tons of phosphorite were mined in Egypt from El-Sebaiya, Red Sea Coast and Abu-Tarture area. Most of these mined phosphates are used in the industry of phosphatic fertilizers and phosphoric acid production and the remainder is exported [3].

The detailed studies for evaluation of phosphorite and uranium contents of El Sebaiya area included several trenches and boreholes drilled by an Egyptian phosphate company to determine the vertical and lateral variations in phosphate. Generally, the detailed lithological, mineralogical and geochemical studies of El Sebaiya phosphate concluded that the inferred phosphorite resources are about 81 million tons with an average of 91 ppm uranium [3]. It is a challenge to evaluate the phosphorite resources and the uranium and REEs contents because they occur over an extensive area and are covered by sandstone and dolomite at the surface.

REFERENCES

[1] ZIDAN I.H., Geological, Mineralogical and Geochemical studies of Abu Tartur phosphate. Western Desert. Egypt PhD thesis. Fac. Sci. Al Azhar Univ. (2002) 235 pp.

[2] ZIDAN I.H., Environmental Impact of the Radioactive and some Heavy Metals in the Egyptian Phosphorite Ores and Fertilizers Product, Jour. Mansoura Environ. Sci. **41** 2 (2012) 153–164.

[3] ZIDAN I.H, Evaluation of phosphorite and Uranium Resources of Duwi Formation at Helal area, South Esna, East Nile Valley, Egypt, Sedimentology of Egypt **23** (2017) 63–80.

[4] SLANSKY M., Geology of Sedimentary Phosphates, North Oxford Academic Publishers. London, 1986, 210 pp.

[5] AMIN M. M., and ZIDAN I. H., Rare earth elements recovery and preparation of phosphoric acid from Abu-Tartur phosphate rock using Penicillium simplicissimum, Chemical Technology, An Indian Journal **10** 3 (2014) 57–61.

INVESTIGATION OF URANIUM ENRICHMENT POTENTIAL IN THE MARINE PHOSPHATES OF THE ISLAMIC REPUBLIC OF IRAN

K. KHOSHNOODI, S. ZIAPOUR
Atomic Energy Organization of Iran,
Nuclear Science and Technology Research Institute,
Material and Nuclear Fuel School,
Tehran, Islamic Republic of Iran

Abstract

Phosphorites are in some cases enriched in uranium and as a result they can be considered as a potential source of uranium. For this study, the behaviour of uranium in phosphates was considered including the eight factors which govern uranium enrichment in phosphate: depositional environment, phosphate mineralogy, organic matter content, P_2O_5 grade, Eh and pH at the time of deposition, paleoclimate and weathering. There are five main phosphate-hosting formations (Pabdeh, Jeiroud, Soltanieh, Gurpi and Shirgesht) in Islamic Republic of Iran. Evaluation of the defined factors in these five main phosphate-bearing formations indicated that the Pabdeh Formation has potential for uranium enrichment. Twenty-six phosphate samples of Jeiroud Formation, 48 phosphate samples of Pabdeh Formation and 11 phosphate samples of Soltanieh Formation were taken and analysed using XRD, ICP-OES and ICP-MS. The uranium concentrations ranged from 18–108 ppm, 2–8 ppm and 2–6 ppm in Pabdeh, Jeiroud and Soltanieh Formations, respectively. The phosphates of Pabdeh Formation are enriched in uranium (average enrichment factor of 8.8). Based on mineralogical study by SEM-EDS, no uranium minerals were identified in the phosphates of Pabdeh Formation and therefore, apatite is most likely the main uranium-bearing mineral. The Jeiroud phosphates do not show uranium enrichment but they are enriched in rare earth elements (REEs) and the main REE-bearing mineral is most likely fluorapatite. The evaluation of uranium enrichment in the marine phosphates in the country using the defined factors confirmed that these factors may be applicable to evaluate uranium enrichment in other sedimentary phosphate deposits globally.

1. INTRODUCTION

Phosphorites can contain high uranium concentrations and in this case could be considered as a potential source of uranium. This feature, first discovered by Strutt [1, 2], attracted the attention of researchers in the second half of the 20th century with the development of the atomic energy industry [3]. The uranium contents in phosphorites on continents and seafloor ranges from 0.n to n*10² ppm (where n is greater than 0 and less than or equal to 1) and with an average of 75 ppm U, which exceeds the Clarke value for sedimentary rocks [4].

The enrichment of rare earth elements (REE) and uranium in francolite occurs in exchange with Ca^{2+} by isomorphic substitution in the francolite lattice [5]. Because of these substitutions, phosphatic rocks can be enriched in REE, U, V, F, Mo, Cd, Ag, Cr, Te, As, Se, Sr, Zn and some other elements [6]. U^{6+} from the near bottom water is reduced in sediments and precipitated as submicroscopic segregations of uranium minerals or absorbed by phosphatic material. In addition, microscopic inclusions of uranium minerals are present in phosphorites [4]. More than 80 phosphate deposits and indications are known to exist in the Iranian plate as a part of a marginal fragment of what was at one time north Gondwana. Both sedimentary and igneous types of phosphate deposits are explored in the country [7].

The aim of this work was the determination of the major factors that govern uranium enrichment in phosphorites, evaluation of these factors in the phosphorite-bearing formations, and the geochemistry and mineralogy of uranium in selected sedimentary phosphates in the Islamic Republic of Iran.

Considering that all phosphorites in the world do not necessarily have significant uranium enrichment, the factors which govern uranium enrichment in phosphorites are discussed in this paper. These factors were applied to studies of the phosphorus-bearing formations in the country which included sampling and geochemical studies.

2. MAIN PHASES OF SEDIMENTARY PHOSPHATIZATION IN ISLAMIC REPUBLIC OF IRAN

The phosphate deposits are located in Central Iran, Central Alborz and Zagros Zones (Table 1). Based on the available exploration data, the Iranian phosphate deposits formed during three geological time periods and are dominated by sedimentary type [7].

2.1 Late Proterozoic-Early Cambrian

These phosphate deposits are either igneous or sedimentary. Sedimentary phosphates are hosted by the Early Cambrian Soltanieh Formation in Alborz and Central Iran and igneous phosphates are found in the rocks of the Rizoo Series in the Bafq area. The phosphatic horizons of the Early Cambrian Soltanieh Formation occur within shale and middle dolomitic members. Some examples of the sedimentary phosphate deposits are Dalir, Valiabad, and Firoozabad in Central Alborz and the Soltanieh Mountains [7]. Presence of phosphate has been reported from the Ordovician sedimentary rocks in the east of Central Iran at Tabas (Shirgesht Formation in Kalmard and Rahdar) and Kerman (Dahuieh, Zarand Region) [8].

2.2. Late Paleozoic-Triassic

The large phosphate deposits and occurrences of the Devonian Jeiroud Formation have been reported from the Jeiroud, Lalun, Firoozkuh, Damavand, Shahroud, and Damghan Regions in the Central Alborz Zone. The phosphatic zone of Devonian Jeiroud Formation occurs within the sandstone layers. This mining zone contains individual layers with higher than 18% P_2O_5 and phosphatic sandstone and limestone with black shale intercalations of lower than 18% P_2O_5 [7].

2.3. Late Cretaceous-Paleogene (Laramide)

Phosphate deposits and occurrences in the Late Cretaceous Gurpi (e.g. Chenareh, Rit, and Tal-e Zang) and Palaeocene to Oligocene Pabdeh Formations (e.g. Kuh-e Lar, Sheikh Habil, Kuh-e Rish, Kuh-e Kumeh, and Kuh-e Sefid deposits) are situated in Zagros Zone of Islamic Republic of Iran [8]. There are seven phosphogenic events recorded during the Coniacian to Oligocene in Zagros Zone, and the most important events both in terms of quality and quantity are Paleocene (occurring at the base of Pabdeh Formation) at Rizroud, Khormoj, and Kuh-e Namak anticlines and Late Eocene-Oligocene at the Dehdasht-Behbahan region [7]. Table 1 shows the major formations hosting sedimentary phosphate deposits in Iran. The major phosphate deposits are located in Central Iran, Central Alborz and Zagros Zones (Figure 1).

TABLE 1. THE MAJOR FORMATIONS HOSTING SEDIMENTARY PHOSPHATE DEPOSITS OF ISLAMIC REPUBLIC OF IRAN

Host formation	Number of deposits	Total reserve P_2O_5 (Mt)	Average P_2O_5 (%)	Important deposits
Pabdeh	56	660	12	Kuh-e Lar anticline (Choram), Kuh-e Rish, Sheikh Habil, Kuh-e Kumeh, Khormoj, Rizroud, Kuh-e Namak anticline, Kuh-e Sefid, Nile anticline
Jeiroud	33	170	13	Jeiroud, Kasil, Lalun, Gaduk-Dogol, Chalmish, Paghaleh, Deh Molla, Margdar
Soltanieh	45	130	8	Dalir, Seyed Kandi, Vali abad, Firouz abad-Kikuh
Gurpi	7	20	4	Chenareh, Rit, Talezang
Shirgesht	11	19	6	Kalmard anticline, Rahdar anticline, Dahuieh

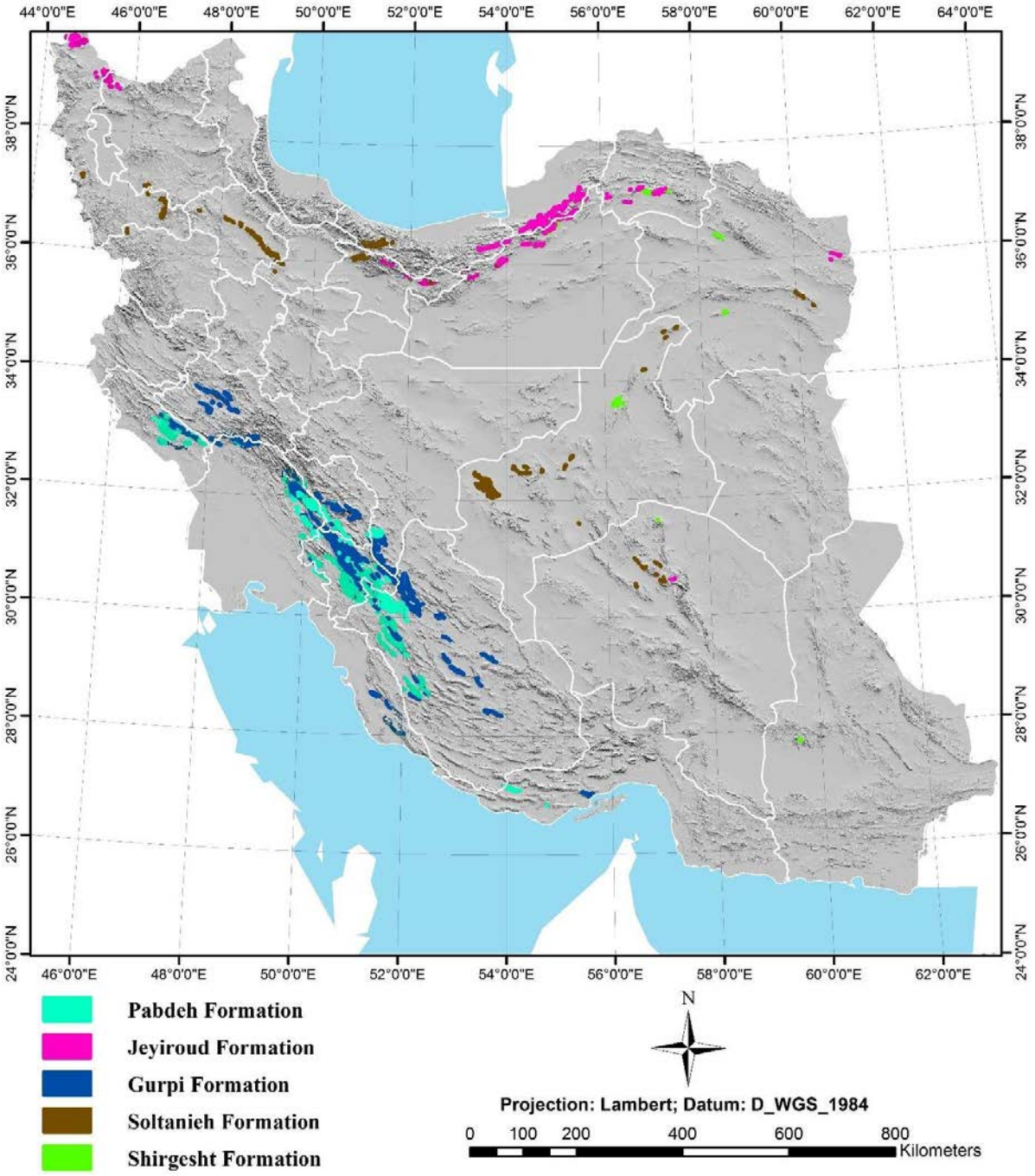

FIGURE 1. Distribution map of outcrops of the marine phosphate hosting formations in Islamic Republic of Iran.

3. MATERIALS AND METHODS

After defining the factors controlling the uranium enrichment in sedimentary phosphate and the phosphatic formations, some major deposits hosted by the formations were selected for sampling.

Twenty six phosphate samples of Jeiroud Formation (from Jeiroud mine, Paghaleh, Lalun, Gaduk; Devonian deposits), 48 phosphate samples of Pabdeh Formation (from Choram, Khormoj, Kuh-e Rish, Kuh-e Kumeh, Sheikh Habil and Rizroud; Paleocene-Eocene-Oligocene deposits) and 11 phosphate samples of Soltanieh Formation (Dalir; Early Cambrian deposit) were collected with a sample interval of one meter from the phosphate layers for geochemical and mineralogical studies. The whole-rock concentrations of major oxides, REE and trace elements were determined by inductively coupled plasma (ICP) optical emission spectroscopy (OES) and mass spectrometry (MS) at the laboratory of the Geological Survey and Mineral Exploration of Iran. Thin sections and thin-polished sections were prepared for detailed petrographic and mineralogical studies. X-ray diffraction (XRD) and Scanning Electron Microscope/Energy-dispersive X-ray spectroscopy (SEM/EDS) were used to analyse the collected samples. Some samples from each phosphate deposit were analysed using XRD instruments at the Zarazma Laboratory, Tehran, Islamic Republic of Iran. Some samples of each phosphate deposit were also studied under SIGMA/VP-ZEISS field emission scanning electron microscope (FESEM), equipped with a X-Max Oxford EDS microanalyzer system at the Center for Applied Research of the Geological Survey and Mineral Exploration of Iran, Karaj. Counting time for peak and background determination was 15–20 s at a voltage of 15–20 keV.

The total gamma activity of natural radionuclides was measured by a gamma spectrometer (model RS-230) in selected phosphate deposits of the Pabdeh, Jeiroud and Soltanieh Formations.

4. MAJOR FACTORS CONTROLLING URANIUM ENRICHMENT IN MARINE SEDIMENTARY PHOSPHATES

The behaviour of uranium in phosphorites is considered and some factors which govern uranium enrichment in phosphorite are introduced. Major factors controlling uranium enrichment in sedimentary phosphates include environment of formation, mineralogy, organic matter, phosphorous grade, redox conditions (Eh), pH, paleoclimatic conditions and weathering (Table 2).

TABLE 2. THE FACTORS CONTROLLING THE URANIUM ENRICHMENT IN MARINE PHOSPHATE

No.	Factors	Favourable conditions
1	Environment of formation	Distal to shoreline (Phosphoria-type) and proximal to shoreline by local reworking (Florida-type).
2	Phosphate mineralogy	Uranium can easily replace Ca in francolite rather than wavellite and crandallite.
3	P_2O_5 grade	Uranium content is proportional to the P_2O_5 grade.
4	Organic matter content	The presence of organic matter is necessary to accumulate uranium in phosphorite.
5	Eh at the time of phosphate deposition	In anoxic conditions, uranium (U^{4+}) is substituted for Ca^{2+} in the apatite or francolite structure.
6	pH at the time of phosphate deposition	Uranium absorption takes place by Ca-phosphate in weakly alkaline pH.
7	Paleoclimatic conditions	In a hot arid climate or during weathering, uranium is leached easily and transported by rivers to the sea.
8	Weathering	During weathering, uranium is leached and can become enriched in apatite at the base of the phosphorite layer.

4.1. Environment of formation

The interpretation of depositional processes and sedimentary paleoenvironment is usually achieved by identifying the lithofacies and biofacies and, in particular, microfacies. Based on depositional environment, two main varieties of uraniferous marine phosphorite are recognized (Figure 2) [9]:

1) Bedded uraniferous phosphorite (Phosphoria-type): Phosphatic shales with oolitic, pisolitic, pelletal, and laminated textures interbedded with fine-grained miogeosynclinal facies (black shale, mudstone, chert, rare carbonate beds), formed in the distal to shore-line environment and which commonly contain high uranium content. Uranium content of the Phosphoria Formation in Idaho ranges between 60 to 200 ppm;
2) Land-pebble phosphate (Florida-type): Uranium enriched in apatite pebbles within nodular phosphorite beds interbedded with fine- to medium-grained shallow marine facies and carbonate beds, formed in the proximal to shoreline marine environment by local reworking and leaching of nodular phosphorite leading to secondary uranium enrichment in the pebbles. Bone Valley Formation in Florida contains an average of 150 ppm uranium.

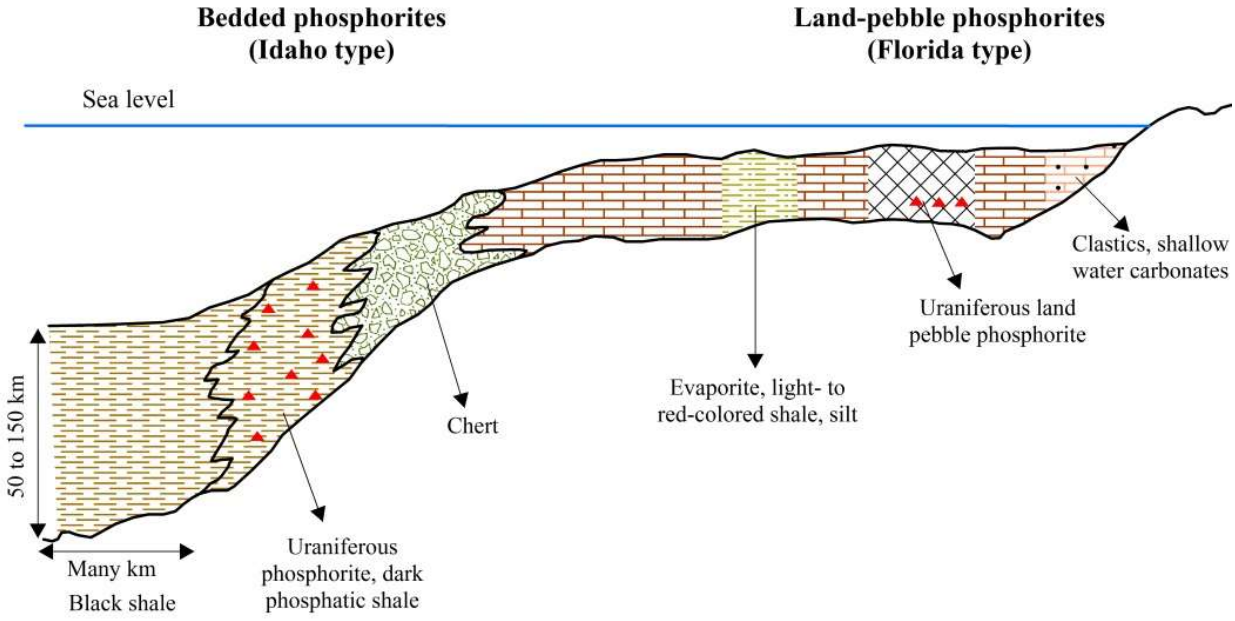

FIGURE 2. Schematic representation of uraniferous phosphorite deposits (modified from Dahlkamp [9]).

4.2. Phosphate mineralogy

Uranium generally occurs in three forms in sedimentary phosphate rocks including replacement of U^{4+} for Ca in apatite structure, adsorption of U^{6+} on the surface of the apatite crystals, and individual U^{4+} minerals (uraninite and ningyoite) [4]. The principal uranium-bearing mineral in sedimentary phosphatic rocks is cryptocrystalline, fluor-carbonate apatite (francolite) containing syngenetic uranium substituting for calcium [10]. According to Dahlkamp [10], unfavourable minerals for uranium accumulation are Al and Ca-Al phosphates (such as wavellite, crandallite and other non-Ca phosphates).

4.3. P_2O_5 grade

In sedimentary phosphate rocks, mostly, but not necessarily, distinct positive correlation between uranium and phosphate contents has been reported [11–13] and the amount of uranium increases with increasing P_2O_5 [3]. Along with organic matter, calcium phosphate plays a substantial role in uranium concentration owing to a high sorption capacity of the calcium phosphate. According to Kochenov and Baturin [3], uranium-bearing sedimentary rocks are characterized by a qualitative relationship between organic matter and calcium phosphate and remains of marine planktonic and nektonic organisms are usually present in the phosphate rocks [3].

4.4. Organic matter content

There are two necessary factors for uranium enrichment in marine sedimentary phosphate rocks including the presence of organic matter and phosphorous. The association of organic matter and calcium phosphate is a necessary condition of uranium enrichment in marine sediments [3, 14]. The average U/P_2O_5 ratio increases from 2.24 to 6.63 towards NW Jordan, indicating that the NW Jordan phosphorites are three times more enriched in uranium. Also, the organic matter shows a

northward increasing trend. Accordingly, it can be concluded that there is a distinct positive correlation between the content of the organic matter and the uranium concentration in sedimentary phosphates [15]. This correlation is linear for the lower and logarithmic for higher carbon contents [3]. The phosphatic sediments which are rich in organic matter have higher uranium concentrations than sediments which do not contain organic substances [16].

4.5. Redox conditions

The most favourable condition for uranium concentration in phosphate is associated with an anoxic bottom water environment combined with a high bioproductivity of aerated surface water [3]. Phosphorites may contain authigenic minerals of U^{4+} such as uraninite-type oxides, ningyoite, coffinite and other tetravalent uranium minerals due to U^{6+} diffusion from the near bottom water into sediments. The above-mentioned minerals are generally formed in a reducing environment [17-21]. For example, the Jordanian phosphorite deposits in the karst pockets had been subjected to a reducing environment [22]. In anoxic condition, uranium (U^{4+}) is substituted for Ca^{2+} in apatite or the francolite structure. High organic matter content, presence of pyrite, absence of benthic fauna, dark color of the peloids, and intense sulphate reduction accompanied by molybdenum accumulation in uranium-bearing phosphatic sediments may serve as an indicator of an anoxic environment in the basin [3, 16, 22, 23].

4.6. pH at the time of phosphate deposition

The specific role of calcium phosphate lies in its ability to extract uranium from low-alkaline solutions, such as seawater [24]. Therefore, pH is another factor in which uranium absorption takes place by Ca-phosphate in weakly alkaline pH conditions.

4.7. Paleoclimatic conditions

The uranium contents in surface water often depend on the climatic zone. In a humid climate with an abundance of moisture, vegetation, precipitation and low evaporation, the water is not very mineralized and mainly contains hydrogen carbonates with nearly neutral pH values. This water does not leach uranium well. In a hot arid climate, with a low amount of precipitation and rapid evaporation, where the active water exchange has a high carbonate content and alkalinity, uranium is leached rapidly. Water with pH>8 are active solvents of the secondary and, to a lesser extent, the primary minerals of uranium [16]. According to Ostrovskaya [25], during the Mesozoic and Cenozoic periods, large deposits of high-grade phosphorites were formed in arid regions and poorer nodular phosphorites in humid zones. The former are frequently uranium-bearing, the latter usually contain no uranium [25]. Since the source of uranium in sedimentary phosphates is transported by rivers from continent to sea, the rivers in hot arid climates contain substantial dissolved uranium as carbonate complexes and provide vital sources for enrichment of sedimentary phosphates in uranium [16].

4.8. Weathering

During weathering, apatite is replaced in the top zone by Al phosphate (wavellite) and in the middle zone by Ca–Al phosphate (crandallite, millisite). During weathering, uranium is leached and liberated easily from apatite in the near-surface levels, remains soluble in the descending acid

solutions, and is preferentially concentrated in apatite at or near the base of the leached zone. As a result of this process, apatite of the bottom zone may be highly enriched in uranium with concentrations as high as 0.3% uranium in the bottom zone pebbles. Highly porous apatite of the bottom zone is enriched in uranium, whereas secondary Al- and Ca-Al phosphates contain only minor amounts of uranium [10, 26]. For example, in Eshidiyya Basin in southern Jordan, the uranium content in Al-Hisa Phosphorite Formation is proportional to the percentage of P_2O_5 and uranium concentration decreases upwards in the sedimentary sequence due to weathering [22]. The type of the source rock, duration and the intensity of weathering control the final weathering products and distribution of uranium [26].

5. EVALUATION OF THE FACTORS CONTROLLING URANIUM ENRICHMENT IN MARINE PHOSPHATES IN ISLAMIC REPUBLIC OF IRAN

These factors are evaluated in various marine phosphate-bearing formations of the Islamic Republic of Iran (Table 3)

TABLE 3. EVALUATION OF FACTORS CONTROLLING URANIUM ENRICHMENT IN THE MAIN PHOSPHATIC FORMATIONS

Factors/Formations	Pabdeh	Jeiroud	Soltanieh	Gurpi	Shirgesht
Depositional Environment	Deep-marine environment (Phosphoria-Type)	Shallow water and near coast (Florida-Type)	Shallow to deep marine water (Florida to Phosphoria-Type)	Deep open marine (Phosphoria-Type)	Shallow water platform (Florida-Type)
Phosphate mineralogy	Francolite	Francolite	Francolite	Collophane	Francolite
Organic matter content	Microfacies with organic matter enrichment	Abundant inclusions of organic matter	Stromatolite and hyoliths	About 0.5%	Abundant organic matter
P_2O_5 grade	11%	26%	8–11%	3–20%	6–16%
Eh at the time of phosphate deposition	Reduced	Reduced	Reduced to weakly oxidized	Reduced	Reduced
pH at the time of phosphate deposition	Weakly alkaline (7.7–8)	Weakly alkaline (7.5–7.8)	Slightly acidic to alkaline	Weakly alkaline to neutral	---
Paleoclimatic conditions	Arid (hot and dry)	Warm and humid	Warm and humid	Warm and dry	Warm and semi humid
Weathering	REE and U are leached and enriched in lower levels	Pyrite altered to goethite	Destruction of organic matter	---	---

5.1. Pabdeh Formation

In the Islamic Republic of Iran, the Tethyan phosphates are restricted to the Eocene-Oligocene Pabdeh Formation located in the Zagros Folded Zone in southwestern Iran [27]. The Pabdeh Formation consists of thin to medium beds of bluish grey shale and marl and interlayers of argillaceous limestones in the lower part, grey shales containing organic matter and marls with interlayers of argillaceous limestone in the middle part, and alternative layers of argillaceous limestone, shale and marl in the upper part. The phosphatic horizons are present in two units in the lower and middle of the formation (Figure 3) [28].

The depositional environment of Pabdeh Formation was a distally steepened ramp (bathymetrical carbonate floored basin or deep shelf or basin margin) [28–30]. The dominant phosphate mineral in unweathered phosphates of Pabdeh Formation is fluor-carbonate apatite (francolite) [31–33].

The microfacies of Pabdeh Formation is enriched in organic matter and planktonic foraminifera indicating local anoxic conditions during phosphate sedimentation [28, 34]. The average content of P_2O_5 is 11% (this study). The pH levels of the sedimentary environment during deposition of the Pabdeh Formation fluctuated between 7.7–8.0 (weakly alkaline) [35]. The climatic conditions were arid (hot and dry) during deposition of the Pabdeh Formation, due to the strong greenhouse effect. Paleogeographic reconstruction during the Eocene period indicates that the Pabdeh Formation was situated in subtropical, storm-dominated paleolatitudes [30, 34]. The phosphate horizons of the Pabdeh Formation were not affected by intense weathering at the surface [31].

Accordingly, evaluation of the major factors controlling the uranium enrichment in sedimentary phosphates in the Pabdeh Formation indicates that it may potentially contain significant enrichment of uranium.

5.2. Jeiroud Formation

The late Devonian Jeiroud Formation consists of black phosphatic sandstones, conglomerates, limestone, basalt and a minor proportion of dark shales (Figure 3) [36]. This formation unconformably sits on the Lashkarak Formation and is overlain by a thick succession of carboniferous carbonates (Mobarak Formation) [37]. In Central Alborz area, the Mila Formation is overlain directly by the Jeiroud Formation. There are phosphate-bearing horizons including nodules, concretions, pellets and bioclasts formed as a result of reworking processes including steep folding during the Alpine Orogeny [36–39].

The origin of the Jeiroud phosphate is by the upwelling of cold, nutrient-rich oceanic water from the deep Paleo-Tethys ocean to the surface which occurred in a warm and shallow near shore sedimentary environment along a passive margin (north of Iran) [40]. The phosphate is present in the form of cryptocrystalline francolite with a relatively small substitution of CO_3F for PO_4 in the lattice [7]. Minor amounts of hydroxyl apatite are also present [40]. In general, organic matter occurs as inclusions in phosphate minerals [41].

There are two phosphate horizons (low- and high-grade) in the Jeiroud Formation; the low-grade phosphate bed (with higher than 10% P_2O_5) and the high-grade phosphate bed (with higher than

20% P_2O_5). The mean P_2O_5 value in the phosphate beds of the Jeiroud Formation is about 26% [8, 42] (and this study). The presence of pyrite in phosphates of the Jeiroud Formation indicates a reduced (anoxic) environment during sedimentation [42, 43]. The depositional environment of the Devonian Jeiroud Formation was weakly alkaline and pH levels at that time ranged between 7.5 and 7.8 [35]. The phosphate deposits of Jeiroud Formation were precipitated in a southern divergent margin of a paleo-Tethys sea under warm and humid (tropical) climatic conditions [44]. During weathering, the pyrite minerals in the phosphate were converted to goethite. The weathered phosphates are reddish brown, whereas unweathered phosphates are completely black [42, 45].

As a result of the climate (one of the major factors in uranium enrichment in sedimentary phosphates) being warm and humid during deposition of the Jeiroud Formation, significant amounts of uranium could not be transported by the river to the sea and therefore there is no potential for uranium enrichment in the sedimentary phosphates of this formation.

5.3. Soltanieh Formation

The Early Cambrian Soltanieh Formation consists of a lower dolomite member (dolomite to cherty dolomite and thin bedded shales), Chopoghloo shale member (black shale with phosphatic pellets), middle dolomite member (dolomite and grey limestone), upper shales member (grey phosphatic shale to silty shale with argillaceous limestone) and an upper dolomite member (Figure 3) [8, 46].

The depositional environment of Soltanieh Formation is different in various areas of the Islamic Republic of Iran. The Dalir deposit formed chemically and biochemically in a shallow marine carbonate environment (in a closed environment). In comparison, the formation environment of the Valiabad phosphates, which contains two types of marginal cements of algal and bacterial origin, correspond with deposition in shallow parts of coastal areas in calm conditions and as deep marine in fine-grained sediments, respectively [8, 47]. The main phosphate mineral in the phosphates of Soltanieh Formation is carbonate fluor-apatite [47–50]. The P_2O_5 grade depends on the region and thickness of phosphatic layers in the Soltanieh Formation. The average concentration of P_2O_5 in Dalir region is 10% P_2O_5 with 23 million tons probable reserve, and in the Valiabad region the average grade of P_2O_5 is 8% with 3 million tons probable reserve [8, 51] (and this study). The pH and redox conditions at the time of deposition of the Soltanieh Formation are completely different in various areas. The Soltanieh Formation in Dalir region has been deposited at a neutral to slightly acidic pH and under reduced conditions [8, 48, 49].

In the Valiabad region, the phosphates of the Soltanieh Formation with marginal cement of algae formed in a weakly oxidized Eh, whereas the phosphates with globular cement formed under reduced conditions at slightly acidic to alkaline pH [47]. According to Mousavi et al. [50], the phosphates of Soltanieh Formation in Zanjan area were deposited under oxidized conditions at an alkaline pH. Cambrian phosphatization was related to sedimentary facies which were deposited in a relatively shallow, warm and nutrient rich marine environment near a tropical latitude when the Alborz was a passive margin of the Proto-Tethys Ocean. The paleoclimate was warm and humid at the time of deposition of the phosphates of the Soltanieh Formation [40]. The organic matter content in phosphates of the Soltanieh Formation is 1.66%. Some organic matter such as stromatolites and hyoliths are abundant in the Soltanieh Formation in Valiabad region and no weathering process has been observed [8, 45].

As the conditions of deposition of the Soltanieh Formation were in a warm/semi-warm and humid climate (one of the major factors in uranium enrichment in sedimentary phosphates), and neutral to acidic pH conditions (Table 3), it was concluded that optimal conditions for uranium enrichment were not present.

5.4. Gurpi Formation

The Gurpi Formation with a thickness of about 400–550 m consists of thin to medium bedded bluish gray marl and marlstone interbedded with thin layers of argillaceous cream limestone. This formation exhibits a low morphology and is of variable thickness because of low rock stability [28]. The Gurpi Formation overlies the Sarvak or Ilam Formation disconformably and is overlain by the Pabdeh Formation [52].

The depositional environment of the Gurpi Formation was a ramp in a deep open marine environment in a transgressive stage (pelagic environment) [28, 52]. Based on Namadmalian et al. [51], the dominant phosphate mineral in the phosphates of the Gurpi Formation is apatite as collophane (cryptocrystalline apatite). The average content of organic matter in the phosphates of the Gurpi Formation is about 0.5% [51].

Oolitic and pelletal phosphates are common in the Gurpi Formation. The average grades of P_2O_5 in phosphate deposits of the Gurpi Formation range between 3 and 20% [51]. The presence of authigenic phosphate and glauconite, primary framboidal pyrite and large percentages of amorphous organic matter (AOM) indicate that the phosphates of the Gurpi Formation were deposited in dysoxic to anoxic (reduced) conditions and a low-energy environment [28, 53, 54]. The depositional conditions of the Gurpi Formation were weakly alkaline to neutral (7.6-7.8 pH). Based on Hadavi and Senemari [55], the existence of index species of calcareous nanofossils in the Gurpi Formation indicate a warm and dry (subtropical) climate and high depths of the basin in low latitudes. The phosphates of the Gurpi Formation were precipitated in warm waters at low latitudes. There is no available data about weathering of phosphate of the Gurpi Formation.

According to the above, it can be concluded that the phosphatic horizons of the Gurpi Formation have some potential for uranium enrichment, however its phosphate deposits are sedimentary Fe-phosphate deposits with high amounts of Al- and Fe-oxides with very low phosphorous contents. Although the phosphates of the Gurpi Formation horizons have some potential for uranium enrichment, they are not similar to other phosphates in terms of processing, so in this case uranium cannot be considered as a highly potential by-product of these phosphates (Table 3).

5.5. Shirgesht Formation

The Lower Ordovician Shirgesht Formation is mainly composed of carbonate and siliciclastic successions that disconformably overlie the Precambrian Kalmard Formation and are overlain by the Carboniferous Gachal or Devonian Rahdar Formations [51, 56–60]. The most important phosphate occurrences are found in the shale-sandstone sequences of the Shirgesht Formation [61].

The Shirgesht Formation was deposited in a barrier island-lagoon depositional system in turbulent, photonic and shallow environments [56, 57]. The dominant mineral in the phosphate horizon of the Shirgesht Formation is francolite [59, 60]. The phosphates of the Shirgesht Formation contain abundant organic matter [56, 59, 60].

The phosphate horizon in Rahdar, Dahuieh and Kalmard deposits is 1.5 m thick with an average grade of 8.17%, 12–16% and 6% P_2O_5, respectively [8, 46]. There is no data about pH at the time of deposition of the Shirgesht Formation, but a reduced condition is indicated by the presence of pyrite and magnetite [60]. According to Bayetgoll and Hosseini Barzi [58], the weathering in the source area of Kalmard block was determined as intensive using the chemical index of alteration (CIA). This reflects the warm and humid paleoclimate of the Shirgesht Formation along an inactive continental margin. Khazaei et al. [62] indicated that the central Iranian micro plate was probably located at a low paleolatitude. Therefore, semi humid climatic conditions could have been dominant in Central Iran in this paleotropical latitude at the paleolatitude of less than 30°S during Ordovician-Silurian time. There is no evidence of alteration of the phosphate of the Shirgesht Formation.

A humid climatic condition during precipitation of the Shirgesht Formation meant that uranium in significant amounts could not be transported by the river to the sea and therefore this formation would not be a suitable host for uranium enrichment.

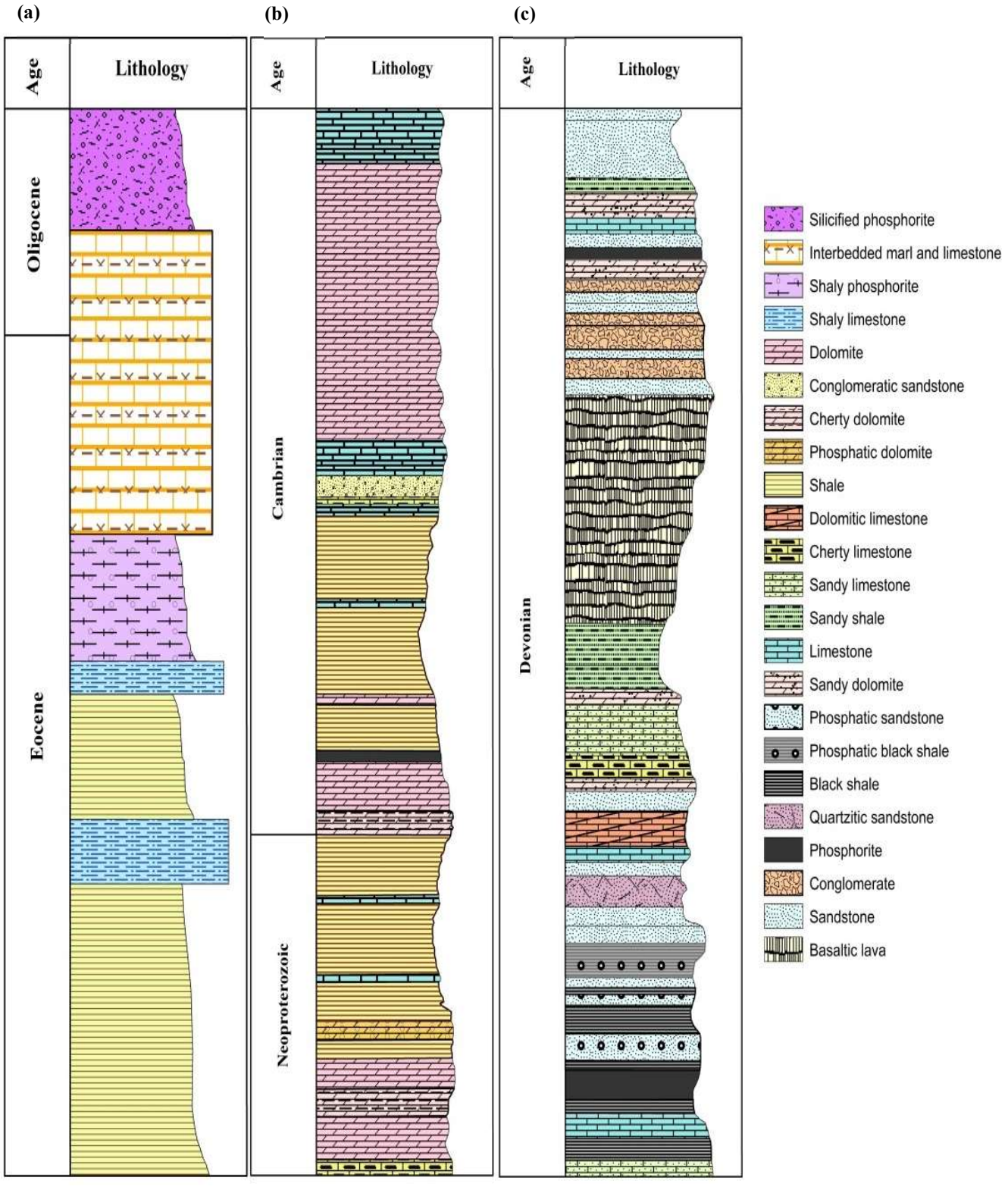

FIGURE 3. Lithostratigraphic columns of: a) Pabdeh Formation in southwestern Iran (modified from Salehi [63]); b) Jeiroud Formation in Central Alborz; and c) Soltanieh Formation in Central Alborz (modified from Ghorbani [7]).

6. GEOCHEMISTRY

The minimum, maximum and average values of the element contents for the phosphates of Pabdeh, Jeiroud and Soltanieh Formations are given in Table 4.

6.1. Phosphatic horizon of Pabdeh Formation

The P_2O_5 values in various deposits of Pabdeh Formation range from 4.3–25.8%. The mean total phosphorus in the phosphates of the Pabdeh Formation is 9.7%. The enrichment factors were calculated by dividing the average concentrations of U, Th and rare earth elements (REE) in the phosphates by the mean concentrations in North American Shale Composite (NASC) [64]. The content of uranium varies from 6 to 108 ppm. The results of the chemical analysis (Table 4) show uranium enrichment compared with NASC values and enrichment factors of 10.9 for Choram, 9.3 for Khormoj, 8.6 for Kuh-e Rish, 6.5 for Kuh-e Kumeh, 37.4 for Sheikh Habil and 2.9 for Rizroud deposits of the Pabdeh Formation. ∑REE ranges from about 57.6 to 707.1 ppm with an average of about 113.6 ppm in the phosphates of the Pabdeh Formation. The enrichment factor of ∑REE ranges between 0.4 and 1.8 in Choram, Kuh-e Rish, Kuh-e Kumeh and Sheikh Habil phosphate deposits, indicating depletion of the REEs. Khormoj and Rizroud phosphate horizons occur at the base of the Pabdeh Formation (Paleocene) and their enrichment factor of ∑REE ranges between 1.7 and 4.4, indicating some enrichment in the REEs.

TABLE 4. CHEMICAL COMPOSITION OF PHOSPHATE SAMPLES OF THE PABDEH, JEIROUD AND SOLTANIEH FORMATIONS (MAJOR ELEMENTS IN WT%; RARE EARTH ELEMENTS, U AND Th IN PPM)

Formation	Elements	U	Th	La	Ce	Pr	Nd	Sm	Eu	Gd	Tb	Dy
Pabdeh	Min.	5.9	0.9	15.6	13.8	2.7	10.5	1.6	0.5	1.8	0.4	2.4
	Max.	107.9	10.9	171.5	162.1	39.2	190.0	23.4	5.6	25.4	4.5	32.7
	Average	33.1	2.7	26.8	37.8	5.1	20.6	4.0	1.0	4.5	0.8	4.8
	Enrich-ment Factor	8.8	0.2	0.9	0.6	0.6	0.8	0.7	0.8	0.9	0.9	-
Jeiroud	Min.	2.3	4.0	36.8	98.0	12.7	56.9	11.5	2.1	11.3	2.7	14.6
	Max.	8.1	26.7	114.9	296.2	38.4	165.6	34.0	9.5	36.3	7.0	40.8
	Average	5.4	11.6	81.5	198.9	25.1	111.3	22.3	5.0	23.2	4.8	27.3
	Enrich-ment Factor	2.1	0.9	2.8	3.2	3.4	4.3	4.1	4.7	4.9	5.9	-
Soltanieh	Min.	1.9	0.2	19.0	6.3	2.2	8.9	1.2	0.4	1.4	0.3	2.1
	Max.	5.5	3.2	42.6	28.4	7.2	30.2	4.6	1.2	5.3	1.1	6.7
	Average	3.4	1.2	30.9	14.6	4.9	19.8	3.2	0.7	2.8	0.7	4.6
	Enrich-ment Factor	1.3	0.1	1.0	0.2	0.6	0.7	0.6	0.6	0.6	0.9	-

TABLE 4 (Cont.). CHEMICAL COMPOSITION OF PHOSPHATE SAMPLES OF THE PABDEH, JEIROUD AND SOLTANIEH FORMATIONS (MAJOR ELEMENTS IN WT%; RARE EARTH ELEMENTS, U AND Th IN PPM)

Formation	Elements	Ho	Er	Tm	Yb	Lu	∑REE	Ce*	Eu*	La/Yb	Y	Sc
Pabdeh	Min.	0.6	1.7	0.29	1.7	0.2	57.6	0.3	0.6	6.8	27.6	2.7
	Max.	9.5	23.1	3.6	24.1	3.0	707.1	0.9	2.0	11.1	303.4	14.0
	Average	1.2	3.3	0.6	3.3	0.6	113.6	0.7	1.0	8.2	53.9	5.6
	Enrich-ment Factor	1.2	1.0	1.1	1.1	1.3	-	-	-	-	-	-
Jeiroud	Min.	3.8	8.7	1.5	8.0	0.7	277.3	0.9	0.8	3.2	101.6	4.8
	Max.	10.1	26.0	5.0	27.4	2.8	803.2	1.2	1.3	7.9	290.1	19.0
	Average	7.0	17.2	3.2	17.8	1.8	546.3	1.0	1.0	4.7	195.3	13.4
	Enrich-ment Factor	6.8	5.2	6.6	5.9	3.9	-	-	-	-	-	-
Soltanieh	Min.	0.6	1.6	0.3	1.3	0.1	45.9	0.2	0.9	8.9	38.3	0.8
	Max.	2.0	5.3	1.0	4.7	0.4	136.9	0.5	1.2	14.4	95.4	4.6
	Average	1.4	3.4	0.6	3.0	0.3	92.8	0.3	1.1	9.7	64.4	1.9
	Enrich-ment Factor	1.3	1.0	1.2	1.0	0.7	-	-	-	-	-	-

TABLE 4 (Cont.). CHEMICAL COMPOSITION OF PHOSPHATE SAMPLES OF THE PABDEH, JEIROUD AND SOLTANIEH FORMATIONS (MAJOR ELEMENTS IN WT%; RARE EARTH ELEMENTS, U AND Th IN PPM)

Formation	Elements	MgO	Na_2O	K_2O	FeO	Al_2O_3	CaO	P_2O_5	MnO_2	TiO_2
Pabdeh	Min.	0.7	0.0	0.1	0.8	0.5	15.4	4.3	0.0	0.0
	Max.	2.6	0.4	2.3	16.6	4.6	50.9	25.8	0.0	0.2
	Average	1.2	0.2	0.4	2.7	2.2	43.1	9.7	0.0	0.1
Jeiroud	Min.	0.2	0.2	0.0	0.9	0.2	10.8	7.2	0.0	0.1
	Max.	2.2	0.6	3.2	13.1	16.4	65.9	41.2	1.1	0.7
	Average	0.5	0.4	0.6	6.2	3.8	38.2	26.0	0.3	0.2
Soltanieh	Min.	1.4	0.1	0.1	0.3	0.3	21.8	5.0	0.1	0.0
	Max.	14.9	0.2	1.3	4.4	4.5	63.9	16.1	0.3	0.2
	Average	4.1	0.2	0.4	1.6	1.2	41.1	9.6	0.2	0.1

The REE patterns of the Choram and Khormoj deposits show flat, slightly rugged parallel curves. In contrast, the REE patterns of the Kuh-e Rish, Kuh-e Kumeh and Sheikh Habil deposits are not flat and show HREE enrichment relative to LREEs (Figure 4). NASC-normalized REE patterns of the phosphate samples in these deposits show a distinct negative Ce anomaly reflecting a reducing condition in the Pabdeh Formation depositional environment. The ratio La/Yb is one of the parameters that has been reported to estimate the degree of REE fractionation in minerals or rocks. In the studied phosphate samples from the Pabdeh Formation, La/Yb ratios are <10 (7.1–9.2) with an average of 8.5 which indicates that no REE fractionation has occurred (except the phosphate samples of Khormoj and one sample from the Choram deposit). La/Yb ratios in the studied phosphate samples of the Khormoj deposit are all >10, ranging from 10.2 to 10.9 with an average of 10.6 which indicates relatively high REE fractionation.

In the studied phosphate samples uranium shows a strong relation with P_2O_5 where the correlation coefficient, r = 0.83, and indicates an intimate relation of uranium during the deposition of the Pabdeh phosphates and the presence of uranium within the apatite structure. The variation of uranium content in the Pabdeh phosphate appears to be generally controlled by the variations of P_2O_5 (Figure 5). The REE are not correlated with P_2O_5 in phosphate samples from the Pabdeh Formation. In general, a distinct positive correlation exists between uranium and phosphorus content in the phosphate samples of the Pabdeh Formation (Figure 5).

6.2. Phosphatic horizon of Jeiroud Formation

Based on geochemical analysis in this study, the P_2O_5 values in various deposits of the Jeiroud Formation range from 7.2–41.2%. The mean total phosphorus in the phosphates of the Jeiroud Formation is 26%. In the phosphates of the Jeiroud Formation, the concentrations of uranium in

the studied phosphates range between 2.3 and 8.1 ppm with an average of 5.4 ppm. The content of ∑REE in the phosphates of the Jeiroud Formation ranges from about 277.3 to 803.2 ppm with an average of about 546.3 ppm. The enrichment factor of ∑REE ranges between 2.8 and 6.8, indicating that REEs are enriched in Jeiroud phosphates. The REE patterns of phosphate deposits of the Jeiroud Formation show flat, slightly rugged parallel curves, reflecting the coherence of REE as a geochemical group in the phosphates (Figure 4). There is a slight enrichment of medium and heavy rare earths (MREE, HREE) relative to light rare earths (LREE) in all phosphate samples of the Jeiroud Formation. NASC-normalized REE patterns of the phosphate samples in the Jeiroud Formation do not show a distinct Ce anomaly (ranging from 0.9 to 1.2 with an average of 1.0).

In the studied phosphate samples of the Jeiroud Formation, La/Yb ratios are all <10 (3.2–7.9) with an average of 4.7 indicating a low degree of REE fractionation. NASC normalized patterns of these deposits show a nearly convex pattern with a moderate positive Eu anomaly, revealing an anoxic (or sulphate reducing) diagenetic environment for the phosphate formation. Uranium shows a moderate relation with P_2O_5 where, r = 0.49 and an even lower correlation between P_2O_5 and ∑REE indicates a low degree of relation between REE during the deposition of the Jeiroud Formation phosphates.

In general, a moderate correlation exists between uranium and phosphorus content in the phosphate samples of the Jeiroud Formation. The correlation coefficients show that uranium in the phosphates of the Jeiroud Formation has a moderate to low positive correlation coefficient with P_2O_5, REE, Y and Sc. This may indicate a moderate relationship between uranium and these elements in the phosphate minerals of the Jeiroud Formation. There are strong positive inter-elemental correlations between all REE which attests to their strong coherence as a geochemical group and common enrichment processes in the phosphates of the Jeiroud Formation (e.g. Er vs Dy=0.97, Eu vs Gd=0.97). The REE show significant positive correlations with uranium in the phosphates of the Jeiroud Formation. The variation of uranium content in Jeiroud phosphate appears to be generally controlled by the variations of P_2O_5 and REEs and is not related to the abundance of other elements such as SiO_2, Al_2O_3, Fe_2O_3, CaO, MgO, Na_2O, K_2O, Co, Cu, Zn, Pb, Ti, Mo, Ni, Zr, Sr, Ba and Cr.

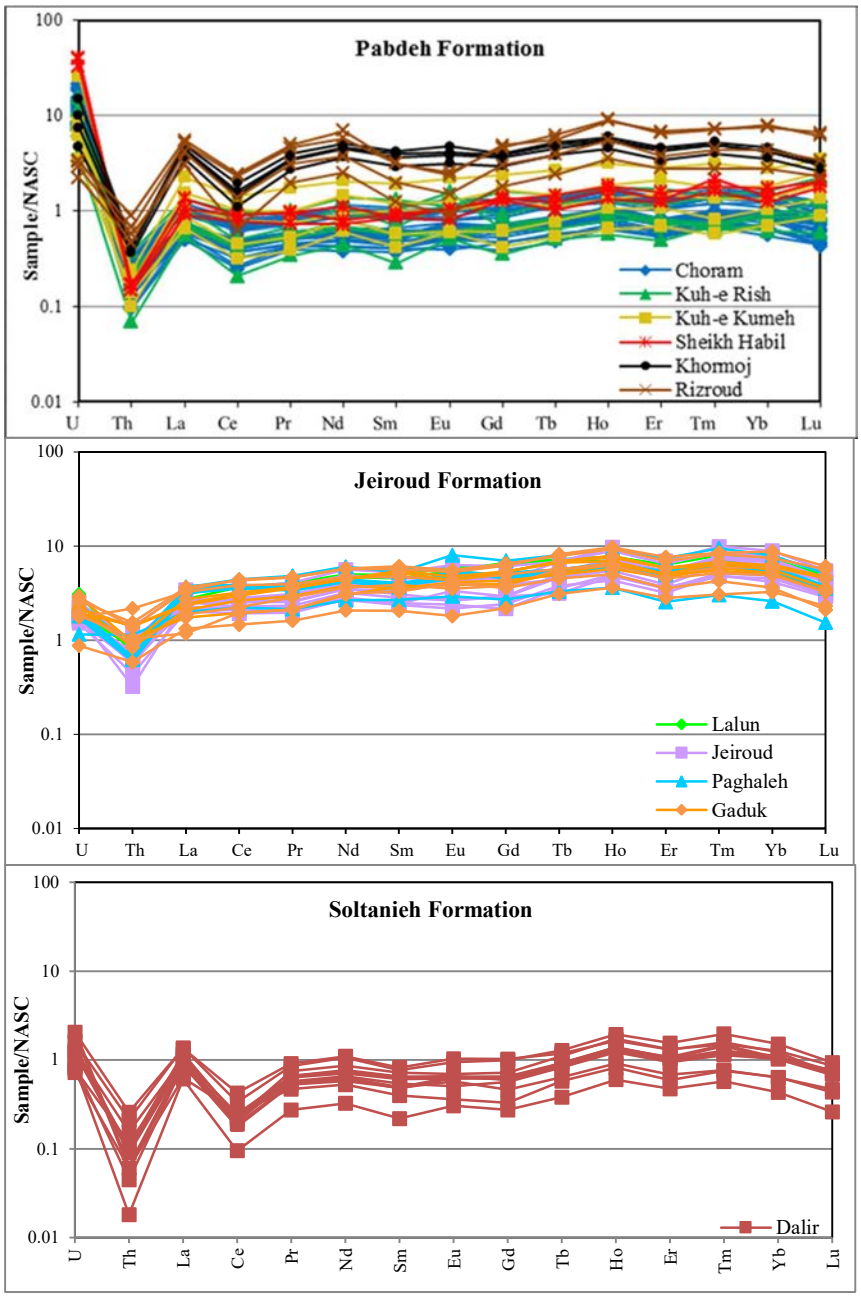

FIGURE 4. NASC normalized REEs, U, and Th distribution patterns for the phosphate deposits of the Pabdeh, Jeiroud and Soltanieh Formations.

6.3. Phosphatic horizon of Soltanieh Formation

The P_2O_5 values of the Dalir deposit range from 5.0–16.1% with an average of 9.6%. In the Dalir deposit, the concentrations of uranium in the studied phosphate samples range between 1.9 and 5.5 ppm with an average of 3.4 ppm. The uranium content is enriched 1.3 times compared with NASC shale values in studied phosphates of the Dalir deposit which indicates that the phosphates are not

enriched in uranium. ∑REE is low in Dalir phosphates and ranges from about 45.9 to 136.9 ppm with an average of about 92.8 ppm. The enrichment factor of ∑REE ranges between 0.3 and 0.8, demonstrating that REE are depleted in Dalir phosphates.

The shale normalized REE, U and Th contents of the studied samples of the Dalir deposit are plotted in Figure 4 which shows slightly flat curves. The cerium is depleted compared to its neighbour REE (Figure 4). In the studied phosphate samples of the Dalir deposit, La/Yb ratios are between 8.9 and 14.4 with an average of 9.7, indicating a moderate fractionation of LREE and HREE.

In the studied phosphate samples, uranium shows weak relation with P_2O_5 where, r = 0.26. The relationship between P_2O_5 and ∑REE shows the antipathetic relation where r = -0.13 (Figure 5). There are strong to moderate positive inter-elemental correlations between all REE which attest their strong coherence as a geochemical group (e.g. Er vs Dy=0.94, Eu vs Gd=0.93). The variation of uranium content in Dalir phosphate appears to be generally controlled by the variations of REEs and is not related to the abundance of P_2O_5 and other elements.

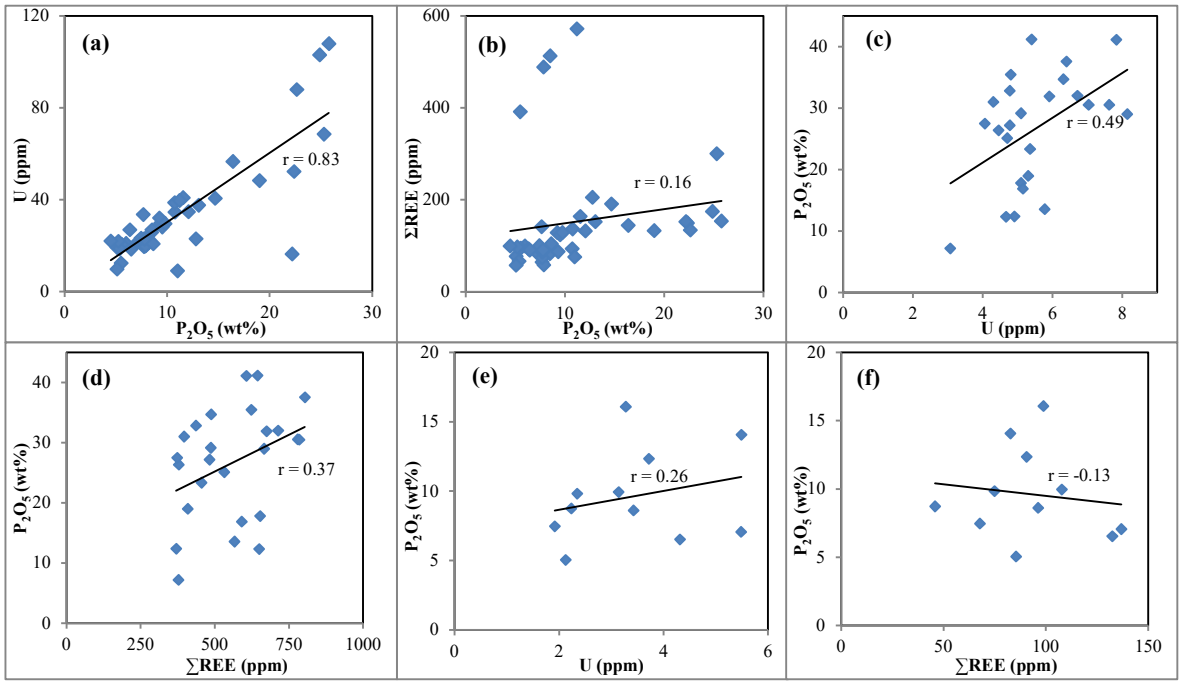

FIGURE 5. Variability of U and ∑REE vs. P_2O_5% in the phosphate samples: a, b) Pabdeh Formation; c, d) Jeiroud Formation; and e, f) Soltanieh Formation.

7. MINERALOGY

Mineralogical studies were carried out by XRD, optical mineralogy and electron microscope analyses (SEM). The list of main, minor and trace minerals in the phosphate rocks of sampled deposits of Pabdeh, Jeiroud and Soltanieh Formations are shown in Table 5.

TABLE 5. MINERALOGY OF THE PHOSPHATE ROCKS IN THE SELECTED DEPOSITS

Formation	Deposit	Mineralogy			
		Main minerals	Minor minerals	Trace minerals	Weathering products
Pabdeh	Choram	fluorapatite, calcite, quartz	illite, glauconite, pyrite, dolomite	barite, chlorite	goethite, crandallite
	Kuh-e Kumeh	fluorapatite, calcite, quartz, glauconite	pyrite, montmorillonite, illite	sphene	crandallite, goethite, hematite
	Sheikh Habil	fluorapatite, quartz, calcite	glauconite, pyrite	barite	goethite, hematite
	Khormoj	fluorapatite, calcite, glauconite, iron oxide (goethite and hematite)	quartz, montmorillonite (illite)	barite	goethite, hematite
	Rizroud	fluorapatite, calcite, glauconite, quartz, montmorillonite, illite	gypsum, pyrite, bassanite, barite	ilmenite, k-feldspar, siderite, Fe-sulphate	goethite
Jeiroud	Jeiroud	fluorapatite, quartz, calcite, ankerite	pyrite, barite, montmorillonite, illite	smectite, kaolinite, zircon, monazite, sphene, native Au	goethite
	Lalun	fluorapatite, quartz, calcite	pyrite, zircon, montmorillonite	rutile, native Fe, ankerite, illite	goethite, hematite
	Paghale	fluorapatite, quartz, calcite	pyrite, zircon, dolomite, illite	rutile, siderite, kaolinite, montmorillonite	goethite
	Gaduk	fluorapatite, quartz, calcite	pyrite, zircon, illite, montmorillonite	feldspar, rutile, barite, siderite, monazite, ilmenite	goethite
Soltanieh	Dalir	fluorapatite, calcite, quartz, dolomite	pyrite, montmorillonite, barite	siderite, rutile, illite	goethite

7.1. Phosphatic horizon of the Pabdeh Formation

The results of XRD and mineralogical studies, optical mineralogy and electron microscope analyses (SEM) on the Choram phosphate deposit indicate that the main minerals include fluorapatite, calcite and quartz accompanied by illite, crandallite, glauconite, pyrite and dolomite in minor amounts; and barite and chlorite in trace amounts. All these minerals occur as secondary replacements of a calcareous matrix and microfossils. Iron oxides like goethite which are final weathering products of pyrite, have filled the pores of calcite and apatite (Figure 6a).

The main minerals identified in the phosphate samples of the Kuh-e Kumeh deposit are fluorapatite, calcite, quartz and glauconite and the minor minerals consist of montmorillonite, illite, pyrite and crandallite. Sphene is present in trace amounts. Iron oxides (hematite and goethite) as final weathering products of pyrite have filled the pores of quartz (cement), calcite and apatite (Figure 6b).

The predominant minerals of the Sheikh Habil deposit are fluorapatite, calcite and quartz. The minor minerals consist of glauconite and pyrite accompanied by barite in trace amounts. Iron oxides like hematite and goethite as final weathering products of framboidal pyrite, have filled the pores of calcite and apatite (Figure 6c).

In the Khormoj deposit, the main minerals are fluorapatite, calcite and glauconite accompanied by quartz and clay minerals (montmorillonite and illite) in minor amounts and barite in trace amounts. Iron oxides (goethite and hematite) as weathering products of pyrite have filled the pores of calcite and apatite (Figure 6d).

The predominant minerals in the phosphates of the Rizroud deposit include fluorapatite, calcite, quartz, glauconite and clay minerals (montmorillonite and illite) accompanied by gypsum, pyrite, barite and bassanite in minor amounts and ilmenite, K-feldspar, siderite and Fe-sulphate in trace amounts. Weathering of pyrite produces iron oxides, including goethite (Figures 6e, f).

According to mineralogical studies on the phosphate deposits of the Pabdeh Formation, uranium minerals have not been observed. The main uranium-bearing mineral is most likely fluorapatite in the Choram, Kuh-e Kumeh, Sheikh Habil, Khormoj and Rizroud deposits. In near-surface samples, apatite is weathered to crandallite and uranium released from the apatite can enter the lattice of crandallite. Therefore, in addition to apatite, crandallite can also be a host of uranium. The phosphatic horizons of the Khormoj and Rizroud deposits in the base of the Pabdeh Formation are enriched in REEs and the main REE-bearing mineral is most likely fluorapatite. The REE and U can replace Ca in the structure of fluorapatite.

7.2. Phosphatic horizon of the Jeiroud Formation

In the phosphate samples of the Jeiroud mine, fluorapatite, quartz and carbonate (ankerite and calcite) are the predominant constituent minerals followed by subordinate amounts of pyrite, montmorillonite, barite and illite. Smectite, kaolinite, zircon, monazite, sphene and native gold occur in trace amounts. Iron oxides (like goethite) are the final product of the weathering of pyrite grains (Figure 7a).

Mineralogical studies on the phosphate samples of the Lalun deposit indicate that fluorapatite, quartz and carbonate (calcite) occur as major minerals. The minor minerals are pyrite, zircon and clay minerals such as montmorillonite accompanied by trace amounts of rutile, native iron, ankerite and illite. Pyrite is weathered to iron-oxides such as goethite and hematite (Figure 7b).

The main minerals of the Gaduk deposit include fluorapatite, quartz and calcite and the minor minerals consist of pyrite, illite, montmorillonite and zircon. The trace minerals are feldspar, rutile, barite, siderite, monazite and ilmenite. Only in one thin section, detrital native gold and copper were observed. The margins of pyrite grains have been replaced by iron oxides such as hematite and goethite during weathering (Figure 7c).

The main minerals in the phosphates of the Paghaleh deposit are fluorapatite, calcite and quartz accompanied by minor amounts of zircon, dolomite, illite and pyrite and trace amounts of rutile, siderite, kaolinite and montmorillonite. Pyrite has been replaced by iron oxides like goethite during weathering (Figure 7d).

According to mineralogical studies, the main REE-bearing mineral in the phosphates of the Jeiroud Formation is most likely fluorapatite and the minor host of REEs is monazite. Zircon in minor amounts and sphene in trace amounts may host some of the REEs. In one thin section from the Gaduk deposit, REE-Ti-Fe minerals were observed as inclusions in quartz grains.

7.3. Phosphatic horizon of the Soltanieh Formation

Mineralogical studies on Dalir Phosphates showed that the main minerals are fluorapatite, calcite, quartz and dolomite. Other important minerals include pyrite, montmorillonite and barite in minor amounts and siderite, rutile and illite in trace amounts. Pyrite in minor amounts, both as individual grains and as aggregates within the phosphate grains and the matrix have been substantially altered to iron oxides, particularly goethite (Figure 8).

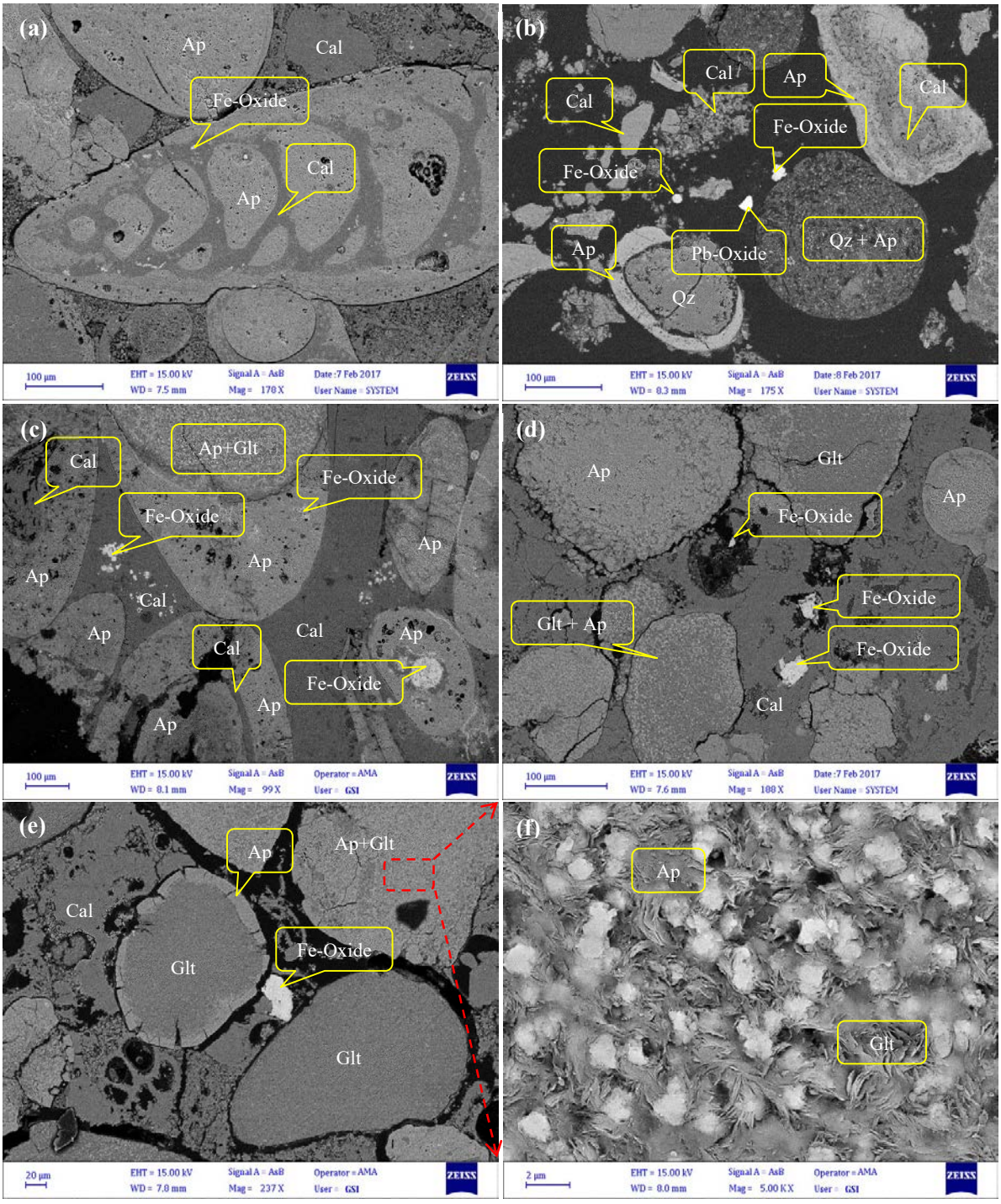

FIGURE 6. BSE images of: a) foraminiferal chambers with calcitic shells filled by phosphate mineral in Choram deposit; b) Pb-mineral in the Kuh-e Kumeh phosphate rock; c) carbonate cement of the Sheikh Habil phosphate rock; d) replacement of glauconite by apatite within calcite cement in Khormoj deposit; e) replacement of glauconite by apatite from margin with endogangue of glauconite in Rizroud deposit. Red box refers to area included for close up; and f) close-up of image (e) showing small flakes of glauconite (Ap: apatite; Cal: Calcite; Glt: Glauconite; Qz: Quartz).

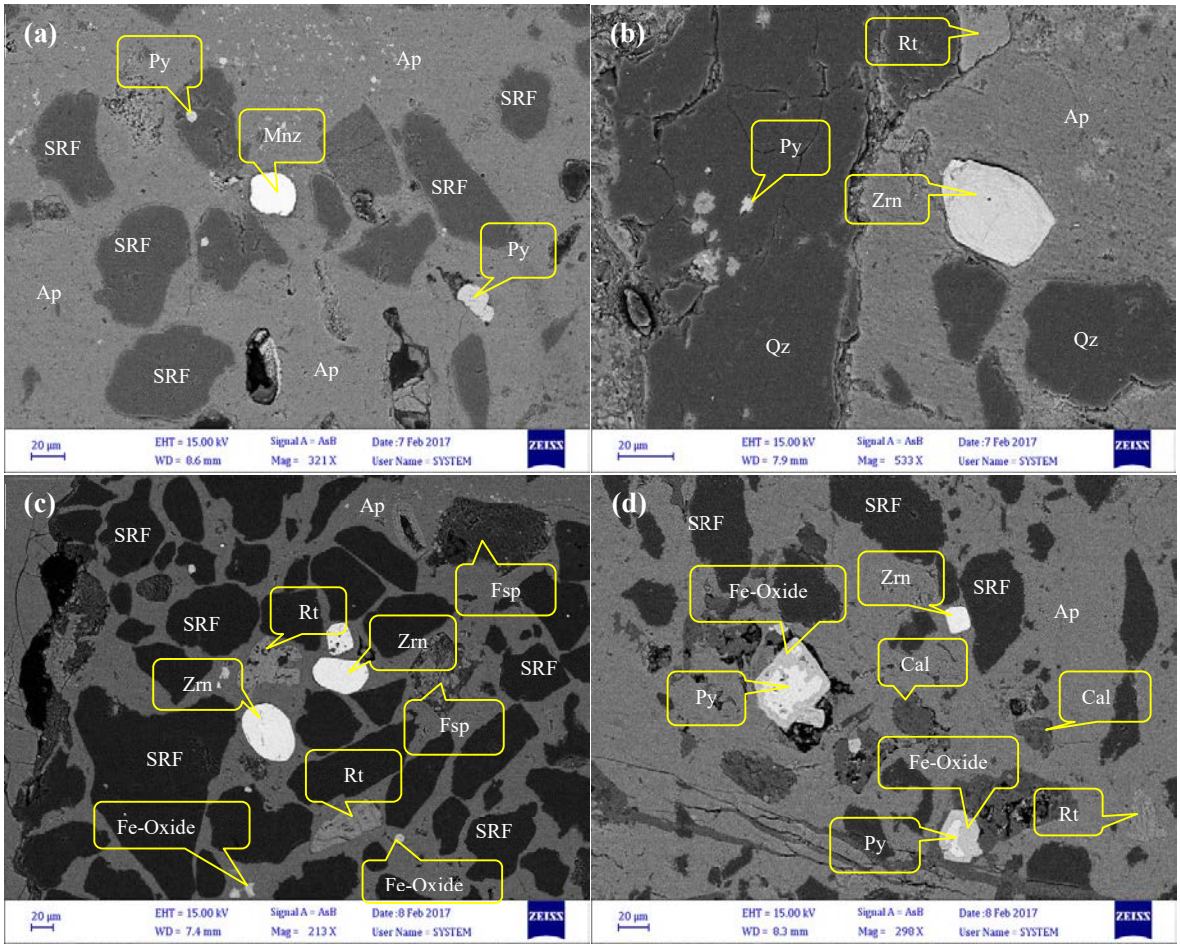

FIGURE 7. BSE images of: a) sedimentary rock fragments within the apatite cement in the phosphate rock of Jeiroud mine; b) detrital zircon and rutile in Lalun phosphate rock; c) detrital zircon and rutile in sedimentary rock fragments within phosphatic cement in Gaduk phosphate rock; and d) weathering of pyrite margins into iron-oxide in the Paghaleh deposit (Ap: apatite; Cal: Calcite; Fsp: Feldspar; Mnz: Monazite; Py: Pyrite; Qz: Quartz; Rt: Rutile; SRF: Sedimentary Rock Fragments; Zrn: Zircon).

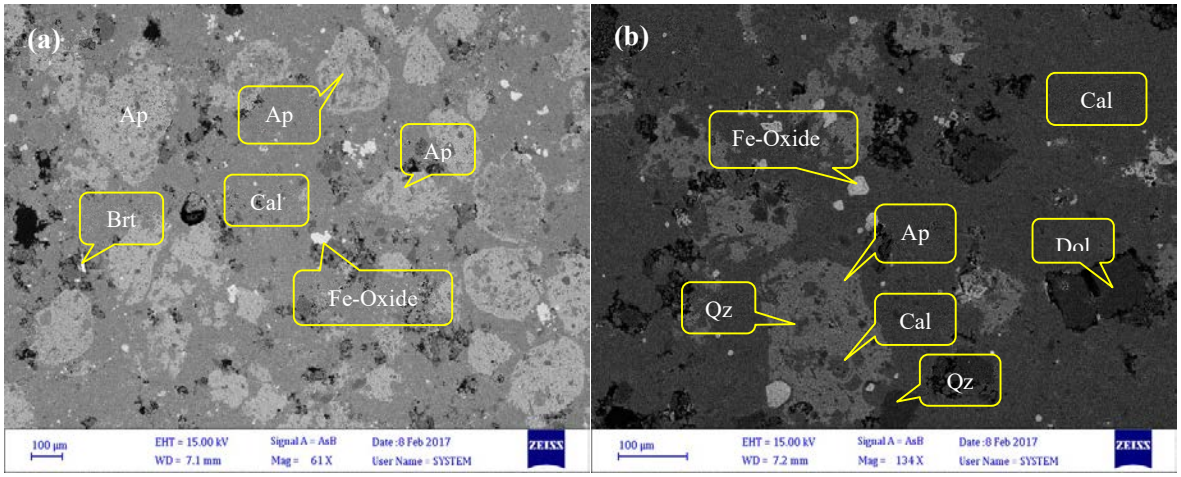

FIGURE 8. BSE images of: a) phosphate pellets with a diameter of 0.1 to 0.4 mm within a carbonate matrix; and b) quartz and calcite inclusions in phosphate pellets (Ap: Apatite; Brt: Barite; Cal: Calcite; Dol: Dolomite; Qz: Quartz).

8. CONCLUSIONS

Considering the behaviour of uranium in phosphates, eight major factors which govern uranium enrichment in phosphorite, including depositional environment, mineralogy, organic matter, phosphorous grade, Eh, pH, paleoclimate and weathering were defined.

Distal shoreline and proximal shoreline marine with local reworking are favourable environments for uranium enrichment in phosphorite. Uranium can easily replace elements such as Ca in francolite but not in minerals such as wavellite and crandallite. The presence of organic matter is necessary to accumulate uranium in phosphorite. In general, uranium content varies directly with P_2O_5 grade. Uranium concentration in phosphorite is favoured in a reducing medium and weakly alkaline pH. In a hot arid climate, leached uranium is transported by rivers from the continent to the sea and provides vital sources of uranium for sedimentary phosphates. During weathering, uranium is leached easily from apatite and can be enriched in the lower part of phosphate.

Based on evaluation of the factors controlling the uranium enrichment in sedimentary phosphate, Pabdeh and Gurpi Formations are predisposed to having the best geological potential for uranium enrichment of the phosphate-bearing formations in Islamic Republic of Iran. Given that the number and tonnage of phosphate deposits of the Gurpi Formation are low and that they are also phosphorous-bearing Fe deposits, the phosphates of this formation were not sampled.

Based on evaluation of the defined factors for uranium enrichment and the hot and humid climate during precipitation of phosphatic horizons, the Jeiroud and Soltanieh Formations have no geological potential for uranium enrichment.

The phosphatic horizon of the Pabdeh Formation contains a relatively high content of uranium (up to 108 ppm). The Eocene-Oligocene phosphatic horizon in the middle Pabdeh Formation is depleted in REEs at the Choram and Kuh-e Rish deposits and not enriched at the Keh-e Kumeh

and Sheikh Habil deposits, however the Paleocene phosphatic horizon at the base of the Pabdeh Formation is relatively enriched in REEs (up to 707 ppm).

The uranium contents of the Jeiroud phosphates vary from 2.3 to 8.1 ppm. The contents of ∑REE in Jeiroud phosphates range from 277.3 to 803.2 ppm (average 546.3 ppm). REE are enriched in the Jeiroud phosphates with an enrichment factor of 2.8–6.8.

The phosphate horizon of the Dalir deposit does not show significant uranium (up to 5.5 ppm) or REE (up to 137 ppm) enrichment. All phosphates of the sampled formations show marked depletion in Th.

Based on mineralogical study by SEM-EDS, no uranium minerals were observed in the phosphates of the Pabdeh Formation. The mineralogical studies and strong positive correlation between uranium and P_2O_5 suggest that the main U-bearing mineral is most likely apatite (substitution of uranium for calcium in apatite). The mineralogical studies suggest that the main REE-bearing mineral in the Pabdeh Formation is most likely apatite and monazite is another minor REE bearing mineral.

The results of this study demonstrate that the defined factors for uranium enrichment can be applicable to evaluate uranium enrichment in other marine phosphate deposits globally and in particular where chemical analysis for uranium has not been carried out.

REFERENCES

[1] STRUTT, R., On the distribution of radium in the earth's crust, Proc. R. Soc. London, Ser. A **78** (1906) 150–153.

[2] STRUTT, R., The accumulation of helium in geological time, Proc. R. Soc. London, Ser. A **81** (1908) 272–277.

[3] KOCHENOV, A.V., BATURIN, G.N., The paragenesis of organic matter, phosphorus, and uranium in marine sediments, Lithology and Mineral Resources **37** 2 (2002) 107–120.

[4] BATURIN, G.N., KOCHENOV, A.V., Uranium in phosphorites, Lithology and Mineral Resources **36** 4 (2001) 303–321.

[5] NATHAN, Y., The mineralogy and geochemistry of phosphorite, In: NRIAGU, J.O., MOORE, P.B., Eds., Phosphate minerals, Springer-Verlag, Berlin (1984) 275–291.

[6] SIMANDL, G.J., PARADIS, S., FAJBER, R., Sedimentary phosphate deposits: Mineral deposit profile F07, Technical Report, British Columbia Ministry of Energy, Mines and Petroleum Resources (2012) 217–222.

[7] GHORBANI, M., The economic geology of Iran: Mineral deposits and natural resources, Springer, Dordrecht, Heidelberg, New York, London (2013) 153–159.

[8] HALALAT, H., BOLOURCHI, M.H., Geology of Iran: Phosphate, Geological Survey and Mineral Exploration of Iran, Tehran (1995) (In Persian).

[9] DAHLKAMP, F.J., Uranium deposits of the world: Asia, Springer-Verlag, Berlin, Heidelberg (2009) 23 pp.

[10] DAHLKAMP, F.J., Uranium ore deposits, Springer-Verlag, Berlin, Heidelberg, New York (1993).

[11] EMEL'YANOV, E.M., Distribution and composition of muds on the shelf of Southwestern Africa, Tr. Inst. Okeanol. Akad. Nauk SSSR **95** (1973) 211–238.
[12] BREMNER, J.M., Brief description of a west coast phosphorite deposit, Geological Survey of South Africa, Report 0100, South Africa (1992).
[13] CALVERT, S.E., PRICE, N.B., Geochemistry of Namibian Shelf Sediments, Coastal Upwelling- Its Sediment Record, Suess, E., Thiede, J., Eds., New York: Plenum, part A (1983) 227–275.
[14] LUCAS, J., ABBAS, M., Uranium in natural phosphorites: Syrian example, Bull. Sci. Geol. Strasbourg **42** (1989) 223–236.
[15] ABED, A.M., Review of uranium in the Jordanian phosphorites: Distribution, genesis and industry, Jordan Journal of Earth and Environmental Sciences **4** 2 (2011) 35–45.
[16] TITAYEVA, N. A., Nuclear geochemistry: Translated from the Russian by Egorov, G., Advances in science and technology in the USSR (1994) 77–78.
[17] BATURIN, G.N., DUBINCHUK, V.T., Modes of uranium occurrence in oceanic phosphorites, Okeanologiya **18** 6 (1978) 1036–1041.
[18] BATURIN, G.N., DUBINCHUK, V.T., Mikrostruktury okeanskikh fosforitov (microtextures of oceanic phosphorites), Moscow: Nauka (1979).
[19] BATURIN, G.N., DUBINCHUK, V.T., Mineralogy of phosphatic sands from the Namibian Shelf, Litol. Polezn. Iskop. **6** (1999) 632–646.
[20] BATURIN, G.N., DUBINCHUK, V.T., KOCHENOV, A.V., Uranium in the process of modern phosphorite formation, Geokhimiya **9** (1986) 1277–1284.
[21] BELOVA, L.N., GORSHKOV, A.I., DOINIKOV, O.A., A new uranous phosphate, Dokl. Akad. Nauk. **349** 3 (1996) 361–363.
[22] ABED, A.M., SADAQAH, R.M., Enrichment of uranium in the uppermost Al-Hisa Phosphorite Formation, Eshidiyya Basin, Southern Jordan, Journal of African Earth Sciences **77** (2013) 31–40.
[23] ALTSCHULER, Z.S., The Geochemistry of trace elements in marine phosphorites: Part 1, characteristic abundances and enrichment, Marine Phosphorites (SEPM Spec. Publ.) 29 (1980) 19–30.
[24] KOCHENOV, A.V., DUBINCHUK, V.T., GERMOGENOVA, E.V., The form of uranium occurrence in phosphate remains of fossil fishes, Sov. Geol. **3** (1973) 60–77.
[25] OSTROVSKAYA, G.Y., Uranium in rocks of phosphorite-bearing formations, Soviet Atomic Energy **36** 3 (1974) 189–194.
[26] CATHCART, J.B., Uranium in phosphate rock. Geological Survey Professional Paper 988-A, U.S. Department of the Interior, Geological Survey (1978).
[27] ABED, A.M., The Eastern Mediterranean phosphorite giants: An interplay between tectonics and upwelling, Geo. Arabia **18** (2013) 67–94.
[28] BAHRAMI, M., SHIRAZI, M.P., Microfacies and sedimentary environments of Gurpi and Pabdeh Formations and the type of Mesozoic- Cenozoic boundary in Fars province, Iran, Journal of Applied Geology **5** 4 (2010) 330–335.
[29] BEHBAHANI, R., MOHSENI, H., KHODABAKHSH, S., ATASHMARD, Z., Depositional environment of the Pabdeh Formation (Paleogene) elucidated from trace fossils, Zagros Basin, Iran; The 1st International Applied Geological Congress, Mashhad, Iran (2010) 26–28.
[30] MOHSENI, H., AL-AASM, I.S., Tempestite deposits on a storm-influenced carbonate ramp: An example from the Pabdeh Formation (Paleogene), Zagros Basin, SW Iran, Journal of Petroleum Geology **27** 2 (2004) 163–178.

[31] CHESHMEHSARI, M., ALIPOUR, S., ABEDINI, A., ZINAT MOTLAQ, A., Mineralogy and geochemistry of REEs and U in Kuh-e Lar phosphatic deposit, SE Dehdasht, Kohgiluyeh and Boyer-Ahmad province. 31st Geology Conference in Iran (2012) (In Persian).
[32] POURKASEB, H., DAMIRI, K., ZARASVANDI, A., CHERCHI, A., Geochemistry of Phosphatic horizons of Kuh-e Sefid and Bonari in SW Iran. Iranian Society of Crystallography and Mineralogy **4** (2011) 749–760 (In Persian).
[33] POURKASEB, H., ZARASVANDI, A., CHERCHI, A., DAMIRI, K., Using mineralogical and textural evidences for determination of occurrence of Bonari phosphate deposit (Kuh-e Lar), Dehdasht, Kohgiluyeh and Boyer-Ahmad Province, 1st Economic Geology Conference of Iran (2012) 96–101 (In Persian).
[34] TABATABAEI, H., MOTAMED, A., SOLEIMANI, B., KAMALI, M.R., Chemical variation during Pabdeh Formation deposition, Zagros Basin: Gurpi-Pabdeh-Asmari boundaries determination and paleoenvironmental condition, Geol Geosci. **1** 1 (2012) 1–8.
[35] ZEEBE, R.E., History of seawater carbonate chemistry, atmospheric CO_2, and ocean acidification. Annual Reviews Earth Planet Sci. **40** (2012) 141–165.
[36] BERBERIAN, M., A Brief Geological Description of North-Central Iran, Geol. Surv. Iran **29** (1974) 127–138.
[37] ASSERETO, R., The Paleozoic formations in Central Elburz (Iran) (preliminary note), Rivista Italiana di Paleontologia e Stratigrafia **69** (1963) 503–543.
[38] SAMIMI, M., MOVAHED AVAL, M., HAGHIPOUR, A., New discoveries of phosphate in Iran, Report of Geological Survey and Mineral Exploration, Iran (1965) (In Persian).
[39] AGHANABATI, M., Geology of Iran, Geological Survey and Mineral Exploration of Iran, Tehran (2004) (In Persian).
[40] KAZEMI, M., SHAFIEI, B., SHAMANIAN, H., AMINI, A., Explaining mineralizations related to genesis and evolution of Proto- and Paleo- Tethys in Alborz Zone, 31st Conference of Earth Science, Tehran, Iran (2012) 1–8 (In Persian).
[41] RAHMANI, B., Studying the environmental effects of Jeiroud phosphate mine on the water and soil of the area, M.Sc Thesis, Shahid Bahonar University, Kerman (2009) (In Persian).
[42] NAMADMALIAN, A., Petrology of Jeiroud phosphorite, north of Tehran, Iran, M.Sc Thesis, Azad University, Tehran, Iran (1989) (In Persian).
[43] KHIREKESH, Z., Mineralogy and geochemistry of phosphate rock in Firuzkuh region, Ph.D. Thesis, Golestan University, Iran (2016) (In Persian).
[44] KOHANSAL GHADIMVAND, N., MANDALZADEH, R., Depositional environment and sequence stratigraphy of Jeiroud Formation in the southern flank of Aynehvarzan- Dalichai anticline, East of Damavand (Central Alborz), Journal of the Earth **3** 3 (2008) 37–48 (In Persian).
[45] ABEDIAN, N., Phosphate prospecting in Gilan Province, Report of Geological Survey and Mineral Exploration of Iran (2008) (In Persian).
[46] AFSHOUN, K., REZAIE, M.H., GHAZIANI, V., HEMMATKHANI, H.R., Comprehensive plan for strategy of phosphate ore mineral in Iran, Report of Ministry of Industries and Mines. Iran (1994) (In Persian).

[47] SHARIFI, J., Geology of Lower Cambrian phosphates of Soltanieh Formation, Central Alborz, PhD Thesis, Geological Engineering Faculty, Ankara University, Turkey (2002).
[48] CHESHMEHSARI, M., ABEDINI, A., ALIZADEH, A., JALILIAN, Z., MORADI, S., Trace element geochemistry of the Dalir phosphate deposit, southwest of Chalous, Mazandaran, 4th Conference of Economic Geology of Iran (2012) 255–260 (In Persian).
[49] CHESHMEHSARI, M., ABEDINI, A., ALIZADEH, A., MOUSAVI, M., REEs mineralogy and geochemistry of the Dalir phosphatic horizon (SW of Chalous, Mazandaran), Journal of Economic Geology **2** 4 (2013) 319–333 (In Persian).
[50] MOUSAVI, H., ABBASSI, N., CALAGARI, A., ABEDIN, A., Geochemical investigation of rare earth elements (REE) in Soltanieh Formation phosphatic horizon, Seyed Kandi section, Southwest Zanjan, 33rd National Geosciences Symposium, Iran (2015) 1–19 (In Persian).
[51] NAMADMALIAN, A., OKHOVAT, Z., MOMENZADEH, M., Phosphate in Iran, Geological Survey and Mineral Exploration of Iran, Tehran (1998) (In Persian).
[52] VAZIRI MOGHADDAM, H., Biostratigraphic study of the Ilam and Gurpi Formations based on planktonic Foraminifer in SE of Shiraz, Iran, Journal of Sciences, Islamic Republic of Iran **13** 4 (2002) 339–356.
[53] BEIRANVAND, B., GHASEMINEJAD, E., KAMALI, M.R., AHMADI, A., Sequence Stratigraphy of the Late Cretaceous–Paleocene Gurpi Formation in southwest Iran, GeoArabia **19** 2 (2014) 89–102.
[54] ZAREI, E., GHASEMINEJAD, E., Sequence stratigraphy of the Gurpi Formation (Campanian–Paleocene) in southwest of Zagros, Iran, based on Palynomorphs and Foraminifera, Arabian Journal of Geosciences **8** 6 (2015) 4011–4023.
[55] HADAVI, F., SENEMARI, S., Calcareous nannofossils from the Gurpi Formation (Lower Santonian-Maastrichtian), Faulted Zagros Range, Western Shiraz, Iran, Stratigraphy and Geological Correlation **18** 2 (2010), 166–178.
[56] HOSSEINI-BARZI, M., BAYETGOLL, A., Facies analysis and sedimentary environment of mixed carbonate-siliciclastic deposits of Shirgesht Formation in Kalmard Block, Central Iran, Journal of Sedimentary Facies of Ferdosi University **2** 1 (2009) 1–24 (In Persian).
[57] BAYETGOLL, A., MOUSAVI-HARAMI, R., MAHBOUBI, A., Sedimentary environments and stratigraphy of the carbonate-siliciclastic deposits of the Shirgesht Formation: Implications for eustasy and local tectonism in the Kalmard Block, Central Iran, Stratigraphy and Sedimentology Researches **31** 3 (2015) 37–68.
[58] BAYETGOLL, A., HOSSEINI-BARZI, M., Major elemental geochemistry of siliciclastic deposits of Shirgesht Formation, in Kalmard Block, Central Iran, for inferring tectonic provenance and parent rock weathering, Journal of Earth Science **79** (2011) 101–112 (In Persian).
[59] ABSHAHI, M., SADRI, M., Prospecting of phosphate in Paleozoic and Upper Cretaceous sedimentary in Kerman region, Report of Geological Survey and Mineral Exploration, Iran, (1986) (In Persian).
[60] HALALAT, H., SALEHI SIAVOSHANI, H., HOSSEINI DOOST, J., MALEKZADEH, L., Prospecting of phosphate in Tabas-Shirgesht, Ozbak Kuh and Kashmar regions, Report of Geological Survey and Mineral Exploration, Iran (1983) (In Persian).

[61] ORRIS, G.J., DUNLAP, P., WALLIS, J.C., Phosphate occurrence and potential in the region of Afghanistan, including parts of China, Iran, Pakistan, Tajikistan, Turkmenistan, and Uzbekistan, U.S. Geological Survey, Reston, Virginia, Open-File Report 2015-1121 (2015).
[62] KHAZAEI, E., MAHMOUDY-GHARAIE, M.H., MAHBOUBI, A., MOUSSAVI-HARAMI, R., TAHERI, J., Petrography, major and trace elemental geochemistry of the Ordovician-Silurian siliciclastics in north of Tabas Block, Central Iran: Implications for provenance and paleogeography, Journal of Sciences: Islamic Republic of Iran **29** 2 (2018) 129–142.
[63] SALEHI, H., The sedimentary phosphate resources of Iran, In: NOTHOLT, A.J.G., SHELDON, R.P., AND DAVIDSON, D.F., Eds., Phosphate deposits of the world, Vol. 2, Phosphate rock resources: Cambridge, Cambridge University Press (1989) 323–328.
[64] GROMET, L.P., HASKIN, L.A., KOROTEV, R.L., DYMEK, R.F., The North American shale composite: Its compilation, major and trace element characteristics, Geochimica et Cosmochimica Acta **48** 12 (1984) 2469–2482.

RADIOMETRIC AND SPECTROANALYTICAL CHARACTERIZATION OF URANIUM- AND THORIUM-BEARING SAMPLES FROM SELECTED ALKALINE CARBONATITE COMPLEXES OF KENYA

H. K. ANGEYO, M. I. KANIU, A. DEHAYEM-MASSOP, J. P. PATEL
Department of Physics,
School of Physical Science,
University of Nairobi,
Nairobi, Kenya

Abstract

Although the alkaline-carbonatite complexes of Kenya, some of which occur in geothermally active high background radiation areas (HBRA), have considerable uranium and thorium potential, they have not been systematically characterized. The challenge of prospecting for and planning towards environmentally friendly mining of uranium and thorium necessitates development of rapid and direct methods for geochemical and mineralogical characterization of these deposits since mineralogical constraints exert significant control over their extraction. This project entailed developing nuclear and laser based spectroscopic methods for trace (elemental, molecular, radiogenic, and isotopic) analysis and spectral imaging utilizing multivariate chemometrics and machine learning techniques towards direct geochemical characterization of thorium- and uranium-bearing samples in Kenya's HBRA. The goals are to understand the genesis and process history of the deposits; how catchment geology is linked to uranium and thorium signatures; and how mineralogical controls influence uranium and thorium occurrences. In this way it is hoped to discriminate new uranium and thorium discoveries and constrain the geological models of deposits. This has significance in the sustainability of Kenya's nuclear power programme (It was envisaged the results of this work will also help to enrich the IAEA databases, World Distribution of Uranium Deposits (UDEPO) and World Thorium Deposits and Resources (ThDEPO). As most of Kenya's HBRA lie in geothermal fields, this study had additional utility in the exploration (geothermal reservoir diagnostics) and development of geothermal resources in the country.

1. INTRODUCTION

Concentrations of uranium and thorium in the continental crust can form ore deposits [1]. Several uranium and thorium mineralizations occurring mostly as carbonatite volcanoes and extrusions are found in Kenya [2]. These include Mrima and Jombo Hills [3], Homa and Ruri Hills [4], Kerio Valley [5], Tinderet [6, 7], and Oldoinyo Nyegi and Shompole [8]. The enhanced radioactivity in these areas has been attributed to sedimentary formations with a provenance comprised of deeply weathered igneous rocks [3, 9].

Mrima Hill is part of the alkaline igneous complex centred on the Jombo Hill whose intrusive rocks have anomalous magnetic properties [2]. Homa and Ruri Hills are carbonatite ring complexes associated with alkaline igneous intrusive activity and so are rich in soda and lime in carbonated condition. It is the iron-stone segregation in these areas that is associated with the abnormally high radioactivity. Kerio Valley lies in a geothermally active field of the North Kenyan Rift [10]. Heavy elements normally associated with fluorite ore deposits have been measured in the area [11]. Studies in the area found uranium concentration ranges of 34– 983 ppm while thorium ranges from 23–166 ppm [5]. The Tinderet volcano is located about 120 km from Kerio Valley. The area is characterized by blocks of carbonatite lavas with calcite, minor apatite, fluorite, spinel-group minerals, accessory perovskite and 'plumbopyrochlore'.

There is a remarkable similarity, in terms of petrography and mineralogy between the carbonatites from the Tinderet and Oldoinyo Lengai volcano [6, 7, 12], the latter being the Earth's sole active carbonatite volcano that erupts and discharges unique natrocarbonatite lava characterized by Na- and K-bearing magmatic carbonatites.

In the parent materials, most of uranium and thorium are bound in accessory minerals such as zircon, alunite, sphene, monazite and apatite [13–16]. Uranium minerals mainly occur as uraninite, pitchblende or as secondary minerals (oxides, silicates, phosphates, vanadates).

The correct identification of such minerals and their chemical composition is critical to the understanding of the genesis and history of a deposit [17]. For this reason, there is a need in the geosciences for direct rapid techniques for mineral identification and chemical analyses.

2. MATERIALS AND METHODS

We used a number of techniques (laser induced breakdown spectroscopy (LIBS) — and its new extension laser ablation molecular isotopic spectrometry (LAMIS); energy dispersive X-ray fluorescence (EDXRF) spectrometry; laser Raman microspectrometry (LRM); laser induced fluorescence (LIF) spectroscopy; and laser scanning microscopy (LSM) towards developing a multimodal protocol for direct geochemical analysis and characterization of thorium- and uranium-bearing samples from Kenya's alkaline-carbonatite complexes. These techniques are targeted for their versatility, potential sensitivity, speed, and in-situ capabilities.

3. RESULTS AND DISCUSSION

3.1. Radiometric surveying and gamma ray spectrometry

The most fundamental task in this work was to perform rapid assessment of radiation levels using in-situ gamma-ray spectrometry [18–20]. In contrast to laboratory measurements, in-situ gamma-ray spectrometry offers a low-cost, rapid, spatially representative radioactivity estimate even in rugged environments.

Characterized by a variety of rock formations namely alkaline, igneous and sedimentary rocks which contain significant deposits of monazite and pyrochlore, Mrima and Jombo Hills are highly heterogeneous with regard to their geochemistry, mineralogy and geological formation. They are one of the several alkaline carbonatite complexes of Kenya that are associated with high natural background radiation and therefore a radioactivity anomaly. However, this high background radiation anomaly has not been systematically assessed and delineated with regard to the spatial, geological, geochemical and anthropogenic variability. We conducted wide-ranging in-situ gamma-ray spectrometric measurements in this area. The goal of the study was to assess the radiation exposure as well as to determine the underlying natural radioactivity levels in the region.

Both 2.0 litre and 0.347 litre NaI(Tl) PGIS-2 portable detectors integrated with GPS were deployed for ground and vehicular radiometric measurements (Figure 1). Window based and spectral stripping methods were used for determination of natural radioactivity concentrations and terrestrial gamma dose-rates. We obtained a spatially representative radioactivity estimate across a

range of landscapes [21, 22] (Figures. 2a, 2b). Results obtained so far include occurrence and radioactivity (U, Th) and radiation maps of the Mrima and Kiruku hill ores are shown in Figure 3.

FIGURE 1. Measurements using PGIS-128 gamma spectrometer at the base of Mrima Hill.

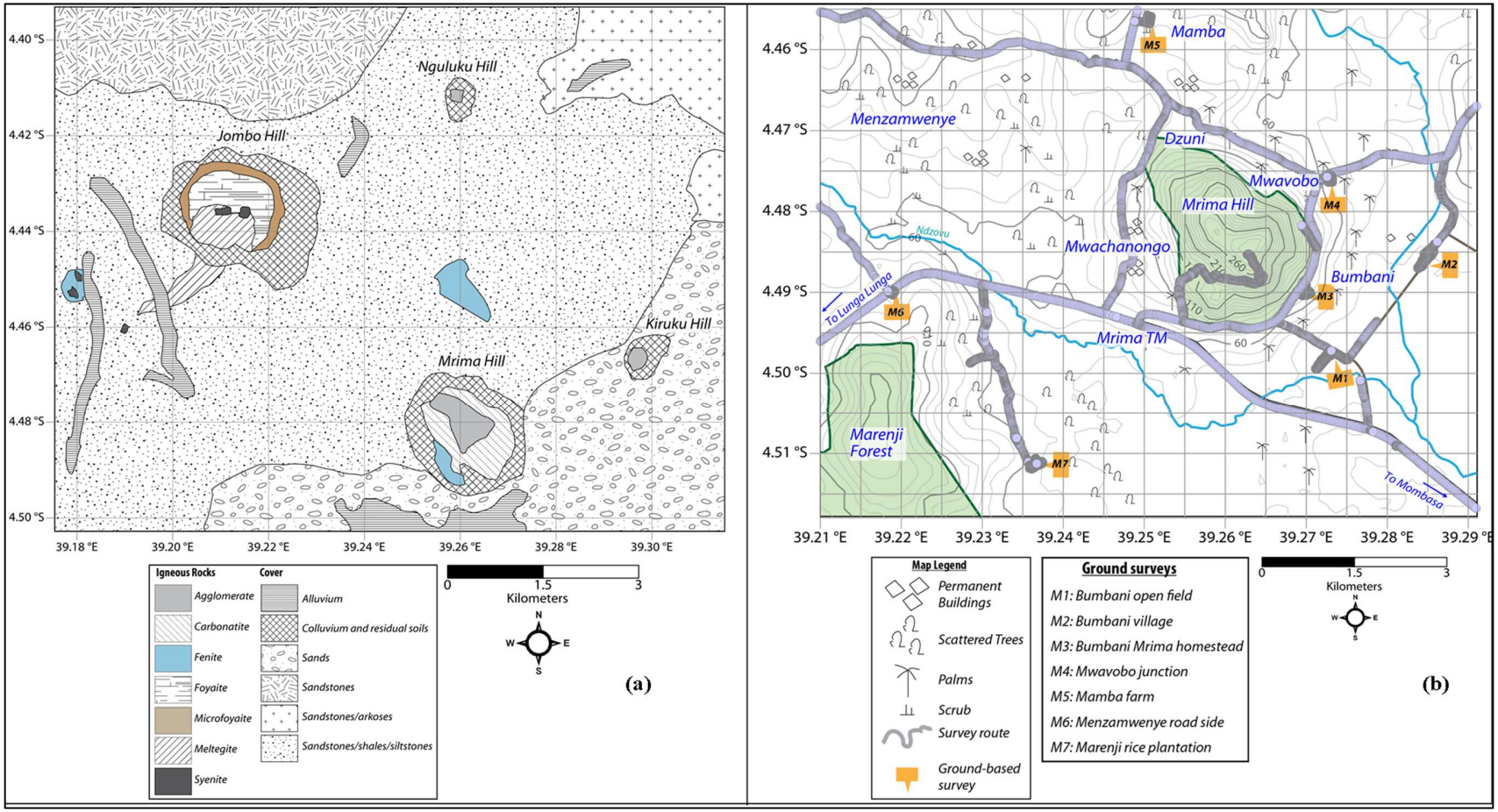

FIGURE 2. Maps indicating (a) geology of Jombo alkaline igneous complex and (b) surveying sites.

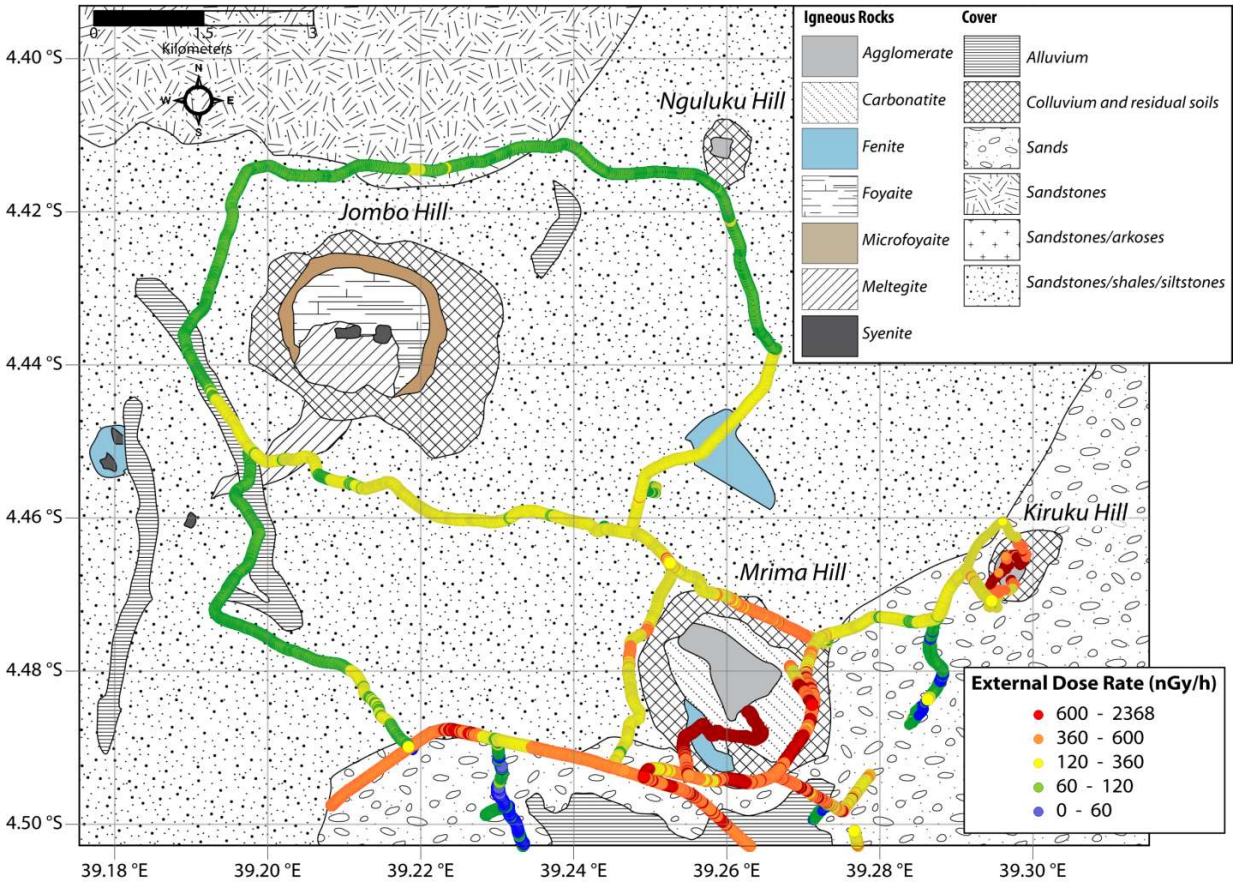

FIGURE 3. Radiometric map of the Jombo complex showing vehicular dose rate measurements.

It was observed that the lower dose rates are associated with sands and sandstones/shales/siltstones, whereas higher dose rates are associated with colluvium and residual soils, agglomerate and carbonatite rocks.

It was found necessary to investigate the accuracy of the spectrometer used for recording dose rate readings by Patel (1991) [3] after a large discrepancy was noted. This was done by comparing the published dose rates of a 5 μCi 133Ba source at various source-detector distances [3] with reverse-calculated values. The comparison indicates that dose rates reported by Patel (1991) [3] were higher by a factor of 1.8 on average suggesting that the calibration factor used to adjust the spectrometer was incorrect. Consequently, the dose rates reported by Patel (1991) [3] were decreased by a factor of 1.8, as shown in Figure4 (a), while interpolated dose rates in the southern part of Mrima Hill (present study) are shown in Figure4 (b).

Mrima and Kiruku Hills are characterized by high ^{40}K, ^{238}U and ^{232}Th but the environs of Mrima Hill show depleted ^{40}K levels (Table 1). Kiruku Hill has the highest and lowest levels of ^{40}K, ^{238}U respectively (Fig 4, Table 1).

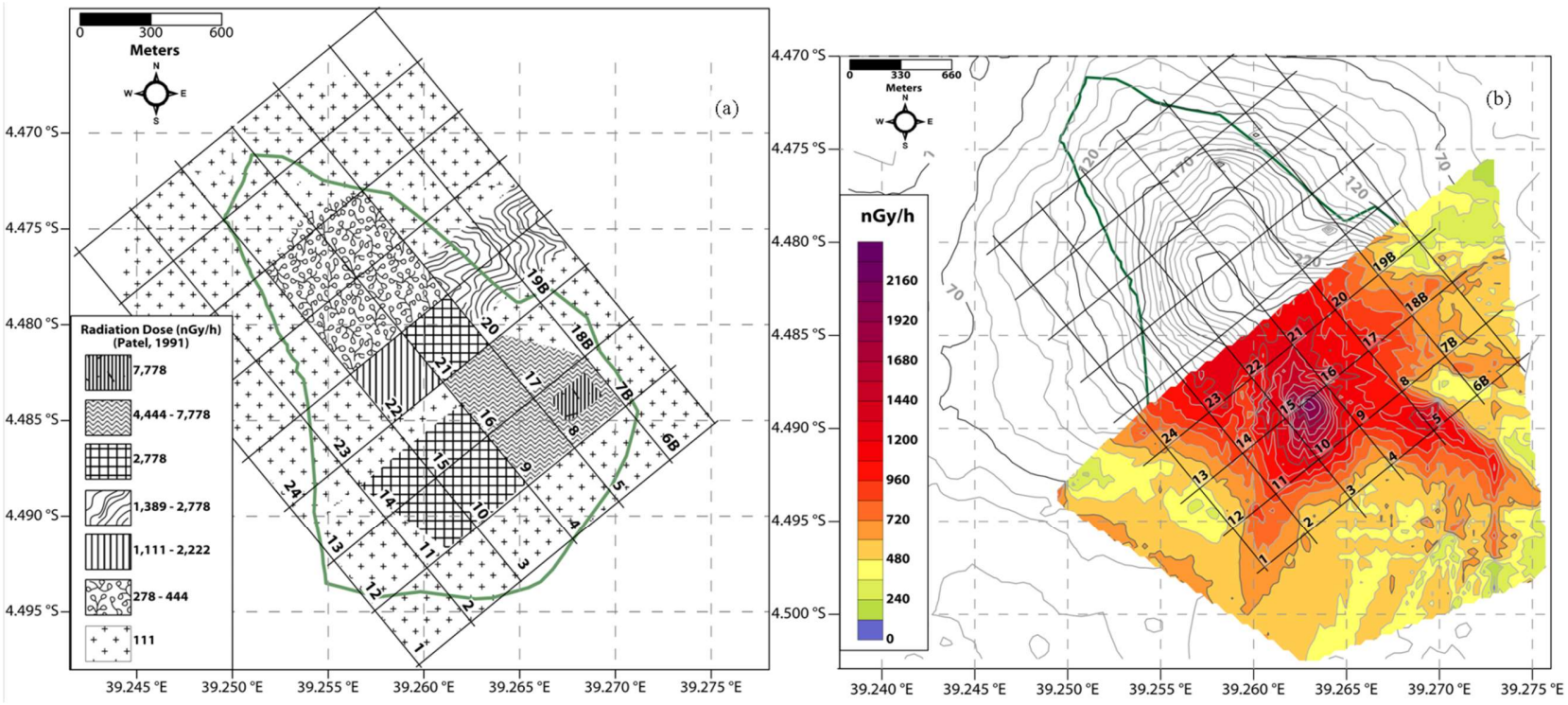

FIGURE 4. (a) Gamma dose rate iso-curves of Mrima Hill (b) Interpolated gamma dose rates by Kriging technique in southern Mrima Hill, overlaid by Patel (1991) sampling grid.

TABLE 1. SUMMARY OF THE RADIOMETRIC SURVEY RESULTS IN THE STUDY AREA (MRIMA-KIRUKU)

	Mean values				
	Number of surveyed sites	Activity concentrations (Bq kg^{-1})			Dose rate (nGy h^{-1})
		^{40}K	^{238}U	^{232}Th	
Mrima Hill[a]	34	313±33	270±28	1515±58	838±41
Mrima Hill environs[b]	16	334±18	288±24	446±28	349±21
Kiruku Hill	29	521±34	86±17	1018±50	601±36
World average for soil[†]		420	33	45	60

[a] Within 1.7 km from Mrima Hill
[b] 1.7 km / 3.5 km away from Mrima Hill
[†] Adapted from UNSCEAR (2000)

Remarkable similarity (petrography, mineralogy) has been noted between the carbonatites from the Tinderet and Oldoinyo Lengai volcanoes. Oldoinyo Nyegi and Shompole volcanoes (carbonatites and trachytes dominate the region) are connected to Lake Magadi. Recharged by highly alkaline hot springs from Lake Naivasha and Lake Natron, Oldonyo Lengai produces natrocarbonatite lava extremely soluble in water and easily washed away in groundwater flows. Soda rich Lake Magadi occurs at the lowest point in Kenya's Southern Rift. All surface ground waters flow to it with no outflows. Lake Magadi is the confluence point for all surface and groundwater flows in the region. The lake is recharged mainly by hot springs (approx. 86° C) around it.

We studied natural radioactivity associated with the Lake Magadi Basin sediment and trachyte rocks as well as its variability in relation to the origin and distribution of geothermal spring waters as we regard it to be a geothermally generated HBRA. The activity concentrations and corresponding gamma-ray spectrometric signatures were explored using multivariate chemometrics to delineate the radionuclide sources, model their occurrence in the basin, and interpret its systematics. The gamma-ray spectrometer used in this work consisted of a vertically mounted HPGe detector in a cylindrical lead shield and cooled by liquid nitrogen in a dewar. It was coupled to a 5 KV voltage bias, amplifier, MCA, and Oxford PCA3 v.1 deconvolution software on a desk top computer. The detector had 144 ml active volume and 76 mm outside diameter. Its average resolution over the period of measurements was 2.83 KeV FWHM at the 1332.50 KeV peak of ^{60}Co while the average efficiency was 30.60%. Each sample and background were counted for between 30 000 to 60 000 seconds for significant peaks to form, depending on their activities. The detector was calibrated for energy using a calibration source SRM1 containing ^{137}Cs, ^{54}Mn and ^{60}Co. A performance test was done using IAEA standard reference materials RGU, RGK, RGTh and Soil-375 under the same counting geometry and environment as the samples to check the efficiency of the energy calibration.

Remarkable spatial variability of radioactivity levels was observed in the rocks. Three regimes of highly alkaline hydrothermal inflows that contribute to and affect the radiogenic quality of trona were delineated: Na_2CO_3 and NaCl-rich inflows from the south; $NaHCO_3$-rich inflows from the north; and saline fluid inflows from the host bedrock on the western edges of the lake. The results show that Lake Magadi Basin is a sink for radionuclides from mostly the weathering of surrounding volcanics making it a quasi-high background radiation area (HBRA) with radioactivity levels of 1880±11 Bq/Kg (^{40}K), 130±10 Bq/Kg (^{238}U) and 190±5 Bq/Kg (^{232}Th) in shore sediment. Log normal distribution of the radionuclides was observed, probably as a result of the different radio-signatures of the spring recharges. Multivariate chemometric exploration of the radionuclide levels and distribution in relation to thermal water temperatures, pH, total dissolved solids (TDS), total organic carbon (TOC), and sediment cation exchange capacity (CEC) revealed marked diversity in the geochemical properties of the source rocks responsible for the spring solutes and more significantly, the possible presence of an underlying uranium-rich rock source. Geochemical immobilization of ^{238}U and ^{232}Th in groundwater flows were found to be the same in the entire basin. Thorium sorption capacity in sediments was observed to be strongly modulated by the thermal water temperatures.

3.2. EDXRF Spectrometry

Energy Dispersive X-ray Fluorescence (EDXRF) spectrometry was used for the determination of major, minor and trace elements in the various matrices. Direct trace analysis of complex matrices is however plagued by challenges. Energy Dispersive X-Ray Fluorescence and Scattering (EDXRFS) spectrometry technique [23–27] was found more appropriate to address some of the challenges encountered in such geoanalysis. The method utilizes, in addition to selected multiple fluorescence peaks corresponding to each element, scatter profiles to determine via multivariate chemometric calibration, elemental concentration and associated speciation.

In an attempt to establish the presence of radioactive monazite with the chemical formula, (Ce, La, Nd, Th)(PO_4, SiO_4) in the samples from Mrima Hill, EDXRF was used to determine the elemental concentrations of the monazite constituents in surface soils (at depths from 0–15 cm). Uranium and thorium atoms are known to bind in accessory minerals such as zircon, alunite, sphene, monazite and apatite. The Spectro X-Lab 2000 (Spectro Analytical Instruments, GmbH) tube excited polarized EDXRF spectrometer was used to perform the elemental analysis of the soil pellets.

The samples were also analyzed to assess the associated elemental composition, particularly rare earth elements (REE) as well as to infer their mineralogy (Table 2). The EDXRF analyses show that Th correlates positively with Ce, Nd, La, and P which implies that the radiation anomaly associated with Mrima Hill may be attributed to the presence of radioactive monazite. A comparison of the elemental concentrations of P, Ce, La, Nd and the results (Table 3) shows that their levels are enhanced in Mrima Hill soil samples.

TABLE 2. ELEMENTAL CONCENTRATIONS AND RATIOS FOR MONAZITE CONSTITUENTS IN MRIMA HILL SOIL SAMPLES CHARACTERIZED BY EDXRF

P (%)	La (µg/g)	Ce (µg/g)	Nd (µg/g)	Th (µg/g)	Th/P	Th/La	Th/Ce	Th/Nd
1.212±0.012	8120±97	10110±91	3580±27	444±10	0.366	0.055	0.044	0.124

TABLE 3. PEARSON'S CORRELATION MATRIX FOR P, Y, LA, CE, ND AND TH MEASURED IN THE SOIL SAMPLES BY EDXRF

	P	Y	La	Ce	Nd	Th
P	1					
Y	0.89	1				
Nb	0.89	0.98				
La	0.78	0.84	1			
Ce	0.81	0.91	0.81	1		
Nd	0.84	0.92	0.88	0.93	1	
Th	0.55	0.85	0.61	0.85	0.77	1

'Strong' correlation coefficient: > 0.75 (in bold)
'Weak' correlation coefficient: 0.35 – 0.50

3.3. Laser Induced Breakdown Spectroscopy (LIBS)

We used LIBS due to its remarkable attributes in geoanalysis [28] that include: (i) real-time response; (ii) in-situ analysis with little or no sample preparation; and (iii) a high sensitivity to low atomic number elements which are often difficult to determine by EDXRF. Further, all components of a LIBS system can be miniaturized for field-portable deployment. The LIBS microplasma that is formed when the laser ablates a sample is a 'spectral fingerprint' of the substance that simultaneously includes all elements.

We explored LIBS in air at atmospheric pressure in conjunction with machine learning towards direct rapid analysis of uranium in carbonatite rocks from Ruri, Mrima, and Magadi. A Q-Switched Nd-YAG laser (Ocean Optics, Quantel Laser), 50 mJ, 1064 nm, pulse frequency 10 Hz. The signal to noise ratio (SNR) was optimized based on U II line 386.592 nm for qualitative analysis of uranium in UO_3 and uranium-bearing samples pelletized in cellulose. We developed a chemometrics enabled LIBS [28] to characterize not only REE, but also uranium and thorium content in the samples. The following lines were identified as analytically useful in the analysis of trace uranium: U I 348.937 nm, U I 356.659 nm, U I 358.488, U I 365.915 nm, U II 367.007 nm, U I 381.199 nm, U I 383.963 nm, U II 385.464 nm, U II 385.957 nm, U I 386.592 nm, U I 387.104 nm, U I 394.382 nm. The limit of detection was found to be 76 ppm U (using U II 385.957 nm line).

The accuracy of analysis was estimated at REP = 4.32% using CRM (IAEA-RGU-1) certified reference material. Using the developed models, uranium levels in the various uranium-bearing carbonatite samples were found to range 103 - 837 ppm U (Table 4).

TABLE 4. URANIUM CONCENTRATION (PPM) IN SELECTED CARBONATITE ROCKS FROM KENYA

Number of samples	Alkaline carbonatite complex		
	Mrima Hill	Lake Magadi	Ruri Hill
1	773	773	Below detection limit
2	394	394	322
3	629	629	199
4	458	458	-
5	410	410	-
6	279	279	-
7	338	-	-
8	103	-	-
9	619	-	-

The samples collected from the different regions of Kenya–Ruri, Lake Magadi and Mrima were observed to form 3 clusters which can be attributed to their sources. The PC1 and PC2 loading spectrum reveals that the source attribution of the samples is closely associated to the rare-earth elements (REE) namely Dy, Ho, Pr, Pm, Sm and also Th and U. Our method therefore not only quantifies uranium but also aids in source attribution.

3.4. Laser Raman Microspectrometry

Laser Raman microspectrometry (LRM) allows molecular and structural analysis with sub-micron spatial resolution (0.1 μm in our case) utilizing little or no sample preparation and therefore may be used to perform quantitative analysis of local molecular composition. Raman spectra also yield information on the individual mineral species and their structural nature that are useful for mineral phase identification [29]. The 3-D imaging capability of confocal LRM is an additional powerful tool for generating detailed chemical images. The instrumentation for this study consisted of confocal laser Raman Spectrometer (STR Raman Spectrum,) equipped with a 300 mm imaging triple grating monochromator spectrograph with two lasers exciting at 532 nm and 785 nm. The 300 mm imaging spectrometer is equipped with 1800, 1200, 600-lines/mm grating and a backscattered-illuminated CCD camera for acquiring spectra within optimized time frames.

Laser Raman spectrometry performed on UCl_3, $UO_3(NO_3)_2.6H_2O$, $UO_2SO_4.3H_2O$ and UO_3 shows bands associated with different uranium molecules as being in range 840 to 867 cm^{-1}. Using the signatures, we performed quantitative spectral imaging of U in microparticles.

The key results obtained in this analysis are:

- Specific and reproducible Raman bands for each uranium compound;
- UO_3, U_3O_8, $UO_4{\cdot}(4H_2O)$, UO_2 particles from bulk materials i.e main uranium oxides can be identified at a particle's level (smallest analyzed uranium oxide particle: ~1 μm);
- Spectra match well with data obtained from the literature (see Table 5).

TABLE 5. ASSIGNMENT OF VIBRATIONAL FREQUENCY TO THE URANIUM COMPOUNDS

Speciation	Band assignment	This work (cm^{-1})	Literature (cm^{-1})
UO_3	U-O stretching	840	846
$UO_3(NO_3)_2.6H_2O$ $UO_3NO_3^+$	UO_2^{2+} symmetric stretch	862	876
NO_3^-	NO_3^- symmetric stretch	1034	1034
	Free NO_3(v1)	1049	1047
UO_2SO_4		867	(860±2)
SO_4^{2-}		1050	1048
$UCl_3UO_2Cl^+$		860	(866±2)
$UO_2SO_4.3H_20$		848	841

Uranium concentration in aerosols is very low (ppb range) hence the associated bands are buried in the fluorescence and background. Laser Raman hyperspectral images obtained from aerosols associated with uranium dust are peak-free, multivariate and thus complex to interpret. We used multivariate curve resolution (MCR) alternate least squares (ALS) to overcome the challenge. Spectra associated with uranium bonds were successfully resolved and consequently it was possible to determine the source of the uranium in the aerosols. Utilizing ANN calibration, uranium in individual aerosols in Mrima Hill were found to range 50−200 ppb.

4. PLANNED FUTURE WORK

4.1. Field sampling campaigns

In the near future we will be extending the study to other alkaline carbonatite complexes: Kerio, Tinderet, Homa, and Ruri. In addition, a more comprehensive survey is needed to complete the radiometric studies of the Mrima-Kiruku-Jombo complex to provide a geo-referenced map and radioactivity baseline. Most of the areas remain inaccessible due to dense forest, etc.

4.2. Laser scanning microscopy and induced fluorescence spectroscopy

Laser scanning microscopy (LSM) can obtain high-resolution images at specified depths on crystals [30, 31]. As elemental uranium does not emit fluorescence whereas U^{4+}, U^{5+}, and U^{6+} emit detectable characteristic fluorescence signals, laser induced fluorescence (LIF) spectroscopy (which is realizable in the LIBS set-up) may be coupled to LSM to determine where uranium occurs within particles, a study that can help elucidate the speciation and mineral forms of uranium. This will give information on individual minerals and their structure (phase identification).

4.3. Confocal laser Raman spectromicroscopy

We are developing calibration strategies for quantitative microanalysis and imaging spectrometry by laser Raman spectromicroscopy and scanning microscopy. Our studies so far show that uranium levels and distribution maps in microsized particles associated with uranium samples can be elucidated. Therefore, studies of micro-inclusions in samples (evidence of mineral genesis or geologic origin) are possible.

4.4. Laser ablation molecular isotopic spectrometry

A new extension of LIBS called Laser Ablation Molecular Isotopic Spectrometry (LAMIS) was reported in 2011 [32] where the laser plasma exhibited large isotopic splitting due to contributions of the rotational and vibrational states of the molecule, making it possible to detect and quantify the different isotopes [33]. An extension of the LIBS method was exploited in LAMIS to perform environmental uranium analysis [34]. This yielded isotopic composition and variability among the samples.

4.5. Machine learning and data fusion

Although the above techniques have high versatility, their utility for geochemical analysis was limited by the complexity of geological samples and interpretation of the generated multivariate data. A variety of machine learning techniques [35] were used to help reduce the complexity, develop multivariate calibration strategies, perform pattern recognition, as well as exploratory analysis and modelling and increased the amount of information obtained [36-38]. Data fusion (the process of integrating information from multiple sources to produce specific, unified data about an entity) techniques was used to arrive at more robust interpretations [39].

5. CONCLUSIONS

The concentrations of uranium and thorium in the Mrima-Kiruku complex are 9–27 ppm, which is 7–24 times the world average in ppm (for soils). Correlation analysis of radioactivity indicated that the high □ dose-rates are due to ^{232}Th. Mrima-Kiruku samples contain enhanced concentrations of Nb, Fe, REEs and Th. LIBS combined with machine learning not only realized direct, rapid detection and quantification of trace levels of uranium in uranium-bearing samples but it also aided in source attribution based on Nd, Pm, Pr, Sm, Sc and Tb. Laser Raman microspectrometry combines the molecular analysis capabilities of Raman scattering and the spatial resolution of optical microscopy which provided key information about uranium on individual micro-sized particles under ambient conditions. The developed analytical protocols should lead to improved reliability owing to the complementarity of the information furnished by the multimodal approaches.

The protocols are attractive as they can be integrated into a suitable software interface in handheld systems for on-site, real-time, stand-off, and direct rapid analysis.

REFERENCES

[1] GUNDERSEN, L. C. and WANTY, R. B., (Eds) (1993). Field studies of radon in rocks, soils, and water. CRC Press, 1971.

[2] YANDA P.Z., MADULU M.F., Water resource management and biodiversity conservation in the Eastern Rift Valley Lakes, Northern Tanzania. Physics and Chemistry of the Earth **30** (2005) 717-725.

[3] PATEL J.P., Environmental radiation survey of the area of high natural radioactivity of Mrima hill of Kenya. Discovery and Innovation **3** 3 (1991) 31–36.

[4] ACHOLA S.O., PATEL J.P., MUSTAPHA AO., ANGEYO H.K., Natural radioactivity in the high background radiation area of Lambwe East, Southwestern Kenya. Radiation Protection Dosimetry **2** (2012) 1–6.

[5] MANGALA J.M., A multichannel X-ray fluorescence analyses of fluorspar ore and rocks from Mrima hills, Kenya. MSc thesis, University of Nairobi, 1987.

[6] ZAITSEV A.N., WENZEL T., VENNEMAN T., MARKL G., Tinderet volcano, Kenya: an altered natrocarbonatite locality? Mineralogical Magazine **77** 3 (2013) 213–226.

[7] DEANS T., ROBERTS B., Carbonatite tuffs and lava clasts of the Tinderet foothills, western Kenya: a study of calcified natrocarbonatites. Journal of the Geological Society, London **141** (1984) 563–580.

[8] MUSTAPHA A.O PATEL, J. P. and RATHORE, I. V. S. (1999). Assessment of human exposures to natural sources of radiation in Kenya. Radiation Protection Dosimetry **82** 4 (1999) 285–292.

[9] MCCALL G.J.H., Geology of the Gwasi Area, Geological Survey of Kenya No. 45 (1958).

[10] WALSH J., Geology of the Eldama Ravine–Kabarnet Area, Kenya Geol. Survey Rept. 83, 1969.

[11] RENAUT R.W., EGO J., TIERCELIN J.J., TURDU L.C. AND OWEN R.B., Saline alkaline palaeolakes of the Tugen Hills–Kerio Valley Region Kenya Rift Valley. In: ANDREWS P., BANHAM P., (Eds), Late Cenozoic Environments and Hominid Evolution: A Tribute to Bill Bishop, Geological Society, London, 1999.

[12] ZAITSEV, A. N. and KELLER, J., Mineralogical and chemical transformation of Oldoinyo Lengai natrocarbonatites, Tanzania. Lithos, **91** 1–4 (2006)191–207.

[13] ANJOS R.M., VEIGA R., MACARIO K., CARVALHO C., SANCHES N., BASTOS J., GOMES P.R.S., Radiometric analysis of Quaternary deposits from the southeastern Brazilian coast. Marine Geology **229** (2006) 29–43.

[14] MOHANTY A.K., SENGUPTA D., DAS S.K., SAHA S. K., VAN K.V., Natural radioactivity and radiation exposure in the high background area at Chhatrapur beach placer deposit of Orissa, India. Journal of Environmental Radioactivity **75** (2004) 15–33.

[15] VASSAS C., POURCELOT L., VELLA C., CARPÉNA J., PUPIN J.P., BOUISSET P., GUILLOT L., Mechanisms of enrichment of natural radioactivity along the beaches of the Camargue, France. Journal of Environmental Radioactivity **91** (2006) 146–159.

[16] LUNDIN, I. A. and BASTANI, M. (2007). Analysis of petrophysical properties of some granitoids in Sweden. Journal of Applied Geophysics **62** 1 (2007) 74–87.

[17] KANIU M.I., DARBY I. G., ANGEYO H.K., Radiological mapping of the alkaline intrusive complex of Jombo, south coastal Kenya by *in-situ g*amma-ray spectrometry. European Geosciences Union General Assembly, Vienna, Austria, 17–22 April 2016.

[18] HARMON R.S., REMUS J., MCMILLAN N.J., MCMANUS C., COLLINS L., GOTTFRIED JR. J.L., DE LUCIA F.C., MIZIOLEK A.W., LIBS analysis of geomaterials: geochemical fingerprinting for the rapid analysis and discrimination of minerals. Applied Geochemistry **24** (2009) 1125–1141.
[19] MILLER K.M., SHEBELL P., KLEMIC G.A., Miller, K. M., Shebell, P., & Klemic, G. A., In situ gamma-ray spectrometry for the measurement of uranium in surface soils. Health Phys. **67** (1994) 140–150.
[20] NANPING W., LEI X., CANPING L., YING H., SHAOYING P., SHAOMIN L., FAN X., YEXUN C., Determination of Radioactivity Level of ^{238}U, ^{232}Th and ^{40}K in Surface Medium in Zhuhai City by in-situ Gamma-ray Spectrometry. Journal of Nuclear Science and Technology **42** 10 (2005) 888–896.
[21] KANIU M.I., ANGEYO H.K., DARBY I.G., MUIA L.M. In situ gamma-ray spectrometric assessment of the Mrima-Kiruku high background radiation anomaly complex of Kenya. Journal of Environmental Radioactivity **188** (2018) 47–57.
[22] KANIU, M. I., DARBY, I. G. and ANGEYO, H. K, Assessment and mapping of the high background radiation anomaly associated with laterite utilization in the south coastal region of Kenya. Journal of African Earth Sciences **160** (2019).
[23] ANGEYO H.K., GARI S., MANGALA J.M., MUSTAPHA A.O., Feasibility for direct rapid energy dispersive X-ray fluorescence (EDXRF) and scattering analysis of complex matrix liquids by partial least squares. Appl Rad Isot **70** (2012) 2596–2601.
[24] ANGEYO H.K., GARI S., MANGALA J.M., MUSTAPHA A.O., Principal component analysis-assisted energy dispersive X-ray fluorescence spectroscopy for non-invasive quality assurance characterization of complex matrix materials. X Ray Spectrom **41** 5 (2012) 321–327.
[25] KANIU M.I., ANGEYO H.K., MANGALA M.J., MWALA A.K., BARTILOL S.K., Feasibility for chemometric energy dispersive X-ray fluorescence and scattering (EDXRFS) spectroscopy method for rapid soil quality assessment. X Ray Spectrom **40** (2011) 432–440.
[26] KANIU M.I., ANGEYO H.K., MWALA A.K. AND MANGALA M.J., Direct rapid analysis of trace bioavailable soil macronutrients by chemometrics-assisted energy dispersive X-ray fluorescence and scattering spectrometry. Anal. Chim. Acta. **729** (2012) 2–25.
[27] KANIU M.I., ANGEYO H.K., MWALA A.K., MWANGI F.K., Energy dispersive X-ray fluorescence and scattering assessment of soil quality via partial least squares and artificial neural networks analytical modeling approaches. Talanta **98** (2012) 236–40.
[28] MUKHONO, P. M., ANGEYO, K. H., DEHAYEM-KAMADJEU, A. and KADUKI, K. A., Laser induced breakdown spectroscopy and characterization of environmental matrices utilizing multivariate chemometrics. Spectrochimica Acta Part B: Atomic Spectroscopy **87** (2013) 81–85.
[29] WHITE S.N., Laser Raman spectroscopy as a technique for identification of seafloor hydrothermal and cold seep minerals. Chemical Geology **259** 3–4 (2009) 240–252
[30] MENE´NDEZA B., DAVIDA C., NISTAL A.M., Confocal scanning laser microscopy applied to the study of pore and crack networks in rocks. Computers & Geosciences **27** (2001) 1101–1109.
[31] MONTOTO M., MARTI'NEZ-NISTAL A., RODRI'GUEZ A., FERNA'NDE MERIYO N., SORIANO P., Microfractography of granitic rocks under confocal scanning laser microscopy. Journal of Microscopy **177** 2 (1995) 138–149.
[32] MAO X., BOL'SHAKOV, A.A., PERRY, D.L., SORKHABI, O., RUSSO, R.E., Laser ablation molecular isotopic spectrometry: parameter influence on boron isotope measurements. Spectrochimi. Acta B **66** (2011) 604–609.

[33] SCHOONOVER J.R., WEESNER F., HAVRILLA G.J., SPARROW M., TREADO P., Integration of elemental and molecular imaging to characterize heterogeneous inorganic materials. Appl. Spectrosc. **52** (1998) 1505–1514.
[34] MALABA J.N., ANGEYO H.K., ODUOR F., Micro extraction of uranium and nuclear forensic analysis by chemometrics based LAMIS. 9th Euro-Mediterranean Symposium on LIBS Colloquium Spectroscopicum International XL, Pisa, Italy, 11–16 June 2017.
[35] MITCHELL T.M., Machine Learning, McGraw Hill, Redmond, 1997.
[36] HENRICH, A., HOFFMANN, P., ORTNER, H. M., GREVE, T. and ITZEL, H., Non-invasive identification of chemical compounds by energy dispersive X-ray fluorescence spectrometry, combined with chemometric methods of data evaluation. Fresenius' journal of analytical chemistry, **368** 2-3 (2000) 130-138.
[37] GOICOECHEA H.C., COLLADO M.S., SATUF M.L., OLIVIERI A.C., Complementary use of partial least-squares and artificial neural networks for the non-linear spectrophotometric analysis of pharmaceutical samples. Anal. Bioanal. Chem. **374** (2002) 460–465.
[38] SCHIMIDT F., CORNEJO-PONCE L., BUENO, M.I., POPPI R.J., Determination of some rare earth elements by EDXRF and artificial neural networks. X-Ray Spectrom. **32** 6 (2003) 423–427.
[39] ACAR E., RASMUSSEN M.A., SAVORANI F., NAES T., BRO R., Understanding data fusion within the framework of coupled matrix and tensor factorizations. Chemometrics and Intelligent Laboratory Systems **129** (2013) 53–63.

ELEMENTAL CHARACTERIZATION OF URANIUM ORE DEPOSITS FROM MONGOLIA

S. TSERENPIL, N. NOROV
Nuclear Research Centre, National University of Mongolia
Ulaanbaatar, Mongolia

Abstract

One of the objectivies of this study was to review literature on the Mongolian uranium deposits. Information on resources, geological age, and mineralization type of the mineral deposits were well documented compared to geochemical data. Furthermore, elemental compositions of the Dornod and Kharaat deposits were analysed and compared to the Dulaan Uul deposit. Three deposits showed encrichment of light rare earth elements (REE) exhibiting average ratio of LREE/HREE from 3.8 to 18.5. Shape of chrondrite normalised REE patterns for the sandstone type Kharaat and Dulaan Uul deposits were similar with negative Eu anomaly.

1. INTRODUCTION

Uranium of Mongolia by Yu.B. Mironov [1] is a major publication on Mongolian uranium mineralization and geology. The work includes reports from the geological expeditions conducted during the 1970s–1990s. The expeditions were carried out jointly by Mongolia and the Soviet Union and included airborne gamma spectrometry (AGS) surveys on various scales. The medium– and small–scale works were performed in the central areas at scales of 1:1,000,000 (300 000 km^2), 1:200 000 (580 000 km^2) and 1:25 000 (171 000 km^2); while specialized geological mapping at scales of 1:200 000–1:10 000 (50 000 km^2) was confined mainly to the east and the west of the territory (total of 1.6 million km^2).

During the joint expeditions, the Dornod uranium deposit in the North Choybalsan district in the northeast of the country was the main discovery and was considered an economically significant deposit with fluorine–molybdenum–uranium (F–Mo–U) type mineralization.

Since 1995, uranium exploration and geotectonic surveys have been conducted in south–eastern Mongolia with the aim to explore for sandstone–type uranium deposits. As a result, several deposits were found, including sandstone roll–front type: Zoovch Ovoo, Dulaan Uul, Kharaat and Khairhan deposits.

Mongolian uranium mineralization is distributed into four metallogenic provinces, and more than 10 deposits and over 100 prospects were found by 2014. Uranium resources are estimated at around 141 500 tU (2% of the world's share) [2] and geological indications show that speculated resources could reach as much as 1.4 million tU [1].

Most of the discovered uranium deposits and occurrences are concentrated in the eastern part of the country: northeast and southeast, and the major types are volcanic– and sandstone–hosted uranium deposits (Table 1).

Uranium deposits in Mongolia are related to the ore–forming epochs during the Late Mesozoic (superimposed volcano tectonic structures) as well as the basins which formed in the Cenozoic epoch of arching and block–faulting.

Geotectonics, ore–bearing process, mineralization, and geological ages and resource estimation have been completed for the Mongolian uranium deposits, while geochemistry and isotopic investigations have not been studied for the majority of the deposits. Such research can be useful for identification of the different stages of mineralization processes and to establish a data set on elemental and rare earth elements (REE) pattern to characterize individual deposits. This project aimed to conduct a geochemical study of known uranium deposits in Mongolia.

TABLE 1. DEPOSIT TYPES AND MINERALIZATION [3]

Deposit type	Deposits	Main minerals	Remarks
Sandstone (roll–front or tabular) (total resource of ca. 80 000 tU)	Kharaat Khairhan Dulaan Uul Zoovch ovoo	Pitchblende Coffinite Poorly expressed U oxide generally associated with coffinite, phosphocoffinite and uranothorite	For Kharaat and Khairhan, both ISL and heap leaching exploitations are recommended. Kharaat deposit contains Ce, La, Re, Ge.
Volcanic deposits (total resource of ca. 48 000 tU)	Dornod Nars Gurvan Bulag Marday Nemer	Mineralization type: Fluorine–molybdenum-uranium Pitchblende-coffinite with brannerite	Open pit, underground Underground mining Open pit and underground

1.1. Uranium mineralization in the late Mesozoic volcano tectonic structures

F–Mo–U type mineralization is one of the important economic uranium mineralization types in Mongolia and includes large and medium–size deposits of the North Choybalsan district (0.03–0.3% U) in the Mongol Priargun metallogenic province. The low– to medium–temperature hydrothermal uranium and complex deposits and prospects are localized in the Late Mesozoic (Late Jurassic–Early Cretaceous) volcano tectonic structures and their crystalline basement.

The mineralized bodies in the Dornod deposit occur at a depth of 100–500 m and are marked by hydrothermally altered rocks and weak primary geochemical haloes along the Central Fault Zone. Mineralized rocks are related to basalt–rhyolite association; uranium minerals include pitchblende–coffinite with brannerite with a uranium resource estimated at around 24 800 tU [1].

TABLE 2. RESOURCES IN SELECTED DEPOSITS [2, 4]

Deposit	Resources, tU	National Resource Category**	Grade, U %
Dornod	24 780	C1+C2	0.154
Kharaat	7 288	B+C	0.026
Zoovch Ovoo	54 640	B+C	0.023
Dulaan Uul	11 006	B+C	0.021
Total	97 714*		

** Represent 69% of U resources of Mongolia.*

***C1+C2 and B+C are equivalent to reasonably assured resources in NEA/IAEA classification*

1.2. Uranium mineralization in terrigenous fill of Mesozoic and Cenozoic depressions

Uranium deposits in the Gobi–Tamsag U province is related to oxidation processes in the terrigenous fill (e.g. lacustrine and alluvial sediments) of the Mesozoic and Cenozoic depressions. In its eastern and northeastern part, this province is superimposed on the older Argun–Mongolian province.

The Kharaat deposit in Choyr uranium–bearing basin in the central Gobi–Tamsag uranium province is one of widespread supergene hydrogenic uranium mineralization. Its grade ranges 0.01–0.04% U with a total resource of 7288 tU [2]. The mineralization is hosted both in the gray rocks at the boundary with limonitized red beds and within the oxidation zone itself, where the mineralization is characterized by low and ordinary uranium grades and largely hosted in sand–shale rocks [5]. Uranium mineralization in Kharaat co–occurs with elements Ce, Re and Sc.

In the Sainshand district, one of the recently discovered typical roll–front type deposits is Dulaan Uul, a narrow ribbon–like mineralized body with a 20 km mineralized front [4]. The Dulaan Uul deposit is in the Uneget Basin with 11 000 tU of resources at an average grade of 0.023% U.

2. MATERIALS AND METHODS

Due to the dormant state of the ore deposits (including Kharaat, Dornod, Gurvanbulag, Nars, Nemer, etc.) as well as limited investment for uranium exploration, we had no direct access to mineralized samples. However, we obtained samples through our colleagues from the Nuclear Research Center (NRC), the National University of Mongolia. Nine samples were from the Marday (Dornod deposit), which were originally obtained during 1988–1995 when the deposit was exploited. Two samples from the Kharaat deposit were also acquired from the time when an insitu leaching (ISL) leaching test was conducted around 2012.

The Dornod U mineralization is related to the volcano tectonic event, while sandstone–types, Kharaat and Dulaan Uul are related to oxidation and reduction in a basinal setting.

Data set [6] on the Dulaan Uul deposit is exclusively on uranium oxide (UO_2) performed by LA-ICP-MS technique.

EDS–X–Ray spectrometry equipped with silicon drift detector (SDD), resolution 155eV at 5.9 keV, at the NRC was used for determination of major elements. As for calibration, a certified reference material (CRM) of uranium tailing sample (UTS–4) and rock (GBW 07109) were used. REE elements for samples from the Dornod and Kharaat deposits were analyzed by ICP–MS after lithium borate fusion decomposition in a furnace at 1000°C by a commercial analytical laboratory.

3. RESULTS

The volcanic related Dornod deposit has higher Mn, Zn, Cs, Y, Pb and As content compared to the sandstone type deposits. However, total concentration of REE (La–Lu) was similar for Dornod and Kharaat with average of 352 and 311 ppm, respectively (Table 3 and Table 4).

TABLE 3. AVERAGE CONTENTS OF ELEMENTS IN DORNOD AND KHARAAT SAMPLES

Elements	Units	Dornod	Kharaat
Al	%	8.24	7.81
K	%	3.30	3.07
Na	%	1.71	1.51
Ca	%	1.08	0.51
Mg	%	0.27	0.36
Fe	%	1.46	2.76
Ti	%	0.26	0.44
Mn	ppm	1268	192
Ba	ppm	995	585
Zn	ppm	1673	66.2
Rb	ppm	221	266
Sr	ppm	366	237
Cs	ppm	112	12.7
Y	ppm	85.7	30.3
Zr	ppm	250	180
V	ppm	74	140
Cr	ppm	36.3	35.5
Cu	ppm	13.2	38.6
Cd	ppm	23.4	0.3
Pb	ppm	72.4	44.7
As	ppm	524.3	9.3

Light REE (LREE) enrichment was observed in both deposits and ratio of LREE/HREE of 8.3 for Dornod and 18.5 for Kharaat. Uranium oxides from the Dulaan Uul deposit showed less fractionation with 3.5–4.0 for LREE/HREE ratio. Shapes of chondrite–normalized REE patterns were similar for the sandstone type deposits of Kharaat and Dulaan Uul. The latter one showed stronger negative Eu anomaly than in Kharaat (Figure 1).

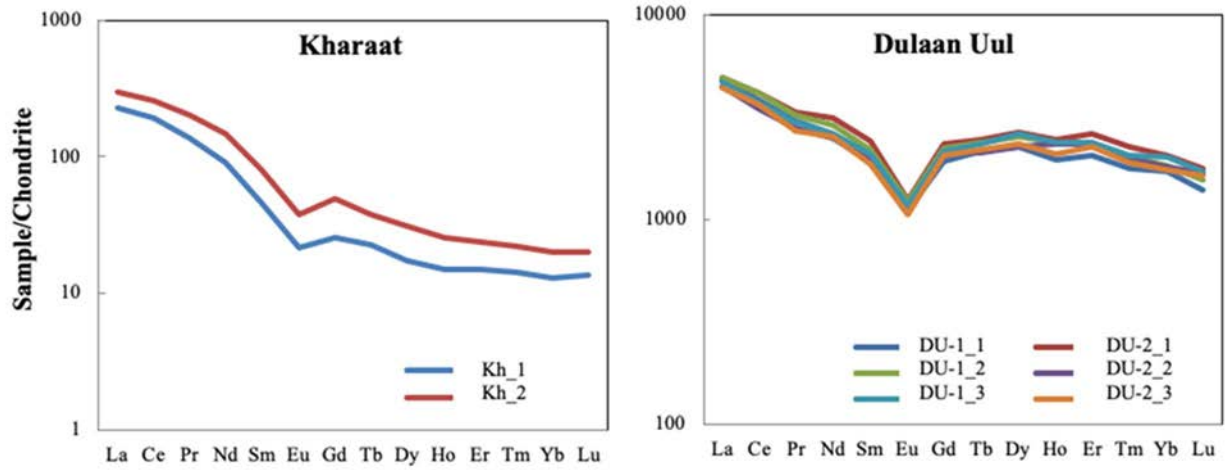

FIGURE 1: Chondrite normalized REE patterns for samples from Kharaat and Dulaan Uul deposits.

TABLE 4. TRACE AND REE CONCENTRATIONS OF URANIUM DEPOSITS, PPM

Element	Dornod (n=8)*	Kharaat (n=2)*	Dulaan Uul $UO_{2\ phase}$ (n=6)**
U	1291	357	731330
Th	18	47	
La	47.65	61.25	1101
Ce	99.2	134.5	2293
Pr	11.63	15	268
Nd	45.7	53.4	1226
Sm	8.75	9.22	306
Eu	1.47	1.65	64
Gd	8.95	7.285	420
Tb	1.46	1.1	83
Dy	9.57	5.84	594
Ho	2.17	1.12	126
Er	6.85	3.09	370
Tm	0.92	0.44	49
Yb	5.6	2.68	303
Lu	0.83	0.41	40
Total	203	236	7241

*Note: *ICP–MS; **LA–ICP–MS; n- number of samples.*

4. CONCLUSION

In roll–front deposits, abundance of REE in uranium oxides is highly fractioned and their patterns, irrelative of temperature, mimic those of the host rock [7]. Also, no major fractionation occurs during source leaching, REE transport and uranium oxide crystallization. Kharaat samples displayed a high fractionation of LREE/HREE=18–21 compared to the volcanic related Dornod sample, LREE/HREE=7–10. For the Dornod deposit, the higher contents of HREE can be explained by a much higher temperature of fluid responsible for the mineralization, which can better mobilize HREE (from the alteration of REE– bearing minerals in the host rock). Though, the chondrite normalized REE pattern did not show a typical volcanic related "bell shape" pattern like in the volcanic type Streltsovshoye deposit. However, it should be noted that the Dornod sample was a composite material sample.

REFERENCES

[1] MIRONOV, YU.B., Uranium of Mongolia. English edition: CERCAMS. London (2006)

[2] OECD NUCLEAR ENERGY AGENCY, INTERNATIONAL ATOMIC ENERGY AGENCY, Uranium 2016: Resources, Production and Demand. NEA No.7301. OECD (2016).

[3] INTERNATIONAL ATOMIC ENERGY AGENCY., World Distribution of Uranium Deposits (UDEPO) with Uranium Deposit Classification, IAEA–TECDOC–1629. IAEA, Vienna (2009).

[4] HOCQUET, S., Zoovch Ovoo and Dulaan Uul Uranium Deposits. IAEA–UNECE Workshop in Ulaanbaatar, August 2016. https://www.unece.org/fileadmin/DAM/energy/se/pp/unfc/ws_UNFC_Mongolia_2016/005_Hocquet_Cogegobi_UB.pdf

[5] BUDUNOV, A.A., Hydrogenic uranium deposits of Mongolia, Proceeding geology of uranium, rare-metal, and rare-earth-metal deposits, Information **144** (2002) 84–89.

[6] LACH, P., Signature géochimique des éléments des terres rares dans les oxydes d'uranium et minéraux associés dans les gisements d'uranium : analyse par ablation laser couplée à l'ICP-MS et étude géochronologique. PhD theses. Université de Lorraine, Faculté des Scineces, Vandoeuvre les Nancy (2012) (In French).

[7] MERCADIER, J., CUNEY, M., LACH, P., BOIRON, M., BONHOURE, J., RICHARD, A., LEISEN, M., KISTER, P., Origin of uranium deposits revealed by their rare earth element signature, Terra Nova **23** (2011) 264–269.

ISOTOPE SYSTEMATICS OF ALBITITE-TYPE URANIUM DEPOSITS, THE CENTRAL UKRAINIAN URANIUM PROVINCE*

L. SHUMLYANSKYY
School of Earth and Planetary Sciences, Curtin University,
Perth, Australia

M. CUNEY
CREGU - CNRS - GeoRessources, University of Lorraine,
Vandoeuvre les Nancy, France

K. BILLSTRÖM
Department of Geosciences, Swedish Museum of Natural History,
Stockholm, Sweden

I. MIKHALCHENKO
State enterprise, Institute of Environmental Geochemistry,
Kyiv, Ukraine

A. SOESOO
Institute of Geology, Tallinn University of Technology,
Tallinn, Estonia

*Preliminary results and some parts of this paper were presented at the IAEA International Symposium on Uranium Raw Material for the Nuclear Fuel Cycle: Exploration, Mining, Production, Supply and Demand, Economics and Environmental Issues (URAM-2018). Vienna, Austria, 25-29 June 2018.

Abstract

The new whole-rock geochemistry and Sr-Nd-Pb isotope data obtained for U-bearing Na-metasomatites (albitites) in the Central Ukrainian Uranium Province (CUUP) are presented and discussed in terms of the possible contribution of different sources of elements to this type of uranium deposit. When compared with the host granite, albitites demonstrate a sharp decrease in the abundances of SiO_2 and K_2O, whereas most other major oxides show significant enrichment. Albitites have Sr isotopic signature typical for crustal rocks. Specifically, rocks of the Novokostyantynivka deposit have $^{87}Sr/^{86}Sr_{(1800)}$ in the range 0.7087–0.7105, whereas rocks of the Novooleksiivka deposit show a variation from 0.7172 to 0.7207. Neodymium isotope compositions allowed construction of the Sm-Nd isochron that yielded an age of 1728 ± 110 Ma. The calculated εNd value of -4.8 indicates that a dominantly crustal source of the fluids was responsible for producing the metasomatic alteration. Lead isotope compositions indicate a prevalence of radiogenic Pb resulting from the decay of uranium, whereas 'common' Pb is negligible. Pb-Pb isochron yielded an age of 1810 ± 17 Ma. The isotope results can be compared with data available for the main rock types present in the area. Albitites of the Novokostyantynivka deposit plot between fields of the Novoukrainka massif and Korsun-Novomyrhorod anorthosite-mangerite-charnockite-granite (AMCG) complex. In contrast, albitites of the Novooleksiivka deposit plot entirely within the field defined by the Inhul granitoid complex. According to Sr-Nd isotope data, the initial fluids could have been derived from or equilibrated with the Palaeoproterozoic felsic rocks widely distributed in the area. However, trace element data indicate an important influence of mantle-derived material. Probably a mantle plume that was active in that area during formation of the albitites was responsible not only for the heating of area and formation of hot fluids but also provided some material necessary for the formation of the albitites.

1. INTRODUCTION

Albitite-type sodium metasomatites occur throughout the world and often contain uranium mineralization that may reach an exploitable scale and grade [1]. Uranium concentrations in albitite-type deposits are rather low but resources can be quite large. Deposits of this type are significantly underexplored and may represent a promising target for further exploration [1].

This is especially true as Na-metasomatites often contain complex mineralization that, besides U, includes Th, Sc, V, Nb, HREE and Ag.

The Central Ukrainian Uranium Province (CUUP) hosts several large deposits and numerous subeconomic deposits and occurrences. Uranium production started in 1951 and since that time two deposits, Zhovta Richka and Pershotravneve, have been completely exhausted. The remaining uranium resources of the CUUP exceed 300 000 tU with grades varying between 0.05 and 0.20 wt% U [1, 2].

In spite of a long history of investigation of albitite-type U deposits in Ukraine, questions regarding their origin remain unanswered. The main questions are related to the sources of the metasomatic fluids and associated mineralizing components. Numerous published studies were focused on the geological structure of uranium deposits in the CUUP, on their mineralogical and chemical compositions, and on stable isotope systematics [3]; whereas radiogenic isotope data were absent, which hampers a fruitful discussion.

Current ideas regarding the origin of metasomatic fluids and their ore load are controversial. Two main unresolved problems are:

(i) The source of the huge volumes of high-temperature hydrothermal solutions evolving over time, with the main alternatives being meteoric waters, basin waters and magmatic fluids;
(ii) The source of U and Na, recalling that large volumes of these elements cannot be derived from low crustal and mantle lithologies. Middle to upper crustal sources may be considered as well. However, calculations indicate that hydrothermal leaching of the upper crustal rocks that host the ores cannot produce such an enrichment of uranium and sodium as these rocks are relatively poor in both of these elements. Besides, there is no field evidence to suggest that a significant leaching of such rocks has taken place.

In this contribution we present new whole-rock geochemistry and Sr-Nd-Pb isotope data obtained for Na-metasomatites in the CUUP and for a large variety of host rocks and discuss the possible contribution of different sources of elements to this type of uranium deposit.

2. GEOLOGICAL SETTING

The CUUP is located in the central part of the Ukrainian Shield, within the predominantly Palaeoproterozoic Inhul mobile belt, and partly within the Mesoarchaean Middle Dnieper domain (Figure 1). Most of the deposits and occurrences are located near the southern contact of the Korsun-Novomyrhorod anorthosite–mangerite–charnockite–granite (AMCG) complex (dated at 1757–1744 Ma [4]) where they are hosted by the Novoukrainka gabbro–monzonite–granite massif (dated at 2038–2028 Ma [5, 6]) and granites and migmatites of the Inhul Complex (dated at 2022–2062 Ma [7–9]). Several deposits are located within the Kryvyi Rih synform structure, which is filled mainly with siliciclastic sediments and banded iron formations. The age of this structure remains poorly understood and is commonly regarded as Palaeoproterozoic–Neoarchaean.

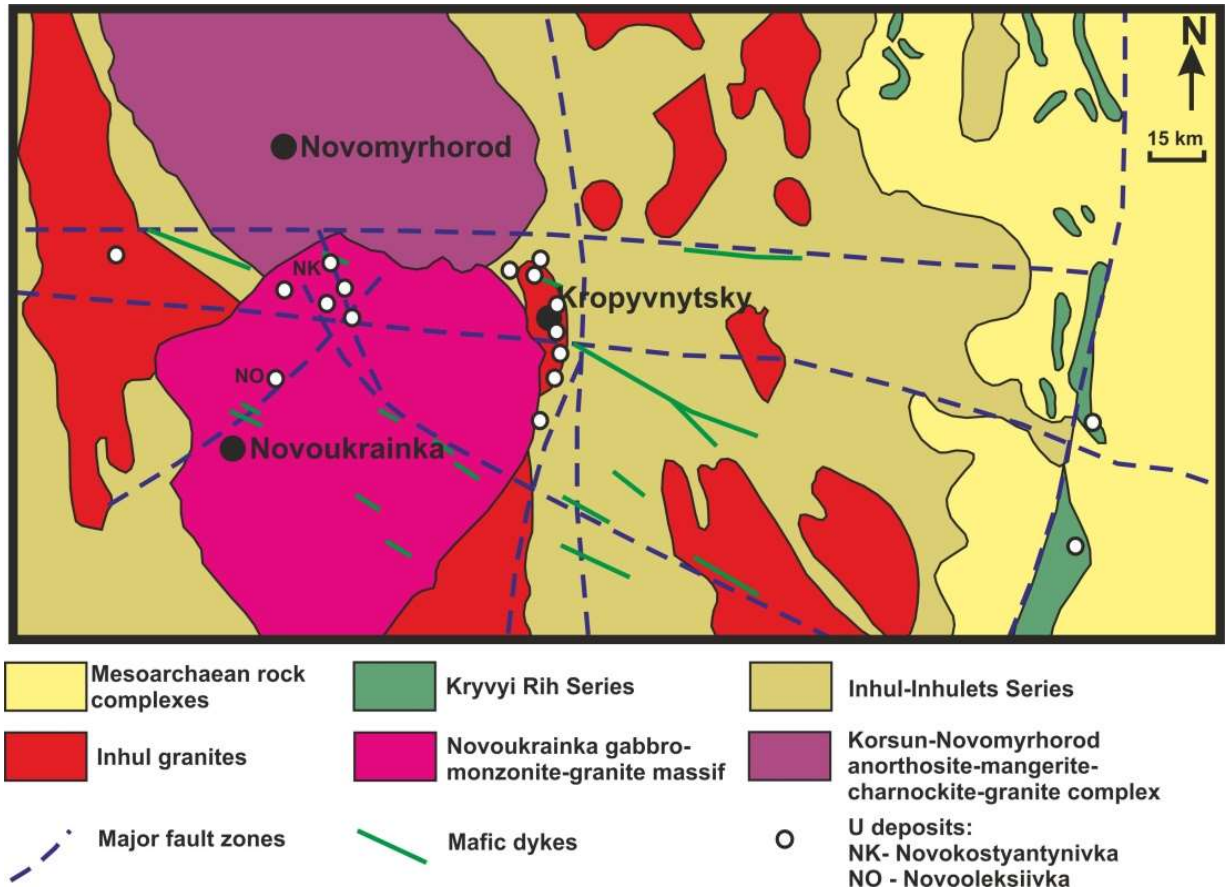

FIGURE 1. Geological overview of the Central Ukrainian Uranium province (reproduced with minor changes from [1] with permission courtesy of Elsevier).

Na-metasomatites are confined to the major fault zones closely associated with the numerous widely distributed mafic dykes. Some of these dykes are older than the metasomatites and can be affected by sodium metasomatism whereas other dykes clearly cut metasomatic bodies. Available geochronological data [10] indicate the formation of the mafic dykes at ~1800 Ma. These dykes are widely distributed across the Ukrainian Shield and indicate emplacement of a mantle plume.

The metasomatic rocks occur as irregular elongated zoned bodies [1, 2] that have been traced along strike for several kilometres whereas their widths may exceed several hundred metres. The largest bodies have been traced by drilling to depths of 1200 m and deeper.

U-bearing albitites develop after felsic igneous and metamorphic rocks. In a generalized form, zoning in these rocks can be described as a gradual transition from unaltered host rock (granite, migmatites, gneiss, etc.) to quartz free (desilicified) microcline–albite metasomatite ('syenite') and then to albitite. This rock succession formed during the progressive (albititic) stage of the alkaline (sodic) metasomatic process. A late-stage mineral assemblage that includes phlogopite (or late chlorite), carbonate, andradite, diopside, Mg-Ca amphibole and haematite are often superimposed on the internal parts of albitites. Besides this, secondary quartz, epidote and microcline are often superimposed on the intermediate and external parts of the metasomatic bodies. These latter minerals are regarded as having developed during removal of silica, calcium and potassium from central (albititic) parts of metasomatic bodies [1–3].

3. MINERALOGY OF ALBITITES

Albite occurs as the main (up to 90%) rock-forming mineral, whereas the amount of mafic minerals usually does not exceed 10%. The typical mafic minerals are alkaline amphibole, alkaline pyroxene, epidote, chlorite, diopside, actinolite and garnet. The proportion of albite and mafic minerals is generally defined by the composition of the initial rock. The amount of pyroxene varies from 0 to 10%. Pyroxenes belong to aegirine composition (the amount of the Ca component varies from 0 to 45 mol.%) and diopside–sahlite composition (the amount of the Na component varies from 0 to 20 mol.%). Amphibole is usually associated with pyroxene and varies in composition from riebeckite to slightly alkaline actinolite. Garnet belongs to the andradite–grossular series and occurs mainly in deposits located in the Novoukrainka granite massif where the amount of garnet may reach 50%. Garnet occurs in association with diopside, actinolite and epidote; sometimes it may be found in association with aegirine. Epidote is a rock-forming mineral in so-called 'syenites' and certain types of albitites. It often replaces garnet in the garnet–diopside metasomatites. Accessory minerals in albitites comprise apatite, zircon, titanite, monazite, uranothorite and allanite, which are present in all types of U-bearing sodic metasomatites. Phenakite, thortveitite and schorlomite are rare minerals. The origin of accessory minerals is not clear as they may represent relict phases left from the initial (pre-metasomatic) rocks.

Albitites also contain various opaque minerals, including haematite, magnetite, titanomagnetite, rutile, ilmenite, galena, pyrite, chalcopyrite, and sphalerite. Native silver in concentrations reaching up to 1% in Na-metasomatites of the Kryvyi Rih–Kremenchuk zone has been known for a long time.

The principal uranium minerals are uraninite (U^{4+}, U^{6+}, Pb, Ca, REE, Zr)O_{2-x}, brannerite (U^{4+}, Ca, Th, Y)[(Ti, Fe)$_2O_6$]·nH_2O and U-ferropseudobrookite (Fe^{2+}[Ti,U^{4+}]$_2O_5$). Uraninite is unevenly distributed and absent in some deposits. Brannerite occurs as the main ore mineral in many of the deposits in the CUUP. It often develops after Ti-bearing minerals; there is a persistent association of brannerite with rutile, anatase, carbonate minerals, quartz and sericite. U-ferropseudobrookite forms anhedral crystals which replace magnetite and generally precedes brannerite and/or uraninite deposition [1].

4. ANALYTICAL METHODS

Altogether twelve rock samples, six each from the Novokostyantynivka and Novooleksiivka deposits, were dissolved in an HF-$HClO_4$ acid mixture before the Sr-Nd-Pb-isotope ratio measurements. The sample solutions were left for three days in Teflon vials at 210 °C in order to ensure total dissolution. Conventional ion exchange techniques, performed in columns filled with AG50W×8, H^+ form resin, were applied to the sample solutions in order to separate and purify the elements whose isotopic compositions were to be determined. Sr was further purified in a second pass through the same columns, whereas Nd was isolated in Ln-spec columns. The Pb fractions were re-dissolved in HBr and treated further in columns with AG1×8, Cl^- form resin.

A Thermo-Finnigan Triton thermal ionization mass spectrometry (TIMS) instrument was used for the Sr and Nd isotope analyses and data were normalized to $^{88}Sr/^{86}Sr = 0.1194$ and $^{146}Nd/^{144}Nd = 0.7219$, respectively. Additionally, replicate analyses of the NBS-987 Sr standard analysed during the course of the study yielded an average $^{87}Sr/^{86}Sr$ of 0.710221 ± 0.000011 (2σ external precision). Given that this value is somewhat low in comparison with most of the published values, a small external correction term was applied to raw data for unknowns.

Corresponding analyses of the La Jolla Nd standard yielded an average $^{143}Nd/^{144}Nd$ of 0.511848 ± 0.000009 (2σ external precision), which is very close to the accepted value. Pb isotope analyses were performed with Tl added to allow for an internal correction of the mass bias, and the measured intensities were corrected for background and Hg interference on mass 204. An ICP-MS instrument (Nu Plasma II hosted by the Vegacenter facility at the Swedish Museum of Natural History) was used for the Pb runs. The NBS-981 Pb standard was run at regular intervals and unknowns were analysed in duplicate. The obtained values for the standard are within error of those given in [11], and the external reproducibility is between 0.04% ($^{206}Pb/^{204}Pb$) and 0.08% ($^{208}Pb/^{204}Pb$). The external reproducibility of the unknowns is of a similar order, but in order to account for errors arising during the chemical treatment in the clean laboratory, an overall uncertainty of ± 0.10% was adopted.

ICP-MS analyses were performed using a quadrupole X-Series 2 instrument at the Institute of Geology, Tallinn University of Technology, Estonia. Whole-rock trace elements were determined from solutions which were prepared following the nitric, hydrofluoric, hydrochloric and boric acids digestion of a 0.250 g pulverized sample in an Anton Paar MW3000 microwave oven.

The whole-rock major elements were analysed by XRF from glass disks, which were prepared using a Li-borate mix with the pulverized sample (using Claisse instrument). The S4 Pioneer Spectrometer , utilizing an X-ray tube with a rhodium anode, operated with a power of 3 kW. Loss on ignition (LOI) was determined from 1 g of the pulverized sample material at 500°C and 920°C.

5. GEOCHEMISTRY

The data obtained demonstrate regular variations of the chemical composition in the vertical profile across the albitite bodies (Table 1, Figure 2). When compared with the host granite, albitites demonstrate a sharp decrease in the abundances of SiO_2 and K_2O. The Al_2O_3 content increases slightly near contacts with the host granites and then decreases in the central part of the metasomatic body. Most other major oxides show significant enrichment in albitites. Oxides such as Fe_2O_3, CaO, TiO_2 and MgO demonstrate pronounced enrichment in the U-rich central (axial) parts of the albitite body. In contrast, Na_2O is sharply increased in metasomatites but demonstrates a moderate decrease in the axial part of the body. The latter decrease can be explained by the effect of the late Ca-Mg-K-rich fluids that were responsible for the transfer and deposition of uranium and some other elements.

The distribution of REE in barren albitites from the outer zone of the metasomatic body is very close to that in the host granite [1]. In general, barren albitites are slightly enriched with respect to LREE, and depleted in HREE, when compared with the host granite, but the difference is insignificant. The new data indicate that albitite samples rich in U are also highly enriched in HREE. It is thought that metasomatic fluids responsible for U enrichment were also rich in HREE. This feature is not typical for felsic rocks that may be considered as the main source of U and Na.

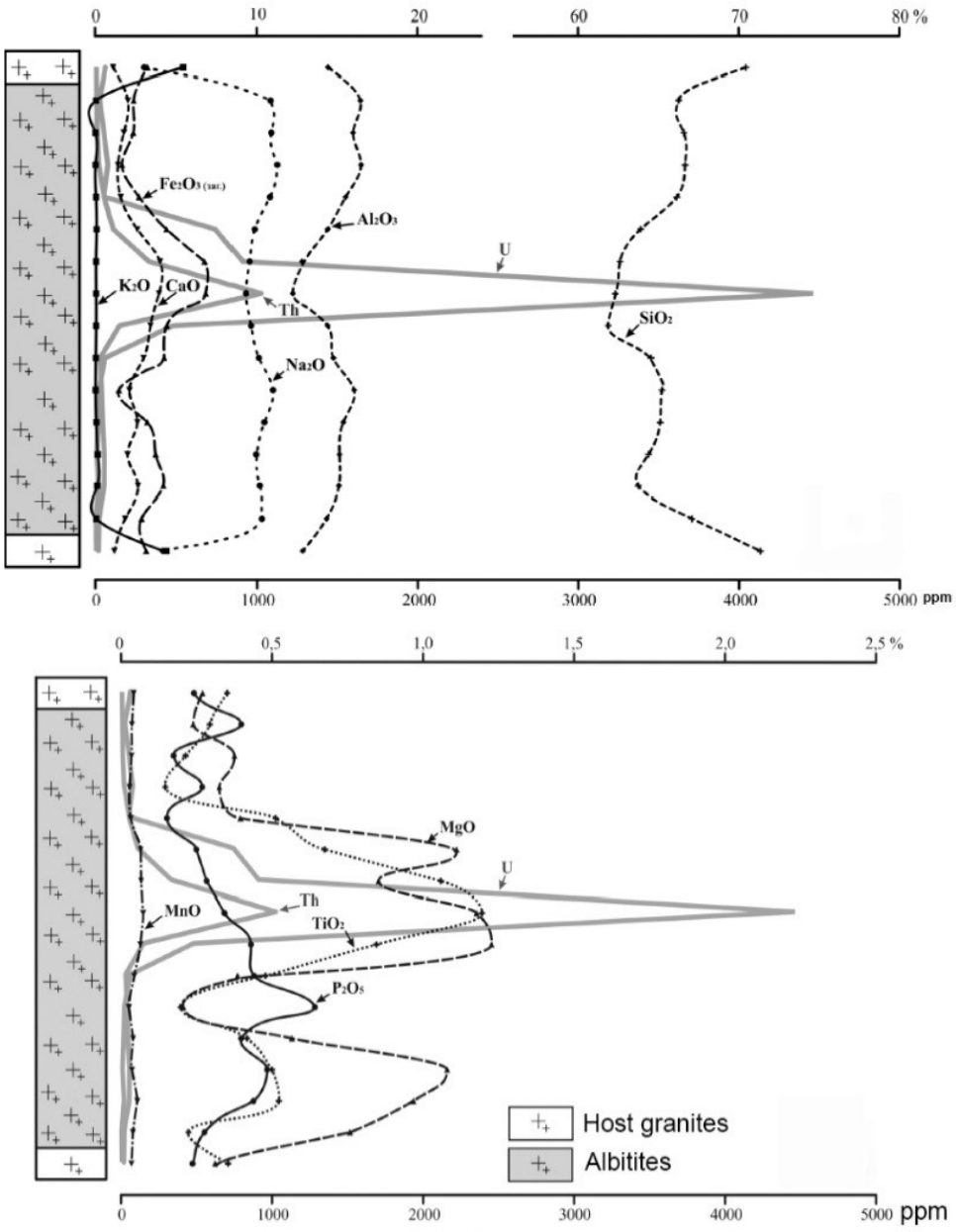

FIGURE 2. Variation of the chemical composition of albitites in the vertical section of the Novooleksiivka deposit. Lines of different styles demonstrate the variation of major oxide and trace element concentrations in a vertical section across the albitite body. Corresponding oxides and trace elements are indicated.

6. Sr-Nd-Pb ISOTOPE SYSTEMATICS

A set of whole rock samples for Pb-Sr-Nd isotope analyses was collected at the Novokostyantynivka and Novooleksiivka albitite-type deposits (Table 2). Both of the deposits are hosted by granitoids of the Novoukrainka massif. As can be seen from Sr isotope data, albitites have an isotopic signature at the time of their crystallization typical for crustal rocks (Figure 3). Specifically, rocks of the Novokostyantynivka deposit have $^{87}Sr/^{86}Sr_{(1800)}$ in the range 0.7087–0.7105, whereas rocks of the Novooleksiivka deposit show a variation from 0.7172 to 0.7207. Although not shown here, there is no strict correlation between $^{87}Rb/^{86}Sr$ and $^{87}Sr/^{86}Sr$ ratios that prevents the construction of isochrons and calculation of reasonable Rb–Sr

isotope ages. This indicates inhomogeneity of the Sr isotope composition that could result from the variable host rock/metasomatic rock ratio in the samples.

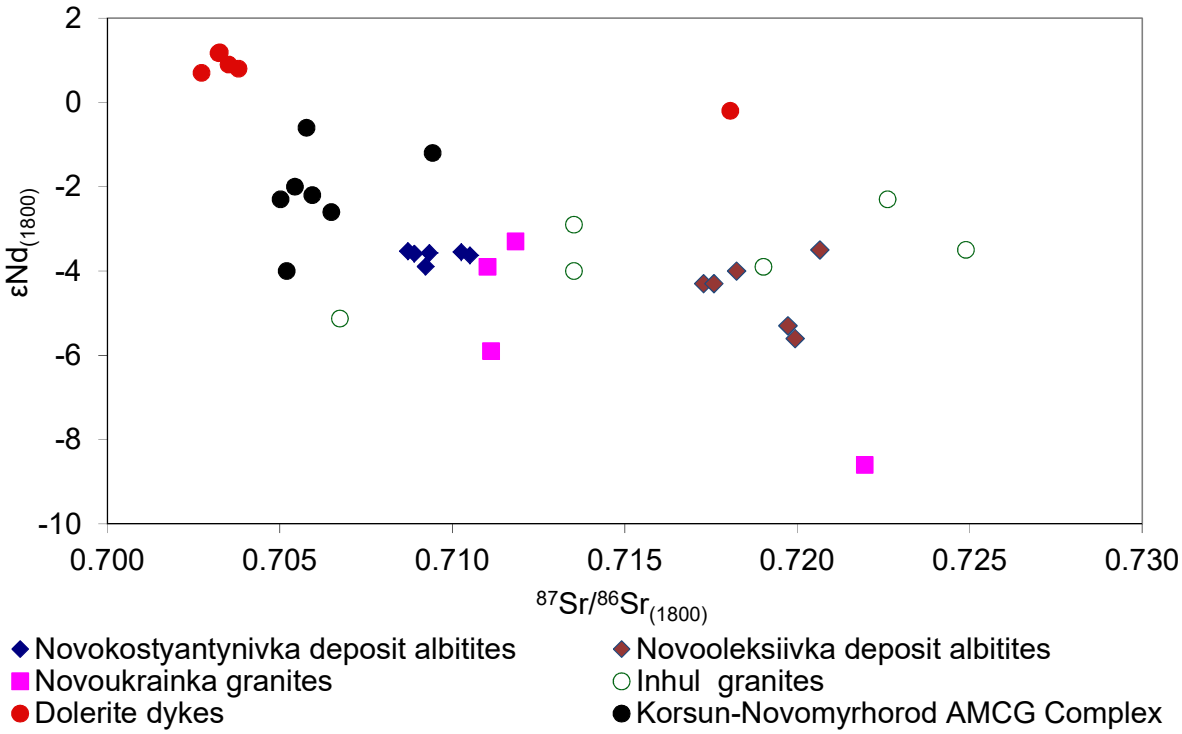

FIGURE 3. Sr-Nd isotope systematics of albitites compared to the most common lithologies in the Central Ukrainian U province.

In the Novooleksiivka deposit, samples were collected systematically across the vertical section of the metasomatic body. The results show that there is a tendency for albitite samples in the axial part of the body to have a less evolved initial Sr isotope composition. This tendency may indicate that the metasomatic fluids were derived from a source that had a lower Rb/Sr ratio than the upper crustal granites. However, this observation requires further confirmation on other deposits.

Neodymium isotope compositions, in contrast to Sr, are much more consistent in both of the deposits studied which allowed construction of a relatively good Sm-Nd isochron (Figure 4). The age obtained from this isochron (1728 ± 110 Ma; based on all results) corresponds within error to the U–Pb age previously obtained for the uranium deposits in the CUUP. The age of 1810 ± 5 Ma reported for the Partisanske deposit [2] which belongs to the same ore field as the Novooleksiivka deposit and the age interval for formation of Na-metasomatites, in general, was previously estimated as 1840–1800 Ma [12]. The calculated εNd value is -4.8, which indicates a dominantly crustal source of the fluids producing the metasomatic alteration, in accordance with Sr isotope data.

There is a small systematic difference between the Novokostyantynivka and the Novooleksiivka deposits; the average $\varepsilon Nd_{(1800)}$ value for the Novokostyantynivka albitites is -3.7, and that for the Novooleksiivka albitites is -4.5. These results are consistent with Sr isotope data, according to which the Novooleksiivka deposit reveals a more 'evolved' crustal source.

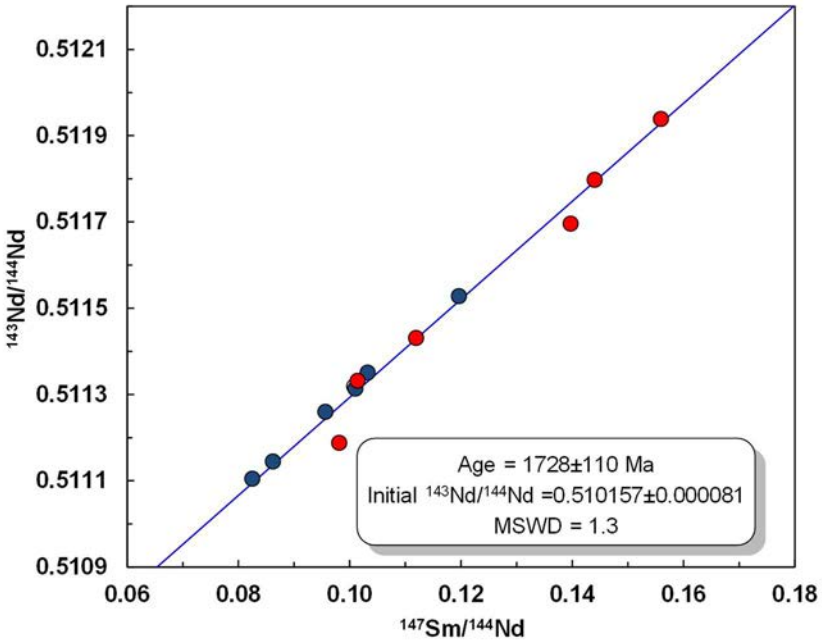

FIGURE 4. Sm-Nd isochron for albitites of the Novooleksiivka (red dots) and Novokostyantynivka (blue dots) deposits.

Lead isotope compositions indicate a prevalence of radiogenic Pb resulting from the decay of uranium, whereas 'common' Pb is negligible. This allows calculation of the Pb–Pb age of deposit formation. There is no significant difference in the age of the Novokostyantynivka and Novooleksiivka deposits and data combined from both deposits yields an age of 1810 ± 17 Ma (Figure 5). This age is in good agreement with the previously reported U–Pb ages [2, 12] and the Sm-Nd isochron age (Figure 4).

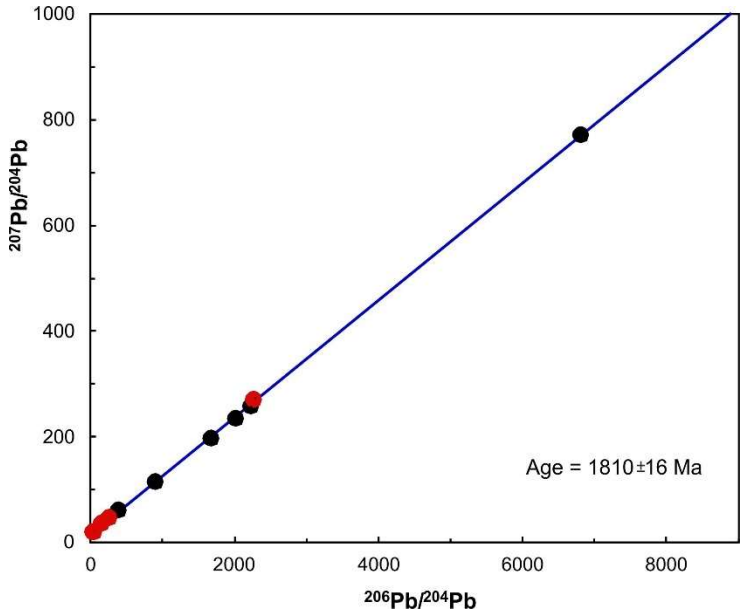

FIGURE 5. Pb-Pb isochron for albitites of the Novooleksiivka (red dots) and Novokostyantynivka (black dots) deposits.

TABLE 1. THE CHEMICAL COMPOSITION OF ALBITITES FROM THE NOVOOLEKSIIVKA DEPOSIT. DATA FOR SAMPLES ARE ORDERED ACCORDING TO THEIR POSITION ALONG THE VERTICAL PROFILE AS SEEN IN FIGURE 2

Rock	Host granite	Barren albitite				Ore-bearing albitite				Barren albitite						Host granite
Sample #	HA23	HA24	HA25	HA26	HA27	HA28	HA29	HA30	HA31	HA32	HA33	HA34	HA35	HA36	HA37	HA38
	%	%	%	%	%	%	%	%	%	%	%	%	%	%	%	%
SiO_2	70.45	66.28	66.59	66.67	66.15	63.90	62.61	62.32	61.89	64.55	65.23	65.11	64.39	63.75	67.09	71.35
Al_2O_3	14.44	16.45	16.01	16.49	15.54	14.43	12.82	12.25	14.42	14.77	16.06	15.39	15.16	15.12	14.35	12.87
Fe_2O_3	3.27	2.40	2.38	1.69	2.75	4.45	6.82	6.89	4.46	4.31	1.49	3.25	3.78	4.25	2.90	3.18
MnO	0.04	0.04	0.04	0.03	0.03	0.06	0.07	0.07	0.06	0.04	0.03	0.04	0.04	0.05	0.04	0.03
MgO	0.27	0.24	0.38	0.33	0.40	1.11	0.85	1.18	1.23	0.39	0.21	0.57	1.08	0.97	0.76	0.31
CaO	1.13	2.05	1.80	1.44	1.61	2.63	4.05	3.99	3.45	3.04	2.14	2.64	2.03	2.68	1.88	1.21
Na_2O	3.07	10.86	10.91	11.28	10.82	9.88	9.56	9.33	9.65	10.14	11.01	10.48	9.96	10.20	10.32	4.04
K_2O	5.49	0.06	0.03	0.04	0.07	0.10	0.07	0.07	0.07	0.06	0.03	0.08	0.18	0.14	0.08	4.44
TiO_2	0.35	0.29	0.21	0.15	0.51	0.67	1.06	1.20	0.85	0.48	0.20	0.42	0.50	0.52	0.22	0.35
P_2O_5	0.24	0.40	0.17	0.27	0.15	0.25	0.28	0.34	0.43	0.44	0.64	0.40	0.48	0.44	0.28	0.24
Total	99.41	99.53	99.32	99.26	99.10	98.64	99.19	98.96	98.51	99.22	98.60	99.26	98.82	99.12	98.95	99.13
	ppm	ppm	ppm	ppm	ppm	ppm	ppm	ppm	ppm	ppm	ppm	ppm	ppm	ppm	ppm	ppm
Be	1.3	1.5	1.5	1.7	1.6	1.7	1.9	1.7	1.7	1.5	1.3	1.8	2.3	2.9	1.6	1.3
V	11.8	25.3	30.1	17.8	41.7	65.1	104.2	115.9	71.1	69.7	32.1	69.0	55.1	58.8	26.2	12.3
Cr	20.9	21.8	20.0	23.2	24.0	19.9	20.8	20.2	18.1	21.6	18.1	30.5	23.2	26.6	25.2	22.3
Co	3.7	2.7	2.9	2.6	2.9	2.4	3.1	3.0	2.5	2.7	2.1	3.8	7.6	5.9	4.5	3.5
Ni	31.1	23.9	18.6	24.2	14.1	15.7	10.7	12.7	11.3	17.7	20.7	23.1	13.2	22.7	17.6	14.8
Cu	17.1	10.8	9.6	9.2	17.1	12.8	15.1	10.2	11.7	10.9	10.5	19.3	16.3	18.4	16.3	16.6
Zn	53.3	17.9	22.1	20.1	23.4	31.8	41.2	42.6	62.2	37.3	20.2	183.1	55	43.1	45.1	50.0
Ga	28.1	25.1	25.1	26.9	25.4	24.8	22.6	22.2	23.3	23.1	24.9	24.2	25	23.5	24.1	25.5
As	1.1	0.7	0.6	0.6	0.6	0.7	0.6	0.7	1.1	1.3	0.6	0.7	0.8	0.8	0.6	0.7
Rb	277.8	2.7	1.5	2.1	4.9	9.5	6.8	6.1	5.4	4.5	1.7	9.7	12.7	10.1	4.9	226.8
Sr	122	96	67	106	116	122	133	144	148	135	169	177	139	169	105	132
Zr	165	72	300	99	203	80	234	215	73	39	34	110	140	100	188	370
Nb	15.0	11.6	9.6	3.5	37.4	59.8	97.8	98.4	38.7	21.4	7.7	14.6	20.4	22.7	14.5	21.5

TABLE 1 (Cont.). THE CHEMICAL COMPOSITION OF ALBITITES FROM THE NOVOOLEKSIIVKA DEPOSIT. DATA FOR SAMPLES ARE ORDERED ACCORDING TO THEIR POSITION ALONG THE VERTICAL PROFILE AS SEEN IN FIGURE 2

Rock	Host granite	Barren albitite				Ore-bearing albitite				Barren albitite						Host granite
Sample #	HA23	HA24	HA25	HA26	HA27	HA28	HA29	HA30	HA31	HA32	HA33	HA34	HA35	HA36	HA37	HA38
	ppm	ppm	ppm	ppm	ppm	ppm	ppm	ppm	ppm	ppm	ppm	ppm	ppm	ppm	ppm	ppm
Mo	2.6	3.5	2.6	3.6	3.1	1.5	1.5	1.5	1.7	4.2	3.6	1.5	1.8	2.0	2.1	1.5
Ag	0.6	0.5	0.7	0.5	0.5	0.4	0.6	0.6	0.5	0.3	0.3	0.4	0.5	0.4	0.5	0.8
Sn	2.4	1.6	2.7	1.2	2.6	2.2	2.7	2.6	1.4	1.6	1.3	2.8	1.5	1.9	2.3	2.3
Cs	1.2	0.1	0.1	0.1	0.2	0.2	0.2	0.2	0.2	0.2	0.1	0.2	0.2	0.2	0.1	0.8
Ba	890.8	109.3	48.7	57.4	115.7	149.5	110.7	195.7	120.3	78.6	47.0	81.6	194.3	231.2	201.5	860.8
Hf	3.7	2.0	8.0	2.7	5.0	1.5	4.8	4.3	1.9	0.9	1.2	2.4	3.5	2.3	4.6	10.2
W	2	1.8	1.3	2.9	1.1	2.6	1.1	1.1	1.3	1.4	1.4	1.6	1.1	4.2	1.5	1.2
Pb	38.4	13.4	9.7	12.9	16.5	26.7	54.0	147.5	26.9	10.7	13.4	10.6	12.6	15.4	12.2	28.4
Th	77.9	32.4	54.3	79.0	57.5	109.5	362.0	1127.0	150.3	36.2	40.6	54.7	67.6	67.3	29	33.2
U	5.4	10.6	13.6	22.5	60.0	739.1	1001.0	4986.0	435.4	67.4	25.9	23.5	14.8	25.7	6.6	4.0
La	142.70	102.50	73.24	143.20	79.66	53.44	59.87	68.69	153.60	56.26	86.43	95.15	113.90	78.90	59.71	72.04
Ce	327.70	223.50	156.90	311.80	176.00	124.90	150.30	185.00	319.40	139.20	211.90	208.20	236.70	174.20	123.90	151.30
Pr	34.13	24.23	16.56	30.25	18.09	15.28	18.82	24.45	37.54	19.31	28.48	26.59	27.08	21.31	14.52	17.59
Nd	133.10	94.90	62.21	107.10	67.36	68.73	85.29	116.00	144.30	82.18	120.50	106.50	99.68	81.41	53.49	63.71
Sm	22.17	15.65	9.43	14.02	10.80	16.07	19.59	29.53	26.62	19.09	26.60	22.05	18.74	16.47	9.85	11.26
Eu	1.17	0.92	0.68	0.90	1.06	1.84	2.23	3.23	2.54	1.87	2.45	2.21	1.57	1.48	0.83	1.19
Gd	16.41	11.98	7.25	10.18	8.30	15.29	18.38	31.67	22.51	16.13	21.87	18.56	15.48	14.14	7.91	8.93
Tb	1.77	1.34	0.83	1.00	1.00	2.40	3.00	5.86	3.21	2.41	3.22	2.67	2.08	1.96	1.01	1.22
Dy	8.32	5.93	4.12	4.39	5.38	15.74	20.65	43.82	19.50	14.06	18.57	15.54	11.39	10.61	4.84	6.76
Ho	1.43	0.91	0.73	0.71	1.00	3.21	4.47	9.95	4.05	2.68	3.55	3.01	2.08	1.91	0.84	1.22
Er	4.28	2.58	2.11	1.91	2.92	9.53	14.03	30.52	11.15	6.74	8.89	7.71	5.47	4.99	2.33	2.90
Tm	0.62	0.39	0.33	0.27	0.46	1.34	1.99	3.97	1.51	0.89	1.11	1.04	0.78	0.71	0.36	0.36
Yb	4.22	2.66	2.48	1.92	3.66	8.25	11.88	20.51	7.96	5.35	5.52	5.93	4.76	4.48	2.26	2.02
Lu	0.63	0.37	0.40	0.32	0.60	1.08	1.51	2.28	1.02	0.84	0.68	0.90	0.76	0.75	0.33	0.29

TABLE 2. Sr, Nd, AND Pb ISOTOPE SYSTEMATICS OF ALBITITES OF THE NOVOKOSTYANTYNIVKA AND NOVOOLEKSIIVKA DEPOSITS

Sample	$^{87}Sr/^{86}Sr$	±2 σ	Rb, ppm	Sr, ppm	$^{87}Rb/^{86}Sr$	$e_{Sr(1800)}$	$^{87}Sr/^{86}Sr_{(1800)}$	$^{143}Nd/^{144}Nd$	±2 σ	Nd, ppm	Sm, ppm	$^{147}Sm/^{144}Nd$	$\varepsilon Nd_{(1800)}$	$^{206}Pb/^{204}Pb$	$^{207}Pb/^{204}Pb$	$^{208}Pb/^{204}Pb$
Novokostyantynivka deposit																
3a	0.710474	0.000015	4.28	257	0.0482	96	0.70923	0.511528	0.000007	58.27	11.54	0.1196	-3.9	2229	257.6	63.48
5	0.712340	0.000008	26.42	576	0.1329	91	0.70890	0.511319	0.000006	27.78	4.63	0.1008	-3.6	6819	770.1	50.62
5 (repeated)	0.712331	0.000012	26.42	576	0.1329	91	0.70889	0.511314	0.000006	28.08	4.69	0.1010	-3.8			
9	0.710737	0.000009	2.97	1000	0.0086	114	0.71051	0.511145	0.000003	62.03	8.85	0.0862	-3.6	395.2	59.38	43.23
10a	0.718104	0.000004	14.03	134	0.3028	110	0.71027	0.511260	0.000005	114.32	18.08	0.0956	-3.6	2022	234	81.57
15	0.710858	0.000005	14.86	520	0.0827	88	0.70873	0.511351	0.000006	62.56	10.68	0.1032	-3.5	1683	196.8	45.35
20a	0.710021	0.000007	2.65	288	0.0266	97	0.70933	0.511105	0.000004	59.20	8.09	0.0825	-3.6	909	114.6	38.97
Novooleksiivka deposit																
HA 24	0.722783	0.000008	2.73	96	0.0821	258	0.72066	0.511332	0.000007	87.86	14.75	0.1014	-3.5	46.60	19.21	57.85
HA 27	0.723128	0.000022	4.95	116	0.1232	248	0.71994	0.511188	0.000004	61.25	9.95	0.0981	-5.6	164.6	34.47	60.11
HA 28	0.723095	0.000007	9.46	122	0.2244	210	0.71729	0.511798	0.000004	66.12	15.75	0.1440	-4.3	2277	269.9	145.7
HA 30	0.720792	0.000016	6.15	144	0.1237	215	0.71759	0.511939	0.000005	109.64	28.28	0.1559	-4.3	10775	1114	865
HA 32	0.722222	0.000021	4.47	135	0.0963	245	0.71973	0.511696	0.000005	82.52	19.08	0.1397	-5.3	262.7	45.35	79.29
HA 35	0.725050	0.000007	12.65	139	0.2630	224	0.71824	0.511431	0.000004	96.97	17.96	0.1119	-4.0	55.09	19.92	69.10

The isotope results can be compared with data available for the main lithologies present in the area (Figure 3). Albitites of the Novokostyantynivka deposit plot between fields of the Novoukrainka massif and Korsun-Novomyrhorod AMCG complex, and closer to the Novoukrainka field. In contrast, albitites of the Novooleksiivka deposit plot entirely within the field defined by the Inhul granitoid complex. It has Nd isotope characteristics similar to the Novoukrainka massif but differs by having much higher Sr isotope values. When these albitites are compared to the coeval mantle-derived dolerite dykes widely distributed in the same area, the difference between these two groups of rocks are evident.

According to Sr-Nd isotope data, the initial fluids that led to the formation of uranium-bearing albitites could have been derived from or equilibrated with the Palaeoproterozoic felsic rocks widely distributed in the area, namely from rocks of the Novoukrainka and Inhul complexes. However, other geochemical data indicate an important influence of mantle-derived material. Probably a mantle plume that was active in that area during formation of the albitites was responsible not only for the heating of area and formation of hot fluids but also provided some material necessary for the formation of the albitites.

7. DISCUSSION ON POSSIBLE SOURCE OF URANIUM-BEARING FLUIDS

Several features of the albitite-type uranium deposits that are important for the understanding of their origin can be recognized. These include:

(i) Close spatial and temporal links with mantle-derived tholeiites and AMCG magmatism. According to the available geochronological data, albitites developed simultaneously with the first phases of AMCG magmatism in the Ukrainian Shield and with numerous mafic and ultramafic dykes. Most of the uranium deposits occur close to the Korsun-Novomyrhorod AMCG complex (see Figure 19.3 in [13]) and are located within fault zones that often host also mafic dykes (Figure 1). Uranium deposits related to Na-metasomatism in the Kryvyi Rih area occur as important exceptions to that rule, as they are located at some distance from the Korsun-Novomyrhorod Complex, but still within fault zones of regional scale;

(ii) Geophysical data [14] indicate, that Na-metasomatites are confined to the major trans-crustal fault zones and to certain crustal anomalies (i.e. to the zones of thickened crust). The fault zones occur as zones of the increased permeability that reach the mantle and could have served as zones of discharge of mantle fluids;

(iii) Results of the fluid inclusion studies (see [1] and references therein) indicate that crystallization of Na-metasomatites was caused by infiltration of hot (up to 380-480 ˚C) fluids. Formation of hot fluids would have required the existence of a thermal anomaly in the crust which probably was caused by the emplacement of hot (mantle) melts;

(iv) Na-metasomatites, besides U, are variously enriched in a wide set of chemical elements. Some of these elements (Na, U, Th, Nb, HREE, Sr, Ag) are more typical for felsic rock, whereas others (Ti, V, Sc, Ni, Zn) are usually related to mafic rocks.

Taken together, geological, geophysical and geochemical data indicate an important role of the magmatism that probably was caused by the mantle plume [4, 10]. The emplacement of large volumes of hot mantle melts into the crust caused abundant crustal melting and formation of huge AMCG plutonic complexes [4]. Inevitably, this event also resulted in the formation of large volumes of hot fluids, of both crustal and mantle origin. Hence, hot mafic melts not only heated the crust, but also provided some metal components for the fluids. This can be seen from enrichments of some elements that are not typical for crustal sources, namely: Ti, V, Sc, Ni, Zn, etc. It is also important to note, that Na-metasomatites are generally very rich in Na, and

poor in K (except products of very small-volume, late stage metasomatic alteration), in contrast to metasomatic fluids that are usually related to felsic rocks and in which K greatly prevails over Na.

However, isotope-geochemical data indicate the predominantly crustal source of the metasomatic rocks. Strontium and neodymium isotopic compositions of the metasomatic rocks is very close (or even identical) to the felsic rocks widely distributed in the area. Additionally, uranium-rich rocks (uranium ores) demonstrate more 'primitive' Sr isotope composition that may indicate a different source of the abundant Na-metasomatites (albitites) of the main metasomatic stage, and of the small-volume uranium ores, which are related to the late K-Mg-Ca metasomatic stage [1]. In spite of some enrichment in K (and Rb), these late metasomatic rocks contain less radiogenic Sr.

8. CONCLUSIONS

In general, geochemical and isotopic data indicate a mixed source of metasomatic fluids and metal components for the albitite-type uranium deposits of the Central Ukrainian Uranium Province. Their formation was likely caused by the emplacement of large masses of hot mantle melts into the crust. Subsequently, hot mantle-derived fluids migrated along the trans-crustal zones of the increased permeability (so-called 'deep faults') and mixed with crustal-derived fluids.

REFERENCES

[1] CUNEY, M., EMETZ, O., MERCADIER, J., MYKHAYLOV, V., SHUNKO, V., YUSLENKO, A., Uranium deposits associated with Na-metasomatism from central Ukraine: a review of some of the major deposits and genetic constraints, Ore Geol. Rev. **44** (2012) 82–106.

[2] BELEVTSEV, YA. N., (Ed.), Genetic types and regularities of the location of uranium deposits in Ukraine, Naukova Dumka, Kyiv, 396 pp (1995) (in Russian).

[3] VERKHOVTSEV, V.G, LISICHENKO, G.V., ZABULONOV, YU.L., VOZNYAK, D.K., DIDENKO, P.I., KOVAL, V.B., KRAMAR, O.O., MELNYCHENKO, B.F., NOZHENKO, O.V., SEMENYUK, M.P., SYNYTSYN, V.O., SUSHCHUK, K.G., TYSHCHENKO, YU.YE., FOMIN, YU.O., SHVAIKO, V.G., YUSKIV, YU.V., YAROSHCHUK, M.O., Prospects for the development of uranium resource base of nuclear power of Ukraine, Naukova Dumka, Kyiv, 356 pp. (2014) (in Ukrainian).

[4] SHUMLYANSKYY, L., HAWKESWORTH, C., BILLSTRÖM, K., BOGDANOVA, S., MYTROKHYN, O., ROMER, R., DHUIME, B., CLAESSON, S., ERNST, R., WHITEHOUSE, M., BILAN, O., The origin of the Palaeoproterozoic AMCG complexes in the Ukrainian Shield: new U-Pb ages and Hf isotopes in zircon, Precam. Res. **292** (2017) 216–239.

[5] CUNEY, M., SHCHERBAK, M.P., EMETZ, A.V., PETRYCHENKO, K.V., SINELU, S., Petrological and geochronological peculiarities of the Novoukrainka massif rocks and age problem of uranium mineralization of the Kirovograd megablock of the Ukrainian Shield, Miner. J. (Ukraine) **30** 2 (2008) 5–16.

[6] STEPANYUK, L.M, ANDRIENKO, O.M., DOVBUSH, T.I., BONDARENKO, V.K., The age of formation of the Novoukrainka massif, Miner. J. (Ukraine) **27** 1 (2005) 44–50 (in Ukrainian).

[7] SHUMLYANSKYY, L., PETRENKO, O., The Palaeoproterozoic granitoid magmatism of the Inhul region of the Ukrainian Shield, Geol. Mineral. Proc. Kryvyi Rih Nat. Univ. **33** 1 (2015) 80–87 (in Ukrainian).

[8] STEPANYUK, L.M, KURYLO, S.I., DOVBUSH, T.I., GRINCHENKO, O.V., SYOMKA, V.O., BONDARENKO, S.M., SHUMLYANSKYY, L.V., Geochronology of granitoids of the eastern part of the Inhul region (the Ukrainian Shield), Geochem. Ore Form. **38** (2017) 3–13.
[9] STEPANYUK, L.M, DOVBUSH, T.I., BONDARENKO, S.M., SYOMKA, V.O., GRINCHENKO, O.V., SKURATIVSKYY, S.E., U-Pb geochronology of the rocks of the K-U formation of the Inhul region of the Ukrainian Shield, Miner. J. (Ukraine) **34** 3 (2012) 55–63 (in Ukrainian).
[10] SHUMLYANSKYY, L., MITROKHIN, O., BILLSTRÖM, K., ERNST, R., VISHNEVSKA, E., TSYMBAL, S., CUNEY, M., SOESOO, A., The ca. 1.8 Ga mantle plume related magmatism of the central part of the Ukrainian Shield, GFF **138** (2016) 86–101.
[11] TODT, W., CLIFF, R.A., HANSER, A., HOFMANN, A.W., Evaluation of ^{202}Pb-^{205}Pb double spike for high-precision lead isotope analysis. In: A. Basu and S. Hart (Editors), Earth Processes: Reading the Isotopic Code, Geophys. Monogr., **95** (1996), Am. Geophys. Union, Washington, DC, 429-437.
[12] SHCHERBAK, N.P., ARTEMENKO, G.V., LESNAYA, I.M., PONOMARENKO, A.N., SHUMLYANSKYY, L.V., Geochronology of the Early Precambrian of the Ukrainian Shield. Proterozoic. Naukova Dumka, Kyiv, 240 p. (2008) (in Russian).
[13] DAHLKAMP, F.J., Uranium Deposits of the World. Europe. Springer-Verlag Berlin Heidelberg, 800 pp. (2016).
[14] STAROSTENKO, V.I., GINTOV, O.B., (Eds.), Kirovohrad ore district. Deep structure. Tectonophysical analysis. Ore deposits, Prastye lyudy, Kyiv (2013), 500 pp. (in Russian).

GEOCHEMICAL AND MINERALOGICAL CHARACTERIZATION OF THE URANIFEROUS PHOSPHATES OF THE NAVAY FORMATION, TÁCHIRA STATE, BOLIVARIAN REPUBLIC OF VENEZUELA, FINAL CONSIDERATIONS*

J. MANRIQUE
Universidad Técnica Particular de Loja,
Loja, Ecuador

E. LINARES, J. MONSALVE, G. VELÁSQUEZ, A. PIÑA
Universidad Central de Venezuela,

H. BARROS
Universidad Simón Bolívar,

Caracas, Bolivarian Republic of Venezuela

*Preliminary results and some parts of this paper were presented at the IAEA International Symposium on Uranium Raw Material for the Nuclear Fuel Cycle: Exploration, Mining, Production, Supply and Demand, Economics and Environmental Issues (URAM-2018). Vienna, Austria, 25-29 June 2018.

Abstract

Through an IAEA CRP, a geochemical and mineralogical characterization study of the uraniferous phosphate rocks of the Navay Formation, Táchira state, Bolivarian Republic of Venezuela, was carried out. Petrographic and mineralogical analyses revealed that the main minerals are fluorapatite ($Ca_5(PO_4)_3F$), quartz (SiO_2) and calcite ($CaCO_3$). This mineralogical association is typical of marine phosphatic deposits. According to the petrographic studies, the rock samples can be classified as phosphatic sandstones and phosphorites. The chemical analyses indicated that the Ca, Sr, Y and U exhibit an excellent positive correlation with the P_2O_5, indicating that the minerals that host these elements is apatite. The average concentration of uranium in the analyzed samples is 90 ppm, with a maximum value of 160 ppm. In addition, anomalous values of V, Mo, and Ni, and sub anomalous values of S, Se, Pb and Zn were determined.

1. INTRODUCTION

As part of an IAEA Coordinated Research Project (CRP) research was conducted on the geochemical and mineralogical characterization of the uraniferous phosphate rocks of the Navay Formation, which is located at Táchira State, Bolivarian Republic of Venezuela. In this framework, a phosphate deposit was discovered in early 1978 by radiometric surveys conducted by The National Commission of Nuclear Affairs (CONAN) of the Ministry of Energy and Mines in Venezuela. The deposit is associated with sandstones in the upper levels of the Navay Formation (Upper Cretaceous) and is hosted by siliceous shales, calcareous shales, uraniferous phosphatic sandstones and cherts (phtanites) [1]. To date, there are few studies on the feasibility for exploitation to produce phosphate fertilizers. To our knowledge, this contribution represents the first approach to characterize the deposit with a focus on the recovery of uranium.

2. GEOLOGICAL SETTING OF THE AREA

2.1. Regional geology

The phosphate deposit studied is located at the Barinas-Apure Basin, in southwestern Venezuela. The geological and tectonic history of this basin is marked by a progressive evolution of the Caribbean-Tethyan passive margin at the edge of the South American plate, taking place from the Jurassic to the Late Cretaceous during the fragmentation of Pangea, which

is correlated with the worldwide eustatic changes of sea level [2]. The chronostratigraphic development of the Barinas-Apure Basin can be divided into two stages (Lower-Middle and Upper): (i) The Barremian-Turonian succession (less than half Cretaceous), which is comprised of the Rio Negro-Aguardiante-Escandalosa Formations, and (ii) the Coniacian-Maastrichtian succession, which is represented by the Navay-Burgüita Formations [3].

The sedimentation of the Navay Formation, considered as the host rock of the mineralization, was controlled by the Arcos de Arauca, Mérida and the Santa Marta and Santander massifs, where this process occurred mainly within a hemipelagic environment, in bottom waters dominated by conditions of little oxygen, and in low energy conditions. Nevertheless, these conditions were not maintained without interruption, triggering bottom currents locally, erosion induced by storms, seismic events and intermittent oxygenation of the bottom waters that affected the sedimentary patterns. According to the lithology and fossil content, the Navay Formation represents a change of sedimentary facies, related to internal platform and transitional environments. Meanwhile an analogous formation to the Navay Formation called La Luna Formation was deposited in deeper marine environments [4–7].

2.2. Local geology

The upper unit of the Navay Formation named the Quevedo Member, consists of siliceous shales, cherts, sandstones and fine-grained and phosphatic layers of remains of organisms. This unit constitutes a lithological facies deposited in shallow water and is locally Campanian-Maastrichtian [8], with thicknesses varying between 100 and 320 m, marked by lateral variations due to the position of high basement rocks, the water depth and the relative position of the outlet conveyor river sediments [1].

Previously determined radiometric anomalies were defined in the Las Tapas–Fila El Toro. These were produced by uranium enrichment in phosphatic minerals (0.01–0.04% U) and are associated with the top of the Navay Formation, equivalent to the base of the Burguita Formation. Pasquali [9] published the first document on the discovery of these phosphate rocks and suggested that the phosphatic sediments of the Navay Formation could be the result of phosphate precipitation in an environment of shallow water, which allowed the formation of phosphate rich streams from the deep basin, Uribante, located northwest of the La Luna Formation.

The radiometric anomalies form strips whose surface width is a function of the dip of phosphatic horizons (phosphatic siltstones, phosphatic sandstones and thin layers with organic remains). The phosphatic sandstones are highly porous and permeable, promoting leaching and P_2O_5 enrichment and mobilization to lower levels and/or fracture zones [10].

3. METHODOLOGY AND RESULTS

3.1. Mineralogical analysis

Mineralogical analyses were carried out at Earth Sciences Institute of the Universidad Central de Venezuela and Diffraction laboratory of the Geology and Mining Engineering of the Universidad Técnica Particular de Loja (Ecuador) on representative samples from different rock facies of the Navay deposit. The selected samples were studied for petrographic and mineralogical analysis using: (i) a polarizing microscope, and (ii) an X-ray diffraction (XRD) analyzer.

The main rock forming minerals were determined and quantified in weight percent (wt%): fluorapatite/chlorapatite ($Ca_5(PO_4)_3(F,Cl)$), collophane or carbonate fluorapatite ($Ca_5(PO_4,CO_3)F$), uranospathite ($Al_{1-xx}[(UO_2)(PO_4)]_2(H_2O)_{20+3x}F_{1-3x}$), quartz ($SiO_2$: 4–88 wt%), calcite ($CaCO_3$; 10–35 wt%), montmorillonite ($(Na,Ca)_{0,3}(Al,Mg)_2Si_4O_{10}(OH)_2$) (maximum 6 wt%) and microcline ($KAlSi_3O_8$) (maximum 1.43 wt%).

3.1.1. X-ray diffraction results

Fluorapatite has been identified as the main phosphate mineral, which in some cases contains carbonate in its structure (CO_3^{2-}), which is common in this group of minerals as carbonate ions can replace phosphate ions (PO_4^{3-}) [11]. The uranium is hosted in the apatite because the U^{4+} (ionic radius 1.00 Å) can replace the Ca^{2+} (ionic radius 1.12 Å and with the same octahedral coordination as U) [12]. The presence of uranospathite, which is a secondary phosphate of Al and U and belongs to the autunite group and formed as a result of the weathering of primary phosphates in humid environments was detected by XRD [13]. The presence of autunite and wavellite cannot be ruled out, as these have been identified in samples from La Lucha River and also in Táchira State [1].

The main uranium-bearing minerals identified include apatite (fluor/chloro apatite and collophane) (28–75 wt%) and uranospathite (2–3 wt%). The distribution of these minerals in the selected samples is shown in the Figure 1.

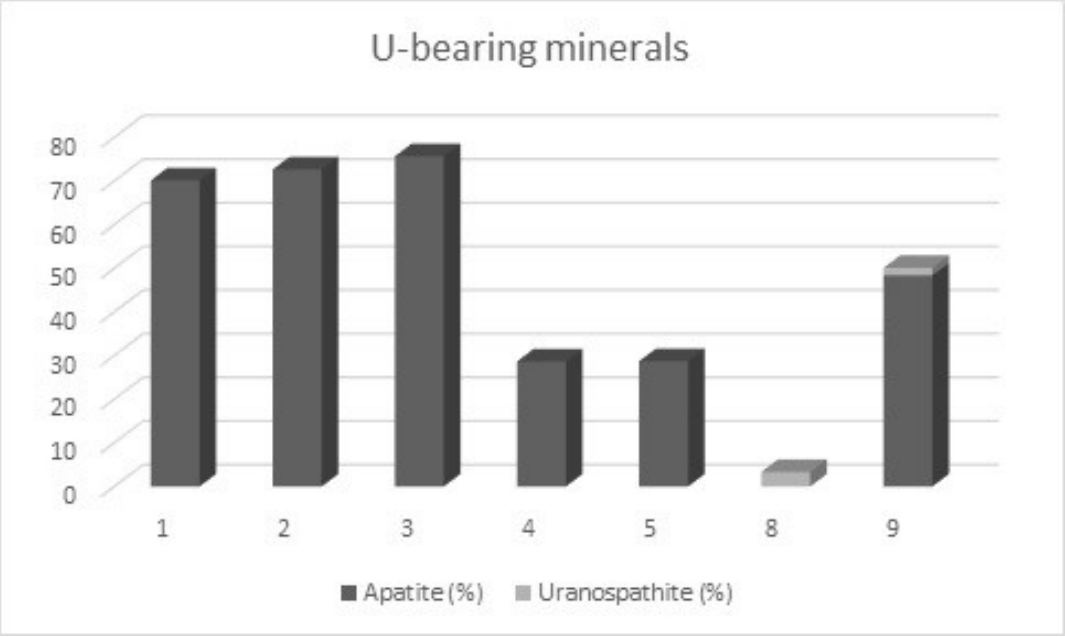

FIGURE 1. Uranium-bearing minerals identified by XRD in selected samples.

3.1.2. Petrographic results

Thin sections were made from some samples for petrographic studies. Results showed that the samples correspond to phosphatic sandstones, some with micritization of peloids. The mineralogy is typical of marine phosphatic deposits.

Petrographic observations of phosphatic sandstones and phosphorites of the Navay Formation indicated that the constituents of these rocks may be classified into two major categories which include phosphatic grains and non-phosphatic grains.

Phosphatic grains form the most important constituent in the investigated samples and are composed of phosphatic mudclasts best described as 'peloids', which are well rounded in shape and lack perceptible internal structure, with sizes ranging from 35 to 100 μm in diameter, and colors that vary from yellow to brown. The samples also contain a fine-grained and homogeneous phosphatic matrix. Some mudclasts are partially replaced with cementing materials, such as chalcedony and calcite (Figure 2).

Non-phosphatic grains are mainly detrital quartz that occur as monocrystalline grains of 30 to 60 μm in diameter, vary in color from pale gray to gray, are angular to subrounded and generally show wavy extinction under crossed polarized light using the polarizing microscope. Also grains of microcline and biotite were identified (Figure 2).

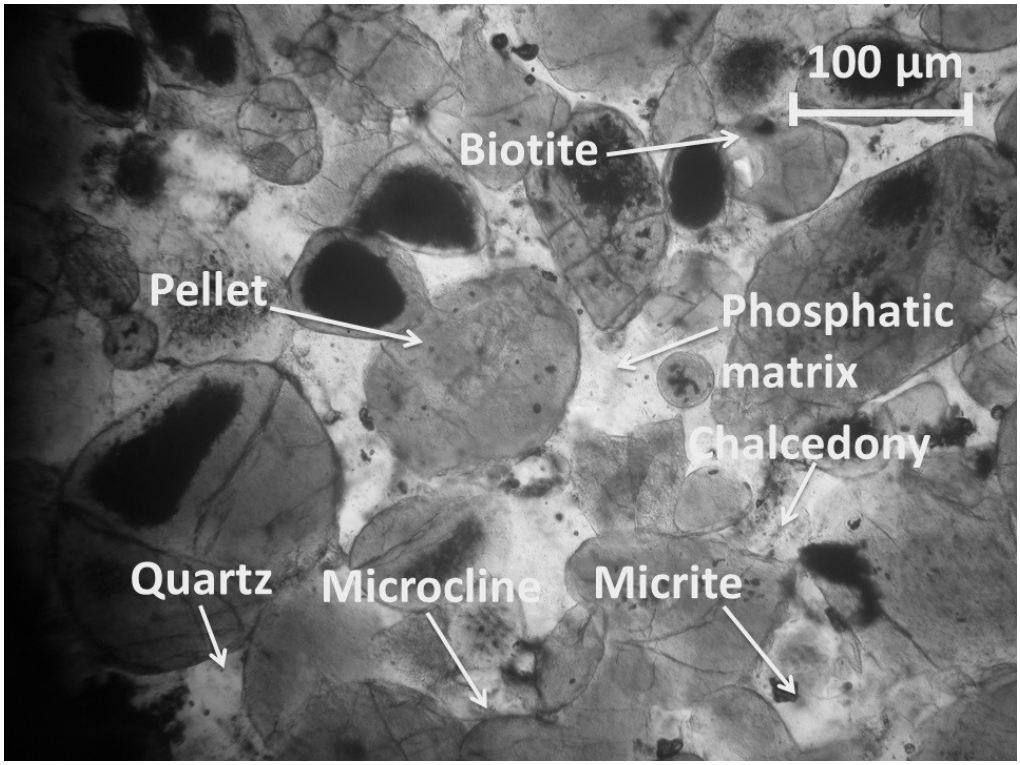

FIGURE 2. Photomicrograph of phosphatic sandstone in thin section.

Intergranular space within the rock samples is composed mainly of chalcedony cement that also replaces the phosphate in phosphatic grains. The chalcedony ranges from colorless and transparent to brown and the calcite occurs as pore-filling microsparite with colorless to pale gray crystals, 10–20 μm in diameter (Figure 2).

3.2. Elemental analysis

Elemental analyses were performed at the Laboratory of Nuclear Physics of the Universidad Simón Bolívar, Laboratory of Analytical Geochemistry of the Geology and Mining Engineering of the Universidad Técnica Particular de Loja (Ecuador) using several techniques: portable X ray fluorescence (pXRF), total reflection X ray fluorescence (TRXRF) and inductively coupled

plasma-atomic emission spectroscopy (ICP-AES). According to these techniques, the background concentration of uranium is 102 ppm, reaching a maximum value of 160 ppm in a calcareous phosphatic sandstone. These values are within the average range of uranium concentrations in marine phosphate rocks (50–300 ppm) [14].

3.2.1. Elemental analysis results

Statistically there were some sub-anomalous values: Cd (82 ppm), Cu (261 ppm), Zn (268 ppm), Sr (1832 ppm) and Zr (510 ppm), as well as anomalous values of Cr (1653 ppm). In addition, maximum values of major, minor and trace element concentrations were determined: MgO (12.40 wt%), Al_2O_3 (9.60 wt%), K_2O (3.07 wt%), Fe_2O_3 (1.25 wt%), MnO (0.05 wt%), TiO_2 (0.35 wt%), S (1.31 wt%), Cl (1.07 wt%), V (82 ppm), Ni (2083 ppm), Pb (86 ppm), Co (199 ppm) and Rb (91 ppm).

According to the chemical composition of the samples (see Figure 3), most of the analyzed samples correspond to phosphatic rocks (median 17.25 wt% and maximum 24.81 wt% P_2O_5), sandstones (median 25.60 wt% and maximum 88.70 wt% of SiO_2) and phosphatic limestones (median 27.88 wt% and maximum 70.40 wt% of CaO) [15].

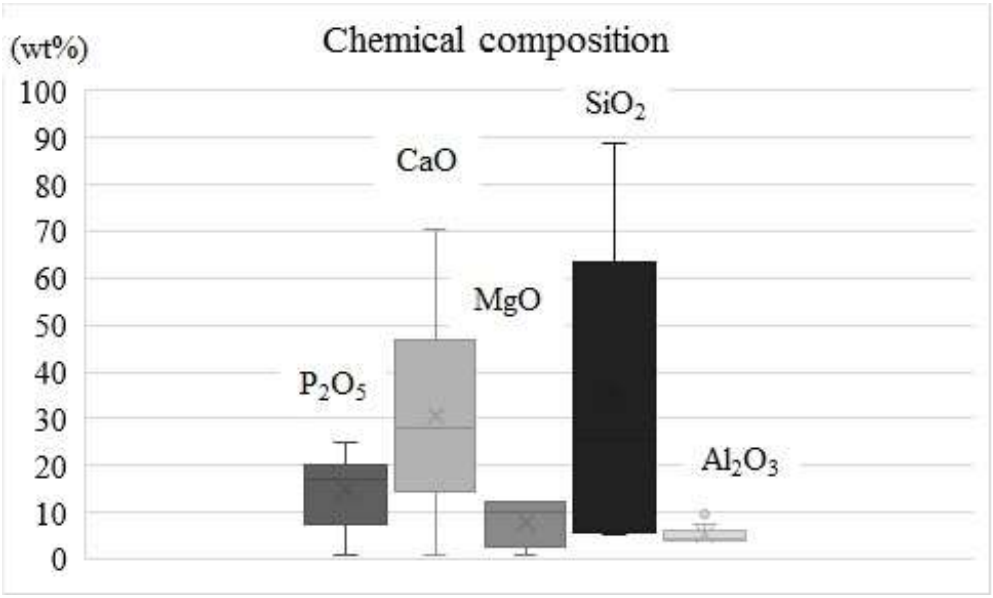

FIGURE 3. Chemical composition (%) of the rock samples.

Further analyses were completed for trace elements which may be geochemically associated with phosphates (U and Y), calcite (Sr) and organic matter and/or sulphide minerals (Ni, Cu, Zn) (Table 1).

TABLE 1. TRACE ELEMENTS CONCENTRATIONS

	U (ppm)	Ni (ppm)	Cu (ppm)	Zn (ppm)	Sr (ppm)	Y (ppm)
Minimum	54	64	14	14	43	24
Maximum	160	819	41	121	691	144
Average	105	182	29	88	388	78
Median	110	26	27	105	376	77

The elemental analyses show that U and Ca are correlated with P, indicating that the mineral hosting uranium can be apatite (Figures 4 and 5). There are strong correlations between P and Y (0.72) which may indicate the presence of yttrium in the phosphatic minerals, Ca–Mg (calcite), Ca–Sr (substitution of Sr^{2+} by Ca^{2+}), Si with Al and K (silicates such as microcline and clays such as montmorillonite), Fe–S (possibly forming sulphides), Fe–V (associated in detrital oxides and/or in organic matter), S–V (possibly in organic matter), U with V and Ni which is probably associated with organic matter, as well as the strong V–Ni correlation, which may be geochemically associated with porphyrins [16, 17].

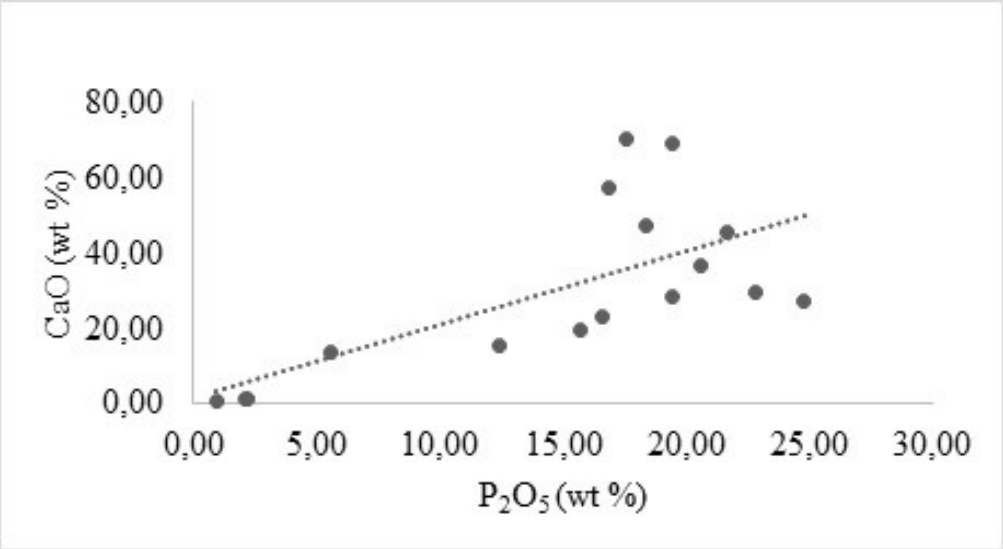

FIGURE 4. Correlation diagram P_2O_5 – CaO.

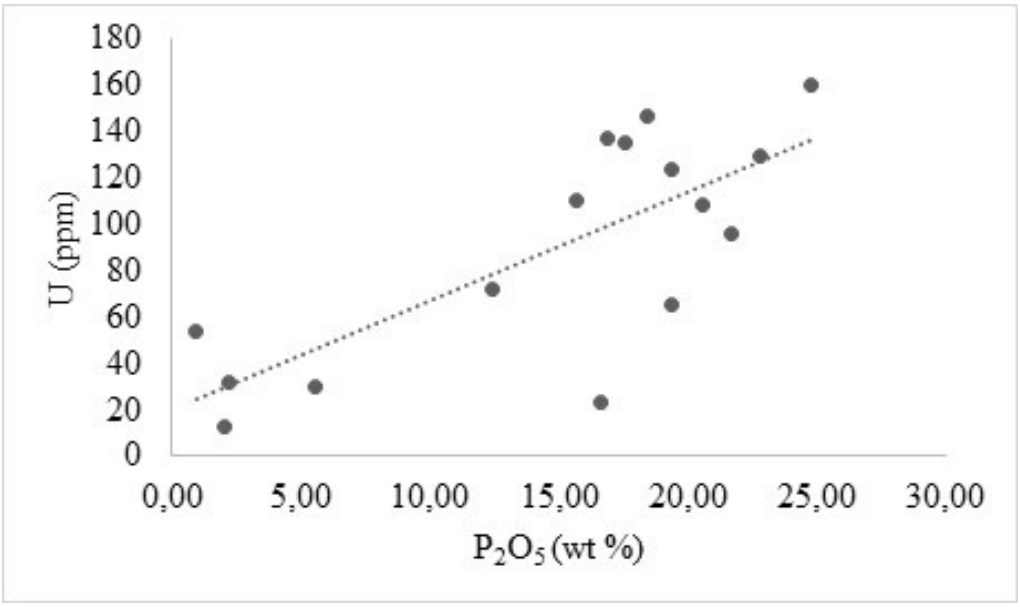

FIGURE 5. Correlation diagram P_2O_5 – U (also see Figure 7).

In several samples, yttrium was detected. Yttrium is associated with phosphates and this behavior may be due to the substitutions of Y^{3+} (ionic radius 0.93 Å) in the structure of the apatite by Ca^{2+} (ionic radius 1.12 Å). It is recommended to do additional REE analysis using an ICP-MS or another analytical technique since REEs cannot be detected using the techniques applied in our study. The REEs can be incorporated into the structure of the phosphate minerals owing to their geochemical affinity [14].

The V:Cr, V:V+Ni and V:Ni ratios indicate that the Navay sediments were deposited under oxic conditions, without replacement. The Ni:Co ratios of several samples indicate that these sediments were deposited under sub-oxic to anoxic conditions [18, 19]. This difference may be due to the evolution of redox conditions during sedimentation as a result of upwelling currents that brought oxygen-poor water from the bottom to the surface. Another interpretation could be that remobilization or a secondary dispersion of several of these redox sensitive elements under oxidative conditions occurred as a result of weathering.

3.3. Gamma spectrometry analysis

According to gamma spectrometric analysis of surface samples and cores, an average activity of 2100 Bq/kg produced by ^{226}Ra was detected, in addition to other isotopes of the decay series of ^{238}U. The ^{226}Ra activity was measured (by measuring ^{214}Pb and ^{214}Bi activities) and ^{234}Th activity directly through the emission at 63 keV. Owing to their low activities, the isotopes of the ^{232}Th series and ^{40}K cannot be detected by this technique.

TABLE 2. GAMMA ANALYSIS OF SELECTED SAMPLES OF PHOSPHATE ROCKS

Radioisotope	In secular equilibrium	Decay series	Energy (keV)	Activity concentrations (Bq/kg))
^{234}Th	^{238}U	^{238}U	63	1500
^{212}Pb	^{208}Tl	^{232}Th	239	31
^{214}Pb	^{226}Ra	^{238}U	295	2200
^{228}Ac	^{228}Ra	^{232}Th	338	35
^{214}Pb	^{226}Ra	^{238}U	352	2100
^{214}Bi	^{226}Ra	^{238}U	608	1900
^{228}Ac	^{228}Ra	^{232}Th	911	32
^{214}Bi	^{226}Ra	^{238}U	1120	2000
^{40}K		^{40}K	1461	LLD

The results imply that the concentrations of thorium in the deposit are low, in agreement with geochemical environments of this type, in which the uranium is mobilized as U^{6+} (uranyl ion UO_2^{2+}) and fixed in the apatite crystal structure as U^{4+} under reducing conditions, while Th^{4+} remains immobile in superficial environments and thus stays at low concentration in this type of deposit.

4. CONCLUSIONS

The Navay phosphate deposit represent lithological facies deposited in shallow water and is locally Campanian – Maastrichtian. Additional studies, including dating by LA-ICP-MS or another suitable technique are required to confirm this.

The mineralogy of the Navay Formation is typical of marine phosphatic deposits with fluorapatite/chlorapatite, collophane or carbonate fluorapatite ($Ca_5(PO_4,CO_3)F$), uranospathite, quartz and calcite as the major phases.

The mineralogical studies show that the uranium is present within two main minerals: apatite (28–75%) and uranospathite (2–3%).

Further studies of the phosphatic minerals to determine REE contents using ICP-MS and LA-ICP-MS are recommended.

According to chemical analysis, the background concentration of uranium is 102 ppm, reaching a maximum value of 160 ppm in a calcareous phosphatic sandstone, so this occurrence can be considered as an unconventional uranium deposit type according to its uranium grade.

REFERENCES

[1] CÁRDENAS, H., Historia de Caso: El descubrimiento e Investigaciones preliminares de los Fosfatos Uraníferos asociados a las Formaciones Navay-Burgüita, sectores Las Tapas–La Lucha-Fila El Toro, Parroquia San Joaquín de Navay, Municipio Libertador, Estado Táchira. Período 1978-1979, Petroquímica de Venezuela S. A. (PEQUIVEN) (unpublished report) (2007) 1–27 (in Spanish) http://699365588.com/descubierto-de-los-fosfatos-de-navay-197879-pdf-free.html.

[2] RUIZ, M., LORENTE, M., DURAN, I., FASOLA, A., Late Cretaceous Upwelling in the Southwest of the Thetys Sea, a Case History from the Barinas Basin, Venezuela. SEPM Research Conference, Paleogeography and Hydrocarbon Potential of the La Luna Formation and Related Cretaceous Anoxic Systems. Society for Sedimentary Geology **6** (2000) Caracas, Venezuela.

[3] CÁRDENAS, H., MOROTE, R., COLMENRAES C., Evaluación geológica de subsuelo de los Yacimientos fosfáticos de Los Monos y Las Tapas, región de Navay, estado Táchira. Sociedad venezolana de geólogos. Jornadas venezolanas de Fosfatos **39** (1991) 35–51 (in Spanish).

[4] SÁNCHEZ, T., LORENTE, M., Paleoecología del miembro Quevedo (Formaci6n Navay) en las proximidades de Santa Bárbara. 5th Venezuelan Geological Congress 1 (1977) 107–133 (in Spanish).

[5] CHIGNÉ, N., Aspectos relevantes en la exploración de Apure. Mem., II Simp. Bolívar, "Exploración petrolera en las cuencas subandinas", Bogotá, Asoc. Colombiana de Geol. y Geof. Petr., **1** 3 (1985) (in Spanish).

[6] MACSOTAY, O., ERLICH, R., PERAZA, T., (2003) Sedimentary Structures of the La Luna, Navay and Querecual Formations, Upper Cretaceous of Venezuela. PALAIOS La Luna Special Issue **18** 4/5 (2003) 334–348.

[7] CRUZ, L. JEREZ, J., AMAYA, H., RUEDA, J. BADILLO. J., VILLAMIZAR, J. (2011). Caracterización físicoquímica, tafonomía y ecología de orthokarstenia ewaldi (foraminiferida: siphogenerinoididae) de la formación los pinos (Cretácico: Maastrichtiano) de Samacá (Boyacá, Colombia). Boletín de geología **33** 2 (2011) (in Spanish).

[8] KISER, G., Review of the Cretaceous Stratigraphy of the Barinas mountain front; Boletín A.V.G.M.P. **11** 1961, 335-359, Caracas.

[9] PASQUALI, J., Uranio en Venezuela, visión para fines de 1978, en Conferencia sobre Yacimientos de Uranio en América Latina, Geología y Exploración, Lima, Perú, Dic. 1978, IAEA-AG Report, Vienna **162**/13 (1980).

[10] CÁRDENAS, E, H.,Informe preliminar de las rocas silícico-fosfato-uraníferas de la región de Navay; Distrito Libertador, Estado Táchira. Informe del CONAN para el Ministerio de Energía y Minas, Caracas SE-MP-115 (1979) 10 pp.

[11] KNUDSEN, A., GUNTER, M., Sedimentary Phosphorites – An Example: Phosphoria Formation, South-eastern Idaho, U.S.A., Reviews in Mineralogy and Geochemistry **48** 1 (2002) 363pp.

[12] BRUNETON, P., CUNEY, M., Geology of uranium deposits, Uranium for Nuclear Power, Resources, Mining and Transformation to Fuel **1** (2016) 11 pp.

[13] LOCOCK, A., KINMAN, W., BURNS, P., The structure and composition of uranospathite, Al1 x_x[(UO2)(PO4)]2(H2O)20+3xF1–3x, 0 < x < 0.33, a non-centrosymmetric fluorine bearing mineral of the autunite group, and of a related synthetic lower hydrate, Al0.67_0.33[(UO2)(PO4)]2(H2O)15.5, The Canadian Mineralogist 43 (2005) 989.

[14] CUNEY, M., KYSER, K., Recent and not-so-recent developments in uranium deposits and implications for exploration, Short Course Series, Mineralogical Association of Canada, Quebec City, Quebec **39** (2008) 259 pp.
[15] BOGGS, S., Petrology of Sedimentary Rocks, 2nd Ed, Cambridge University Press (2009) 612 pp.
[16] HUANG, J., HUANG, F., EVANS, L., GLASAUER, S., Vanadium: Global (bio) geochemistry, Chemical Geology 417 (2015) 68.
[17] GAO, Y., SHEN, B., LIU, J., Distribution of Nickel and Vanadium in Venezuelan Crude Oil, Petroleum Science and Technology 31 (2013) 509.
[18] SÁEZ, R., MORENO, C., GONZÁLEZ, F., ALMODÓVAR, G., Black shales and massive sulphide deposits: causal or casual relationships? Insights from Rimersburg, Tharsis, and Draa Sfar, Miner Deposita 46 (2011) 585.
[19] JONES, B., MANNING, D., Comparison of geochemical indices used for the interpretation of paleoredox conditions in ancient mudstones, Chemical Geology **111** (1994) 111 pp.

Appendix I

PUBLICATIONS RESULTING FROM THE CRP

Member State: Ukraine

Contract title: Geochemical and mineralogical characterization of Palaeoproterozoic albitite-type uranium deposits of the Ukrainian Shield.

MYKHALCHENKO I.I., SHUMLYANSKYY L.V., SOESOO A., Rare earth elements in Th-U-bearing albitites of the Novooleksiivka occurrence, the Ukrainian shield. In: abstract volume of the X international conference, Kryvyi Rih national University, 24–26 November 2016, 34–39.

MYKHALCHENKO I.I., SHUMLYANSKYY L.V., SOESOO A., Correlation of thorium with lanthanides in Th-U-bearing albitites of the Novooleksiivla occurrence. In: Abstract volume of the XIII Ukrainian conference, Kryvyi Rih national University, 2017, 22–28 (In Ukrainian).

MYKHALCHENKO I.I., SHUMLYANSKYY L.V., SOESOO A., Correlation of uranium with lanthanides in Th-U-bearing albitites of the Novooleksiivla occurrence. In: Abstract volume of the conference dedicated to the 50th anniversary of the M.P. Semenenko Institute of geochemistry, mineralogy and ore formation, Kyiv, 2019, **1**, 86–87 (In Ukrainian).

SHUMLYANSKYY L., Sr-Nd-Pb isotope systematics of U-bearing albitites of the Central Ukrainian Uranium Province: implication for the source of metasomatizing fluids, International Symposium on Uranium Raw Material for the Nuclear Fuel Cycle: Exploration, Mining, Production, Supply and Demand, Economics and Environmental Issues (URAM 2018) 25–29 June 2018, Vienna, Austria.

SHUMLYANSKYY L.V., MYKHALCHENKO I.I., Isotope composition of Sr, Nd and Pb in albitites of the Central Ukrainian Uranium Province. In: Abstract volume of the conference dedicated to the 50-th anniversary of the M.P. Semenenko Institute of geochemistry, mineralogy and ore formation, Kyiv, 2019, **1**, 124–125, (In Ukrainian).

SHUMLYANSKYY L.V., LI Z.Y., The source of metasomatic fluids for U-bearing albitites of the Central Ukrainian Uranium Province according to the data about Sr and Nd isotope compositions. In: Abstract volume of the XXII conference on isotope geochemistry dedicated to the Academician A.P. Vinogradov, Moscow, 2019 (In Russian).

Member State: Argentina

Contract title: Metallogenesis of granite-related uranium deposits in Argentina.

ALVAREZ J., LOPEZ L., PARRA F., BELLO C., ANZIL P., SALVATORE M., SCARLATTA L., FERREYRA P., MIYNO S., FELKAI E., HANLY A., CUNEY M., MERCADIER J., LIRA R., New studies of uranium deposits related to granites in Argentina. IAEA International Symposium on Uranium Raw Material for the Nuclear Fuel Cycle: Exploration, Mining, Production, Supply and Demand, Economics and Environmental Issues (URAM-2018) 25–29 June 2018, Vienna, Austria.

ANZIL P., SALVATORE M., PARRA F., SCARLATTA L., MIYNO S., BELLO F., Análisis textural y química mineral de la mineralización de uranio Alipan, Sierra de Velasco, La Rioja. Implicancias sobre la edad de la mineralización (Textural analysis and chemical composition of the Alipan uranium mineralization, Sierra de Velasco, La Rioja, Argentina. Implications about the age of mineralization) XX Congreso Geológico Argentino, 2017, ST 4: 2–4, Tucuman, Argentina.

BELLO C., LOPEZ L., FERREYRA P., Uranium potential assessment of Argentina using qualitative and quantitative approaches. Proceedings of the XI Argentine Congress of Economic Geology, Salta, Argentina, 7–9 September 2016.

CEBALLOS E., ZELAYA A., GORUSTOVICH S., Estudios complementarios de alteración hidrotermal en el depósito de uranio Mina Franca, provincia de Catamarca, Argentina (Complementary studies of hydrothermal alteration in the Mina Franca uranium deposit, Catamarca province, Argentina). XX Congreso Geológico Argentino, 2017, ST 4: 16–19 p, Tucuman, Argentina.

CEBALLOS E., ZELAYA A., MOLINA CASTILLO J., GORUSTOVICH S., GUIDI F., Hydrothermal alteration, structure and metallogenesis in the Central Sector of the Franca uranium mine (Catamarca). Proceedings of the XI Argentine Congress of Economic Geology, Salta, Argentina, 7–9 September 2016.

DE LA HOZ G., Supergenic mineralization of Las Termas uranium deposit, Fiambala Ranges, Catamarca. Proceedings of the XI Argentine Congress of Economic Geology, Salta, Argentina, 7–9 September 2016.

LIRA R., PARRA F., BARDELLI F., GALLISKI M., SCARLATTA L., Amazonite from miarolitic NYF-pegmatites and primary accessory minerals of the A-type La Chichilla granite, Sierra de Velasco, La Rioja Province, Argentina. Proceedings of the 7th International Symposium on Granitic Pegmatites, PEG 2015 Książ, Poland.

LOPEZ L., Uranium resources and perspectives for nuclear supply in Argentina, IAEA International Symposium on Uranium Raw Material for the Nuclear Fuel Cycle: Exploration, Mining, Production, Supply and Demand, Economics and Environmental Issues (URAM-2018), 25–29 June 2018, Vienna, Austria.

MOLINA CASTILLO J., ZELAYA A., GORUSTOVICH S., GUIDI F., Alteration belts in the Center - South Sector of the Franca uranium mine (Catamarca). Proceedings of the XI Argentine Congress of Economic Geology, Salta, Argentina, 7–9 September 2016.

Member State: China

Contract title: The relations of A-type igneous rocks to uranium mineralization in south China.

WANG, K. X., YU C. D., YAN J., LIU X.-D., LIU, W.-H., PAN, J.Y., Petrogenesis of Early Silurian granitoids in the Longshoushan area and their implications for the extensional environment of the North Qilian Orogenic Belt, China. Lithos, 2019, 342-343, 152-174.

YU C.D, WANG K.W., DONG LIU X.D., CUNEY M., PAN J.Y., WANG G., ZHANG L., ZHANG J., Uranium mineralogical and chemical features of the Na-metasomatic type uranium deposit in the Longshoushan Metallogenic Belt, Northwestern China, Minerals 2020, 10 (4), 335.

Member State: China

Contract title: Mineralogical characterization of sandstone uranium deposits in China

LIAO W., QUE W., WANG L., DU Z., Synergetic oxidation in alkaline in-situ leaching uranium a preliminary case study, Proceedings of the 28th International Conference on Nuclear Engineering (ICONE 28), 2020, 2–6 August, California, 6 p.

Member State: Ghana

Contract title: Geochemical and mineralogical studies of potential co-products; uranium resources in Ghana.

AGBETSOAMEDO J.E., ASIEDU D.K., DAMPARE S.B., KWAYISI, D., Geochemistry and uranium potential of black shales from the late Devonian to early Carboniferous Takoradi Shale Formation, Sekondian Group, Ghana. 26th Colloquium of African Geology (CAG26) and the 16th Congress of the Geological Society of Africa (GSAF), 23–27 November 2016, Ibadan, Nigeria., Abstracts Volume, p.78

DAMPARE S.B., ASIEDU D.K., AGBETSOAMEDO J.E., AIDOO F., HANSON J., BLAY S.S., Geochemical and mineralogical studies of uranium potential of the late Devonian to early Carboniferous Takoradi Black Shale, Sekondian Group, Ghana. International Symposium on Uranium Raw Material for the Nuclear Fuel Cycle: Exploration, Mining, Production, Supply and Demand, Economics and Environmental Issues (URAM-2018), 25–29 June 2018, Vienna, Austria.

Member State: Kenya

Contract title: Multimodal spectrometric characterization of uranium and thorium bearing mineral ores from Kenya's High Background Radiation Areas (HBRA).

BHATT B., ANGEYO K. H., DEHAYEM-MASSOP A., LIBS Development methodology for forensic nuclear materials analysis and attribution. Analytical Methods 2018, **10**, 791–798.

BHATT B., ANGEYO H. K., DEHAYEM-MASSOP A., Rapid nuclear forensics analysis via machine learning enabled LIBS. International Conference on Women in Physics, July16 – July20, 2017, Birmingham, United Kingdom.

KANIU M. I., ANGEYO K.H., Occurrence and multivariate exploratory analysis of the natural radioactivity anomaly in the south coastal region of Kenya. Radiation Physics and Chemistry, 2018, **146**, 34–41.

KANIU I., ANGEYO K.H., DARBY I., MUIA L.M., Rapid in situ gamma-ray spectrometric assessment of the Mrima-Kiruku high background radiation anomaly complex of Kenya. Journal of Environmental Radioactivity, 2017, **188**, 47–57.

KANIU M. I., DARBY I. G., ANGEYO K. H., In-situ gamma-ray spectrometric assessment of the radiation anomaly associated with Kenya's south coast paved road and adjoining environs. 7th International Symposium on IN SItu NUclear MEtrology as a tool for radioecology –INSINUME 2017, 24–28 April 2017, Ohrid, Macedonia.

WABWILE M.J., ANGEYO K.H., DEHAYEM-MASSOP A., Characterization of uranium bearing aerosols utilizing drop coating deposition based peak free Raman microspectrometry combined with multivariate curve resolution, 26th International Conference on Raman Spectroscopy, August 26–31 2018, Jeju, Korea.

WABWILE J. M., ANGEYO K.H., DEHAYEM-MASSOP A., Quantitative Raman microspectrometry of uranium in individual aerosols over a model nuclear atmosphere. Colloquium Spectroscopic International XL, 11–16 June 2017, Pisa, Italy.

Organization: International Atomic Energy Agency

HANLY A., IAEA Coordinated research project: Geochemical and mineralogical characterization of uranium and thorium deposits, IAEA International Symposium on Uranium Raw Material for the Nuclear Fuel Cycle: Exploration, Mining, Production, Supply and Demand, Economics and Environmental Issues (URAM-2018), 25–29 June 2018, Vienna, Austria.

Appendix II

GRADUATE STUDIES SUPPORTED BY THE CRP

This appendix provides additional information on graduate level studies that were fully or partly supported by the CRP.

Member State: Ukraine

Title of research contract: Geochemical and mineralogical characterization of Palaeoproterozoic albitite-type uranium deposits of the Ukrainian Shield

Type: Doctor of Sciences

Type of support: Partially supported

Title of thesis: Geology of the ore fields and deposits of the Central Ukrainian Uranium Province

Name of Student: Ivan Mykhalchenko

Institution: Institute of environmental geochemistry of the National Academy of sciences of Ukraine

Member State: Argentina

Title of research contract: Metallogenesis of granite-related uranium deposits in Argentina

Type: MSc.

Type of support: Partially supported

Title of thesis: Caracterización petrológica y geoquímica del plutón La Punta y sus manifestaciones uraníferas asociadas (Sierra de Velasco, La Rioja)/ Petrological and geochemical characterization of La Punta pluton and associated uranium showings (Velasco Range, La Rioja).

Name of Student: A. Cima

Institution: National University of Cordoba (UNC)

Member State: China

Title of research contract: The relations of A-type igneous rocks to uranium mineralization in south China

Type: Masters

Type of support: Partially supported

Title of thesis: Geochemical characteristics of Zoujiashan uranium deposit in Xiangshan uranium ore-field

Name of Student: Yu Chida

Institution: East China University of Technology

Member State: Ghana

Title of research contract: Geochemical and mineralogical studies of potential co-products; uranium resources in Ghana

Type: MSc.

Type of support: Partially supported

Title of thesis: Geochemistry of the Takoradi shales from the Sekondian Group, southwestern Ghana: implications for provenance, tectonic setting and source area weathering

Name of Student: Ms. Joyce Doku

Name of Institution: Department of Earth Science, University of Ghana, Legon, Accra

Type: MSc

Type of support: Partially supported

Title of thesis: Geochemical evaluation of uranium potential of the Takoradi Shale Formation, Sekondian Group, southern Ghana.

Name of Student: Mr. Godfred Ekye

Name of Institution: Department of Earth Science, University of Ghana, Legon, Accra

Member State: Kenya

Title of research contract: Multimodal spectrometric characterization of uranium and thorium bearing mineral ores from Kenya's high background radiation areas

Type: Doctor of Sciences

Type of support: Information was not provided

Title of thesis: In-situ gamma ray spectrometry and associated radiometric assessment of the Mrima-Kiruku high background radiation anomaly Complex of Kenya

Name of Student: Mr I. Kaniu

Institution: Information was not provided

Type: MSc

Type of support: Information was not provided

Title of thesis: Laser Raman microspectrometric assessment of uranium forensics signature in aerosols over a model nuclear atmosphere.

Name of Student: Mr J. Wabwile

Institution: Information was not provided

Member State: Bolivarian Republic of Venezuela

Title of research contract: Geochemical and mineralogical characterization of the uraniferous phosphates of the Navay Formation, Táchira state, Venezuela.

Type: Masters in Geochemistry

Type of support: Fully supported

Title of thesis: Mineralogical and geochemical characterization of phosphate rocks of the Navay Formation, Táchira state, Venezuela/Caracterización mineralógica y geoquímica de rocas fosfáticas de la Formación Navay, estado Táchira, Venezuela (in Spanish).

Name of Student: Eduard Linares

Institution: Universidad Central de Venezuela

LIST OF ABBREVIATIONS

ANN	Artificial neural networks
AOM	Amorphous organic matter
ASI	Aluminium saturation index
BSE	Back scattered electron
CCD	Charge coupled device
CNEA	National Atomic Energy Commission of Argentina
CRM	Certified reference material
CRP	Coordinated Research Project
CUUP	Central Ukrainian Uranium Province
EDS	Energy dispersive spectroscopy
EDXRFS	Energy dispersive X-ray fluorescence and scattering spectrometry
EPMA	Electron probe microanalyzer
eTh	Equivalent thorium
eU	Equivalent uranium
FESEM	Field emission scanning electron microscopy
FWHM	Full width half maximum
HBRA	High background radiation area(s)
HREE	Heavy rare earth elements
GPS	Global positioning system
GT	Grade-thickness
IC	Inorganic carbon
ICP-AES	Inductively coupled atomic emission spectrometry
ICP-OES	Inductively coupled plasma optical emission spectrometry
ICP-MS	Inductively coupled mass spectrometry
ID-TIMS	Isotopic dilution-thermal ionization mass spectrometry

I/M	Illite/montmorillonite mixed layer clay
I/S	Illite/smectite mixed layer clay
ISL	Insitu leaching
K	Permeability
LA-ICP-MS	Laser ablation inductively coupled mass spectrometry
LAMIS	Laser ablation isotopic spectrometry
LIBS	Laser induced breakdown spectroscopy
LIF	Laser induced fluorescence
LREE	Light rare earth elements
LRM	Laser Raman microspectrometry
l/s	Litres per second
LSM	Laser scanning microscopy
m	metre
Ma	Million years
mD	Millidarcies
NAA	Neutron activation analysis
NASC	North American Shale Composite
Nd-YAG	Neodymium-doped yttrium aluminium garnet
NEA	Nuclear Energy Agency
No.	Number
PIMA	Portable infrared mineral analyser
ppb	parts per billion
ppm	parts per million
REE	Rare earth elements
SDD	Silicon drift detector
SEM	Scanning electron microscopy
SHRIMP	Sensitive high-resolution ion microprobe

SNR	Signal to noise ratio
SWIR	Short wave infrared
TIMS	Thermal ionization mass spectrometry
TOC	Total organic carbon
TSF	Takoradi Shale Formation
UDEPO	World distribution of uranium deposits
UNSCEAR	United Nations Scientific Committee on the Effects of Atomic Radiation
WDS	Wavelength Dispersive XRF Spectroscopy
XRD	X-ray diffraction
XRF	X-ray fluorescence

CONTRIBUTERS TO DRAFTING AND REVIEW

Angeyo, H.K.	University of Nairobi, Kenya
Álvarez, J.	National Atomic Energy Commission (CNEA), Argentina
Anzil, P.	National Atomic Energy Commission (CNEA), Argentina
Barros, H.	Universidad Simón Bolívar, Bolivarian Republic 0f Venezuela
Bello, C.	National Atomic Energy Commission (CNEA), Argentina
Billström, K.	Swedish Museum of Natural History, Sweden
Ceballos, E.	National Atomic Energy Commission (CNEA), Argentina
Cuney, M.	Université de Lorraine, France
Dehayem-Massop, A.	University of Nairobi, Kenya
Farag, N.	Nuclear Materials Authority, Egypt
Felkai, E.	National Atomic Energy Commission (CNEA), Argentina
Ferreyra, P.	National Atomic Energy Commission (CNEA), Argentina
Gado, H.	Nuclear Materials Authority, Egypt
Hanly A.	International Atomic Energy Agency
He, K.	Beijing Research Institute of Chemical Engineering and Metallurgy, China
Jiang, G.	Beijing Research Institute of Chemical Engineering and Metallurgy, China
Kaniu, M.I.	University of Nairobi, Kenya
Khoshnoodi, K	Atomic Energy Organization of Iran, Islamic Republic of Iran
Li., P.	Beijing Research Institute of Chemical Engineering and Metallurgy, China
Liao, W.	Beijing Research Institute of Chemical Engineering and Metallurgy, China
Linares, E.	Universidad Central de Venezuela, Bolivarian Republic of Venezuela
Lira, R.	Universidad Nacional de Córdoba, Argentina

López, L.	National Atomic Energy Commission (CNEA), Argentina
Manrique, J.	Universidad Técnica Particular de Loja, Ecuador
Mercadier, J.	Université de Lorraine, France
Mikhalchenko, I.	State enterprise, Institute of Environmental Geochemistry, Ukraine
Mira, H.	Nuclear Materials Authority, Egypt
Miyno, S.	National Atomic Energy Commission (CNEA), Argentina
Monsalve, J.	Universidad Central de Venezuela, Bolivarian Republic of Venezuela
Norov, N.	National University of Mongolia, Mongolia
Parra, F.	National Atomic Energy Commission (CNEA), Argentina
Patel, J.P.	University of Nairobi, Kenya
Piña, A.	Universidad Central de Venezuela, Bolivarian Republic of Venezuela
Pohjolainen, E.	Geological Survey of Finland (GTK)
Salvatore, M.	National Atomic Energy Commission (CNEA), Argentina
Scarlatta, L.	National Atomic Energy Commission (CNEA), Argentina
Shumlyanskyy, L.	Curtin University, Australia
Soesoo, A.	Tallinn University of Technology, Estonia
Tserenpil, S.	National University of Mongolia, Mongolia
Velásquez, G.	Universidad Central de Venezuela, Bolivarian Republic of Venezuela
Wang., L.	Beijing Research Institute of Chemical Engineering and Metallurgy, China
Zelaya, A.	National Atomic Energy Commission (CNEA), Argentina
Zhengbang, L.	Beijing Research Institute of Chemical Engineering and Metallurgy, China
Ziapour, S.	Nuclear Science and Technology Research Institute, Islamic Republic of Iran
Zidan, I.	Nuclear Materials Authority, Egypt

Research Coordination Meetings

Vienna, Austria: 10–13 November 2015; 4–7 June 2018

Kingston, Canada: 30 May–2 June 2017

IAEA
International Atomic Energy Agency

No. 26

ORDERING LOCALLY

IAEA priced publications may be purchased from the sources listed below or from major local booksellers.

Orders for unpriced publications should be made directly to the IAEA. The contact details are given at the end of this list.

NORTH AMERICA

Bernan / Rowman & Littlefield

15250 NBN Way, Blue Ridge Summit, PA 17214, USA
Telephone: +1 800 462 6420 • Fax: +1 800 338 4550

Email: orders@rowman.com • Web site: www.rowman.com/bernan

REST OF WORLD

Please contact your preferred local supplier, or our lead distributor:

Eurospan Group

Gray's Inn House
127 Clerkenwell Road
London EC1R 5DB
United Kingdom

Trade orders and enquiries:

Telephone: +44 (0)176 760 4972 • Fax: +44 (0)176 760 1640
Email: eurospan@turpin-distribution.com

Individual orders:

www.eurospanbookstore.com/iaea

For further information:

Telephone: +44 (0)207 240 0856 • Fax: +44 (0)207 379 0609
Email: info@eurospangroup.com • Web site: www.eurospangroup.com

Orders for both priced and unpriced publications may be addressed directly to:

Marketing and Sales Unit
International Atomic Energy Agency
Vienna International Centre, PO Box 100, 1400 Vienna, Austria
Telephone: +43 1 2600 22529 or 22530 • Fax: +43 1 26007 22529
Email: sales.publications@iaea.org • Web site: www.iaea.org/publications

20-02965E

International Atomic Energy Agency
Vienna